

Edited by  
Bogdana Gayvas, Veronika Dmytruk

# DRYING PROCESSES: APPROACHES TO IMPROVE EFFICIENCY

Collective monograph

**UDC 65**  
**P93**

Published in 2025  
by TECHNOLOGY CENTER PC®  
Kharkiv, Ukraine

**P93**

**Authors:**

Edited by **Bogdana Gayvas, Veronika Dmytruk**

Bogdana Gayvas, Bogdan Markovych, Anatolii Dmytruk, Veronika Dmytruk, Yevhen Chaplya

Drying processes: approaches to improve efficiency: collective monograph. – Kharkiv: TECHNOLOGY CENTER PC, 2025. – 208 p.

This monograph is dedicated to the mathematical modeling of heat and moisture transfer in the drying of capillary-porous materials. It presents advanced theoretical and numerical approaches to describing the drying process, considering key factors such as phase transitions, diffusion mechanisms, electroosmotic effects, and mechanical stresses. The book provides a comprehensive analysis of drying kinetics under various conditions, integrating experimental validation and optimization strategies to enhance industrial drying efficiency.

This monograph will be particularly useful for researchers, engineers, and professionals working in the fields of heat and mass transfer, material science, and industrial drying technologies. It provides theoretical foundations and practical insights for optimizing drying processes in industries such as wood processing, food production, pharmaceuticals, and construction materials. By bridging the gap between fundamental research and real-world applications, the book serves as a critical reference for those seeking to enhance drying efficiency, reduce energy consumption, and ensure material durability in various industrial settings.

Figures 24, Tables 6, References 200 items.

This book contains information obtained from authentic and highly regarded sources. Reasonable efforts have been made to publish reliable data and information, but the author and publisher cannot assume responsibility for the validity of all materials or the consequences of their use. The authors and publishers have attempted to trace the copyright holders of all material reproduced in this publication and apologize to copyright holders if permission to publish in this form has not been obtained. If any copyright material has not been acknowledged please write and let us know so we may rectify in any future reprint.

The publisher, the authors and the editors are safe to assume that the advice and information in this book are believed to be true and accurate at the date of publication. Neither the publisher nor the authors or the editors give a warranty, express or implied, with respect to the material contained herein or for any errors or omissions that may have been made.

Trademark Notice: product or corporate names may be trademarks or registered trademarks, and are used only for identification and explanation without intent to infringe.

**DOI: 10.15587/978-617-8360-09-2**

**ISBN 978-617-8360-09-2 (on-line)**

*Cite as: Gayvas, B., Dmytruk, V. (Eds.) (2025). Drying processes: approaches to improve efficiency: collective monograph. Kharkiv: TECHNOLOGY CENTER PC, 208. <http://doi.org/10.15587/978-617-8360-09-2>*



Copyright © Author(s) 2025  
This is an open access paper under the Creative  
Commons Attribution-NonCommercial-NoDerivatives  
4.0 International License (CC BY-NC-ND 4.0)

## AUTHORS

### BOGDANA GAYVAS

(Chapter 1, 3, 4, 5)

Doctor of Technical Sciences, Leading Researcher  
Laboratory of Mathematical Modeling of Nonequilibrium  
Processes

Pidstryhach Institute for Applied Problems of Mechanics  
and Mathematics

National Academy of Sciences of Ukraine

 ORCID: <https://orcid.org/0000-0003-0788-506X>


### BOGDAN MARKOVYCH

(Chapter 1, 3, 4, 5)

Doctor of Physical and Mathematical sciences, Professor

Department of Applied Mathematics

Lviv Polytechnic National University


 ORCID: <https://orcid.org/0000-0002-8813-9108>

### ANATOLII DMYTRUK

(Chapter 1, 2, 3, 4, 5)

Department of Applied Mathematics

Lviv Polytechnic National University

 ORCID: <https://orcid.org/0000-0002-2393-0193>

### VERONIKA DMYTRUK

(Chapter 1, 3, 4, 5)

PhD, Associate Professor

Department of Applied Mathematics

Lviv Polytechnic National University

 ORCID: <https://orcid.org/0000-0002-3692-7110>

### YEVHEN CHAPLYA

(Chapter 3, 4)

Doctor of Physical and Mathematical Sciences, Professor


Department No. 20 Mathematical Problems of Mechanics

of Heterogeneous Bodies

Pidstryhach Institute for Applied Problems of Mechanics

and Mathematics

National Academy of Sciences of Ukraine

 ORCID: <https://orcid.org/0000-0002-5504-0419>

## ABSTRACT

This monograph explores the mathematical modeling of heat and moisture transfer processes in the drying of capillary-porous materials. It presents advanced models that account for the dynamics of moisture evaporation, convective and conductive drying, and the influence of external factors such as airflow, temperature gradients, and electric fields. Special attention is given to thermodynamic principles, diffusion mechanisms, and mechanical stresses that arise during drying, providing a comprehensive framework for understanding and optimizing drying technologies.

A significant portion of the monograph is devoted to the development of nonstationary and quasi-stationary mathematical models that describe the behavior of moisture and temperature fields over time. These models incorporate the effects of phase transitions, electroosmotic forces, and capillary interactions, allowing for a detailed analysis of drying kinetics under various conditions. Numerical simulations and experimental validation are employed to assess the accuracy and applicability of the proposed approaches, offering valuable insights for both theoretical research and industrial implementation.

The monograph also addresses the structural characteristics and mechanical properties of drying materials, highlighting the role of material deformation, shrinkage, and potential stress accumulation that may lead to cracking. Empirical criteria such as the Kirpichov, Nusselt, and Postnov numbers are examined as key parameters for evaluating drying efficiency and ensuring material integrity. Additionally, optimization strategies for industrial drying processes are discussed, incorporating mathematical and experimental methodologies to enhance energy efficiency and product quality.

By bridging the gap between fundamental research and industrial applications, this work provides engineers, researchers, and professionals in material science and heat transfer with a solid foundation for improving and innovating drying processes. The insights presented in this book contribute to the development of more efficient, sustainable, and cost-effective drying technologies, fostering advancements in industries such as wood processing, food production, pharmaceuticals, and materials engineering.

## KEYWORDS

Mathematical modeling, drying, electroosmotic drying, unilateral drying, bilateral drying, isothermal drying, drying kinetics, convection, diffusion, heat and mass transfer, capillary-porous material, capillary effects, continuum thermodynamics, moisture, moisture transport, multi-component system, phase, phase transition, structural model, ponderomotive force, sustainable technology, dispersed materials, gas-suspended state, fluidization, stress, optimization, deformation, anisotropy, numerical methods.

## CIRCLE OF READERS AND SCOPE OF APPLICATION

This monograph is dedicated to the mathematical modeling of heat and moisture transfer in the drying of capillary-porous materials. It presents advanced theoretical and numerical approaches to describing the drying process, considering key factors such as phase transitions, diffusion mechanisms, electroosmotic effects, and mechanical stresses. The book provides a comprehensive analysis of drying kinetics under various conditions, integrating experimental validation and optimization strategies to enhance industrial drying efficiency.

A significant focus is placed on the development of nonstationary and quasi-stationary models that account for convective, conductive, and electroosmotic drying, incorporating the effects of external factors such as airflow, temperature gradients, and electric fields. The work explores how these parameters influence moisture migration, heat transfer, and the structural integrity of materials, making it a valuable resource for improving industrial drying processes.

This monograph will be particularly useful for researchers, engineers, and professionals working in the fields of heat and mass transfer, material science, and industrial drying technologies. It provides theoretical foundations and practical insights for optimizing drying processes in industries such as wood processing, food production, pharmaceuticals, and construction materials. By bridging the gap between fundamental research and real-world applications, the book serves as a critical reference for those seeking to enhance drying efficiency, reduce energy consumption, and ensure material durability in various industrial settings.

# CONTENTS

<b>List of Tables</b> .....	xi
<b>List of Figures</b> .....	xiii
<b>Introduction</b> .....	1
<b>1 Convective drying of wood of cylindrical shape</b> .....	
1.1 Convective drying of wood of cylindrical shape: nonstationary case .....	
1.2 Solving Stefan's linear problem for drying cylindrical beam under quasi-averaged formulation .....	
Conclusions .....	
References .....	
<b>2 Drying process models for a multi-component system of capillary-porous structure based on thermodynamic relationships of mixture theory</b> .....	
2.1 Entropy balance equation .....	
2.2 Convection-diffusion equation for mass transfer .....	
2.3 Compatibility equation .....	
2.4 Momentum balance equation .....	
2.5 The key system of equations .....	
2.6 Numerical experiment .....	
Conclusions .....	
References .....	
<b>3 Mathematical modeling of drying processes in porous materials considering capillary properties</b> .....	
3.1 Mathematical modeling of the drying process .....	
3.1.1 Heat and mass transfer with the external environment .....	
3.1.2 Equations of thermo-hygro-mechanical processes in a porous body in the homogeneous approximation (generalized coordinates: temperature, deformation, moisture content) .....	
3.1.3 Mathematical modeling of the drying process of porous bodies considering capillary properties .....	
3.1.4 Capillary model of a porous body. Problem statement .....	
3.2 Mathematical modeling and computational analysis of moisture, temperature, and stress distribution in grain in convective drying. Problem formulation and key system of equations .....	

3.2.1	Development of solution algorithms for moisture content and stress-strain state of the grain .....	
	Conclusions .....	
	References.....	

#### **4 Drying of a porous layer in an external constant electric field (electroosmotic drying) .....**

4.1	Electroosmosis drying a porous layer .....	
4.1.1	Capillary moisture flow.....	
4.1.2	Electroosmotic liquid flow.....	
4.1.3	Solution of the problem and results of quantitative analysis .....	
4.2	Enhancement of convective drying of a porous layer surface by electroosmosis .....	
4.2.1	Numerical analysis of parameter influence on convective electroosmotic drying .....	
4.3	Influence of an external constant electric field on bilateral natural drying of a porous layer .....	
4.3.1	Mass transfer in the surrounding gas.....	
4.3.2	Mass transfer in the zone of dried pores .....	
4.3.3	Liquid flow under the influence of capillary forces.....	
4.3.4	Mass balance equation for liquid .....	
4.3.5	Solution of the problem and analysis of the obtained results .....	
4.3.6	Estimation of temperature change in the layer due to the influence of the electric field.....	
4.4	The influence of electroosmosis on bilateral convective drying of a porous layer .....	
4.4.1	Object of study and problem formulation.....	
4.4.2	Solution and quantitative analysis of the problem.....	
	Conclusions .....	
	References.....	

#### **5 On the issues of optimization and regulation of the convective drying process of materials in drying units.....**

5.1	Fundamentals of heterogeneous media description.....	
5.2	Statistical methods for studying the drying of capillary-porous bodies.....	
5.3	Drying process control and optimization for energy efficiency and sustainability .....	
5.3.1	General information on convective drying of porous materials in drying installations .....	
	Conclusions .....	
	References.....	

## LIST OF TABLES

- 4.1 Consideration of capillary imbibition ( $t = 104$  s,  $L_0 = 0.1$  m)
- 4.2 Influence of electric field intensity on relative moisture content at  $E = 200$  V/m
- 4.3 Influence of electric field intensity on relative moisture content at  $E = 400$  V/m
- 4.4 Dependence of relative moisture content  $\bar{z}_m = 1 - \bar{z}_m^*$  on temperature at a mass transfer coefficient  $b = 0.01$  for  $E = 200$  V/m, and  $E = 400$  V/m
- 4.5 Dependence of relative moisture content  $\bar{z}_m$  on the mass transfer coefficient  $b$  at  $T = 300$  K,  $E = 200$  V/m, and  $E = 400$  V/m
- 5.1 Constants for relationships heat and mass transfer



## LIST OF FIGURES

- 1.1 Schematic representation of the wooden cylindrical beam
- 1.2 Control function  $T_a(\tau)$
- 1.3 Temperature distributions on the surface and inside the cylindrical beam at a drying agent temperature of 302 K (soft regime)
- 1.4 Temperature distributions on the surface and inside the cylindrical beam at a drying agent temperature of 370 K (hard regime)
- 1.5 The dependence of thickness of layer of the dried area on time of drying (curves 1–3 correspond to sort of materials: spruce, pine, birch, respectively)
- 1.6 Change in relative moisture of beam skeleton in time (curves 1–3 correspond to materials: spruce, pine, birch, respectively)
- 2.1 Schematic representation of the model
- 2.2 Temperature variations in time for  $\Pi = 0.9$  and  $\alpha_0 = 0.8$ . The curves 1, 2, 3 correspond to the  $q = 10^4, 5 \cdot 10^3, 3 \cdot 10^3$ , respectively
- 2.3 Change in volumetric saturation in time on the outer surface for  $\alpha_0 = 0.8$ . The curves 1, 2, 3 correspond to the  $q = 3 \cdot 10^3, 5 \cdot 10^3, 10^4$ , respectively
- 2.4 Temperature variations in time under the action of the flow  $q = 5 \cdot 10^3$ . The curves 1, 2, 3 correspond to the porosity  $\Pi = 0.4, 0.6, 0.8$ , respectively
- 2.5 Change in volumetric saturation in time on the outer surface for  $q = 5 \cdot 10^3, \alpha_0 = 0.8$ . The curves 1, 2, 3 correspond to the porosity  $\Pi = 0.4, 0.6, 0.8$ , respectively
- 2.6 Temperature variations in time on the heating surface (curves 1); external surface (curves 2) for  $q = 10^4, \alpha_0 = 0.8$  for different values of porosity (dashed curves for  $\Pi = 0.4$ ; solid curves for  $\Pi = 0.6$ , dotted curves for  $\Pi = 0.8$ )
- 2.7 Change in air density in time on the heating surface (curves 1); external surface (curves 2) for  $q = 10^4, \alpha_0 = 0.8$  for different values of porosity (dashed curves for  $\Pi = 0.4$ ; solid curves for  $\Pi = 0.6$ , dotted curves for  $\Pi = 0.8$ )
- 4.1 Dependence of relative moisture content on time at different temperatures for  $\delta = 0.001$  m
- 4.2 Dependence of relative moisture content on time at different temperatures for  $\delta = 0.1$  m
- 4.3 Time variation of relative moisture content for different temperature values in the absence of an external electric field
- 4.4 Time variation of relative saturation as a function of temperature at a given electric field strength  $E = 200$  V/m
- 4.5 Time dependence of relative moisture content for different values of the mass transfer coefficient at  $E = 200$  V/m

- 4.6 Temporal dependence of the relative moisture content of the layer during the second stage of drying at  $E = 200$  V/m for temperatures of 300 K, 310 K, 320 K, and 330 K
- 4.7 Temporal dependence of the relative moisture content of the layer during the second stage of drying for a temperature of 300 K at  $E = 200$  V/m, 400 V/m, and 1000 V/m
- 4.8 Dependence of relative saturation on the mass transfer coefficient  $\beta_2$
- 4.9 The effect of electric field intensity on humidity variation over time
- 4.10 Time dependence of relative moisture content for different temperatures
- 5.1 Changes of  $T_c$  and  $T_m$  in the process of drying

# INTRODUCTION

Drying is a fundamental process widely applied in various industrial sectors, from wood processing to food production and material science. The efficiency and quality of drying largely depend on understanding the complex interplay between heat and mass transfer, as well as the thermodynamic and mechanical properties of the material being dried. Over the years, mathematical modeling has become an essential tool for analyzing and optimizing drying processes, providing valuable insights into moisture migration, temperature distribution, and stress formation within porous media.

This monograph presents a comprehensive study of mathematical models describing the drying process of capillary-porous materials. The focus is on the development and application of nonstationary and quasi-stationary heat and moisture transfer models, incorporating external influences such as convective airflow and electric fields. The models account for moving moisture evaporation boundaries and various drying regimes, offering a detailed analysis of drying kinetics under different conditions.

The chapters of this book explore the fundamental thermodynamic principles governing moisture transfer in deformable porous media, formulating a complete system of equations to describe heat and mass transport phenomena. By leveraging continuum mechanics and mixture theory, the book systematically examines the role of diffusion, capillarity, electroosmotic forces, and thermal gradients in optimizing the drying process. Additionally, numerical simulations are carried out to validate theoretical models, with a particular emphasis on industrial applications where precise control of drying conditions is critical.

Special attention is given to the influence of external factors such as airflow velocity, temperature gradients, and electric fields on drying efficiency. The research presented provides a solid foundation for optimizing drying strategies, reducing energy consumption, and enhancing material durability. Moreover, empirical criteria such as the Kirpichov, Nusselt, and Postnov numbers are discussed as essential parameters for assessing and controlling drying performance.

This monograph serves as a valuable resource for engineers, researchers, and professionals involved in material drying and heat transfer processes. By integrating advanced mathematical modeling techniques with practical considerations, it contributes to the ongoing development of more efficient and sustainable drying technologies. Through rigorous theoretical analysis and experimental validation, this work aims to bridge the gap between fundamental research and industrial application, ensuring the advancement of drying science and technology.

## CHAPTER 1

## CONVECTIVE DRYING OF WOOD OF CYLINDRICAL SHAPE

ABSTRACT

---

In this Chapter, the mathematical nonstationary and quasi-stationary models of the heat and moisture transfer in convective drying of a long wooden beam with a circular cross-section of the radius  $R$  ( $0 \leq r \leq R$ ) are constructed, taking into account the moving boundary of the moisture evaporation zone under the action of the convective-thermal unsteady flow of the drying agent, as well as the calculation schemes for the implementation of these models into practice. Numerical experiments are carried out. The regularities of distribution of temperature and moisture in a capillary-porous body of a cylindrical shape at an arbitrary moment of drying depending on the coordinate of the phase transition, thermophysical characteristics of the material, and parameters of the drying agent have been established.

KEYWORDS

---

Mathematical model, initial boundary value problem, heat and mass transfer, convection, diffusion, Stefan's problem, Kontorovich-Lebedev transform, Pochhammer's polynomials, Green's function, Steklov's theorem, Poiseuille's equation, capillary-porous material, phase transition, cylindrical shape.

Drying is the process of removing moisture from the body, which changes the structural-mechanical, technological and biological properties of the material, caused by the change in bonding forms of moisture with the material [1, 2]. When moisture is removed, capillary-porous bodies become brittle, slightly compressible and can be turned into powder; colloidal bodies significantly change their size with changing moisture content, but retain plasticity or elastic properties; capillary-porous colloidal bodies have a capillary-porous structure, with capillary walls having the properties of limitedly swollen colloidal bodies (skin, tissue, wood) [3–5].

Convective-heat drying is classified into subtypes: steam-air, gas, steam, moisture and others [6]. The uniformity of drying materials in drying plants is achieved by the drying agent circulation. The drying agent circulation with velocity  $v$  can be natural and forced, unilateral and reversible. It is carried out by fans in a chamber or through ejector nozzles [6]. The drying agent is characterized

additionally by humidity  $\phi = \frac{\gamma_v}{\gamma_n}$  and temperature  $t$ . Here,  $\gamma_v$  is the density of vapor, and  $\gamma_n$  is the

density of saturated vapor. Parameters  $t$ ,  $\phi$ ,  $v$  define the drying mode [6].

The change of local moisture content  $U$  and local temperature  $t$  in a capillary-porous body with time depends on the relationship between the mechanism of moisture and heat transfer inside the wet material as well as the mass and heat exchange of the body surface with the drying agent [7–9].

In drying plants, the regime changes with time. A rigorous analysis of drying kinetics is complex. Increasing temperature intensifies the drying process [10, 11]. Increasing the moisture content of the drying agent reduces the intensity and critical moisture content [12, 13]. Increasing the velocity of the drying agent leads to higher drying intensity at the beginning of the process and has much less effect at the end [14].

The whole process of drying porous materials can be divided into three stages [6]:

1. Disordered irregular regime at the beginning of the process. The initial distribution of temperature and moisture in the body is important here.
2. From some time on, the body enters a regular heating regime, when the initial distribution no longer has an effect. Body heating is described by a simple exponent.
3. The final stage of heating corresponds to the stationary state, at which the temperature is equal to the ambient temperature at all points of the body.

During the drying process, three characteristic zones can be formed in the body: the outer gas zone, where all the pores are dried; the middle two-phase zone, where the dried pores and the pores filled with moisture; and the inner moisture zone, where all the pores are filled with moisture. The two-phase zone emerges due to the release of moisture through evaporation, and on the other hand, through the flow of moisture by the action of capillary forces from wide moisture pores into narrow dried pores and recondensation of moisture. In the elementary physical volume of the two-phase zone, the moisture phase may exist in the form of a connected network of wet pores and in the form of unconnected inclusions, blocked by gas from all sides. Their fates depend on the specific moisture content. In the process of evaporation with a decrease in specific moisture content, redistribution and fragmentation of the cohesive system occur. Upon reaching a critical moisture content, the bonds are completely broken. The capillary inflow is possible only through the connected moisture network. For moisture contents less than critical, the transfer through the moisture phase is impossible. The cohesive system of moisture pores is also heterogeneous due to one-side open pores [4]. The dimension of these zones depends on the pore radius distribution function, which characterizes the structure of the porous body. During evaporation, the boundaries of the zones move into the middle of the body.

**Forms of moisture bonding with the material.** The velocity of moisture movement inside the material depends on the form of its connection with the material. The main forms of moisture connection with the body are adsorption and capillary bonds [15]. The amount of adsorption-bound and microcapillary moisture depends on the temperature and pressure in the environment. This moisture is called hygroscopic moisture. Changes in material dimensions (shrinkage-soaking) are

linked to the change in the amount of hygroscopic moisture. Bound moisture is uniform and depends on the structure of the surface interacting with it. There arises a density gradient in the layer thickness of the water bound to the body surface. Capillary forces and gravity do not occur in this bound water. The evaporation heat of bound water is higher than the one of free water by the energy amount of adsorption water bounding with the surface of  $E \approx 280$  cal/g [15].

In the macrocapillaries of a capillary-porous body, the laminar flow satisfies Poiseuille's equation

$j = \frac{\rho^2}{8\nu} \frac{P_1 - P_2}{l}$ , with  $P_1, P_2$  as the pressure at the ends of the capillary of length  $l$ . Poiseuille's equation and Fick's law of diffusion are not satisfied in microcapillaries, with

$$j = \frac{8}{3} \sqrt{\frac{\mu}{2\pi RT}} \frac{\varepsilon}{l} \left( \frac{P_2}{\sqrt{T_2}} - \frac{P_1}{\sqrt{T_1}} \right)$$

being the flow [16], where  $\mu$  is the dynamic viscosity,  $\varepsilon$  is a constant for a capillary-porous body, it is called the coefficient of the molecular gas flow. The heat conduction coefficient for gas in

microcapillaries is defined as  $\lambda = 2\varepsilon c_v \sqrt{\frac{\mu}{3RT}} \rho$ , where  $c_v$  is the specific heat capacity of gas for

the constant volume and  $\rho$  is the capillary radius [16].

The forms of moisture bonding with the material play a major role in the mechanism of heat and moisture transfer inside the body.

The main mechanisms of moisture transfer in the porous medium are [17]:

- diffusion of vapor-air mixture in the gas zone by the action of density difference in the direction opposite to the gradient and recondensation by the action of partial pressure gradient of vapor over menisci of different curvature;
- thermal diffusion of vapor in the direction of heat flow from areas with higher temperature to areas with lower temperature;
- convective transfer of vapor and moisture by the action of external pressure drop;
- capillary movement of moisture in the pores that depends on the structure of the porous medium, i.e. the capillary leakage from wide to narrow pores due to the difference in capillary pressure;
- moisture film transfer by the action of gradients of the wedge and capillary pressures.

Experimental studies of these transfer mechanisms carried out on real and model systems indicate the decisive effect of capillary and surface forces on the mass transfer process and drying intensity. These forces regulate the mutual distribution of phases in the pore space and determine the conditions of transfer, causing the mechanisms of transfer.

The amount of adsorption-bound and microcapillary moisture depends on the temperature and vapor pressure in the environment. The relationship between moisture and the body is characterized by the differential and integral curves of pore radius distribution.

The area under the differential curve on its arbitrary part provides the moisture volume (saturation) within the range of capillary radii change. The curves of pore distribution by radii show a wide variation in the size of voids in the body pores.

To determine the rational drying regime, the choice of which depends on technological changes in the drying process, it is important to study the regularities of moisture transfer for the purpose of its control. One of the possible ways to control the moisture transfer mechanism is by affecting the processes of diffusion and thermal diffusion.

The moisture movement by the action of temperature (heat and moisture conduction) includes the following phenomena [1, 3–5, 10, 17]:

1. Molecular diffusion of moisture in the form of molecular vapor flow, which occurs due to different velocities of molecules of heated and cold material layers.

2. Capillary conduction caused by the change in capillary potential, which depends on the surface tension, decreasing with rising temperature. Since the capillary pressure over the concave meniscus is negative, the decrease in pressure increases the suction force, resulting in moisture leaving the heated body to colder layers in the form of liquid.

3. The movement of fluid in a porous body in the direction of heat flow is caused by trapped air. When the material is heated, the pressure of the trapped air increases, and the air bubbles expand. As a result, the liquid in the capillary pore is pushed in the direction of heat flow.

Heat moisture conduction is the reason for the movement of moisture in the direction of heat flow. During convective drying, a temperature gradient opposite to the moisture gradient is created, which prevents the movement of moisture from the bulk to the surface of the material. The flow of moisture directed to the surface of the material is reduced by the value of the flow of moisture due to thermal diffusion. The temperature gradient is an obstacle to the movement of moisture from the central layers to the surface. With a constant intensity of drying, conditions are created that help the evaporation of moisture inside the material. Thermal diffusion reduces the moisture gradient and reduces the speed of movement of liquid moisture and the amount of water-soluble substances on the surface of the material. With a change in the value and direction of the temperature gradient, the conditions for the movement of moisture and substances dissolved in it change. This leads to a change in the physical and chemical properties of the material [3–5].

## 1.1 CONVECTIVE DRYING OF WOOD OF CYLINDRICAL SHAPE: NONSTATIONARY CASE

One of the important areas of modern mathematical modeling is the construction of adequate mathematical models for the description of the technological processes of drying capillary-porous materials. Such models, as a rule, are based on the thermodynamics of irreversible processes and must take into account the peculiarities of the kinetics of internal transformations, in particular, phase transitions. The problems of mathematical physics based on them also require the development of appropriate analytical and numerical methods for their solution.

Drying of wood includes taking into account the heat-mass exchange between the wood surface and wet air and the internal heat and moisture exchange in the material [18]. The relationship between the distribution of moisture content and temperature fields depends on the geometric

dimensions of the material to be dried. In this chapter, the mathematical nonlinear and linear models of the moisture transfer in drying of a long wooden beam with a circular cross-section of the radius  $R$  ( $0 \leq r \leq R$ ) is constructed, taking into account the moving boundary of the moisture evaporation zone under the action of the convective-thermal unsteady flow of the drying agent as well as the calculation schemes for the implementation of these models into practice. Numerical experiments are carried out. The regularities of distribution of temperature and moisture in a capillary-porous body of a cylindrical shape at an arbitrary moment of drying depending on the coordinate of the phase transition, thermophysical characteristics of the material, and parameters of the drying agent have been established.

When developing the models, it was taken into account that wood shrinkage along the fibers is negligibly small (0.1–0.3 %). The cross-section shrinkage is from 2 to 10 % [6].

Since the length of the considered cylindrical beam is much greater than the dimensions of its cross-section, and the coefficient of moisture conductivity along the fibers is much larger than that coefficient across the fibers, and due to the great complexity of the structure of the wood material, a plane averaged thermal conductivity problem is considered. As a tool for describing thermal conductivity, differential equations were used to model non-stationary processes [19]. The method of integral transformations was used to find solutions [20].

To simplify the models, it is assumed that the gas phase is water vapor, which is an ideal gas.

The aim of this work is the determination of optimal wood drying parameters, at which energy consumption will be minimal.

**Problem formulation.** Let's consider a cylinder with a radius  $R$  ( $0 \leq r \leq R$ ) shown in **Fig. 1.1**. Given the symmetry of the boundary conditions of this problem, it is possible to introduce a polar coordinate system  $(r, \varphi)$ , the polar axis of which is directed along the axis of the cylinder. The cylinder is under the action of convective-thermal non-stationary flow of the drying steam-air agent of the velocity  $v$ . It is possible to assume that the drying agent regime is three-stage, non-stationary, and includes heating, keeping, and cooling.

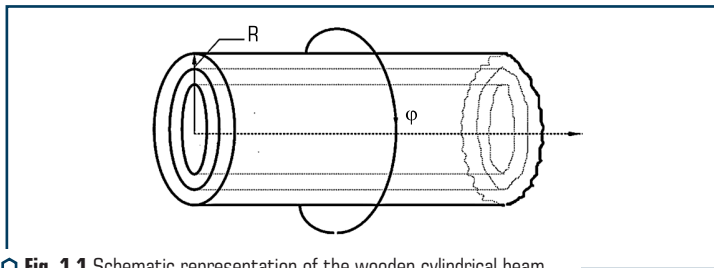


**Fig. 1.1** Schematic representation of the wooden cylindrical beam

The control parameter in this process is the temperature of the drying agent  $T_a$ . In convective drying, the heat supplied by the gas is used to evaporate the liquid, heat the material, and overcome



the energy of moisture bonds with the material. It is possible to assume that the moisture in the dried area is removed and in the rest of the volume it is preserved, known and its density is  $\rho_l$ . The moisture content  $W$  retained in the body is calculated by the formula:

$$W = \rho_l \left( \frac{V - V_m}{V} \right),$$

where  $V$  is the body volume;  $V_m$  is the volume of the dried area. Note that when hot air contacts with moisture particles, the latter break down into steam and smaller liquid particles.

The process of heat conduction in the body is described by the equation:

$$\begin{aligned} & \left[ \Pi (\mathcal{C}_v \rho_v + \mathcal{C}_a \rho_a) + (1 - \Pi) \mathcal{C}_s \rho_s \right] \frac{\partial T}{\partial \tau} + \gamma_1^2 T = \\ & = \lambda \left[ r^2 \frac{d^2 T}{dr^2} + (2\alpha + 1) r \frac{dT}{dr} + (\alpha^2 - \lambda^2 r^2) T \right], \quad (2\alpha + 1 > 0). \end{aligned} \quad (1.1)$$

where  $\tau$  is time;  $r$  is the radius of running point ( $0 \leq r \leq R$ );  $\gamma_1^2$  is the particle decomposition coefficient.

Equation (1.1), using the Bessel differential operator, takes the form:

$$B_\alpha [T] = \left[ r^2 \frac{d^2 T}{dr^2} + (2\alpha + 1) r \frac{dT}{dr} + (\alpha^2 - \lambda^2 r^2) T \right],$$

for the given volumetric heat capacity  $c_p$  and averaged thermal conductivity  $\lambda$  in the quasi-homogeneous approximation, which can be used in wood drying problems with acceptable temperature gradients, has the form [20]:

$$\frac{\partial T}{\partial \tau} + \gamma^2 T = a^2 B_\alpha [T, r], \quad \gamma^2 = \frac{\gamma_1^2}{c_p}, \quad \alpha > 0, \quad (1.2)$$

where  $a^2 = \frac{\lambda}{\left[ \Pi (\mathcal{C}_v \rho_v + \mathcal{C}_a \rho_a) + (1 - \Pi) \mathcal{C}_s \rho_s \right]}$  is the averaged thermal diffusivity coefficient.

Let's construct the solution of Equation (1.2) under the following boundary conditions:

$$T(\tau, r)|_{\tau=0} = g(r), \quad r \in (0, R), \quad (1.3)$$

$$\lim_{r \rightarrow 0} \frac{\partial}{\partial r} (r^\alpha T) = 0, \quad \left( \alpha_{11}^1 \frac{\partial}{\partial r} + \beta_{11}^1 \right) T|_{r \rightarrow R} = T_a(\tau), \quad (1.4)$$

where  $T_a$  is the temperature of the drying agent;  $\gamma^2$  is responsible for the multiplication of particles of the steam-air mixture (averaged coefficient of decomposition) in the porous material under the action of the drying agent; indices  $v, a, s$  indicate the components of steam, air, and skeleton, respectively;  $\Pi, C_v, C_a, C_s, \rho_v, \rho_a, \rho_s$  are porosity, heat capacity, and density of steam, air, and skeleton, respectively;  $\lambda$  is the averaged coefficient of thermal conductivity;  $\alpha_{11}^1, \beta_{11}^1$  are coefficients of thermal conductivity and heat transfer on the outer surface of the cylinder.

The temperature of the drying agent  $T_a(\tau)$  is as follows:

$$T_a(\tau) = \begin{cases} T_0 + \frac{T_{\max} - T_0}{\tau_1} \tau, & 0 \leq \tau \leq \tau_1; \\ T_{\max}, & \tau_1 \leq \tau \leq \tau_2; \\ \frac{T_{\max} \tau_3 - T_1 \tau_2}{\tau_3 - \tau_2} - \frac{T_{\max} - T_1}{\tau_3 - \tau_2} \tau, & \tau_2 \leq \tau \leq \tau_3. \end{cases} \quad (1.5)$$

The scheme of  $T_a(\tau)$  behavior is shown in **Fig. 1.2**.

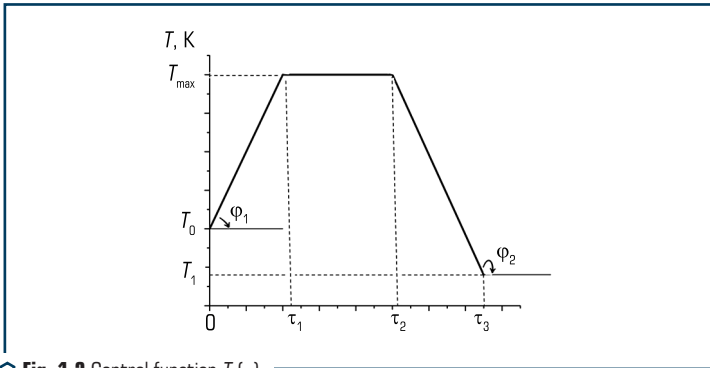


**Fig. 1.2** Control function  $T_a(\tau)$

Here  $T_0$  is the initial temperature of the drying agent; cooling is carried out to some equilibrium temperature.

It is possible to expand this function into a trigonometric Fourier series with respect to cosines:

$$T_a(\tau) = \alpha_0 + \sum_{n=1}^{\infty} \alpha_n \cos \frac{n\pi}{\tau_3} \tau, \quad v_n^2 = \frac{n\pi}{\tau_3}.$$

$$\alpha_0 = \frac{2}{\tau_3} \left[ T_{\max} \left( -\frac{\tau_1}{2} + \frac{\tau_2}{2} + \frac{\tau_3}{2} \right) + T_0 \frac{\tau_1}{2} + T_1 \left( -\frac{\tau_2}{2} + \frac{\tau_3}{2} \right) \right],$$

$$\alpha_n = \frac{2}{\tau_3} \left[ \frac{(T_{\max} - T_0)}{\tau_1 v_n^4} (\cos v_n^2 \tau_1 - 1) + \frac{T_{\max}}{v_n^2} (\sin v_n^2 \tau_2 - \sin v_n^2 \tau_1) \right] +$$

$$+ \frac{2}{\tau_3} \left\{ -\frac{T_{\max} \tau_3 - T_1 \tau_2}{\tau_3 - \tau_2} \frac{\tau_2}{n\pi} \sin v_n^2 \tau_2 - \frac{T_{\max} - T_1}{\tau_3 - \tau_2} \left( \frac{1}{v_n} \right)^4 \left[ (-1)^n - \cos v_n^2 \tau_2 - \frac{n\pi \tau_2}{\tau_3} \sin v_n^2 \tau_2 \right] \right\}.$$

Let  $T^*(p, r)$  be the image of the Laplace transform of the temperature  $T(\tau, r)$ :

$$L[T(\tau, r)] = \int_0^{\infty} T(\tau, r) e^{-p\tau} d\tau = T^*(p, r).$$

Then, in accordance with the problem (1.1)–(1.4), it is possible to obtain the following boundary value problem with respect to the function  $T^*(p, r)$ :

$$(B_{v,\alpha} - \lambda^2) T^* = \frac{d^2 T^*}{dr^2} + \frac{2\alpha + 1}{r} \frac{dT^*}{dr} - \left( \lambda^2 + \frac{v^2 - \alpha^2}{r^2} \right) T^* = -\tilde{g}(r), \quad (1.6)$$

$$\lim_{r \rightarrow 0} \frac{\partial}{\partial r} (r^{\alpha-v} T^*(p, r)) = 0, \quad \left( \alpha \frac{1}{r} \frac{d}{dr} + \beta \frac{1}{r} \right) T^* \Big|_{r=R} = T_a^*(p), \quad (1.7)$$

$$\tilde{g}(r) = a^{-2} r^{-2} g(r), \quad v^2 = a^{-2} (p + \gamma^2), \quad p = \sigma + i\tau, \quad i^2 = -1.$$

Let's fix  $\operatorname{Re} v = \operatorname{Re} \left[ a^{-1} (p + \gamma^2)^{1/2} \right] > 0$ . Construct a Cauchy function for equation (1.6) to

satisfy homogeneous boundary conditions. A fundamental function  $\varepsilon_\alpha^*(p, r, \rho)$  satisfying the homogeneous equation corresponding to equation (1.6) and the homogeneous conditions corresponding to the conditions (1.7) is the Cauchy function. The solution of equation (1.6) satisfying the homogeneous conditions corresponding to the conditions (1.7), has the form:

$$T^*(p, r) = \int_0^R \varepsilon_\alpha^*(p, r, \rho) \tilde{g}(\rho) \rho^{2\alpha+1} d\rho,$$

where  $\varepsilon_\alpha^*(p, r, \rho)$  is a fundamental function of the boundary value problem (1.6), (1.7) with the following properties:

– the function  $\varepsilon_\alpha^*(p, r, \rho)$  satisfies the homogeneous equation corresponding to equation (1.6) and the following boundary conditions [20]:

$$\lim_{r \rightarrow 0} \frac{\partial}{\partial r} (r^{\alpha-\nu} \varepsilon^*) = 0, \quad \left( \alpha_1^1 \frac{d}{dr} + \beta_1^1 \right) \varepsilon^* \Big|_{r=R} = 0.$$

With this,  $\varepsilon_\alpha^*(p, r, \rho) \Big|_{r=\rho+0} - \varepsilon_\alpha^*(p, r, \rho) \Big|_{r=\rho-0} = 0$ .

The following holds  $d / dr \varepsilon_\alpha^*(p, r, \rho) \Big|_{r=\rho+0} - d / dr \varepsilon_\alpha^*(p, r, \rho) \Big|_{r=\rho-0} = \rho^{-(2\alpha+1)}$ .

Let's put:

$$\varepsilon_\alpha^*(p, r, \rho) = \begin{cases} A_1 I_{\nu, \alpha}(\lambda r), & 0 < r < \rho < R; \\ A_2 I_{\nu, \alpha}(\lambda r) + B_2 K_{\nu, \alpha}(\lambda r), & 0 < \rho < r < R, \end{cases}$$

where  $I_{\nu, \alpha}(\lambda r)$ ,  $K_{\nu, \alpha}(\lambda r)$  are modified Bessel functions of the first and second kind  $\nu = i\alpha^{-1}\beta$ ,

$\operatorname{Re} \nu \geq \alpha \geq -\frac{1}{2}$ , write down in the form:

$$\rho = -(\beta^2 + \gamma^2) = (\beta^2 + \gamma^2) e^{i\pi},$$

$$d\rho = -2\beta d\beta, \quad b(\beta) = \alpha^{-1}\beta.$$

Returning to the original, it is possible to obtain:

$$T(\tau, r) = \frac{\bar{a}^{-2}}{2\pi i} \int_0^R \int_{\sigma_0 - i\infty}^{\sigma_0 + i\infty} \varepsilon_\alpha^*(p, r, \rho) e^{p\tau} dp \, \lambda g(\rho) \rho^{2\alpha-1} d\rho,$$

where  $\bar{a}^{-2}$  is a weight function [20]. The special points of the Cauchy function  $\varepsilon^*(p, r, \rho)$  are the branching points  $p = -\gamma^2 \leq 0$  and the point  $p = \infty$ .

Let's denote:

$$\begin{aligned} X_{\alpha, 11}^{11}(\lambda R, b) &= \alpha_{11}^1 \frac{d}{dr} C_\alpha(\lambda r, b) + \beta_{11}^1 C_\alpha(\lambda r, b) \Big|_{r=R} = \alpha_{11}^1 \lambda \left[ \frac{d I_{\beta, \alpha}(\lambda R)}{dr} + \frac{i}{\pi} sh\pi b \frac{d K_{\beta, \alpha}(\lambda R)}{dr} \right] + \\ &+ \beta_{11}^1 \left[ I_{\beta, \alpha}(\lambda R) + i\pi^{-1} sh\pi b K_{\beta, \alpha}(\lambda R) \right] = \tilde{X}_{\alpha, 11}^{11}(\lambda R) + i \frac{sh\pi b}{\pi} \tilde{X}_{\alpha, 11}^{12}(\lambda R); \\ X_{\alpha, 11}^{12}(\lambda R, b) &= \left( \alpha_{11}^1 \frac{d}{dr} + \beta_{11}^1 \right) D_\alpha(\lambda r, b) \Big|_{r=R} = \\ &= \alpha_{11}^1 \lambda \left[ \frac{1}{\pi} sh\pi b \frac{d K_{\beta, \alpha}(\lambda R)}{dr} \right] + \beta_{11}^1 \pi^{-1} sh\pi b K_{\beta, \alpha}(\lambda R) = \\ &= \pi^{-1} sh\pi b \left[ \alpha_{11}^1 \lambda \frac{d}{dr} K_{\beta, \alpha}(\lambda R) + \beta_{11}^1 K_{\beta, \alpha}(\lambda R) \right] = \tilde{X}_{\alpha, 11}^{12}(\lambda R) \frac{sh\pi b}{\pi}; \end{aligned} \quad (1.8)$$

$$\begin{aligned}\tilde{X}_{\alpha,11}^{11}(\lambda R) &= \alpha_{11}^1 \lambda \frac{dI_{\beta,\alpha}(\lambda R)}{dR} + \beta_{11}^1 I_{\beta,\alpha}(\lambda R); \\ \tilde{X}_{\alpha,11}^{12}(\lambda R) &= \alpha_{11}^1 \lambda \frac{dK_{\beta,\alpha}(\lambda R)}{dR} + \beta_{11}^1 K_{\beta,\alpha}(\lambda R).\end{aligned}$$

If to pass to the Bessel functions of a real argument  $J_{\nu,\alpha}(\lambda R, b)$ ,  $N_{\nu,\alpha}(\lambda R, b)$ , then:

$$\begin{aligned}X_{\alpha,11}^{11}(\lambda R, b) &= \left( \alpha_{11}^1 \frac{\nu - \alpha}{R} + \beta_{11}^1 \right) J_{\nu,\alpha}(\lambda R, b) - \alpha_{11}^1 R \lambda^2 J_{\nu+1,\alpha+1}(\lambda R, b), \quad b = a^{-1}\beta; \\ X_{\alpha,11}^{12}(\lambda R, b) &= \left( \alpha_{11}^1 \frac{\nu - \alpha}{R} + \beta_{11}^1 \right) N_{\nu,\alpha}(\lambda R, b) - \alpha_{11}^1 R \lambda^2 N_{\nu+1,\alpha+1}(\lambda R, b).\end{aligned}$$

Let's determine functions:

$$\begin{aligned}U_{\nu,\alpha,11}^{11}(\lambda R, b) &= X_{\alpha,11}^{11}(\lambda R, b) - i X_{\alpha,11}^{12}(\lambda R, b) = \tilde{X}_{\alpha,11}^{11}(\lambda R) = \alpha_{11}^1 \lambda \frac{dI_{\beta,\alpha}(\lambda R)}{dR} + \beta_{11}^1 I_{\beta,\alpha}(\lambda R) = \\ &= \left( \alpha_{11}^1 \frac{\nu - \alpha}{R} + \beta_{11}^1 \right) I_{\nu,\alpha}(\lambda R, b) + \alpha_{11}^1 R \lambda^2 I_{\nu+1,\alpha+1}(\lambda R, b), \quad \nu = a^{-1}\beta; \\ U_{\nu,\alpha,11}^{12}(\lambda R) &= \pi(\sin b\pi)^{-1} X_{\alpha,11}^{12}(\lambda R, b) = \left( \alpha_{11}^1 \frac{d}{dR} + \beta_{11}^1 \right) K_{\nu,\alpha}(\lambda R) \Big|_{r=R} = \tilde{X}_{\alpha,11}^{12}(\lambda R, b) = \\ &= \left( \alpha_{11}^1 \frac{\nu - \alpha}{R} + \beta_{11}^1 \right) K_{\nu,\alpha}(\lambda R) + \alpha_{11}^1 R \lambda^2 K_{\nu+1,\alpha+1}(\lambda R).\end{aligned}\tag{1.9}$$

Satisfying the condition (1.7), it is possible to obtain the algebraic system of equations for determining the coefficients  $A_1, A_2, B_2$ :

$$\begin{aligned}(A_2 - A_1)I_{\nu,\alpha}(\lambda \rho) + B_2 K_{\nu,\alpha}(\lambda \rho) &= 0, \\ (A_2 - A_1)I'_{\nu,\alpha}(\lambda \rho) + B_2 K'_{\nu,\alpha}(\lambda \rho) &= -\frac{1}{\lambda \rho^{2\alpha+1}}.\end{aligned}$$

Given the relation:

$$I_{\nu,\alpha}(\lambda \rho) K'_{\nu,\alpha}(\lambda \rho) - I'_{\nu,\alpha}(\lambda \rho) K_{\nu,\alpha}(\lambda \rho) = -(\lambda \rho)^{-(2\alpha+1)},$$

let's obtain:

$$(A_2 - A_1) = -\lambda^{2\alpha} K_{\nu,\alpha}(\lambda \rho), \quad B_2 = \lambda^{2\alpha} I_{\nu,\alpha}(\lambda \rho).\tag{1.10}$$

Satisfying the boundary condition for  $r = R$ , it is possible to obtain:

$$A_2 U_{v,\alpha;11}^{11}(\lambda R) + B_2 U_{v,\alpha;11}^{12}(\lambda R) = 0 \quad (1.11)$$

$$A_2 = \lambda^{2\alpha} \frac{\Psi_{v,\alpha;11}^{1*}(\lambda R, \lambda \rho)}{U_{v,\alpha;11}^{11}(\lambda R)} - \lambda^{2\alpha} K_{v,\alpha}(\lambda \rho) = \lambda^{2\alpha} \left\{ \frac{\Psi_{v,\alpha;11}^{1*}(\lambda R, \lambda \rho) - U_{v,\alpha;11}^{11}(\lambda R) K_{v,\alpha}(\lambda \rho)}{U_{v,\alpha;11}^{11}(\lambda R)} \right\} =$$

$$= -\lambda^{2\alpha} \frac{U_{v,\alpha;11}^{12}(\lambda R)}{U_{v,\alpha;11}^{11}(\lambda R)} I_{v,\alpha}(\lambda \rho) = -B_2 \frac{U_{v,\alpha;11}^{12}(\lambda R)}{U_{v,\alpha;11}^{11}(\lambda R)},$$

$$A_1 = \frac{B_2 K_{v,\alpha}(\lambda \rho)}{I_{v,\alpha}(\lambda \rho)} + A_2,$$

where

$$A_1 = \lambda^{2\alpha} \left( U_{v,\alpha;11}^{11}(\lambda R) \right)^{-1} \Psi_{v,\alpha;11}^{1*}(\lambda R, \lambda \rho);$$

$$U_{v,\alpha;11}^{12}(\lambda R) = \frac{A_2 \left( U_{v,\alpha;11}^{11}(\lambda R) \right)}{\lambda^{2\alpha} I_{v,\alpha}(\lambda R)};$$

$$\Psi_{v,\alpha;11}^{1*}(\lambda R, \lambda \rho) = U_{v,\alpha;11}^{11}(\lambda R) K_{v,\alpha}(\lambda \rho) - U_{v,\alpha;11}^{12}(\lambda R) I_{v,\alpha}(\lambda \rho).$$

Then the function  $\varepsilon_{\alpha}^*(p, r, \rho)$  due to the symmetry relative to the diagonal  $r = \rho$  has the form:

$$\varepsilon_{\alpha}^*(p, r, \rho) = \frac{\lambda^{2\alpha}}{U_{v,\alpha;11}^{11}(\lambda R, b)} \begin{cases} I_{v,\alpha}(\lambda r) \Psi_{v,\alpha;11}^{1*}(\lambda R, \lambda \rho), & 0 < r < \rho < R; \\ I_{v,\alpha}(\lambda \rho) \Psi_{v,\alpha;11}^{1*}(\lambda R, \lambda r), & 0 < \rho < r < R. \end{cases} \quad (1.12)$$

The roots  $p_n = -(\beta_n^2 + \gamma^2)$  of the transcendental equation  $U_{v,\alpha;11}^{11}(\lambda R, b) = 0$  are simple poles of  $\varepsilon_{\alpha}^*(p, r, \rho)$ .

Let's consider the transcendental equation:

$$\left( \alpha_{11}^1 \frac{v-\alpha}{R} + \beta_{11}^1 \right) I_{v,\alpha}(\lambda R, b) - \alpha_{11}^1 \lambda^2 R I_{v+1,\alpha+1}(\lambda R, b) = 0,$$

where  $p = -(\beta^2 + \gamma^2) = (\beta^2 + \gamma^2) e^{\pi i}$ ,  $b(\beta) = a^{-1} \beta$  form a discrete spectrum  $\{b_n\}_{n=1}^{\infty}$ .

Let's denote  $\Psi_{v,\alpha;11}^1(\lambda R, \lambda r, b) = \pi^{-1} (sh \pi b) \times \Psi_{v,\alpha;11}^{1*}(\lambda R, \lambda r, b)$ .

Here  $\Psi_{v,\alpha,11}^1(\lambda R, \lambda r, b)$  is the eigenfunction of the problem that satisfies equation (1.2) and homogeneous boundary conditions. It is possible to use it to construct a solution of the problem that satisfies the inhomogeneous condition at the outer surface of the cylinder, i.e., reflects the effect of the drying agent.

The original of the fundamental function:

$$\begin{aligned}\varepsilon_\alpha(t, r, \rho) &= \int_0^\infty e^{-(\beta^2 + \gamma^2)t} \Psi_{v,\alpha,11}^1(\lambda R, \lambda r, b) \Psi_{v,\alpha,11}^1(\lambda R, \lambda \rho, b) \frac{2\beta \lambda^{2\alpha} d\beta}{\left(X_{\alpha,11}^{11}\right)^2 + \left(X_{\alpha,11}^{12}\right)^2} = \\ &= \int_0^\infty e^{-(\beta^2 + \gamma^2)t} V_\alpha(r, \beta) V_\alpha(\rho, \beta) \Omega_\alpha(\beta) d\beta; \\ \Omega_\alpha(\beta) &= \frac{2\beta \lambda^{2\alpha}}{\left(X_{\alpha,11}^{11}(\lambda R, \beta)\right)^2 + \left(X_{\alpha,11}^{12}(\lambda R, \beta)\right)^2}.\end{aligned}\quad (1.13)$$

By the generalized development theorem:

$$\varepsilon_\alpha(t, r, \rho) = \sum_{n=1}^\infty e^{-(\beta_n^2 + \gamma^2)t} \frac{V_\alpha(b_n r) V_\alpha(b_n \rho)}{\|V_\alpha(b_n r)\|_1^2},$$

where  $\|V_\alpha(b_n r)\|_1^2$  is the square of the norm of its own function;  $b_n$  are roots of the function  $U_{v,\alpha,11}^{11}(\lambda R, b)$ .

$$\begin{aligned}\Psi_{v,\alpha,11}^{1*}(i\lambda R, i\lambda \rho) &= -\frac{\pi}{2} e^{-\pi i \alpha} \Psi_{v,\alpha,11}^1(\lambda R, \lambda \rho), \\ V_\alpha(r, \beta) &= \Psi_{v,\alpha,11}^1(\lambda R, \lambda r, \beta) = X_{\alpha,11}^{11}(\lambda R, \beta) D_\alpha(\lambda r, \beta) - X_{\alpha,11}^{12}(\lambda R, \beta) C_\alpha(\lambda r, \beta), \\ \Psi_{v,\alpha,11}^{*1}(i\lambda R, i\lambda r) &= -\frac{\pi}{2} e^{-\pi i \alpha} \Psi_{v,\alpha,11}^1(\lambda R, \lambda r).\end{aligned}\quad (1.14)$$

Here  $V_\alpha(r, \beta) = \Psi_{v,\alpha,11}^1(\lambda R, \lambda r, \beta)$  is eigenfunction (spectral function) of the problem (1.6);  $\Omega_\alpha(\beta)$  is a spectral density.

Returning in equation (1.13) to the original, it is possible to obtain a solution  $T_{odn}(t, r)$  of the homogeneous parabolic Cauchy problem (1.2), (1.3):

$$T_{odn}(t, r) = \int_0^R \varepsilon_\alpha(t, r, \rho) g(\rho) \rho^{2\alpha-1} d\rho =$$

$$= \int_0^{\infty} e^{-(\beta^2 + \gamma^2)t} V_{\alpha}(r, \beta) \int_0^R g(\rho) V_{\alpha}(\rho, \beta) \sigma \rho^{2\alpha-1} d\rho \Omega_{\alpha}(\beta) d\beta, \quad \sigma = a^{-2}. \quad (1.15)$$

From equation (1.15) for  $t = 0$ , it is possible to obtain the integral image:

$$g(r) = \int_0^{\infty} V_{\alpha}(r, \beta) \int_0^R g(\rho) V_{\alpha}(\rho, \beta) \sigma \rho^{2\alpha-1} d\rho \Omega_{\alpha}(\beta) d\beta. \quad (1.16)$$

From equation (1.16), it follows that the function  $\varepsilon_{\alpha}(t, r, \rho)$  defined by equation (1.13) is a delta-shaped sequence with respect to  $t$  for  $t \rightarrow 0+$ .

The integral image (1.16) defines a direct:

$$H_{\alpha}[g(r)] = \int_0^R g(r) V_{\alpha}(r, \beta) \sigma r^{2\alpha-1} dr \equiv \tilde{g}(\beta); \quad (1.17)$$

and inverse:

$$H_{\alpha}^{-1}[\tilde{g}(r)] = \int_0^{\infty} \tilde{g}(\beta) V_{\alpha}(r, \beta) \Omega_{\alpha}(\beta) d\beta \equiv g(r). \quad (1.18)$$

Kontorovich-Lebedev transform over the interval  $[0, R]$ .

Given the theorem on the basic identity of the integral transform [20] of a differential operator  $B_{\alpha}$ , i.e., if the function  $g(r)$  is such that the function  $f(r) = B_{\alpha}[g(r)]$  is continuous on the set  $(0, R)$  and the boundary conditions hold:

$$\lim_{r \rightarrow 0} r^{2\alpha+1} \left( \frac{dg}{dr} V_{\alpha}(r, \beta) - g(r) \frac{dV_{\alpha}}{dr} \right) = 0, \quad \left( \alpha_{11}^1 \frac{d}{dr} + \beta_{11}^1 \right) g(r) \Big|_{r=R} = g_R(\tau), \quad (1.19)$$

then for any  $\lambda \in (0, \infty)$ , the following equality holds:

$$H_{\alpha} \left[ a^2 B_{\alpha} [g(r)] \right] = -\beta^2 \tilde{g}(\beta) + \frac{sh \pi \beta}{\pi \lambda^{2\alpha}} g_R(\tau). \quad (1.20)$$

Therefore, based on relation (1.17), it follows:

$$H_{\alpha} \left[ a^2 B_{\alpha} [g(r)] \right] = -\beta^2 \int_0^R g(r) V_{\alpha}(r, \beta) \sigma r^{2\alpha-1} dr + \frac{sh \pi \beta}{\pi \lambda^{2\alpha}} J_{\alpha}(R, \tau). \quad (1.21)$$

From the properties of the eigenfunction  $V_{\alpha}(r, \beta)$ , it follows that:



$$\left( \alpha_{11}^1 \frac{dV_\alpha(r, \beta)}{dr} + \beta_{11}^1 V_\alpha(r, \beta) \right) \Big|_{r=R} = 0, \quad (a^2 B_\alpha + \beta^2) V_\alpha(r, \beta) = 0.$$

From equation (1.21), taking into account equation (1.19), it is possible to obtain:

$$\begin{aligned} H_\alpha \left[ a^2 B_\alpha [g(r)] \right] &= a^2 \int_0^R B_\alpha [g(r)] V_\alpha(r, \beta) \sigma r^{2\alpha-1} dr = \\ &= \int_0^R \left[ r^2 \frac{d^2 g}{dr^2} + (2\alpha + 1) r \frac{dg}{dr} - \lambda^2 r^2 g(r) + \alpha^2 g(r) \right] V_\alpha(r, \beta) r^{2\alpha-1} dr = \\ &= a^2 \sigma r^{2\alpha+1} \left[ g'(r) V_\alpha(r, \beta) - g(r) V'_\alpha(r, \beta) \right] \Big|_0^R + \int_0^R g(r) a^2 \sigma B_\alpha [V_\alpha(r, \beta)] r^{2\alpha-1} dr = \\ &= R^{2\alpha+1} \left[ g'(r) V_\alpha(r, \beta) - g(r) V'_\alpha(r, \beta) \right] \Big|_{r=R} - \beta^2 H_\alpha [g(r)]. \end{aligned}$$

where  $H_\alpha[g(r)]$  is defined by the expression (1.17);  $g_R = T_{aR}(R, t)$  is the temperature of the drying agent.

Then from equation (1.21), it is possible to obtain:

$$\begin{aligned} \frac{g_R}{\alpha_{11}} V_\alpha(R, \beta) &= \frac{g_R}{\alpha_{11}} \left[ X_{\alpha, 11}^{11}(\lambda R, b) D_\alpha(\lambda R, b) - X_{\alpha, 11}^{12}(\lambda R, b) C_\alpha(\lambda R, b) \right] = \\ &= g_R \left[ C'_{r\alpha}(\lambda R, b) D_\alpha(\lambda R, b) - D'_{r\alpha}(\lambda R, b) C_\alpha(\lambda R, b) \right] = \frac{sh\pi b}{\pi \lambda^{2\alpha} R^{2\alpha+1}} T_{aR}. \end{aligned} \quad (1.22)$$

The equations of thermal conductivity and boundary conditions have the following form:

$$\frac{\partial T}{\partial \tau} + (\beta^2 + \gamma^2) T = 0; \quad T(\tau, \beta) \Big|_{\tau=0} = g(\beta), \quad \left( \alpha_{11}^1 \frac{dT}{dr} + \beta_{11}^1 T \right) \Big|_{r=R} = T_{aR}(\tau).$$

As a result of identity (1.21):

$$\frac{\partial \tilde{T}}{\partial \tau} + (\beta^2 + \gamma^2) \tilde{T} = \frac{sh\pi b}{\pi \lambda^{2\alpha}} T_{aR}(\tau); \quad \tilde{T}(\tau, \beta) \Big|_{\tau=0} = \tilde{g}(\beta). \quad (1.23)$$

The solution of the Cauchy problem (1.23) is the function:

$$\tilde{T}(\tau, \beta) = e^{-(\beta^2 + \gamma^2)\tau} \tilde{g}(\beta) + \int_0^\tau e^{-(\beta^2 + \gamma^2)(\tau-t)} \left[ \frac{sh\pi b}{\pi \lambda^{2\alpha}} \left( \alpha_0 + \sum_{n=1}^\infty \alpha_n \cos v_n^2 t \right) \right] dt. \quad (1.24)$$

Let's apply the integral operator  $H_\alpha^{-1}$  (1.18) to  $\tilde{T}(\tau, \beta)$ , and obtain the solution of the problem (1.24):

$$T(t, r) = \int_0^t \int_0^R \int_0^\infty e^{-(\beta^2 + \gamma^2)(t-\tau)} V_\alpha(r, \beta) V_\alpha(\rho, \beta) \Omega_\alpha(\beta) d\beta [\delta_+(\tau) g(\rho)] \sigma \rho^{2\alpha-1} d\rho d\tau + \\ + \int_0^\infty \int_0^t e^{-(\beta^2 + \gamma^2)(t-\tau)} \frac{sh\pi b}{\pi \lambda^{2\alpha}} T_s(\tau) V_\alpha(r, \beta) \Omega_\alpha(\beta) d\beta d\tau. \quad (1.25)$$

From equations (1.17), (1.18) and Steklov's theorem, any vector-function  $f(r) = B_\alpha[g(r)]$  continuous on  $(0, R)$  satisfying zero boundary conditions can be decomposed in terms of a system of eigenfunctions  $V_\alpha(r, \beta_j)_{j=1}^\infty$  into an absolutely and uniformly convergent Fourier series.

It is known that one eigenvector-function  $V_\alpha(r, \beta_j)$  corresponds to each eigenvalue  $\beta_j$  and the system of spectral functions  $V_\alpha(r, \beta_j)_{j=1}^\infty$  is complete and closed. The square of the norm of eigenfunction  $\|V_\alpha(r, \beta_j)\|^2 = \int_0^R [V_\alpha(r, \beta_j)]^2 \sigma r^{2\alpha-1} dr$ .

Thus, given equation (1.17), the inverse integral operator (1.18) can be written down as follows:

$$H_\alpha^{-1}[\tilde{g}(r)] = \sum_{j=0}^\infty \tilde{g}(\beta_j) V_\alpha(r, \beta_j) \left( \|V_\alpha(r, \beta_j)\|^2 \right)^{-1} \equiv g(r),$$

and the function:

$$G_\alpha(t, r, \rho) = \int_0^\infty e^{-(\beta^2 + \gamma^2)t} V_\alpha(r, \beta) V_\alpha(\rho, \beta) \Omega_\alpha(\beta) d\beta, \quad (1.26)$$

by taking into account the initial temperature state of the body, according to the theory of surpluses can be represented as calculated integral in the form:

$$G_\alpha(t, r, \rho) = \sum_{j=1}^\infty e^{-(\beta_j^2 + \gamma^2)t} \frac{V_\alpha(r, \beta_j) V_\alpha(\rho, \beta_j)}{\|V_\alpha(r, \beta_j)\|^2} \sigma \beta_j^2,$$

where

$$V_\alpha(r, \beta_j) = \Psi_{\alpha, 11}^1(\lambda R, \lambda r, \beta_j) = \frac{sh\pi \beta_j}{\pi} \left[ X_{\alpha, 11}^{11}(\lambda R, \beta_j) D_\alpha(\lambda r, \beta_j) - X_{\alpha, 11}^{12}(\lambda R, \beta_j) C_\alpha(\lambda r, \beta_j) \right];$$

as well as the Green's function generated by the thermal regime at the boundary:

$$r = R;$$

$$W_{\alpha}(t, r) = \int_0^{\infty} e^{-(\beta^2 + \gamma^2)t} V_{\alpha}(r, \beta) \frac{sh\pi\beta}{\pi\lambda^{2\alpha}} \Omega_{\alpha}(\beta) d\beta, \quad b = a^{-1}\beta;$$

$$W_{\alpha}(t, r) = \sum_{j=1}^{\infty} e^{-(\beta_j^2 + \gamma^2)t} \frac{sh\pi\beta_j}{\pi\lambda^{2\alpha}} \frac{V_{\alpha}(r, \beta_j)}{\|V_{\alpha}(r, \beta_j)\|^2} \sigma a^2. \quad (1.27)$$

Then the solution will take the form:

$$T(t, r) = \int_0^t \int_0^R G_{\alpha}(t - \tau, r, \rho) [\delta_+(\tau) g(\rho)] \sigma \rho^{2\alpha-1} d\rho d\tau + \int_0^t W_{\alpha}(t - \tau, r) T_a(\tau) d\tau. \quad (1.28)$$

Here  $\delta_+(\tau)$  is a delta-function concentrated at the point  $0+$ .

According to equation (1.28), taking into account the properties of delta-function and equation (1.17), it is possible to obtain:

$$T(t, r) = \int_0^{\infty} e^{-(\beta^2 + \gamma^2)t} \tilde{g}(\beta) V_{\alpha}(r, \beta) \Omega_{\alpha}(\beta) d\beta + \int_0^t e^{-(\beta^2 + \gamma^2)(t-\tau)} \frac{sh\pi\beta}{\pi\lambda^{2\alpha}} T_{aR}(\tau) V_{\alpha}(r, \beta) \Omega_{\alpha}(\beta) d\beta.$$

Let's denote  $\int_0^t e^{-(\beta^2 + \gamma^2)(t-\tau)} \frac{sh\pi\beta}{\pi\lambda^{2\alpha}} T_{aR}(\tau) d\tau = T_{wa}(t, \beta)$ . It is possible to transit to impro-

per integrals:

$$T(t, r) = \int_0^{\infty} e^{-(\beta^2 + \gamma^2)t} \tilde{g}(\beta) V_{\alpha}(r, \beta) \Omega_{\alpha}(\beta) d\beta + \int_0^{\infty} T_{wa}(t, \tau) V_{\alpha}(r, \beta) \Omega_{\alpha}(\beta) d\beta.$$

Taking into account equation (1.26), (1.27), let's obtain:

$$T(t, r) = \sum_{j=1}^{\infty} e^{-(\beta_j^2 + \gamma^2)t} \tilde{g}(\beta_j) \frac{V_{\alpha}(r, \beta_j)}{\|V_{\alpha}(r, \beta_j)\|^2} \sigma a^2 + \sum_{j=1}^{\infty} T_{wa}(t, \tau) \frac{V_{\alpha}(r, \beta_j)}{\|V_{\alpha}(r, \beta_j)\|^2} \sigma a^2.$$

Let's determine the effect of initial conditions and temperature of the drying agent on the drying process. Given equation (1.16), the initial condition  $\left(g(r) = \sum_{j=0}^2 g_{j0} r^j\right)$  is chosen. Then:

$$\begin{aligned} \tilde{g}(\beta) = & \frac{1}{a^2} \int_0^R \sum_{j=0}^2 (g_{j0} r^{j+2\alpha-1}) \times \left[ X_{\alpha 11}^{11}(\lambda R, \beta) (\pi^{-1} sh \pi \beta K_{\beta, \alpha}(\lambda r)) - \right. \\ & \left. - X_{\alpha 11}^{12}(\lambda R, \beta) (I_{\beta, \alpha}(\lambda r) + i(\pi^{-1} sh \pi \beta K_{\beta, \alpha}(\lambda r))) \right] dr. \end{aligned}$$

Given expressions for the Bessel functions:

$$I_{v, \alpha}(\lambda \rho) = (\lambda \rho)^{-\alpha} I_v(\lambda \rho), \quad K_{v, \alpha}(\lambda \rho) = (\lambda \rho)^{-\alpha} K_v(\lambda \rho).$$

Let's determine:

$$\begin{aligned} \tilde{g}(\beta) = & \frac{1}{a^2} \left\{ X_{\alpha 11}^{11}(\lambda R, \beta) \pi^{-1} sh \pi \beta \int_0^R \sum_{j=0}^2 (g_{j0} r^{j+\alpha-1}) K_{\beta}(\lambda r) dr - \right. \\ & - X_{\alpha 11}^{12}(\lambda R, \beta) \int_0^R \sum_{j=0}^2 (g_{j0} r^{j+\alpha-1}) I_{\beta}(\lambda r) dr - \\ & \left. - i X_{\alpha 11}^{12}(\lambda R, \beta) \pi^{-1} sh \pi \beta \int_0^R \sum_{j=0}^2 (g_{j0} r^{j+\alpha-1}) K_{\beta}(\lambda r) dr \right\} = \\ = & \frac{1}{a^2} \left\{ \left[ X_{\alpha 11}^{11}(\lambda R, \beta) - X_{\alpha 11}^{12}(\lambda R, \beta) \right] \pi^{-1} sh \pi \beta \int_0^{\lambda R} \sum_{j=0}^2 \lambda^{-(2\alpha+j)} (g_{j0} r^{j+\alpha-1}) K_{\beta}(\lambda r) dr - \right. \\ & \left. - X_{\alpha 11}^{12}(\lambda R, \beta) \int_0^{\lambda R} \sum_{j=0}^2 \lambda^{-(2\alpha+j)} (g_{j0} r^{j+\alpha-1}) I_{\beta}(r) dr \right\}. \end{aligned}$$

$$\begin{aligned} \tilde{T}_{go}(\tau, \beta) = & e^{-(\beta^2 + \gamma^2)\tau} \left\langle \frac{1}{a^2} U_{\alpha, 11}^{11}(\lambda R) \pi^{-1} sh \pi \beta \lambda^{-\alpha} \sum_{j=0}^2 g_{j0} \frac{1}{\lambda^{j+\alpha}} \times \right. \\ & \times \left\{ \frac{2^{\beta-1} \Gamma(i\beta)}{j+\alpha-i\beta} (\lambda R)^{j+\alpha-i\beta} {}_1F_2 \left( \frac{j+\alpha-i\beta}{2}; 1-i\beta, \frac{j+\alpha-i\beta+2}{2}, \frac{(\lambda R)^2}{4} \right) + \right. \\ & \left. \frac{2^{-i\beta-1} \Gamma(-i\beta)}{j+\alpha+i\beta} (\lambda R)^{j+\alpha+i\beta} {}_1F_2 \left( \frac{j+\alpha+i\beta}{2}; 1+i\beta, \frac{j+\alpha+i\beta+2}{2}, \frac{(\lambda R)^2}{4} \right) \right\} - X_{\alpha 11}^{12}(\lambda R, \beta) \frac{\lambda^{-\alpha}}{a^2} \times \\ & \times \sum_{j=0}^2 g_{j0} \frac{1}{\lambda^{j+\alpha}} \left\{ \frac{1}{2^{i\beta} (j+\alpha+i\beta) \Gamma(1+i\beta)} (\lambda R)^{j+\alpha+i\beta} {}_1F_2 \left( \frac{j+\alpha+i\beta}{2}; 1+i\beta, \frac{j+\alpha+i\beta+2}{2}, \frac{(\lambda R)^2}{4} \right) \right\} \end{aligned}$$

$$F_2 \left( \frac{j + \alpha + i\beta}{2}, \frac{j + \alpha + i\beta + 2}{2}, 1 + i\beta; \frac{(\lambda R)^2}{4} \right) \left\{ \right\}.$$

Here  ${}_1F_2 \left( (a_1)_k; (b_1)_k, (b_2)_k; z \right) = \sum_{k=0}^{\infty} \frac{(a_1)_k}{(b_1)_k (b_2)_k} \frac{z^k}{k!}$  are generalized hypergeometric function,

where  $(a_1)_k = \frac{j + \alpha \pm i\beta}{2}$ ;  $(b_1)_k = \frac{j + \alpha \pm i\beta + 2}{2}$ ;  $(b_2)_k = 1 \pm i\beta$ ;  $z = \frac{(\lambda R)^2}{4}$  are Pochhammer's

polynomials [21]. Let's write these functions.

Let's write the first of these functions:

$$\begin{aligned} (a_1)_k &= \frac{j + \alpha - i\beta}{2}; (b_1)_k = 1 - i\beta; (b_2)_k = \frac{j + \alpha - i\beta + 2}{2}; z = \frac{(\lambda R)^2}{4}; \\ \Phi_1 &= {}_1F_2 \left( \frac{j + \alpha - i\beta}{2}; 1 - i\beta, \frac{j + \alpha - i\beta + 2}{2}, \frac{(\lambda R)^2}{4} \right) = 1 + \frac{\left( \frac{j + \alpha - i\beta}{2} \right) \frac{(\lambda R)^2}{4}}{(1 - i\beta) \left( \frac{j + \alpha - i\beta + 2}{2} \right) 1!} + \\ &+ \frac{\left( \frac{j + \alpha - i\beta}{2} \right) \left( \frac{j + \alpha - i\beta}{2} + 1 \right) \left( \frac{(\lambda R)^2}{4} \right)^2}{(1 - i\beta)(1 - i\beta + 1) \left( \frac{j + \alpha - i\beta + 2}{2} \right) \left( \frac{j + \alpha - i\beta + 2}{2} + 1 \right) 2!} + \\ &+ \frac{\left( \frac{j + \alpha - i\beta}{2} \right) \left( \frac{j + \alpha - i\beta}{2} + 1 \right) \left( \frac{j + \alpha - i\beta}{2} + 2 \right) \left( \frac{(\lambda R)^2}{4} \right)^3}{(1 - i\beta)(1 - i\beta + 1)(1 - i\beta + 2) \left( \frac{j + \alpha - i\beta + 2}{2} \right) \left( \frac{j + \alpha - i\beta + 2}{2} + 1 \right) \left( \frac{j + \alpha - i\beta + 2}{2} + 2 \right) 3!} + \dots \end{aligned}$$

The second function:

$$\begin{aligned} (a_1)_k &= \frac{j + \alpha + i\beta}{2}; (b_1)_k = 1 + i\beta; (b_2)_k = \frac{j + \alpha + i\beta + 2}{2}; z = \frac{(\lambda R)^2}{4}; \\ \Phi_2 &= {}_1F_2 \left( \frac{j + \alpha + i\beta}{2}; 1 + i\beta, \frac{j + \alpha + i\beta + 2}{2}, \frac{(\lambda R)^2}{4} \right) = 1 + \frac{\left( \frac{j + \alpha + i\beta}{2} \right) \frac{(\lambda R)^2}{4}}{(1 + i\beta) \left( \frac{j + \alpha + i\beta + 2}{2} \right) 1!} + \end{aligned}$$

$$\begin{aligned}
 & \left( \frac{j+\alpha+i\beta}{2} \right) \left( \frac{j+\alpha+i\beta}{2} + 1 \right) \left( \frac{(\lambda R)^2}{4} \right)^2 \\
 & + \frac{\left( \frac{j+\alpha+i\beta}{2} \right) \left( \frac{j+\alpha+i\beta}{2} + 1 \right) \left( \frac{j+\alpha+i\beta+2}{2} \right) \left( \frac{j+\alpha+i\beta+2}{2} + 1 \right) \left( \frac{(\lambda R)^2}{4} \right)^3}{(1+i\beta)(1+i\beta+1)(1+i\beta+2) \left( \frac{j+\alpha+i\beta+2}{2} \right) \left( \frac{j+\alpha+i\beta+2}{2} + 1 \right) \left( \frac{j+\alpha+i\beta+2}{2} + 2 \right) 3!} + \dots
 \end{aligned}$$

The third function [21]:

$$(a_1)_k = \frac{j+\alpha+i\beta}{2}; \quad (b_1)_k = \frac{j+\alpha+i\beta+2}{2}; \quad (b_2)_k = 1+i\beta; \quad z = \frac{(\lambda R)^2}{4};$$

$$\begin{aligned}
 \Phi_3 = {}_1F_2 \left( \frac{j+\alpha+i\beta}{2}; \frac{j+\alpha+i\beta+2}{2}, 1+i\beta; \frac{(\lambda R)^2}{4} \right) &= 1 + \frac{\left( \frac{j+\alpha+i\beta}{2} \right) \left( \frac{(\lambda R)^2}{4} \right)}{\left( \frac{j+\alpha+i\beta+2}{2} \right) (1+i\beta) 1!} + \\
 & + \frac{\left( \frac{j+\alpha+i\beta}{2} \right) \left( \frac{j+\alpha+i\beta}{2} + 1 \right) \left( \frac{(\lambda R)^2}{4} \right)^2}{\left( \frac{j+\alpha+i\beta+2}{2} \right) \left( \frac{j+\alpha+i\beta+2}{2} + 1 \right) (1+i\beta)(1+i\beta+1) \cdot 2!} + \\
 & + \frac{\left( \frac{j+\alpha+i\beta}{2} \right) \left( \frac{j+\alpha+i\beta}{2} + 1 \right) \left( \frac{j+\alpha+i\beta+2}{2} \right) \left( \frac{(\lambda R)^2}{4} \right)^3}{\left( \frac{j+\alpha+i\beta+2}{2} \right) \left( \frac{j+\alpha+i\beta+2}{2} + 1 \right) \left( \frac{j+\alpha+i\beta+2}{2} + 2 \right) (1+i\beta)(1+i\beta+1)(1+i\beta+2) \cdot 3!} + \dots
 \end{aligned}$$

Comparing the expressions for  $\Phi_2$  and  $\Phi_3$ , it is possible to see that  $\Phi_2 = \Phi_3$ . Let's consider the expressions of the first three coefficients of each of these generalized hypergeometric functions. Let's determine the real and imaginary parts in them. Let's consider the function:

$$\Phi_1 = {}_1F_2 \left( \frac{j+\alpha-i\beta}{2}; 1-i\beta; \frac{j+\alpha-i\beta+2}{2}, \frac{(\lambda R)^2}{4} \right) = {}_1F_2(a_1 + a_1^i; b_1 + b_1^i; b_2 + b_2^i) =$$

$$= 1 + A_1 + A_2 + A_3 \dots$$

Let's introduce the denotations:

$$(a_1)_k = \frac{j + \alpha - i\beta}{2}; (b_1)_k = 1 - i\beta; (b_2)_k = \frac{j + \alpha - i\beta + 2}{2}; z = \frac{(\lambda R)^2}{4};$$

$$a_1 = \frac{j + \alpha}{2}; a_1^i = -\frac{\beta}{2}; b_1 = 1; b_1^i = -\beta; b_2 = \frac{j + \alpha + 2}{2}; b_2^i = -\frac{\beta}{2}.$$

Here

$$A_1 = \frac{\frac{j + \alpha - i\beta}{2} \frac{(\lambda R)^2}{4}}{(1 - i\beta) \frac{j + \alpha - i\beta + 2}{2}} = A_{11} + A_{11}^i i,$$

where

$$A_{11} = \frac{\left\{ a_1 (b_1 b_2 - b_1^i b_2^i) + a_1^i (b_1 b_2^i + b_1^i b_2) \right\} \frac{(\lambda R)^2}{4}}{\left[ (b_1^2 + b_1^{i2}) (b_2^2 + b_2^{i2}) \right]},$$

$$A_{11}^i = \frac{\left\{ a_1^i (b_1 b_2 - b_1^i b_2^i) - a_1 (b_1 b_2^i + b_1^i b_2) \right\} \frac{(\lambda R)^2}{4}}{\left[ (b_1^2 + b_1^{i2}) (b_2^2 + b_2^{i2}) \right]};$$

$$A_2 = \frac{\left( \frac{j + \alpha - i\beta}{2} \right) \left( \frac{j + \alpha - i\beta}{2} + 1 \right) \left( \frac{(\lambda R)^2}{4} \right)^2}{(1 - i\beta) (1 - i\beta + 1) \left( \frac{j + \alpha - i\beta + 2}{2} \right) \left( \frac{j + \alpha - i\beta + 2}{2} + 1 \right) 2!} = A_{12} + A_{12}^i i =$$

$$= (A_{11} + A_{11}^i i) \left\langle \left[ (b_1 + 1)(b_2 + 1) - b_1^i b_2^i \right] a_1 + a_1^i \left[ (b_1 + 1)b_2^i + b_1^i (b_2 + 1) \right] \right\rangle +$$

$$+ \left\langle \left[ (b_1 + 1)(b_2 + 1) - b_1^i b_2^i \right] a_1^i - \left[ (b_1 + 1)b_2^i + b_1^i (b_2 + 1) \right] a_1 \right\rangle i \times$$

$$\times \frac{\frac{(\lambda R)^2}{4}}{\left[ \left( (b_1 + 1)^2 + b_1^{i2} \right) \left( (b_2 + 1)^2 + b_2^{i2} \right) \right] 2};$$

$$A_{12} = \frac{\left\{ \left[ (b_1 + 1)(b_2 + 1) - b_1' b_2' \right] a_1 + a_1' \left[ (b_1 + 1) b_2' + b_1' (b_2 + 1) \right] \right\} (\lambda R)^2}{\left[ \left( (b_1 + 1)^2 + b_1'^2 \right) \left( (b_2 + 1)^2 + b_2'^2 \right) \right] 2} \frac{1}{4},$$

$$A_{12}' = \frac{\left\{ \left[ (b_1 + 1)(b_2 + 1) - b_1' b_2' \right] a_1' - \left[ (b_1 + 1) b_2' + b_1' (b_2 + 1) \right] a_1 \right\} (\lambda R)^2}{\left[ \left( (b_1 + 1)^2 + b_1'^2 \right) \left( (b_2 + 1)^2 + b_2'^2 \right) \right] 2} \frac{1}{4};$$

$$(A_2 + A_2' i) = (A_{11} + A_{11}' i)(A_{12} + A_{12}' i) = (A_{11} A_{12} - A_{11}' A_{12}') + (A_{11}' A_{12} + A_{12}' A_{11}) i;$$

$$\begin{aligned} A_3 &= \frac{\left( \frac{j + \alpha - i\beta}{2} \right) \left( \frac{j + \alpha - i\beta}{2} + 1 \right) \left( \frac{j + \alpha - i\beta}{2} + 2 \right) \left( \frac{(\lambda R)^2}{4} \right)^3}{(1 - i\beta)(1 - i\beta + 1)(1 - i\beta + 2) \left( \frac{j + \alpha - i\beta + 2}{2} \right) \left( \frac{j + \alpha - i\beta + 2}{2} + 1 \right) \left( \frac{j + \alpha - i\beta + 2}{2} + 2 \right) 3!} + \dots = \\ &= A_1 A_2 (A_{13} + A_{13}' i) = A_1 A_2 \left\{ \left[ (b_1 + 2)(b_2 + 2) - b_1' b_2' \right] a_1 + a_1' \left[ (b_1 + 2) b_2' + b_1' (b_2 + 2) \right] \right\} + \\ &\quad + \left\{ \left[ (b_1 + 2)(b_2 + 2) - b_1' b_2' \right] a_1' - \left[ (b_1 + 2) b_2' + b_1' (b_2 + 2) \right] a_1 \right\} i \left\{ \frac{(\lambda R)^2}{4} \right\} \frac{1}{\left[ \left( (b_1 + 2)^2 + b_1'^2 \right) \left( (b_2 + 2)^2 + b_2'^2 \right) \right] 3!}. \end{aligned}$$

$$\begin{aligned} (A_3 + A_3' i) &= (A_{11} + A_{11}' i)(A_{12} + A_{12}' i)(A_{13} + A_{13}' i) = \\ &= \left[ (A_{11} A_{12} - A_{11}' A_{12}') A_{13} - (A_{11}' A_{12} + A_{12}' A_{11}) A_{13}' \right] + \left[ (A_{11} A_{12} - A_{11}' A_{12}') A_{13}' - (A_{11}' A_{12} + A_{12}' A_{11}) A_{13} \right] i. \end{aligned}$$

For the functions  $\Phi_2, \Phi_3$ , the representation of the coefficients  $A_1, A_2, A_3, \dots$  remain the same:

$$\Phi_2 = {}_1F_2 \left( \frac{j + \alpha + i\beta}{2}, 1 + i\beta, \frac{j + \alpha + i\beta + 2}{2}, \frac{(\lambda R)^2}{4} \right) = {}_1F_2 \left( a_1 + a_1' i; b_1 + b_1' i; b_2 + b_2' i, \frac{(\lambda R)^2}{4} \right) =$$

$$= 1 + (A_1 + A_1' i) + (A_2 + A_2' i) + (A_3 + A_3' i) + \dots,$$

$$a_1 = \frac{j + \alpha}{2}; a_1' = +\frac{\beta}{2}; b_1 = 1; b_1' = +\beta; b_2 = \frac{j + \alpha + 2}{2}; b_2' = +\frac{\beta}{2};$$

$$\Phi_3 = {}_1F_2 \left( \frac{j + \alpha + i\beta}{2}, \frac{j + \alpha + i\beta + 2}{2}, 1 + i\beta, \frac{(\lambda R)^2}{4} \right) = {}_1F_2 \left( a_1 + a_1' i; b_1 + b_1' i; b_2 + b_2' i \right),$$



$$a_1 = \frac{j + \alpha}{2}; a_1^i = \frac{\beta}{2}; b_1 = \frac{j + \alpha + 2}{2}; b_1^i = \frac{\beta}{2}; b_2 = 1; b_2^i = \beta.$$

Thus, recurrent relations are obtained for real and imaginary parts of generalized hypergeometric functions of complex arguments, which allows to determine the temperature distribution depending on the parameters of the structure of wood and other porous materials.

Let's determine the solution  $\tilde{T}_{wa}(\beta)$  caused by the drying agent  $\tilde{T}_{wa} = \frac{sh\pi b}{\pi\lambda^{2\alpha}} \int_0^\tau e^{-(\beta^2 + \gamma^2)(\tau-t)} T_a(t) dt$ .

$$\begin{aligned} \tilde{T}_{wa}(\tau) &= \int_0^\tau e^{-(\beta^2 + \gamma^2)(\tau-t)} \left[ \frac{sh\pi b}{\pi\lambda^{2\alpha}} \left( \alpha_0 + \sum_{n=1}^\infty \alpha_n \cos v_n^2 t \right) \right] dt = \\ &= e^{-(\beta^2 + \gamma^2)\tau} \frac{sh\pi b}{\pi\lambda^{2\alpha}} \left[ \frac{e^{(\beta^2 + \gamma^2)t}}{(\beta^2 + \gamma^2)^2} a_0 + \sum_{n=1}^\infty a_n \frac{e^{(\beta^2 + \gamma^2)t} \left[ (\beta^2 + \gamma^2) \cos v_n^2 t + v_n^2 \sin v_n^2 t \right]}{(\beta^2 + \gamma^2)^2 + (v_n^2)^2} \right] \Bigg|_0^\tau = \\ &= e^{-(\beta^2 + \gamma^2)\tau} \frac{sh\pi b}{\pi\lambda^{2\alpha}} \left[ \frac{e^{(\beta^2 + \gamma^2)\tau} - 1}{(\beta^2 + \gamma^2)^2} a_0 + \right. \\ &\quad \left. + \sum_{n=1}^\infty a_n \frac{e^{(\beta^2 + \gamma^2)\tau} \left[ (\beta^2 + \gamma^2) \cos v_n^2 \tau + v_n^2 \sin v_n^2 \tau \right] - (\beta^2 + \gamma^2)^2}{(\beta^2 + \gamma^2)^2 + (v_n^2)^2} \right] = \\ &= \frac{sh\pi b}{\pi\lambda^{2\alpha}} \left[ \frac{1 - e^{-(\beta^2 + \gamma^2)\tau}}{(\beta^2 + \gamma^2)^2} a_0 + \sum_{n=1}^\infty a_n \frac{\left[ (\beta^2 + \gamma^2) \cos v_n^2 \tau + v_n^2 \sin v_n^2 \tau \right] - e^{-(\beta^2 + \gamma^2)\tau} (\beta^2 + \gamma^2)^2}{(\beta^2 + \gamma^2)^2 + (v_n^2)^2} \right]. \quad (1.31) \end{aligned}$$

The solution of a Cauchy problem is the function:

$$\begin{aligned} \tilde{T}(\tau, \beta) &= e^{-(\beta^2 + \gamma^2)\tau} \tilde{g}(\beta) + \int_0^\tau e^{-(\beta^2 + \gamma^2)(\tau-t)} \left[ \frac{sh\pi b}{\pi\lambda^{2\alpha}} \left( \alpha_0 + \sum_{n=1}^\infty \alpha_n \cos v_n^2 t \right) \right] dt = \\ &= e^{-(\beta^2 + \gamma^2)\tau} \tilde{g}(\beta) + \tilde{T}_{wa}(\tau) = e^{-(\beta^2 + \gamma^2)\tau} \left\langle \frac{1}{a^2} U_{\alpha, 11}^{11}(\lambda R) \pi^{-1} sh\pi \beta \lambda^{-(2\alpha+i)} \sum_{j=0}^2 g_{j0} \times \right. \\ &\quad \left. \times \left\{ \frac{2^{i\beta-1} \Gamma(i\beta)}{j + \alpha - i\beta} (\lambda R)^{j + \alpha - i\beta} {}_1F_2 \left( \frac{j + \alpha - i\beta}{2}; 1 - i\beta, \frac{j + \alpha - i\beta + 2}{2}; \frac{(\lambda R)^2}{4} \right) \right\} + \right. \end{aligned}$$

$$\begin{aligned}
 & + \frac{2^{-i\beta-1}\Gamma(-i\beta)}{j+\alpha+i\beta}(\lambda R)^{j+\alpha+i\beta} {}_1F_2\left(\frac{j+\alpha+i\beta}{2}; 1+i\beta, \frac{j+\alpha+i\beta+2}{2}; \frac{(\lambda R)^2}{4}\right) \Bigg\} - \\
 & - X_{\alpha 11}^{12}(\lambda R, \beta) \frac{1}{a^2} \lambda^{(j+2\alpha)} \sum_{j=0}^2 g_{j0} \left\{ \frac{(\lambda R)^{j+\alpha+i\beta}}{2^{i\beta} (j+\alpha+i\beta) \Gamma(1+i\beta)} \times \right. \\
 & \times {}_1F_2\left(\frac{j+\alpha+i\beta}{2}; \frac{j+\alpha+i\beta+2}{2}, 1+i\beta; \frac{(\lambda R)^2}{4}\right) \Bigg\} + \\
 & + \frac{sh\pi b}{\pi \lambda^{2\alpha}} \left[ \frac{1 - e^{-(\beta^2 + \gamma^2)\tau}}{(\beta^2 + \gamma^2)} a_0 + \sum_{n=1}^{\infty} a_n \frac{\left[ (\beta^2 + \gamma^2) \cos v_n^2 t + v_n^2 \sin v_n^2 t \right] - e^{-(\beta^2 + \gamma^2)\tau} (\beta^2 + \gamma^2)}{(\beta^2 + \gamma^2)^2 + (v_n^2)^2} \right]. \quad (1.32)
 \end{aligned}$$

Let's apply to the function  $\tilde{T}(\tau, \beta)$  the integral operator  $H_{\alpha}^{-1}(\tau, \beta)$ .

For non-stationary case:

$$\begin{aligned}
 & \int_0^{\infty} e^{-(\beta^2 + \gamma^2)t} \frac{sh\pi b V_{\alpha}(r, \beta) \Omega(r, \beta) d\beta}{\pi \lambda^{2\alpha}} g_R = \frac{I_{q, \alpha}(\lambda r)}{U_{q, \alpha}^{11}(\lambda R)} g_R(t), \\
 & \int_0^{\infty} e^{-(\beta^2 + \gamma^2)t} V_{\alpha}(r, \beta) V_{\alpha}(\rho, \beta) \Omega(r, \beta) d\beta = \varepsilon(r, \rho, q) = \\
 & = \frac{\lambda^{2\alpha}}{U_{q, \alpha, 11}^{11}(\lambda R)} \left\{ I_{q, \alpha}(\lambda r) \psi_{q, \alpha, 11}^{1*}(\lambda R, \lambda \rho) \quad 0 < \rho < r < R, \right. \\
 & \left. I_{q, \alpha}(\lambda \rho) \psi_{q, \alpha, 11}^{1*}(\lambda R, \lambda r) \quad 0 < \rho < r < R. \right.
 \end{aligned}$$

**Numerical analysis.** Based on the obtained formulas for determining the temperature at any point of the radius of wooden cylindrical beam at any time of drying depending on the effect of thermal diffusion, initial values of temperature and moisture, thermophysical characteristics of the material and parameters of the drying agent on the temperature of phase transitions, a software program is designed, the work of which is demonstrated for solving a specific application problem of wood drying.

To implement the numerical experiment, the characteristics of the thermophysical properties of wood were used. The dependence of the hydro conductivity of wood on temperature and moisture was derived on the basis of experimental data [6].

Numerical simulation of drying of a sample of a cylindrical pine timber beam of a circular cross-section of the temperature  $T_0$  with a 50 % moisture content was carried out. The following

basic parameters of the problem were accepted: ambient temperature  $T_a$ , which is determined by the temperature of the steam-air mixture measured by a dry bulb thermometer. The drying process lasted until the temperature of the beam reached the ambient temperature  $T_1 = 289$  K. Drying agent velocity  $v = 2$  m/s; saturated vapor density  $\rho_v = 0.013188$  kg/m<sup>3</sup>; air density  $\rho_{a0} = 1.29$  kg/m<sup>3</sup>. Physical parameters of wood: the radius of cross-section of a beam  $R = 0.25$  m; density  $500$  kg/m<sup>3</sup>; moisture  $0.7$  kg/kg; porosity  $\Pi = 0.672$ . Thermal parameters of wood: initial temperature  $T_0 = 290$  K, thermal conductivity coefficient  $\lambda = 0.14$  W/(m·K).

Computer simulation of the drying of a cylindrical beam was carried out for soft ( $\approx 300$  K) and hard regimes ( $\approx 370$  K), which were determined by the control functions of temperature and moisture of the steam-air mixture, which is fed into the drying chamber.

In **Fig. 1.3** and **1.4**, the temperature distributions in the structural elements of the cylindrical beam are presented. **Fig. 1.3** characterizes the change in temperature in the wooden beam during drying at  $300$  K; and so, does **Fig. 1.4** at  $370$  K, respectively.

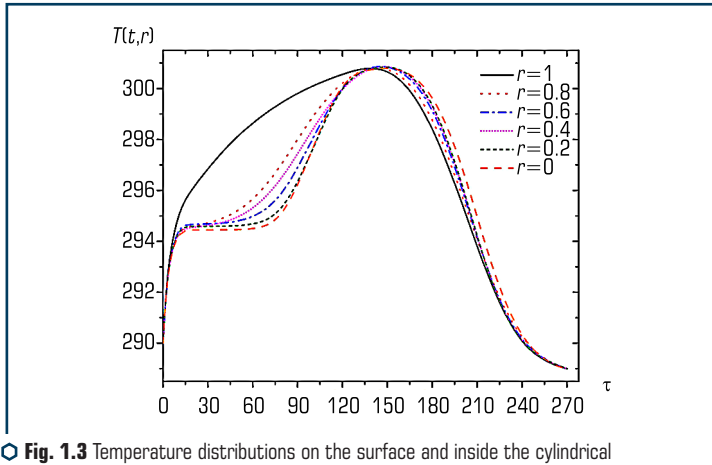


Fig. 1.3 Temperature distributions on the surface and inside the cylindrical beam at a drying agent temperature of  $302$  K (soft regime)

Here, the curve 1 corresponds to a unit value of dimensionless radius  $\bar{r} = 1$ , i.e., it shows the temperature on the surface of the cylinder; curve 2:  $\bar{r} = 0.8$ ; curve 3:  $\bar{r} = 0.6$ ; curve 4:  $\bar{r} = 0.4$ ; curve 5:  $\bar{r} = 0.2$ ; curve 6 corresponds to zero value of dimensionless radius:  $\bar{r} = 0$ .

Analyzing the graphical dependences, it is possible to see that in the process of drying cylindrical wood with the specified initial parameters, three characteristic stages are observed: heating, stabilization, and cooling.

The graphical analysis of the drying process for wood with a circular cross-section ( $\rho = 500$  kg/m<sup>3</sup>) and an initial moisture content  $0.7$  kg/kg reveals several key insights for both hard and soft

drying regimes. Throughout the entire drying process, the temperature of the wood's surface layer is consistently higher than that of the inner layers for both drying regimes. By the end of the first drying period, the surface layer reaches a maximum temperature. The inner layers experience different heating patterns: in the hard drying regime, they experience more rapid temperature increases, indicating quicker heat penetration and more aggressive moisture removal leading to faster vaporization within the wood. In contrast, for the soft drying regime, the bulk of the wood remains within the 294–295 K range for a significant portion of the first period, only beginning to increase in temperature two-thirds of the way through this period. During the second drying period, the temperature growth stabilizes across the layers, attributed to the absorption of heat for internal vaporization. The onset of the constant drying rate period varies with depth, showing significant delays in the wood's inner layers. For hard drying regimes, maximum temperatures are achieved mid-way through this period, followed by a gradual decline. During the period of decreasing drying rate, a noticeable temperature rise occurs throughout the entire material volume until the central layer's temperature matches the surface layer's temperature. This period is dominated by the release of bound moisture, which dictates the duration of the drying process.

It should be noted that the temperature distributions in the cross-sectional layers of wood for the two considered drying regimes differ qualitatively and quantitatively. The temperature of the outer layer of the cylindrical beam during the entire drying period is much higher than the temperature of the middle layers, and, here, the maximum residual pressure is maintained until the end of  $\tau_1$ . A temperature gradient appears, which causes the flow of moisture to move towards low temperatures, and its place is filled by steam.

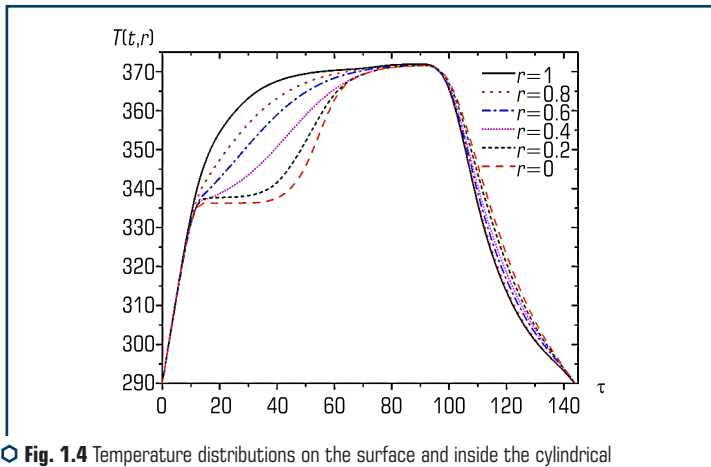


Fig. 1.4 Temperature distributions on the surface and inside the cylindrical beam at a drying agent temperature of 370 K (hard regime)

At hot drying modes during the second period of stabilization we observe a significant difference in the values of the temperature of wood layers in depth, sometimes up to 10 K (**Fig. 1.4**, measurement time  $0.5 \tau_2$ , layers  $\bar{r} = 0.2, 0.4, 0.6$ ). Just at this time it is possible to observe the maximum values of internal residual pressures in these layers. In mild regime, an increase in the temperature of the central part of the beam is observed at the time  $2/3 \tau_2$  and a corresponding decrease in moisture content in its core layers (**Fig. 1.3**, time curve  $0.7 \tau_2$ ). From the third period  $\tau_3$ , the rate of moisture removal decreases until the state of equilibrium moisture content.

In conclusion, the hard drying regime leads to a quicker internal temperature rise, suggesting faster drying but potentially greater risk of stress and cracking. The soft drying regime offers a gentler approach, with slower internal temperature increases, potentially reducing stress and maintaining structural integrity. This analysis underscores the importance of selecting an appropriate drying regime based on the desired balance between drying speed and material quality preservation.

## 1.2 SOLVING STEFAN'S LINEAR PROBLEM FOR DRYING CYLINDRICAL BEAM UNDER QUASI-AVERAGED FORMULATION

When solving the problem of drying objects with a capillary-porous structure, in particular wood, they usually are described in terms of a quasi-homogeneous medium [22–25] with effective coefficients, which are chosen so that the solution to the problem in a homogeneous medium would coincide with the solution of the problem in a porous medium. The effect of the porous structure is taken into account by introducing the effective coefficients of binary interaction into the Stefan-Maxwell equation. The problem of mutual distribution of phases is solved according to the principle of local equilibrium of phases [26–31]. The given properties of the material, namely: heat capacity, density, thermal conductivity coefficients are functions of material porosity, density and heat capacity of body components.

The plain problem of drying of a cylindrical timber beam in average statement is considered. The thermal diffusivity coefficients are expressed in terms of the porosity of the timber, the density of the components of vapor, air, and timber skeleton. The problem of mutual phase distribution during drying of timber has been solved using the energy balance equation. The indicators of the drying process of the material depend on the correct choice and observance of the parameters of the drying medium [32].

In stationary mode, the relationship between temperature and moisture gradients is determined by the formula:

$$\frac{\partial U}{\partial r} + \frac{\beta}{a} U = \frac{\delta \partial T}{\partial r} - \frac{\beta}{a} U_p,$$

where  $\delta$  is the thermogradient coefficient;  $\beta$  is the mass transfer coefficient;  $a$  is the thermal diffusivity coefficient. In this dependence, the rate of moisture transfer is affected by the rate of

heat transfer and by the equilibrium moisture content  $U_p$  [19]. The relationship between the distribution of moisture content and temperature fields depends on the geometric dimensions of the timber material in length and radius. Since the length of the beam of material is much larger than the cross-sectional size and the coefficient of moisture conductivity is much larger along the fibers than this coefficient across the fibers and due to the great complexity of the structure of timber material, consider the plane average problem of heat conduction.

When the hot air of the drying agent contacts with the moisture of the dried material, the moisture particles disintegrate and multiply, turning into steam and rarefied moisture particles, the number of which increases [7]. Thus, there is a multiplying of particles of a two-phase zone. At the same time there occurs a gradual deepening of the front of moisture evaporation. Heat is supplied to the evaporation front by heat conduction from the drying agent across the dried layer of material. Excess pressure is formed in the front zone, under the action of which the vapor is filtered to the outer surface. The total rate of moisture removal depends on the thermal and filtration resistance. The vapor pressure and the temperature at the front are related as parameters of saturated vapor. The slow movement of the front into depth allows to consider the fields of temperature and excess pressure in the dried material to be quasi-stationary. The drying process with a variable phase transition boundary is described by the equation [19]:

$$\frac{\partial T}{\partial \tau} + \gamma^2 T = a^2 B_\alpha [T, r], \quad \gamma^2 = \frac{\gamma_1^2}{C_p}, \quad \alpha > 0, \quad (1.33)$$

where  $a^2 = \frac{\lambda}{[\Pi(C_v \rho_v + C_s \rho_s) + (1 - \Pi)C_s \rho_s]}$  is averaged thermal diffusivity coefficient.

Let's solve (1.33) under the initial condition:

$$T(\tau, r)|_{\tau=0} = g(r), \quad r \in (0, R), \quad (1.34)$$

and under the boundary conditions on  $r = 0$  and  $r = R$ , which express heat exchange in the cylinder and between the surface of the cylinder and the drying agent:

$$\lim_{r \rightarrow 0} \frac{\partial}{\partial r} (r^\alpha T) = 0, \quad \left( \alpha_{11}^1 \frac{\partial}{\partial r} + \beta_{11}^1 \right) T|_{r=R} = T_s(\tau). \quad (1.35)$$

The process of penetration of hot air, the rate of which is proportional to the concentration, leads to the problem of phase transition if  $\gamma^2 < 0$  (diffusion with decomposition), the indices of a series:

$$T(M, t) = \sum_{n=1}^{\infty} T_n e^{(\gamma^2 - a^2 \lambda_n) t} v_n(M),$$

obtained by expansion in terms of eigenvalues functions  $v_n(M)$ , are less than the indices of a series if not to take into account changes in temperature over time without a phase transition. In the case  $\gamma^2 > 0$  (penetration with multiplication), if at least one of the indices  $(\gamma^2 - a^2\lambda) > 0$ , then there is an increase by the exponential law. The value  $\gamma^2$  is a characteristics of the material (multiplication factor),  $\lambda$  significantly depends on the shape and size of the area (pores). If  $\lambda = \frac{\gamma^2}{a^2}$ ,

then the area where the phase transition occurs has critical dimensions. For a plane problem, the smallest value of  $\lambda$  corresponds to the eigenfunction, which has radial symmetry and is equal

to  $\lambda_1 = \frac{\mu_1^{(0)}}{R}$ ,  $\mu_1^{(0)} = 2.4048$  [19].

For the critical diameter, the formula  $d_{kp} = \frac{2\mu_1^{(0)}a}{\gamma} = \frac{4.80a}{\gamma}$  is obtained [29].

When solving the problem of drying objects with a capillary-porous structure, in particular wood, in order not to consider the porous body in all its complexity, it is described in terms of a quasi-homogeneous medium with effective coefficients, which are chosen so that the solution of the problem in a homogeneous medium coincides with the solution in a porous medium. The influence of the porous structure is taken into account by introducing the effective binary interaction coefficients into the Stefan-Maxwell equation. The problem of mutual phase distribution is solved using the principle of local phase equilibrium. It is possible to consider that the averaged properties of the material, namely: heat capacity  $C$ , density  $\rho$ , and thermal conductivity coefficients  $\lambda$  are functions of porosity of material, densities and heat capacities of body components.

**Problem statement.** Let's consider the problem of drying a wet long wooden beam of cylindrical cross section in a drying plant. In solving this problem, it is possible to neglect the discrete structure of the material at the molecular level and come to the equation of heat conduction:

$$\frac{\partial T}{\partial \tau}(\rho, \tau) = a\Delta T + \gamma^2 T, \gamma^2 > 0.$$

Here,  $a$  is the thermal diffusivity coefficient,  $\gamma$  is a variable equivalent to the presence of sources of diffusing substance in the pores,  $T$  is the body temperature. The higher the temperature is the higher the rate of drying. The temperature in the drying chamber is the temperature in the vapor-gas mixture, which is determined by a dry bulb thermometer. The temperature determined by a wet bulb thermometer is the temperature at the boundary of the phase transition, which moves inside the material. The difference between the readings of dry and wet bulb thermometers is used to determine the relative humidity. For successful air drying, a continuous flow of air throughout the beam must be ensured. In the drying chambers, unsaturated air is used as a drying agent. Successful operation of drying chambers is achieved by regulating the temperature and humidity at the right time [33–37].

The volume of the dried area is a function of time. In the this case, the body to be dried is a cylindrical beam, the outer surface of which  $F(r, \tau) = 0$  is described by the equation:

$$F(r, \tau) = r - 1 = 0, \tau = 0. \quad (1.36)$$

At the time moment  $\tau = 0$ , the temperature  $T_0(\tau)$  is applied to the outer surface of the cylinder and from this time the drying process begins, and at the interface of the phase transition the curve of separation of dry and wet zones is the temperature  $T_c(\tau)$  curve.

In the process of drying, this curve moves, forming a closed curve  $F_k(r, \tau) = 0$ , which is an isotherm  $T = T_c$ . In the zone where the drying has already taken place, the temperature is described by the equation of heat conduction and by boundary conditions, these boundary conditions can be written as:

– on the outer contour of the cylinder  $F_k(r, \tau) = 0$ :

$$T = T_c, \quad (1.37)$$

– and the following initial conditions:

$$T = T_0, F_0 = F_k, \tau = 0. \quad (1.38)$$

Let  $V(F_k, F_0)$  be the volume of the dried area at the time  $t$  per unit length of the beam in the direction of the axis  $Oz$ . Then, over a period of time  $\Delta t$ , the volume will increase by  $\Delta V(F_k, F_0)$ , and the amount of heat spent is:

$$\Delta Q = \rho_k c_k (T - T_c) \Delta V(F_k, F_0). \quad (1.39)$$

Determine this amount of heat through the flow on the surface  $F_k(r, \tau) = 0$ :

$$\Delta Q = -\lambda_k \int_{F_k=0} \frac{\partial T}{\partial n} ds \Delta t. \quad (1.40)$$

Passing in (1.40) to the limit at  $\Delta t \rightarrow 0$ , given (1.39), let's obtain:

$$\lambda_k \int_{F_k=0} \frac{\partial T}{\partial n} ds = -\rho_k c_k (T - T_c) \frac{dV(F_k, F_0)}{dt}, \quad (1.41)$$

$$V(F_k, F_0) = \int_{F_k=0}^{F_0=0} ds. \quad (1.42)$$



If to pass to the variables:

$$\eta = \frac{T - T_c}{T_0 - T_c}, \beta = \frac{\rho_k c_k a}{\lambda_k}, \vartheta = \frac{V}{R^2}, l = \frac{s}{R}, \sigma = \frac{s}{R^2}, \quad (1.43)$$

then dimensionless coefficients will satisfy the equation of heat conduction and the boundary conditions (1.37), (1.38):

$$\text{at } F_0 = 0,$$

$$\eta = 1;$$

$$\text{at } F_k = 0,$$

$$\eta = 0; \quad (1.44)$$

$$\eta = 1, \tau = 0. \quad (1.45)$$

Let's consider the equation of the Stefan's boundary change:

$$\beta \eta \frac{d\vartheta}{d\tau} = - \frac{\partial T}{\partial n} dl, \quad (1.46)$$

$$\vartheta(F_0, F_k) = \int_{F_k=0}^{F_0=0} \int d\sigma. \quad (1.47)$$

It is possible to note that at the beginning of the drying process:

$$F_k(x, y, \tau) = F_0(x, y), \varepsilon^*(t) = 0. \quad (1.48)$$

Over a short period of time, the contour of the boundary of the dried and wet zones will be as follows:

$$F_k(x, y, t) - F_0(x_1, y_1) = \varepsilon^*(t), \quad (1.49)$$

where  $\varepsilon^*(t)$  is the thickness of the layer of the dried area (1.49). From the symmetry of the problem it follows that the contours  $F_0, F_k$  are concentric circles, the equations of which in a dimensionless polar system are:

$$F_0 = r - 1 = 0, F_k(t) = r - 1 + \varepsilon(t) = 0, \varepsilon = \frac{\varepsilon^*}{R}. \quad (1.50)$$

With this  $\varepsilon(\tau) = 0$  for  $\tau = 0$ .

From (1.50) it follows that at the time of complete drying of the beam  $\varepsilon^*(t) = R$ , and, respectively,  $\varepsilon(\tau) = 1$ .

Write the equation of heat balance for the area bounded by the contours  $F_0, F_k(t)$ . In integral form, this equation can be written as:

$$\int_{F_k=0}^{F_0=0} \frac{\partial \eta}{\partial \tau} d\sigma = \int_{F_0} \frac{\partial \eta}{\partial n} dl - \int_{F_k} \frac{\partial \eta}{\partial n} dl, \quad (1.51)$$

where  $F_0, F_k$  are contours of cross-sections of surfaces  $F_0 = 0, F_k = 0$ , respectively.

If to take into account the boundary condition (1.46), it is possible to obtain:

$$\int_{F_k=0}^{F_0=0} \frac{\partial \eta}{\partial n} d\sigma = \int_{F_0} \frac{\partial \eta}{\partial n} dl + \beta \eta \frac{\partial \eta}{\partial \tau}. \quad (1.52)$$

Equation (1.52) is the main one, which takes into account the factor of the moving boundary.

Introduce the function  $\eta^*(r, \tau)$  so that it satisfies the initial and boundary conditions (1.45). This function will establish the relationship between the relative saturation and temperature in the cross section in time.

$$\eta^*(r, \tau) = \frac{r - 1 + \varepsilon(\tau)}{\varepsilon(\tau)}. \quad (1.53)$$

Let's take  $\eta^*(r, \tau)$  as an approximate solution, which at a certain value  $\varepsilon(\tau)$  must satisfy (1.51). There is a relationship between it and  $\varepsilon$ :

$$\frac{\partial \eta^*}{\partial \tau} = (1-r) \frac{1}{\varepsilon^2} \frac{d\varepsilon}{dt}, \quad \frac{\partial \eta^*}{\partial n} = \frac{\partial \eta^*}{\partial r} = \frac{1}{\varepsilon}, \quad (1.54)$$

$$\int_{F_0} \frac{\partial \eta^*}{\partial n} dl = \frac{2\pi}{\varepsilon}, \quad \int_{F_k=0}^{F_0=0} \frac{\partial \eta^*}{\partial n} d\sigma = \int_0^{2\pi} d\varphi \int_{1-\varepsilon}^1 \frac{1-r}{\varepsilon^2} \frac{d\varepsilon}{d\tau} r dr = \frac{\pi}{3} (3-2\eta) \frac{d\varepsilon}{d\tau}.$$

From (1.52) it is possible to obtain:

$$\varepsilon^2 + \varepsilon \frac{1-2\beta\eta^*}{2(3\beta\eta^*-1)} \frac{d\varepsilon}{d\tau} = \frac{3\beta\eta^*}{3\beta\eta^*-1}, \quad (1.55)$$

or

$$d\tau = \frac{1}{B}(\varepsilon^2 + A\varepsilon)d\varepsilon, \tau(0) = 0, \quad (1.56)$$

$$B = \frac{3\beta\eta^*}{3\beta\eta^* - 1}, A = \frac{1 - 2\beta\eta^*}{2(3\beta\eta^* - 1)}. \quad (1.57)$$

The solution of (1.56) is:

$$\tau = \frac{1}{B} \left( \frac{\varepsilon^3}{3} + A \frac{\varepsilon^2}{2} \right). \quad (1.58)$$

From (1.46) and (1.58), taking into account (1.47) and (1.50), it is possible to obtain the equation describing the change in the unit of length of the volume of the dried zone over time:  $V_d = \pi R^2 [1 - \varepsilon^2(\tau)]$  and, thus, now it is possible to calculate the relative moisture of the timber

beam during drying  $W = \frac{V - V_d}{V}$ . Simple formulae for approximation of the experimental data allow

to calculate the total duration of the drying process from the initial to the final moisture content of the material.

**Numerical experiment.** Based on the obtained solutions, the numerical simulation of drying of samples of timber circular beams of pine, spruce, and birch of the same size has been carried out. The material after preliminary natural drying had been brought to 15 % of moisture content. The following basic parameters of the problem have been accepted: the ambient temperature  $T_c = 313$  K; the velocity of the drying agent  $v = 2$  m/s; the saturated vapor density  $\rho_s = 0.013188$  kg/m<sup>3</sup>; the air density  $\rho_{a0} = 1.29$  kg/m<sup>3</sup>. Physical parameters of timber: the radius of a circular beam  $R = 0.07$  m; wood density: spruce 450 kg/m<sup>3</sup>, pine 500 kg/m<sup>3</sup>, birch 750 kg/m<sup>3</sup>; the porosity: pine  $\Pi = 0.672$ , spruce  $\Pi = 0.654$ , birch  $\Pi = 0.591$ . Thermal parameters of wood: the initial temperature  $T_0 = 293$  K, the thermal conductivity coefficient at moisture of 15 % across fibers: spruce  $\lambda = 0.11$  W/(m·K), pine  $\lambda = 0.14$  W/(m·K), birch  $\lambda = 0.14$  W/(m·K).

**Fig. 1.5** shows the changes in the thickness of the layer of the dried area  $\varepsilon$  in time of drying  $\tau$ .

In **Fig. 1.6**, the distributions of relative moisture of wood in time are presented.

The analysis of the relative moisture content for different species of wood: spruce, pine, and birch, during the drying process reveals distinct drying dynamics for each wood type.

It is possible to observe that the samples with greater porosity and lower density lose moisture faster (**Fig. 1.6**, curves 1, 2); the moisture from wood with less porosity is removed more slowly (**Fig. 1.6**, curve 3). The obtained results correspond to the experimental data given in the literature [38–40].

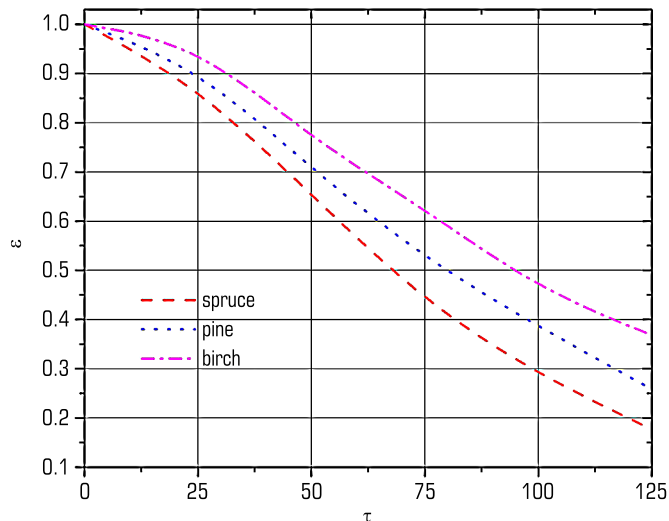


Fig. 1.5 The dependence of thickness of layer of the dried area on time of drying (curves 1–3 correspond to sort of materials: spruce, pine, birch, respectively)

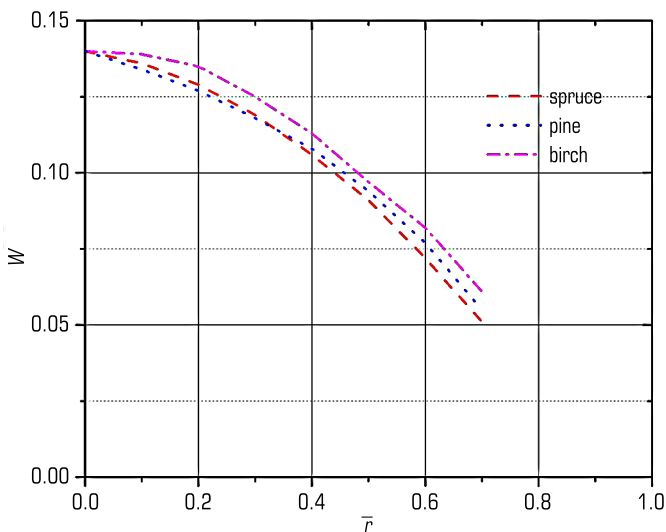


Fig. 1.6 Change in relative moisture of beam skeleton in time (curves 1–3 correspond to materials: spruce, pine, birch, respectively)

## CONCLUSIONS

The two problems of convective drying of wood of the circular cross-section in nonstationary and quasi-stationary formulations have been solved taking into account given properties of the material: heat capacity, density, thermal diffusivity coefficients, which are expressed as functions of the porosity of the material, densities, and heat capacities of the components.

In the first problem, a nonlinear mathematical model for forecasting the drying behavior of cylindrical beams of capillary-porous material under convective conditions is constructed, enabling more accurate control and optimization of the drying process in industrial applications. The governing equations for heat transfer are formulated, which are discretized using finite difference approximations for derivatives. The Kontorovich-Lebedev transform is used to simplify the complex differential equations that arise due to the cylindrical symmetry of the wood. Green's functions are employed to address the inhomogeneous differential equations representing the system's response to initial and boundary conditions. Analytical dependences are obtained for determining the temperature based on the thermophysical characteristics of the material and the parameters of the drying agent in non-isothermal conditions. The solution to Bessel equations involved Bessel functions of the first and the second kinds, which were computed using their series expansions as well as numerical libraries of special functions in Python. When approximating series solutions, Pochhammer's polynomials are utilized, making it easier to capture the behaviors of heat distribution in the wood profile. Steklov's theorem ensures that the series solutions used in the model are convergent and orthogonal. The resulting system of algebraic equations is solved iteratively to obtain the temperature distributions within the wood. Boundary conditions are applied to simulate real drying conditions, ensuring that the model accurately reflects the physical processes involved.

For the second problem about mutual phase distribution, the relationship is established between the drying time and the average parameters of porous cylindrical timber, in particular the relative saturation of moisture, the thermal conductivity of timber, which take into account the factor of movement of the transient boundary of the dried zone. It has been established that in the process of drying timber materials, the movable surface of the phase transition, which separates the dried and wet zones, depends on the properties of the material and temperature, which is a function of coordinates and time. The results are in good agreement with experimental data and results of other research.

The study bridges the gap between theoretical models and practical applications by providing a robust framework that accommodates the complex interactions involved in wood drying.

## REFERENCES

1. Burak, Ya. Y., Chaplia, Ye. Ya., Chernukha, O. Yu. (2006). *Kontynualno-termodynamichni modeli mekhaniky tverdykh rozchyniv*. Kyiv: Naukova dumka, 272.

2. Sokolovskyy, Y., Levkovych, M., Mysyk, M. (2023). Matrix Approach to Numerical Modeling of Heat-and-Moisture Transfer Processes in a Medium with a Fractal Structure. 2023 17th International Conference on the Experience of Designing and Application of CAD Systems (CADSM), 44–48. <https://doi.org/10.1109/cadsm58174.2023.10076519>
3. Lykov, A. V. (1968). *Teoriia sushki*. Moscow: Energiia, 472.
4. Hachkevych, O. R., Kushnir, R. M., Terletskii, R. F. (2022). Mathematical Problems of Thermomechanics for Deformable Bodies Subjected to Thermal Irradiation. *Ukrainian Mathematical Journal*, 73 (10), 1522–1536. <https://doi.org/10.1007/s11253-022-02011-7>
5. Kheifitc, L. I., Neimark, A. V. (1982). *Mnogofaznye protsessy v poristyykh sredakh*. Moscow: Khimiia, 320.
6. Pyanylo, Y. (2022). Analysis of Filtration Processes in Porous Environments Taking Into Account the Movement of Capillaries. 2022 12th International Conference on Advanced Computer Information Technologies (ACIT), 9–12. <https://doi.org/10.1109/acit54803.2022.9913087>
7. Gayvas, B., Markovych, B., Dmytruk, A., Havran, M., Dmytruk, V. (2024). The methods of optimization and regulation of the convective drying process of materials in drying installations. *Mathematical Modeling and Computing*, 11 (2), 546–554. <https://doi.org/10.23939/mmc2024.02.546>
8. Hayvas, B., Dmytruk, V., Torsky, A., Dmytruk, A. (2017). On methods of mathematical modeling of drying dispersed materials. *Mathematical Modeling and Computing*, 4 (2), 139–147. <https://doi.org/10.23939/mmc2017.02.139>
9. Baranovsky, S. V., Bomba, A. Ya. (2024). The diffusion scattering parameters identification for a modified model of viral infection in the conditions of logistic dynamics of immunological cells. *Mathematical Modeling and Computing*, 11 (1), 59–69. <https://doi.org/10.23939/mmc2024.01.059>
10. Mozhaev, A. P. (2001). Chaotic homogeneous porous media. 1. Theorems about structure. *Engineering-Physical Journal*, 74 (5), 196–201.
11. Lutcyk, P. P. (1988). *Issledovanie protsessov teplomassopere nosa pri sushke kapillarno-poristyykh tel s ucheto m vnutrennikh napriazhenii. Teplomassoobmen*. Minsk: Institut teplo- i massoobmena im. A. V. Lykova, 184–197.
12. Khoroshun, L. P., Maslov, B. P., Leshchenko, P. V. (1989). *Prognozirovanie effektivnykh svoystv pezoaktivnykh kompozitsionnykh materialov*. Kyiv: Naukova dumka, 208.
13. Burak, Y., Kondrat, V., Gayvas, B. (2002). On the mathematical modeling of drying processes of porous bodies. *Informational-Mathematical Modeling of Complex Systems*. Lviv: CMM IPPMM named after Y. S. Pidstryhach NAS of Ukraine, Akhil Publishing House, 153–159.
14. Dibagar, N., Kowalski, S. J., Chayjan, R. A., Figiel, A. (2020). Accelerated convective drying of sunflower seeds by high-power ultrasound: Experimental assessment and optimization approach. *Food and Bioproducts Processing*, 123, 42–59. <https://doi.org/10.1016/j.fbp.2020.05.014>

15. Shlikhting, G. (1974). *Teoriia pogranichnogo sloia*. Moscow: Nauka, 690.
16. Gayvas, B. I., Dmytruk, V. A., Semerak, M. M., Rymar, T. I. (2021). Solving Stefan's linear problem for drying cylindrical timber under quasi-averaged formulation. *Mathematical Modeling and Computing*, 8 (2), 150–156. <https://doi.org/10.23939/mmc2021.02.150>
17. Gayvas, B. I., Dmytruk, V. A. (2022). Investigation of drying the porous wood of a cylindrical shape. *Mathematical Modeling and Computing*, 9 (2), 399–415. <https://doi.org/10.23939/mmc2022.02.399>
18. Gayvas, B. I., Markovych, B. M., Dmytruk, A. A., Havran, M. V., Dmytruk, V. A. (2023). Numerical modeling of heat and mass transfer processes in a capillary-porous body during contact drying. *Mathematical Modeling and Computing*, 10 (2), 387–399. <https://doi.org/10.23939/mmc2023.02.387>
19. Gera, B., Kovalchuk, V., Dmytruk, V. (2022). Temperature field of metal structures of transport facilities with a thin protective coating. *Mathematical Modeling and Computing*, 9 (4), 950–958. <https://doi.org/10.23939/mmc2022.04.950>
20. Gayvas, B., Markovych, B., Dmytruk, A., Dmytruk, V., Kushka, B., Senkovych, O. (2023). Study of Contact Drying Granular Materials in Fluidized Bed Dryers. 2023 IEEE XXVIII International Seminar/Workshop on Direct and Inverse Problems of Electromagnetic and Acoustic Wave Theory (DIPED), 238–241. <https://doi.org/10.1109/diped59408.2023.10269464>
21. Alaa, K., Atounti, M., Zirhem, M. (2021). Image restoration and contrast enhancement based on a nonlinear reaction-diffusion mathematical model and divide & conquer technique. *Mathematical Modeling and Computing*, 8 (3), 549–559. <https://doi.org/10.23939/mmc2021.03.549>
22. Alaa, H., Alaa, N. E., Aqel, F., Lefraich, H. (2022). A new Lattice Boltzmann method for a Gray–Scott based model applied to image restoration and contrast enhancement. *Mathematical Modeling and Computing*, 9 (2), 187–202. <https://doi.org/10.23939/mmc2022.02.187>
23. Baala, Y., Agmour, I., Rachik, M. (2022). Optimal control of tritrophic reaction–diffusion system with a spatiotemporal model. *Mathematical Modeling and Computing*, 9 (3), 647–662. <https://doi.org/10.23939/mmc2022.03.647>
24. Bounkaicha, C., Allali, K., Tabit, Y., Danane, J. (2023). Global dynamic of spatio-temporal fractional order SEIR model. *Mathematical Modeling and Computing*, 10 (2), 299–310. <https://doi.org/10.23939/mmc2023.02.299>
25. Gouasnouane, O., Moussaid, N., Boujena, S., Kabli, K. (2022). A nonlinear fractional partial differential equation for image inpainting. *Mathematical Modeling and Computing*, 9 (3), 536–546. <https://doi.org/10.23939/mmc2022.03.536>
26. Najm, F., Yafia, R., Aziz Alaoui, M. A., Aghriche, A., Moussaoui, A. (2023). A survey on constructing Lyapunov functions for reaction-diffusion systems with delay and their application in biology. *Mathematical Modeling and Computing*, 10 (3), 965–975. <https://doi.org/10.23939/mmc2023.03.965>

27. Suganya, G., Senthamarai, R. (2022). Mathematical modeling and analysis of Phytoplankton–Zooplankton–Nanoparticle dynamics. *Mathematical Modeling and Computing*, 9 (2), 333–341. <https://doi.org/10.23939/mmc2022.02.333>
28. Ben-Loghfyry, A., Hakim, A. (2022). Time-fractional diffusion equation for signal and image smoothing. *Mathematical Modeling and Computing*, 9 (2), 351–364. <https://doi.org/10.23939/mmc2022.02.351>
29. Kostrobij, P. P., Markovych, B. M., Ryzha, I. A., Tokarchuk, M. V. (2021). Statistical theory of catalytic hydrogen oxidation processes. Basic equations. *Mathematical Modeling and Computing*, 8 (2), 267–281. <https://doi.org/10.23939/mmc2021.02.267>
30. Kostrobij, P. P., Ivashchysyn, F. O., Markovych, B. M., Tokarchuk, M. V. (2021). Microscopic theory of the influence of dipole superparamagnetics (Type  $\langle\beta\text{-CD(FeSO}_4\rangle\rangle$ ) on current flow in semiconductor layered structures (type gas, inse). *Mathematical Modeling and Computing*, 8 (1), 89–105. <https://doi.org/10.23939/mmc2021.01.089>
31. Aberqi, A., Elmassoudi, M., Hammoui, M. (2021). Discrete solution for the nonlinear parabolic equations with diffusion terms in Museilak-spaces. *Mathematical Modeling and Computing*, 8 (4), 584–600. <https://doi.org/10.23939/mmc2021.04.584>
32. Bazirha, Z., Azrar, L. (2024). DDFV scheme for nonlinear parabolic reaction-diffusion problems on general meshes. *Mathematical Modeling and Computing*, 11 (1), 96–108. <https://doi.org/10.23939/mmc2024.01.096>
33. Baranovsky, S., Bomba, A., Lyashko, S., Pryshchepa, O. (2024). Diffusion Perturbations in Models of the Dynamics of Infectious Diseases Taking into Account the Concentrated Effects. *Computational Methods and Mathematical Modeling in Cyberphysics and Engineering Applications* 1, 273–303. <https://doi.org/10.1002/9781394284344.ch11>
34. El Hassani, A., Bettoui, B., Hattaf, K., Achtaich, N. (2024). Global dynamics of a diffusive SARS-CoV-2 model with antiviral treatment and fractional Laplacian operator. *Mathematical Modeling and Computing*, 11 (1), 319–332. <https://doi.org/10.23939/mmc2024.01.319>
35. Tokarchuk, M. V. (2023). Unification of kinetic and hydrodynamic approaches in the theory of dense gases and liquids far from equilibrium. *Mathematical Modeling and Computing*, 10 (2), 272–287. <https://doi.org/10.23939/mmc2023.02.272>
36. Belhachmi, Z., Mghazli, Z., Ouchtout, S. (2022). A coupled compressible two-phase flow with the biological dynamics modeling the anaerobic biodegradation process of waste in a landfill. *Mathematical Modeling and Computing*, 9 (3), 483–500. <https://doi.org/10.23939/mmc2022.03.483>
37. Pukach, P. Y., Chernukha, Y. A. (2024). Mathematical modeling of impurity diffusion process under given statistics of a point mass sources system. I. *Mathematical Modeling and Computing*, 11 (2), 385–393. <https://doi.org/10.23939/mmc2024.02.385>
38. Laham, M. F., Ibrahim, S. N. I. (2023). Penalty method for pricing American-style Asian option with jumps diffusion process. *Mathematical Modeling and Computing*, 10 (4), 1215–1221. <https://doi.org/10.23939/mmc2023.04.1215>



39. Dmytryshyn, L. I., Dmytryshyn, M. I., Olejnik, A. (2023). Model of money income diffusion in the European integration context. *Mathematical Modeling and Computing*, 10 (2), 583–592. <https://doi.org/10.23939/mmc2023.02.583>
40. Patil, J. V., Vaze, A. N., Sharma, L., Bachhav, A. (2021). Study of calcium profile in neuronal cells with respect to temperature and influx due to potential activity. *Mathematical Modeling and Computing*, 8 (2), 241–252. <https://doi.org/10.23939/mmc2021.02.241>

## CHAPTER 2

# DRYING PROCESS MODELS FOR A MULTI-COMPONENT SYSTEM OF CAPILLARY-POROUS STRUCTURE BASED ON THERMODYNAMIC RELATIONSHIPS OF MIXTURE THEORY

## ABSTRACT

In this Chapter, the main statements are formulated and fundamental thermodynamic relations for moisturized capillary-porous deformable systems are obtained when describing them using continuum representations. Possible methods of choosing the parameters of the local thermodynamic state of a solid deformable multi-component system are presented, being consistent with their choice of the liquid (gaseous) phase. A complete system of equations is constructed to describe the drying process of dense packing of capillary-porous materials, based on the approaches of the theory of the mixtures of porous and dense packing of disperse materials of multicomponent three-phase media.

There have been analysed the influence of the external heat flow, the initial volumetric moisture saturation on changes in temperature, volumetric moisture saturation, and air density in body pores in time by the example of conductive drying.

## KEYWORDS

Mathematical modeling, continuum thermodynamics, drying, moisture, diffusion, capillary-porous, multi-component system, phase.

Recently, increased interest among scientists and researchers burst out for developing new and improving existing mathematical models and analytical-numerical methods for studying heat and mass transfer and the stress-strain state of porous materials, taking into account the influence of filtration, diffusion, and other physical processes due to the environmental situation on the planet. Problems of drying belong to such energy-consuming processes requiring new sustainable solutions.

To most accurately reproduce the physical content of the heat and moisture transfer processes in drying and adequately treat input data, such models are predominantly constructed based on general approaches and methods of thermodynamics of nonequilibrium processes. Integrating principles from thermodynamics, heat and mass transfer, and porous media mechanics, the model

offers valuable insights and practical solutions for improving drying efficiency and effectiveness in various applications.

The application of heat and mass transfer models covers numerous engineering tasks, from agriculture and food processing to pharmaceuticals, construction, chemical engineering, environmental engineering, the energy sector, and the textile industry. These models are valuable for improving process efficiency, reducing energy consumption, and achieving sustainable development goals, making them reliable tools in modern engineering.

As a particular case of the heat and mass transfer model in an  $n$ -component, three-phase, deformable porous wet medium with phase transitions and chemical reactions, the mathematical model of drying capillary-porous bodies, examines the evolution of temperature, moisture content, pressure, kinematic characteristics of the process, and sensitivity to the influence of parameters and boundary conditions.

Mathematical models of drying of capillary-porous bodies are based on the laws of conservation of mass, momentum and energy, as well as known experimental dependencies, on the basis of which the equations of heat-mass-moisture transfer in the body are constructed. The ability to quantify the heat passing inside the body due to thermal conductivity is based on the Fourier hypothesis. At the same time, diffusion flows are taken into account on the basis of Fick's laws, filtration flows on the basis of Darcy's law.

Essential for advancing knowledge in science and engineering was a noticed similarity between heat and mass transfer processes and the universality of diffusion equations. By using common principles and mathematical descriptions, scientists and engineers develop more efficient and effective solutions for a wide range of applications.

Consider the results of state-of-the-art investigations in complex systems, which use models of heat and mass transfer.

B. Alaa et al. [1, 2] proposed a novel approach for image restoration and contrast enhancement using a nonlinear reaction-diffusion model. This model is based on the similarity of its behavior to a heat equation in low-gradient areas, while in high-gradient regions, diffusion is halted to preserve edges. The algorithm utilizes a divide-and-conquer technique coupled with a reaction-diffusion system. In [3], a new numerical approach is introduced using a Lattice Boltzmann method for a Gray-Scott based reaction-diffusion model aimed at image restoration and contrast enhancement. This method, traditionally used in fluid dynamics, effectively handles noisy images by comparing pixel motion to fluid motion.

V. Baala et al. [4] propose a new model of spatio-temporal dynamics concerning the tritrophic reaction-diffusion system, offering methodologies for managing optimal control of the system. G. Bounkaicha et al. [5] investigated spatio-temporal dynamics using a fractional order SEIR model, relevant for understanding drying processes. D. Gouasnouane et al. [6] developed a nonlinear fractional partial differential equation for image inpainting, applying nonlinear diffusive filters. M. Najm et al. [7] surveyed the construction of Lyapunov functions for reaction-diffusion systems with delay, providing stability analysis techniques necessary for drying process models. T. Suganya

and S. Senthamarai [8] formulated a diffusive phytoplankton – zooplankton – nanoparticle model with a density-dependent death rate of predators, constructed it, and analyzed its local stability. D. Ben-Loghfry and N. Hakim [9], based on a time-fractional diffusion equation, performed image and signal smoothing, offering an idea of using anomalous diffusion behaviors for modeling different phenomena of image processing.

A statistical description of catalytic hydrogen oxidation applied by Kostrobij [10] provides a comprehensive understanding of the complex interactions involved in catalytic reactions on metal surfaces, incorporating both the diffusion of reactants and the magnetic properties of the ions and atoms involved. A generalized Cattaneo-type diffusion equation in time fractional derivatives is obtained in [11] for electrons with a characteristic relaxation time, and a generalized model is proposed based on a statistical approach that accounts for the complexity of relaxation electromagnetic diffusion processes for electrons in layered nanostructures. T. Aberqi et al. [12] provided a discrete solution for nonlinear parabolic equations with diffusion terms. They proved the existence and uniqueness of a weak solution using an approximation approach combining internal approximation with the backward Euler scheme, and provided a priori error estimates for temporal semi-discretization. F. Bazirha and S. Azrar [13] developed a DDFV scheme for nonlinear parabolic reaction-diffusion problems on general meshes, applicable to complex geometries in capillary-porous structures. B. Gayvas et al. [14] addressed solving Stefan's linear problem for drying cylindrical timber, offering solutions for phase change problems in drying.

Important practical problems in medicine are proposed in [15, 16]. D. Baranovsky and T. Bomba identified diffusion scattering parameters for a modified model of viral infection [15]. M. El Hassani et al. examined the dynamics of a diffusive SARS-CoV-2 model using fractional Laplacian operators [16].

Consideration of a broader range of conditions and parameters that affect heat and mass transfer processes is realized in [17], where S. Tokarchuk has unified kinetic and hydrodynamic approaches in the theory of dense gases and liquids far from equilibrium, under arbitrary Knudsen number conditions. The collision integral of this equation includes the diffusion coefficient in velocity space. Insights into liquid and gas interactions are provided by L. Belhachmi et al. [18], who discussed coupled compressible two-phase flow.

E. Pukach and T. Chernukha [19] focused on impurity diffusion processes, essential for accurately describing mass transfer equations. O. Ogunmiloro et al. [20] focused on fractional order spatial models, highlighting computational analysis to ensure the existence and uniqueness of solutions, which is critical for the reliability of drying process models.

A. Dmytryshyn et al. [21] modeled the diffusion of money income, providing methodologies for solving this problem. D. Laham and H. Ibrahim [22] proposed a penalty approach for pricing the American-style Asian option under the Merton model, which is particularly relevant for today's global financial markets. By including jump-diffusion in the models, Laham's approach captures the skewness and kurtosis features of return distributions often observed in several assets.

S. Pradhan et al. [23] modeled mixed-traffic in urban areas, where advection equation captures the bulk movement of cars, while the advection-diffusion equation includes the effects of diffusion, providing a more detailed description of the motorbike flow. In [24], B. Gayvas et al. presented an approach to optimizing the convective drying process by leveraging empirical relationships and drying technology principles through improved accounting for thermal diffusion.

Models of capillary-porous materials require researchers to carefully study the effects on the transfer processes of capillary forces and diffusion processes, so let's proceed to the theory.

The drying process is characterized by changes in temperature, volume, and composition of the system. Let's assume that the change in composition is possible only due to the phase transformation of liquid into vapor and vapor into liquid, and is determined by the change in the density of the

components  $\rho_i = \lim_{\Delta V \rightarrow 0} \frac{\Delta m_i}{\Delta V}$ , ( $i = 0, L, v, a$ ). No chemical reactions are involved. Let  $S_i$  be the partial entropy;  $\varepsilon_{ij}$ ,  $\sigma_{ij}^0$  are the strain and stress tensors of the solid skeleton;  $P_i$  is the pressure tensor of the  $i$ -th component;  $T_i$  is the temperature;  $\rho_i$  is the density;  $\mu_i$  is the chemical potential. All the functions depend on the parameters  $\varepsilon_{ij}$ ,  $T_i$ ,  $\rho_i$ ,  $P_i$ , with  $\varepsilon_{ij} = 0$ ,  $T = T_0$ ,  $\rho = \rho_0$  in the initial state.

Let's elaborate on describing the densities of the porous (granular) medium  $\rho_i = \frac{M_i}{V}$ , where

$M_i$  is the mass of the system components,  $M = \sum_i M_i$ ,  $V = V_0 + V_H$ , and  $V_H$  is the volume of

the carrier (continuous phase)  $V_H = V_a + V_L + V_v$ .  $v_H = \frac{1}{\rho_a} + \frac{1}{\rho_L} + \frac{1}{\rho_v}$  is the specific volume of

the carrier phase. Let  $\Pi = \frac{V_H}{V_H + V_0}$  be the porosity of the medium and  $V_0$  the volume of the solid

phase. Also, let's introduce the true densities of the components  $\rho_i^0 = \frac{M_i}{V_i}$ . To derive the main

equations describing the transfer processes in a thick layer, the method of local volume averaging will be employed. According to this method, each point of the porous medium is mapped to the small volume  $V_i$ , bounded by the closed surface  $S$ . There are two types of parameter averaging in the main equations: averaging values of local volume and averaging phase values (true). The averaging volume

values  $\Phi$  for a phase  $i$  are defined as follows:  $\langle \Phi \rangle = \frac{1}{V} \int_{V_i} \Phi dV$ , and the averaging phase ones are

defined as  $\langle \Phi \rangle^i = \frac{1}{V_i} \int_{V_i} \Phi dV$ , where  $V_i$  is the volume occupied by the  $i$ -th phase. Assuming that the

carrier phase is a mixture of liquid and gas, with the latter being a homogeneous mixture of an ideal gas – air and vapor, the following is obtained:

$$\rho_a = \frac{M_a}{V} = \frac{M_a}{V_a} \frac{V_a}{V_H} \frac{V_H}{V_H + V_0}, \quad \rho_v = \frac{M_v}{V} = \frac{M_v}{V_v} \frac{V_v}{V_H} \frac{V_H}{V_H + V_0},$$

$$\rho_l = \frac{M_l}{V} = \frac{M_l}{V_l} \frac{V_l}{V_H} \frac{V_H}{V_H + V_0}, \quad V_H = V_l + V_g.$$

Let's introduce the volume saturation with liquid  $\alpha = \frac{V_l}{V_H}$ ,  $1 - \alpha = \frac{V_g}{V_H}$ , and considering that

$V_v = V_a = V_g$ , the expressions for the scaled densities in terms of the true  $\rho_i^0$  can be obtained in the following form [25]:

$$\rho_0 = (1 - \Pi)\rho_0^0 = \alpha_l\rho_0^0, \quad \rho_l = \Pi\alpha\rho_l^0 = \alpha_l\rho_l^0, \quad \rho_v = \Pi(1 - \alpha)\rho_v^0 = \alpha_v\rho_v^0,$$

$$\rho_a = \Pi(1 - \alpha)\rho_a^0 = \alpha_a\rho_a^0, \quad \rho_g = \rho_a + \rho_v = \Pi(1 - \alpha)(\rho_a^0 + \rho_v^0) = \alpha_g(\rho_a^0 + \rho_v^0).$$

During evaporation, the volume saturation  $\alpha$  changes. Assuming that drying loss is possible during the drying process, the volume of the skeleton decreases, with the positions of the skeleton particles in space undergoing change. The drying-up can be characterized by a changing volume concentration  $\Pi$ . At constant temperature and volume, the chemical potential  $\mu_\beta$  according to the formulas for internal energy  $du_\beta = T_\beta dS_\beta + \mu_\beta d\rho_\beta - P_\beta dV_\beta$  ( $\beta = a, v, l$ ),  $du_0 = TdS + \mu_0 d\rho_0 - \sigma_\beta d\epsilon_\beta$

and heat of phase transition, can be given in the form  $\mu_\beta \Big|_{T, V_\beta} = \frac{\partial u_\beta}{\partial \rho_\beta} - \frac{1}{2} \sum_{\gamma=1}^{\beta} r_{\beta\gamma} \frac{\partial \rho_{\beta\gamma}}{\partial \rho_\beta}$ , where  $\partial \rho_{\beta\gamma}$

is the change in density of a component  $\beta$  due to phase or chemical transformation of the component  $\gamma$ ,  $r_{\beta\gamma}$  being the specific heat of phase transition or chemical transformation of the component  $\gamma$

in the component  $\beta$ . The derivative  $\frac{\partial u_\beta}{\partial \rho_\beta}$  determines the change in the specific internal energy

caused by the change in the mass of the component  $\beta$  due to phase and chemical transformations. To express the free energy of an elementary volume, let the free energy components be averaged by phase. Moving from phase averaging to volume averaging, the ratio  $\langle f \rangle_v = \alpha_i \langle f \rangle_i$  is taken into account. Then the brackets denoting volume averaging are omitted. Provided that there is no deformation  $\epsilon_\beta$  and no change in volume  $V$ , the free energy function of the  $i$ -th phase can be expressed as follows:

$$F_i = \int_{T_0}^T \left( \frac{\partial F_i}{\partial T_i} \right)_{\rho, \epsilon=0} dT_i + \int_{\rho_{i0}}^{\rho_i} \left[ \frac{\partial u_i}{\partial \rho_i} - \frac{1}{2} \sum_{\gamma=1}^i r_{i\gamma} \frac{\partial \rho_{i\gamma}}{\partial \rho_i} \right] d\rho_i. \quad (2.1)$$

The free energy function of an elementary volume is of the form:

$$F^0 = \alpha_0 \int_{T_0}^T \left( \frac{\partial F_0}{\partial T_0} \right)_{\rho, \varepsilon=0} dT_0 + \alpha_i \sum_i \int_{T_0}^T \left( \frac{\partial F_i}{\partial T_i} \right)_{\rho, \varepsilon=0} dT_i + \sum_{\beta} \alpha_{\beta} \int_{\rho_{\beta 0}}^{\rho_{\beta}} \left[ \frac{\partial u_{\beta}}{\partial \rho_{\beta}} - \frac{1}{2} \sum_{\gamma=1}^{\rho_{\beta}} r_{\beta\gamma} \frac{\partial \rho_{\beta\gamma}}{\partial \rho_{\beta}} \right] d\rho_{\beta}.$$

Let's assume a single-phase model for heat transfer ( $T = T_i$ ,  $dT = dT_i$ ) and introduce the scaled heat capacity of wet material. To this end, the entropy dependence on the temperature at constant

volume and concentration is expressed in the form  $S_{\varepsilon_i, \rho_{\beta}} = \int_{T_0}^T \rho_0 [C_{ef} / T] dT$ . In expressions (2.1),

the derivatives  $\left( \frac{\partial F_i}{\partial T} \right)_{\rho, \varepsilon=0}$  are defined through the heat capacities of the  $G_i$  system components

in the isochoric process  $\rho_i G_i|_{\rho, \varepsilon} = T_i \left( \frac{dS_i}{dT_i} \right)_{\rho, \varepsilon} = -T_i \frac{d^2 F_i}{dT_i^2} \quad (i=0, L, v, a)$ , which follows that

$\left( \frac{\partial F_i}{\partial T} \right)_{\rho, \varepsilon} = - \int_{T_i}^T \frac{\rho_i G_i}{T_i} dT_i$ . The expression for the effective heat capacity in terms of the heat capa-

cities of the components is of the form:

$$C_{ef} = C_0 + \frac{\alpha_L \rho_L^0 G_L + \alpha_v \rho_v^0 G_v + \alpha_a \rho_a^0 G_a}{\rho_0} = C_0 + \frac{\rho_L G_L + \rho_v G_v + \rho_a G_a}{\rho_0}.$$

The explicit form of the functions  $S$ ,  $\sigma_{ij}$ ,  $\mu_i$  can be found by expanding the function  $F = F_0 + \sum_i F_i$

in a Taylor series in powers  $\varepsilon_{ij}$  through the first two invariants  $I_1 = \varepsilon_1 = \varepsilon_{kk}$ ,  $I_2 = \varepsilon_2 = \varepsilon_{ij}$  of this tensor ( $k = i = j = 1, 2, 3$ ) and by retaining terms  $F^0$  in the expansion no higher than the second order of smallness [26]. As in the previous paragraph, the effective stresses on the elementary site  $\sigma_{ij} = \sigma_{ij}^e (1 - \Pi) + \sigma_{ij}^H \Pi = \sigma_{ijc} + \sigma_{ijH}$ .

The application of surface forces  $\sigma_{ijH}$  leads to the movement of the load-bearing phase and system deformation. The determination of the stress tensor  $\sigma_{ijH}$  is related to solving the problem of the flow of a continuous phase in the system.

The volume-averaged free energy of elastic deformation can be determined by analogy with a continuous medium. Then the total free energy is expressed as follows [29]:

$$F(\varepsilon_{ij}, T, w) = 1/2 (K - 2/3G) \varepsilon_{kk}^2 + \\ + 1/3K \left[ \alpha_{\varepsilon 0} (T - T_0) + \sum_{\beta=0, L, v, a} \alpha_{\beta 0} (\rho_{\beta} - \rho_{\beta 0}) (2/3G + \lambda) - \alpha_{\rho} P_H \right] \varepsilon_{kk} +$$

$$+G\varepsilon_{ij}\varepsilon_{ij} + \sum_{\beta=0,L,V,a} \alpha_{\beta} \int_{\rho_{\beta 0}}^{\rho_{\beta w}} \left[ \frac{\partial u_{\beta}}{\partial \rho_{\beta}} - \frac{1}{2} \sum_{\gamma=1}^{\beta} r_{\beta\gamma} \frac{\partial \rho_{\beta\gamma}}{\partial \rho_{\beta}} \right] d\rho_{\beta} - \int_{T_0}^T dT \int_{T_0}^T \frac{\rho_0 G_{ef,w,\varepsilon}}{T} dT, \quad (2.2)$$

$$\text{where } \frac{\partial F}{\partial l_1} = -\frac{K}{3} \varepsilon_{kk}, \quad \frac{\partial F}{\partial l_2} = G = \frac{E}{2(1+\nu)}, \quad \frac{\partial^2 F}{\partial l_1^2} = (K - 2/3G) = \lambda = \frac{Ev}{(1+\nu)(1-2\nu)},$$

$$\text{with Poisson's ratio } \nu; \text{ Laham's ratio } \lambda, \text{ Young's modulus } E = \frac{(1+\nu)(1-2\nu)}{\nu} (K - 2/3G);$$

the bulk elasticity modulus  $K$ ; the shear modulus  $G$ ; the resultant change in the unit volume of the body in the absence of stresses  $\varepsilon$ ; the initial temperature  $T_0$ ; the current temperature  $T$ ; the pore pressure  $P$ ; the atmospheric pressure  $P_0$ ;  $P_H = P - P_0$ ; the linear thermal expansion coefficient  $\alpha_{TW}$ ; the linear shrinkage coefficient  $\beta_{TW}$ .

The relationship between the average stress tensor, which determines the contribution to the macrodeformation of a granular heterogeneous system under drying conditions, is given as follows:  $\sigma_{ij} = (\sigma_{ij}^f - P_H \delta^{ij})$ , where  $\sigma_{ij}^f$  is the effective stress tensor and is expressed by Hooke's law through the solid phase strain tensor as follows:

$$\sigma_{ij}^f = (1 - \Pi) \left\{ \lambda_i^{\sigma} \varepsilon_{mm} \delta^{ij} + 2\mu_i^{\sigma} \varepsilon_{ij}^0 + \nu_i^{\sigma} P \delta^{ij} - \nu_i^{\sigma} \left[ \lambda_0^{\sigma} + 2/3\mu_0^{\sigma} \right] \times \right. \\ \left. \times \left[ \alpha_{t0} (T - T_0) + \sum_{\beta=0,L,V,a} \alpha_{\beta 0} (\rho_{\beta} - \rho_{\beta 0}) \right] \delta^{ij} \right\}.$$

Here,  $\lambda_i^{\sigma}$ ,  $\mu_i^{\sigma}$ ,  $\nu_i^{\sigma}$  are the effective coefficients, the volume fraction of the skeleton in the system being  $1 - \Pi$ . As regards a capillary-porous elastic-plastic body,  $(1 - \Pi)\mu_i^{\sigma}(1 - \omega) = \mu(1 - \omega) = G$  is the effective strain shear modulus, with  $\omega = \omega(\varepsilon, T, \rho_i)$  as a function of relative shear in the plastic strain region determined from measurements of generalized strains

$$\varepsilon = \frac{\sqrt{2}}{2(1+\nu)} \left[ (\varepsilon_{ij} - \varepsilon_{ji})^2 + 6\varepsilon_{ij}^2 \right]^{0.5} \quad (i \neq j), \quad \nu \text{ as Poisson's ratio and generalized stresses for}$$

simple loading cases;  $(1 - \Pi)\lambda_i^{\sigma} = \lambda$  is the generalized Laham's constant. As far as a granular medium

$$\text{is concerned, } (1 - \Pi)\mu_i^{\sigma} = (1 - \Pi)\mu^{\sigma} \left( 1 + \frac{\mu^{\sigma}}{\mu_0^{\sigma}} \right)^{-1}; \quad (1 - \Pi)\lambda_i^{\sigma} = (1 - \Pi)\lambda^{\sigma} \left( 1 + 0 \left( \frac{\lambda^{\sigma}}{\lambda_0^{\sigma}}, \frac{\mu^{\sigma}}{\mu_0^{\sigma}} \right) \right)^{-1};$$

$(1 - \Pi)\lambda_i^{\sigma}$ ,  $(1 - \Pi)\mu_i^{\sigma}$  are the elastic moduli of the granular skeleton depend on the structure and bonds between the grains (the greater the porosity, the lower the elastic moduli, other parameters being equal). Here,  $\lambda_0^{\sigma}$ ,  $\mu_0^{\sigma}$  are Laham's constants of an elastic grain;



$(1-\Pi)(\lambda_f^\sigma + 2/3\mu_f^\sigma) = \lambda + 2/3\mu$ ,  $\mu = \frac{E}{2(1+\nu)}$ ,  $E$  is the effective Young's modulus. For a

granular medium, the effective coefficients of thermal expansion and shrinkage, expressed through the effective elastic moduli, are as follows:

$$\alpha_t = (1-\Pi)\nu_f^\sigma(\lambda_0^\sigma + 2/3\mu_0^\sigma)\alpha_{t0}; \quad \alpha_\beta = (1-\Pi)\nu_f^\sigma(\lambda_0^\sigma + 2/3\mu_0^\sigma)\alpha_{\beta0},$$

$$\nu_f^\sigma = \frac{\lambda^\sigma + 2/3\mu^\sigma}{(\lambda_0^\sigma + 2/3\mu_0^\sigma)} \left[ 1 + 0 \left( \frac{\lambda^\sigma}{\lambda_0^\sigma}, \frac{\mu^\sigma}{\mu_0^\sigma} \right) \right], \quad K = (1-\Pi)(\lambda^\sigma + 2/3\mu^\sigma),$$

are the elastic deformation coefficients averaged over the elementary volume. For a wet porous material, all these values are determined on the basis of experimental studies, and as practice shows, they are functions of moisture content and temperature. Based on the above, the expressions of entropy and chemical potential have the following form:

$$S = -\varepsilon_{ij}\varepsilon_{ij} \frac{\partial \mu}{\partial T} - \varepsilon_{kk}^2 \frac{\partial \lambda}{\partial T} + K\varepsilon_{kk} \frac{\partial}{\partial T} \left[ \alpha_t(T - T_0) + \sum_\beta \alpha_\beta(\rho_\beta - \rho_{\beta0}) \right] - \frac{\partial \alpha_1}{\partial T} \frac{P_1}{E_0} + \int_{T_0}^T \frac{\rho_0 C_{eff}}{T} dT, \quad (2.3)$$

$$\begin{aligned} \rho_0 \mu_\beta = & \varepsilon_{ij}\varepsilon_{ij} \frac{\partial \mu}{\partial \rho_\beta} + \varepsilon_{kk}^2 / 2 \frac{\partial \lambda}{\partial \rho_\beta} - K\varepsilon_{kk} \frac{\partial}{\partial \rho_\beta} \left[ \alpha_t(T - T_0) + \sum_\beta \alpha_\beta(\rho_\beta - \rho_{\beta0}) \right] - \\ & - \frac{\partial u_\beta}{\partial \rho_\beta} - \frac{1}{2} \sum_\gamma r_{\beta\gamma} \frac{\partial \rho_{\beta\gamma}}{\partial \rho_\beta} + E_0 \varepsilon_{kk} \frac{\partial (\alpha_1 P_1)}{\partial \rho_\beta}. \end{aligned} \quad (2.4)$$

## 2.1 ENTROPY BALANCE EQUATION

According to the basic principles of the thermodynamics of irreversible processes, the product of absolute temperature and entropy growth rate is equal to the sum of the products of fluxes and the corresponding thermodynamic forces. Then, the energy transfer equations can be expressed in the form [30]:

$$\rho \frac{\partial S}{\partial \tau} = \vec{\nabla} \cdot (\lambda_q \vec{\nabla} T) + \vec{\nabla} \cdot (\lambda_{t\beta} \vec{\nabla} \rho_\beta) + \vec{\nabla} \cdot (\lambda_{tp} \vec{\nabla} P) + \rho_\beta \mu_\beta \frac{\partial \rho_\beta}{\partial \tau} + \Pi_t. \quad (2.5)$$

Here,  $\lambda_q$ ,  $\lambda_{t\beta}$ ,  $\lambda_{tp}$  are the coefficients of heat transfer;  $\Pi_t$  is the part of entropy production

related to the redistribution of heat and mass in the body volume; the quantity of  $\rho_\beta \mu_\beta \frac{\partial \rho_\beta}{\partial \tau}$ , resulting from the part of entropy production due to evaporation.

For small changes in temperature, and mass content, at which the characteristics of the medium can be considered constant, equations (2.3), (2.4) have the form:

$$S = K\alpha_T \varepsilon_{kk} - \frac{\partial}{\partial T}(\alpha_T P_1) + \frac{\rho_0 C_{ef}}{T_0}(T - T_0);$$

$$\rho_0 \mu_\beta = -K\alpha_\beta \varepsilon_{kk} + \frac{\partial}{\partial \rho_\beta}(\alpha_T P_1) - \varepsilon_{\Phi\beta} r^*, \quad \varepsilon_{\Phi 0} = \varepsilon_{\Phi a} = 0, \quad (2.6)$$

where  $r^* = 1/2r_{lv}$ ,  $\varepsilon_{\Phi l} = \frac{\partial \rho_{lv}}{\partial \rho_l}$  is the degree of phase transition completeness;  $r^*$  is heat of the phase transition. In equations (2.6), it is assumed that  $\ln \frac{T}{T_0} = \ln \left( 1 + \frac{\theta}{T_0} \right) \approx \frac{T - T_0}{T_0}$ . Let's consider

$\alpha_T P_1 = P$ ,  $\lambda_{tp} = 0$ ,  $\lambda_{t\beta} = 0$ . The entropy balance equation in this case is expressed as follows:

$$T \frac{d}{d\tau} \left[ K\alpha_T \varepsilon_{kk} + \frac{\partial P}{\partial T} \varepsilon_{kk} + T \frac{\rho_0 C_{ef}}{T_0} \right] = \lambda_q \nabla^2 T - K\alpha_{l0} \varepsilon_{kk} \frac{d\rho_l}{d\tau} - K\alpha_{v0} \varepsilon_{kk} \frac{d\rho_v}{d\tau} - K\alpha_{a0} \varepsilon_{kk} \frac{d\rho_a}{d\tau} -$$

$$-K\alpha_{00} \varepsilon_{kk} \frac{d\rho_0}{d\tau} - \varepsilon_{kk} \frac{dP}{d\rho_l} \frac{d\rho_l}{d\tau} - \varepsilon_{kk} \frac{dP}{d\rho_v} \frac{d\rho_v}{d\tau} - \varepsilon_{kk} \frac{dP}{d\rho_a} \frac{d\rho_a}{d\tau} - \varepsilon_{\Phi} r \frac{d\rho_v}{d\tau} + I_g, \quad (2.7)$$

where  $\alpha_{i0}$  are the initial volume concentrations. Here, all the quantities included in equation (2.7) are averaged over a variable volume. Considering the formula for differentiating integrals over a

variable volume  $\frac{d}{dt} \int_{V_i} f_i dV = \int_{V_i} \frac{\partial f_i}{\partial t} dV + \int_{\Sigma} f_i V_{ni} dS$  and the expression of the effective heat capacity in

terms of components, as well as the fact that the first two terms are related to the deformability of the skeleton, the following is obtained (nonlinear terms above the second order of smallness are discarded):

$$T \frac{d}{d\tau} \left[ K\alpha_T \varepsilon_{kk} + \frac{\partial P}{\partial T} \varepsilon_{kk} + T \frac{\rho_0 C_{ef}}{T_0} \right] = \lambda_q \nabla^2 T - K\varepsilon_{kk} \left[ \alpha_{l0} \frac{d\rho_l}{d\tau} + \alpha_{v0} \frac{d\rho_v}{d\tau} + \alpha_{a0} \frac{d\rho_a}{d\tau} + \alpha_{00} \frac{d\rho_0}{d\tau} \right] -$$

$$- \varepsilon_{kk} \left[ \frac{dP}{d\rho_l} \frac{d\rho_l}{d\tau} + \frac{dP}{d\rho_v} \frac{d\rho_v}{d\tau} + \frac{dP}{d\rho_a} \frac{d\rho_a}{d\tau} \right] - \varepsilon_{\Phi} r \frac{d\rho_v}{d\tau} - J_L \left( C_L T + \frac{P}{\rho_L} \right) \Big|_{S_L} -$$

$$- (J_a C_{pa} + J_v C_{pv}) T \Big|_{S_g} - \sum_i (\lambda_i \nabla T) \Big|_{S_i} + (\lambda \nabla T_g - \lambda \nabla T_0) \Big|_{S_{g0}} +$$

$$+ (\lambda \nabla T_l - \lambda \nabla T_0) \Big|_{S_{l0}} + (\lambda \nabla T_g - \lambda \nabla T_l) \Big|_{S_{lg}} + (C_l - C_{pl}) J_L T - \frac{P}{\rho} J_L, \quad (2.8)$$

with the fluxes  $J_i = \rho_i v_i$  ( $i = l, v, a$ );  $J_e = \rho_l (v_l - D_{gl})$ ;  $D_{gl}$  is the velocity of the liquid and gas phases, provided that at the interface ( $gl$ ):  $v_a = D_{gl}$ ;  $J_e = \rho_v (v_v - D_{gl})$ .

In this case, the nonlinear entropy balance equation takes the form:

$$\begin{aligned} T \frac{d}{d\tau} \left[ \left( K\alpha_T + \frac{\partial P}{\partial T} \right) \varepsilon_{kk} + T \frac{\rho_0 C_{ef}}{T_0} + r_0 \rho_v \right] = \nabla \left[ \lambda_{ef} \nabla T - r_0 J_v - \right. \\ \left. - K \varepsilon_{kk} \left[ \alpha_{l0} \frac{d\rho_l}{d\tau} + \alpha_{v0} \frac{d\rho_v}{d\tau} + \alpha_{a0} \frac{d\rho_a}{d\tau} + \alpha_{00} \frac{d\rho_0}{d\tau} \right] - \varepsilon_{kk} \left[ \frac{dP}{d\rho_l} \frac{d\rho_l}{d\tau} + \frac{dP}{d\rho_v} \frac{d\rho_v}{d\tau} + \frac{dP}{d\rho_a} \frac{d\rho_a}{d\tau} \right] + \right. \\ \left. + (Q_{g0} - Q_{0g}) + (Q_{l0} - Q_{0l}) + (Q_{gl} - Q_{lg}) - T_0 \left( K\alpha_T + \frac{\partial P}{\partial T} \right) \frac{\partial \varepsilon_{kk}}{\partial \tau} \right]. \end{aligned} \quad (2.9)$$

Here  $Q_j$  is the intensity of heat exchange at the interface;  $r_0 = r + (C_l - C_{pv})T$ . The densities included in the heat transfer equation are scaled, not true.

## 2.2 CONVECTION-DIFFUSION EQUATION FOR MASS TRANSFER

Equation (2.9) includes the time derivatives of  $\rho_v$ ,  $\rho_a$ ,  $\rho_l$ , which follow from the mass balance equation of the  $k$ -th component [31]:

$$\frac{\partial \rho_k}{\partial \tau} + \vec{\nabla} J_k = \sum_{k \neq l} \rho_{kl}, \quad (k = l, v, a), \quad (2.10)$$

where  $J_k = \rho_k \vec{v}_k$ ,  $\vec{v}_k$  is the velocity of the  $k$ -th component of the carrier phase, with  $\rho_{kl}$  as the production capacity of the  $k$ -th component corresponding to the phase transition of the  $l$ -th component to the  $k$ -th. These equations can be written as follows:

$$\frac{\partial \rho_k}{\partial \tau} + \vec{\nabla} \cdot (D_{kT} \vec{\nabla} T + (D_{kP} \vec{\nabla} P) + (D_{kj} \vec{\nabla} \rho_j)) = \sum_{k \neq l} \rho_{kl}, \quad (k = l, v, a). \quad (2.11)$$

The heating of the material induces the filtration flow of liquid and gas. The liquid flow is caused by a gradient of liquid concentration in the pores  $\alpha$ , temperature  $T$ , and pressure of the vapor-air mixture  $P$ . The flows of steam and air are caused by the gradients of pressure and mass concentration of steam in the mixture. Assuming that the vapor-air mixture forms a homogeneous phase and the liquid is water, the velocity of the components satisfies Darcy's equation, the fluxes of the components of the carrier phase are presented as follows [31, 32]:

$$\vec{J}_l = -D_l (\Pi \rho_l^0 \vec{\nabla} \alpha + \rho_0 \delta \vec{\nabla} T) - \tilde{K} \frac{\rho_l^0}{\mu_l} K_l \vec{\nabla} (P - P_{cap} + \rho_l^0 g),$$

$$\bar{J}_v = -\tilde{K} \frac{\rho_v^0}{\mu_{e\Phi}} K_g \bar{\nabla} P - (1-\alpha) \Pi D_{e\Phi} \rho_g^0 \bar{\nabla} \frac{\rho_v^0}{\rho_g^0}, \quad (2.12)$$

$$\bar{J}_a = -\tilde{K} \frac{\rho_a^0}{\mu_{e\Phi}} K_g \bar{\nabla} P + (1-\alpha) \Pi D_{e\Phi} \rho_g^0 \bar{\nabla} \frac{\rho_v^0}{\rho_g^0}.$$

Here  $D_L, D_{e\Phi}, \tilde{K}, K_g, K_l, \mu_{e\Phi}, P_{cap}, g$  are the effective diffusion coefficients of liquid, gas, permeability, the relative permeability of gas and liquid, effective viscosity of the gas mixture, capillary pressure, acceleration of the earth's gravity;  $J_i$  are the flows of liquid, steam, and air;  $\delta$  is the

thermogradient coefficient;  $\tilde{K} = \frac{r^2}{1-\Pi}$ , with  $r$  as the characteristic radius of the pores in the

skeleton. The filtration coefficient  $\tilde{K}$  depends on the pore size in the sample and the characteristics of the pore space. As a rule, it is assumed that the relative permeability of a substance is proportional to the volume fraction of the substance in the pores [33, 34]:  $K_g = 1-\alpha, K_l = \alpha$ .

When a liquid phase is present in the pores, zones of entrapped air can occur. In those zones of the material where the air is entrapped, the velocities of liquid and gas are equal and the flows

of liquid and vapor are determined by the following relations  $J_{a2} = \frac{1-\alpha}{\alpha} \frac{\rho_a}{\rho_l} J_l, J_{v2} = \frac{\rho_a}{\rho_l} J_{a2}$ , with

the first relation  $J_l$  being satisfied [35].

Let the transition from the entrapped state to independent phase motion occur when the value  $\alpha$  decreases in a certain range of the two-phase zone  $\alpha_g \leq \alpha \leq \alpha_l$ , where  $\alpha_g, \alpha_l$  depend on the structure of the medium and are considered to be given. To describe the movement of phases in the entire region of moisture content change, the air and vapor flows are presented in the form  $J_i = f J_{i1} + (1-f) J_{i2}$ , ( $i = v, a$ ), with the continuous function  $f$ , along with its derivative, changing from 1 to 0 for  $\alpha_g \leq \alpha \leq \alpha_l$  and being equal to one for  $\alpha \leq \alpha_g$  and zero for  $\alpha \geq \alpha_l$ . Let it be expressed in the form:

$$f(\alpha) = 1 - \left[ \left( \frac{\alpha - \alpha_g}{\alpha_l - \alpha_g} \right) \sigma_0(\alpha - \alpha_g) - \left( \frac{\alpha - \alpha_l}{\alpha_l - \alpha_g} \right) \sigma_0(\alpha - \alpha_l) \right].$$

In this case, it is possible to study the behavior of the quantities in question at different ratios of flux rates. Summing the first and third equations of system (2.10), the equations of moisture and air transfer are obtained:

$$\frac{\partial}{\partial \tau} \Pi \left[ (\rho_l^0 - \rho_v^0) \alpha + \rho_v^0 \right] + \nabla J_m = 0, \quad J_m = J_l + J_v,$$

$$\frac{\partial}{\partial \tau} \left[ \Pi (1-\alpha) \rho_a^0 \right] + \nabla J_a = 0. \quad (2.13)$$

If the porosity is considered constant, then the unknowns in these equations are  $\alpha$  and  $\rho_a$ . Defining the fluxes of the component velocities as functions of the liquid volume fraction  $\alpha$ , pressure  $P$ , and mass fraction of vapor in the vapor-air mixture, the following equations will be satisfied:

$$v_{L1} = \left\{ -D_l \left( \frac{\nabla \alpha}{\alpha} + \frac{\rho_v^0 \delta}{\Pi \alpha \rho_l^0} \nabla T \right) - \frac{\tilde{K}}{\mu_l \Pi} \nabla P \right\},$$

$$v_{v1} = \left\{ -\frac{D_{ef}}{\rho_v^0 / \rho_g^0} \nabla (\rho_v^0 / \rho_g^0) - \frac{\tilde{K}}{\mu_{ef} \Pi} \nabla P \right\},$$

$$v_{a1} = \left\{ \frac{D_{ef}}{\rho_a^0 / \rho_g^0} \nabla (\rho_v^0 / \rho_g^0) - \frac{\tilde{K}}{\mu_{ef} \Pi} \nabla P \right\}.$$

With this representation of the fluxes, the problem of heat and mass transfer can be solved in a one-dimensional formulation. This is possible when the layer thickness is small compared with the length and width. With  $\alpha = 0$ , the first equation of system (2.13) becomes the equation for determining the density of unsaturated steam  $\rho_v^0$ . The value of  $D_l$  is determined as in [35]:

$$D_l(T, \alpha) = \begin{cases} \left[ D_{L0} + (D_{LL} - D_{L0}) \sin \frac{\pi \alpha}{2\alpha_a} \right] \left( \frac{T}{273} \right)^{20}, & \alpha \leq \alpha_a, \\ D_{LL} \left( \frac{T}{273} \right)^{20}, & \alpha > \alpha_a, \end{cases}$$

where  $D_{L0}$ ,  $D_{LL}$  are the diffusion coefficients of the liquid in the solid skeleton and in the liquid, respectively.

The effective viscosity coefficient of the vapor-air mixture is a function  $\alpha$ . Moreover,  $\mu_l = \mu_g$ , where  $\mu_g$  is the viscosity of the gas mixture for  $0 < \alpha < \alpha_g$ , after which  $\mu_{ef}$  increases from  $\mu_g$  to  $\mu_l$  for  $\alpha_g < \alpha < \alpha_L$  and remains constant if  $\alpha_L < \alpha < 1$ . The thermogradient coefficient is also a function  $\alpha$ :

$$\delta(\alpha) = \delta_0 \left[ 1 - 4(\alpha - 0.5)^2 \right].$$

In the state of entrapped gas, for  $\alpha > \alpha_L$ ,  $\mu_{ef}$  and the effective vapor diffusion coefficient  $D_{ef}$  are also a function  $\alpha$ , with  $D_{ef} = D_{max}$  for  $0 < \alpha < \alpha_g$  and decreasing to zero for  $\alpha_g < \alpha < \alpha_L$ . In the entrapped state, no vapor diffusion occurs in the material  $v_{v2} = v_{a2} = v_{12}$ .

The vapor-air mixture is considered an ideal gas. Pressure  $P_g = \left( \frac{\rho_v^0}{M_v} + \frac{\rho_a^0}{M_a} \right) RT$ . The density of

saturated vapor is a function of temperature and for water is approximated by the Filonenko formula (no hygroscopic state of the material is considered here)

$\rho_v^0 = 133 \frac{M_v}{RT} \exp\left(18.681 - \frac{4105}{T-35}\right)$  when  $\alpha > 0$ . If the deformation of a solid skeleton is

subject to Hooke's law, then linear relationships can be assumed for the fluid, which links overpressure, density, and temperature. The state equation for a fluid can be expressed as

$\frac{\rho_L^0}{\rho_{L0}^0} = 1 + \beta_{pl}(P_L - P_0) - \alpha_{TL}(T - T_0)$ . Therefore,  $P_{L1} = \frac{1}{\beta_{pl}} \left[ \frac{\rho_L^0 - \rho_{L0}^0}{\rho_{L0}^0} + \alpha_{TL}(T - T_0) \right]$  is the over-

pressure in the fluid. Here,  $\beta_{pl}$ ,  $\alpha_{TL}$  are the coefficients of volume and temperature expansion, respectively. The overpressure in the carrier phase is  $P = (1 - \alpha)P_g + \alpha P_L$ . The expression for  $P_L$  may include the capillary pressure, which depends on the surface tension.

### 2.3 COMPATIBILITY EQUATION

If the porosity  $\Pi$  changes during the drying process, it is necessary to have an equation to determine it. Thus, the elasticity relations for a solid skeleton are considered. By Hooke's law for a micro-volume of a solid skeleton:

$$\varepsilon_0^{kl} = \frac{1}{2\mu_0^\sigma} \left[ \sigma_0^{kl} - \frac{\lambda_0^\sigma}{3\lambda_0^\sigma + 2\mu_0^\sigma} \sigma_0^{mm} \delta^{kl} \right] + 1/3 \alpha_{T0} (T'/T^0 - 1) \delta^{kl}.$$

Let the expression be averaged by convolving it by the indices:

$$\langle \varepsilon_0^{kk} \rangle_0 = \frac{1}{2\mu_0^\sigma} \left[ \langle \sigma_0^{kk} \rangle \frac{1}{3\lambda_0^\sigma + 2\mu_0^\sigma} \right] + \alpha_{T0} (T'/T^0 - 1) = P_0 \frac{1}{3\lambda_0^\sigma + 2\mu_0^\sigma} + \alpha_{T0} \frac{T' - T^0}{T^0},$$

$$P_0 = 1/3 \langle \sigma_0^{kk} \rangle, \quad \langle \varepsilon_0^{kk} \rangle_{00} = P_0 \frac{1}{3\lambda_0^\sigma + 2\mu_0^\sigma}, \quad \langle \varepsilon_0^{kk} \rangle = \frac{1}{V_0} \int \varepsilon_0^{kk} dV.$$

The first invariant of the averaged strain tensor  $\langle \varepsilon_0^{kk} \rangle_0$  determines the change in the true

density  $\rho_0^0$ :  $\langle \varepsilon_0^{kk} \rangle_0 - \langle \varepsilon_0^{kk} \rangle_{00} = -\frac{\rho_0^0 - \rho_{00}^0}{\rho_{00}^0}$ . For the averaged quantities over the volume of the

solution  $\varepsilon_0^{kk}$  is obtained:

$$\varepsilon_0^{kk} - \varepsilon_{00}^{kk} = \frac{\rho_0 - \rho_{00}}{\rho_{00}}. \quad (2.14)$$

By Hooke's law for fictitious stresses:

$$P_1 - P_0 = \left[ \lambda_f^\sigma + 2 / 3 \mu_f^\sigma \right] \varepsilon_0^{kk} + v_f^\sigma P_1 - v_f^\sigma \left[ \lambda_f^\sigma + 2 / 3 \mu_f^\sigma \right] \alpha_T^0 \left( \frac{T}{T_0} - 1 \right), \quad (2.15)$$

$$P_1 = \frac{V_H}{V_H + V_0} (\alpha_l P_l + \alpha_g P_g). \quad (2.16)$$

Differentiating expression (2.15) by  $\tau$  and considering relation (2.14):

$$-\left[ \lambda_f^\sigma + 2 / 3 \mu_f^\sigma \right] \frac{1}{\rho_{00}} \frac{\partial \rho_0}{\partial \tau} - (1 - v_f^\sigma) \frac{\partial P_1}{\partial \tau} + \frac{\partial P_0}{\partial \tau} - v_f^\sigma \left[ \lambda_f^\sigma + 2 / 3 \mu_f^\sigma \right] \alpha_{T0} / T_0 \frac{\partial T}{\partial \tau} = 0. \quad (2.17)$$

By definition,  $\rho_0 = (1 - \Pi) \rho_0^0$ . Given that:

$$\begin{aligned} \frac{\partial P_{1g}}{\partial \tau} &= \left( \frac{1}{M_v} \frac{\partial \rho_v^0}{\partial \tau} + \frac{1}{M_g} \frac{\partial \rho_g^0}{\partial \tau} \right) RT + \left( \frac{\rho_v^0}{M_v} + \frac{\rho_g^0}{M_g} \right) R \frac{\partial T}{\partial \tau}, \\ \frac{\partial P_{1l}}{\partial \tau} &= \frac{1}{\beta_{p1}} \left( \frac{1}{\rho_{l0}^0} \frac{\partial \rho_l^0}{\partial \tau} + \frac{\alpha_{Tl}}{T_0} \frac{\partial T}{\partial \tau} \right), \\ \frac{\partial P_0}{\partial \tau} &= \frac{1}{\beta_{p0}} \left( \frac{1}{\rho_{00}^0} \frac{\partial \rho_0^0}{\partial \tau} + \frac{\alpha_{T0}}{T_0} \frac{\partial T}{\partial \tau} \right), \end{aligned} \quad (2.18)$$

and by substituting (2.18) into (2.17), the compatibility equation that relates the true densities to the porosity is obtained:

$$\begin{aligned} &-\left[ \lambda_f^\sigma + 2 / 3 \mu_f^\sigma \right] \frac{1}{\rho_{00} \beta_{p0}} \left[ \frac{\partial}{\partial \tau} (1 - \Pi) \rho_0^0 \right] \frac{\partial P}{\partial \tau} - (1 - v_f^\sigma) \left\{ \frac{\alpha}{\beta_{pl}} \left( \frac{1}{\rho_{l0}^0} \frac{\partial \rho_l^0}{\partial \tau} + \frac{\alpha_{Tl}}{T_0} \frac{\partial T}{\partial \tau} \right) + \right. \\ &+ (1 - \alpha) \left[ \left( \frac{1}{M_v} \frac{\partial \rho_v^0}{\partial \tau} + \frac{1}{M_g} \frac{\partial \rho_g^0}{\partial \tau} \right) RT + \left( \frac{\rho_v^0}{M_v} + \frac{\rho_g^0}{M_g} \right) R \frac{\partial T}{\partial \tau} \right] \left. \right\} + \\ &+ \frac{1}{\beta_{p0}} \left( \frac{1}{\rho_{00}^0} \frac{\partial \rho_0^0}{\partial \tau} + \frac{\alpha_{T0}}{T_0} \frac{\partial T}{\partial \tau} \right) = 0. \end{aligned} \quad (2.19)$$

## 2.4 MOMENTUM BALANCE EQUATION

To determine the deformations and average displacements in a solid skeleton, the momentum balance equation for a saturated porous medium is obtained in the form [27]:

$$\rho_1 \frac{d_1 \vec{v}_1}{d\tau} = -\vec{\nabla}(\Pi P) - \vec{R}_{10} + \rho_1 \vec{g}_1, \quad (2.20)$$

$$\rho_0 \frac{d_0 \vec{v}_0}{d\tau} = -\vec{\nabla}[(1-\Pi)P] + \vec{\nabla} \cdot \hat{\sigma}_f + \vec{R}_{10} + \rho_0 \vec{g}_0, \quad (2.21)$$

where  $\vec{v}_1 = \frac{\rho_L \vec{v}_L + \rho_v \vec{v}_v + \rho_a \vec{v}_a}{\rho_L + \rho_v + \rho_a}$ ;  $\vec{R}_{10}$  is an interfacial variable. By determining  $\vec{R}_{10}$  from equations (2.20) and substituting into (2.21):

$$\rho_0 \frac{d_0 \vec{v}_0}{d\tau} = -\vec{\nabla}P + \vec{\nabla} \cdot \hat{\sigma}_f - \rho_1 \frac{d_1 \vec{v}_1}{d\tau} + \rho_1 \vec{g}_1 + \rho_0 \vec{g}_0, \quad (2.22)$$

with

$$\vec{v}_1 = \frac{\rho_L^0 \left\{ -D_L \vec{\nabla} \alpha + \frac{\rho_0^0 \delta}{\Pi \rho_L^0} \vec{\nabla} T \right\} - \frac{\tilde{K}}{\Pi} \vec{\nabla} P \left\{ \frac{\alpha \rho_L^0}{\mu_L} + \frac{(1-\alpha)(\rho_v^0 + \rho_a^0)}{\mu_{ef}} \right\}}{\alpha \rho_L^0 + (1-\alpha)(\rho_v^0 + \rho_a^0)}, \quad (2.23)$$

$$\vec{v}_0 = \frac{\partial}{\partial \tau} \begin{Bmatrix} \vec{u}_1 \\ \vec{u}_2 \\ \vec{u}_3 \end{Bmatrix}, \quad \rho_1 = \Pi \left[ \alpha \rho_L + (1-\alpha)(\rho_v^0 + \rho_a^0) \right], \quad (2.24)$$

where  $\vec{u}_1, \vec{u}_2, \vec{u}_3$  is the displacement vector in the direction of the axes  $Ox_1, Ox_2, Ox_3$ .

To solve the system of equations (2.9), (2.13), (2.19), (2.22), it is necessary to set the single-valued conditions for heat and mass transfer, as well as the mechanical and initial conditions. The mechanical conditions at the boundary are given by the surface force vector  $\vec{f}$ , or the displacement vector  $\vec{h}$ , or the ratio between the vectors  $\vec{f}$  and  $\vec{h}$ . The condition  $\sigma_{ij} n_j = f_i$  reflects the equilibrium of the stresses and forces applied to the boundary distributed over the body volume. For the bearing medium at the boundary, the heat and mass flows of moisture and air are specified. Initial conditions are set at the initial temperature  $t = 0$ , liquid concentration  $\alpha$ , air concentration

$\rho_a = \rho_0 - \frac{\rho_{vs}(T_0)}{M_v} RT$ , and zero initial stresses. Besides, when setting the heat flux in the case of

contact drying,  $q_e = -\lambda \nabla T + r^* j_v + \rho_p C_p h \frac{\partial T}{\partial \tau}$ , where  $\rho_p, C_p$  are the specific density and heat



capacity of the sieve (the thin plate) on which the grain layer lies. In particular, for a multicomponent inhomogeneous linear viscoelastic body, the momentum balance equations are as follows [27]:

$$\rho \frac{\partial^2 u_i}{\partial \tau^2} = \left[ \mu(1-\omega) u_{i,j} \right]_{,j} + \left[ (\lambda + 2/3 \mu \omega) u_{j,i} \right]_{,i} + \left[ \mu(1-\omega) u_{j,i} \right]_{,j} - \left[ \alpha_T (T - T_0) + \sum_{\beta} \alpha_{\beta} (\rho_{\beta} - \rho_{\beta 0}) \right]_{,i} (\lambda + 2/3 \mu) - \Pi P_{,i} + X_i. \quad (2.25)$$

Here,  $u_i$  is the displacement, a comma marking the differentiation along the  $i$ -th coordinate.

## 2.5 THE KEY SYSTEM OF EQUATIONS

The obtained relations allow writing a complete system of equations for determining functions  $\Pi, \hat{N}, P, \alpha, \rho_v, \rho_a$  and  $u_i, \varepsilon_{ij}, \sigma_{ij}$  ( $i = 1, 2, 3$ ), namely the heat conduction equation:

$$\begin{aligned} T / T_0 \frac{d}{d\tau} \left[ \left( K \alpha_T + \frac{\partial P}{\partial T} \right) \varepsilon_{kk} + (1 - \Pi) \rho_0^0 C_{ef} T + r_0 \Pi (1 - \alpha) \rho_v^0 \right] = \\ = \nabla \left[ \lambda_{ef} \nabla T - r_0 J_v - (C_{pa} J_a + C_{pv} J_v + C_{pl} J_l) T - K \varepsilon_{kk} \left[ \Pi \alpha_L \frac{d(\Pi \alpha \rho_l^0)}{d\tau} + \right. \right. \\ \left. \left. + \Pi (1 - \alpha) \frac{d[(1 - \alpha)(\rho_v^0 + \rho_a^0)] \rho_v}{d\tau} + (1 - \Pi) \frac{d[(1 - \Pi)] \rho_0^0}{d\tau} \right] - \right. \\ \left. - \varepsilon_{kk} \left[ \frac{dP}{d\rho_l} \frac{d(\Pi \alpha \rho_l^0)}{d\tau} + \frac{dP}{d\rho_v} \frac{d[\Pi (1 - \alpha) \rho_v^0]}{d\tau} + \frac{dP}{d\rho_a} \frac{d[\Pi (1 - \alpha) \rho_a^0]}{d\tau} \right] - T_0 \left( K \alpha_T + \frac{\partial P}{\partial T} \right) \frac{\partial \varepsilon_{kk}}{\partial \tau} \right]; \quad (2.26) \end{aligned}$$

– the equation for the pressure:

$$(1 - \Pi) P_1 = \Pi (1 - \alpha) P_g + \Pi \alpha P_L, \quad (2.27)$$

$$P_g = \left( \frac{\rho_v^0}{M_v} + \frac{\rho_a^0}{M_a} \right) RT, \quad (2.28)$$

$$P_L = \frac{1}{\beta_{pl}} \left[ \frac{\rho_L^0 - \rho_{L0}^0}{\rho_{L0}^0} + \alpha_{TL} (T - T_0) \right], \quad (2.29)$$

where  $\alpha_{\text{TL}}$ ,  $\beta_{\text{PL}}$  are the coefficients of temperature and volume expansion of the liquid;  
 – the equation for the density of saturated vapor:

$$\rho_v^0 = 133 \frac{M_v}{RT} \exp\left(18.681 - \frac{4105}{T - 35}\right); \quad (2.30)$$

– the equation of mass balance:

$$\frac{\partial[(1-\Pi)]\rho_0^0}{\partial\tau} + \bar{\nabla}(\rho_0 v_0) = 0, \quad (2.31)$$

$$\alpha_l + \alpha_g = \Pi, \quad \Pi = \frac{V_H}{V_H + V_0}, \quad (2.32)$$

$$\frac{\partial[\Pi(1-\alpha)]\rho_a^0}{\partial\tau} + \bar{\nabla}J_a = 0, \quad (2.33)$$

$$\frac{\partial[\Pi(1-\alpha)]\rho_v^0}{\partial\tau} + \bar{\nabla}J_v = I_{\text{vl}}, \quad (2.34)$$

$$\frac{\partial[\Pi\alpha\rho_l^0]}{\partial\tau} + \bar{\nabla}J_l = -I_{\text{vl}}; \quad (2.35)$$

$$J_l = -D_l(\Pi\rho_l^0\nabla\alpha + \rho_0\delta\nabla T) - \tilde{K}\frac{\rho_l^0}{\mu_l}K_l\nabla P, \quad (2.36)$$

$$J_v = -\tilde{K}\frac{\rho_v^0}{\mu_{\text{v}\Phi}}K_g\nabla P - (1-\alpha)\Pi D_{\text{v}\Phi}\rho_g^0\nabla\frac{\rho_v^0}{\gamma_g}, \quad (2.37)$$

$$J_a = -\tilde{K}\frac{\rho_a^0}{\mu_{\text{a}\Phi}}K_g\nabla P + (1-\alpha)\Pi D_{\text{a}\Phi}\rho_g^0\nabla\frac{\rho_v^0}{\rho_g^0}. \quad (2.38)$$

Summing the mass balance equations for vapor and liquid, two equations for determining  $\rho_a^0$  and  $\alpha$  are obtained:

$$\frac{\partial}{\partial\tau}\Pi[(\rho_l^0 - \rho_v^0)\alpha + \rho_v^0] + \nabla J_m = 0, \quad J_m = J_l + J_v, \quad (2.39)$$

$$\frac{\partial}{\partial\tau}[\Pi(1-\alpha)\rho_a^0] + \nabla J_a = 0. \quad (2.40)$$

Invariants for the averaged values over the volume of the solution  $\varepsilon_0^{kk} - \varepsilon_{00}^{kk} = -\frac{\rho_0 - \rho_{00}}{\rho_{00}}$ .  
The equation of compatibility:

$$\begin{aligned} & -\left[\lambda_f^\sigma + 2/3\mu_f^\sigma\right] \frac{1}{\rho_{00}\beta_{\rho 0}} \left[ \frac{\partial}{\partial \tau} (1-\Pi) \rho_0^0 \right] - (1-\nu_f^\sigma) \left\{ \frac{\alpha}{\beta_{\rho l}} \left( \frac{1}{\rho_{l0}^0} \frac{\partial \rho_l^0}{\partial \tau} + \frac{\alpha_{\tau l}}{T_0} \frac{\partial T}{\partial \tau} \right) + \right. \\ & \left. + (1-\alpha) \left[ \left( \frac{1}{M_v} \frac{\partial \rho_v^0}{\partial \tau} + \frac{1}{M_s} \frac{\partial \rho_s^0}{\partial \tau} \right) RT + \left( \frac{\rho_v^0}{M_v} + \frac{\rho_s^0}{M_s} \right) R \frac{\partial T}{\partial \tau} \right] + \frac{1}{\beta_{\rho 0}} \left( \frac{1}{\rho_{00}^0} \frac{\partial \rho_0^0}{\partial \tau} + \frac{\alpha_{\tau 0}}{T_0} \frac{\partial T}{\partial \tau} \right) \right\} = 0. \end{aligned} \quad (2.41)$$

Momentum balance equation:

$$\rho_0 \frac{d_0 \bar{v}_0}{d\tau} = -\bar{\nabla} P + \bar{\nabla} \cdot \hat{\sigma}_f - \rho_1 \frac{d_1 \bar{v}_1}{d\tau} + \rho_l \bar{g}_1 + \rho_0 \bar{g}_0, \quad (2.42)$$

where

$$\bar{v}_1 = \frac{\rho_l^0 \left\{ -D_l \bar{\nabla} \alpha + \frac{\rho_0^0 \delta}{\Pi \rho_l^0} \bar{\nabla} T \right\} - \frac{K}{\Pi} \bar{\nabla} P \left\{ \frac{\alpha \rho_l^0}{\mu_l} + \frac{(1-\alpha)(\rho_v^0 + \rho_s^0)}{\mu_{ef}} \right\}}{\alpha \rho_l^0 + (1-\alpha)(\rho_v^0 + \rho_s^0)}, \quad (2.43)$$

$$\bar{v}_0 = \frac{\partial}{\partial \tau} \left\{ \begin{matrix} \bar{u}_1 \\ \bar{u}_2 \\ \bar{u}_3 \end{matrix} \right\}, \quad \rho_1 = \Pi \left[ \alpha \rho_l + (1-\alpha)(\rho_v^0 + \rho_s^0) \right], \quad (2.44)$$

$$\sigma_{ij} = \sigma_{ij}^f - P_H \delta^{ij}, \quad (2.45)$$

$$\begin{aligned} \sigma_{kl}^f &= (1-\Pi) \left\{ \lambda_f^\sigma \varepsilon_0^{mm} \delta^{kl} + 2\mu_f^\sigma \varepsilon_2^{kl} + \nu_f^\sigma P_1 \delta^{kl} - \right. \\ & \left. - \nu_f^\sigma \left[ \lambda_0^\sigma + 2/3\mu_0^\sigma \right] \left[ \alpha_{t0} (T - T_0) + \sum_{\beta} \alpha_{\beta 0} (\rho_{\beta} - \rho_{\beta 0}) \right] \delta^{ij} \right\}. \end{aligned} \quad (2.46)$$

The pressure difference between the carrier and solid phases due to strength:

$$P_1 - P_0 = \left( \lambda_f^\sigma + \frac{2}{3} \mu_f^\sigma \right) \varepsilon_2 + \nu_f^\sigma P_1 - \left[ \alpha_f (T - T_0) + \beta_f \sum_{\beta} (\rho_{\beta} - \rho_{\beta 0}) \right], \quad (2.47)$$

where  $\nu_f^\sigma$ ,  $\alpha_f$ ,  $\beta_f$  are the effective moduli of elasticity and expansion. Average velocities and strains:

$$v_0 = \frac{\partial \langle u_0 \rangle_0}{\partial t}, \quad \varepsilon_0^{kl} = 0.5 \left( \frac{\partial u_0^{kl}}{\partial x^k} + \frac{\partial u_0^{lk}}{\partial x^l} \right), \quad \varepsilon_0^{kl} = 0.5 \left( \frac{\partial \langle u_0^{kl} \rangle_0}{\partial x^k} + \frac{\partial \langle u_0^{lk} \rangle_0}{\partial x^l} \right), \quad (2.48)$$

$$\varepsilon_0^{kl} = \langle \varepsilon_0^{kl} \rangle_0 + \varepsilon_f^{kl},$$

$$\varepsilon_{kl}^f = -0.5 \left[ \langle u_0^{kl} \rangle_0 \frac{\nabla^k (1-\Pi)}{(1-\Pi)} + \langle u_0^{lk} \rangle_0 \frac{\nabla^l (1-\Pi)}{(1-\Pi)} \right] - \sum_j \frac{S_{0j}}{2(1-\Pi)} \langle u_0^{kl} u_0^{lk} + u_0^{lk} u_0^{kl} \rangle_{0j}, \quad (2.49)$$

where  $S_{0j}$  is the inner surface of the porous body.

## 2.6 NUMERICAL EXPERIMENT

Let's consider a thin plane plate, a surface of which from one side is subjected to the external heat flow  $q_e(t)$  (Fig. 2.1).

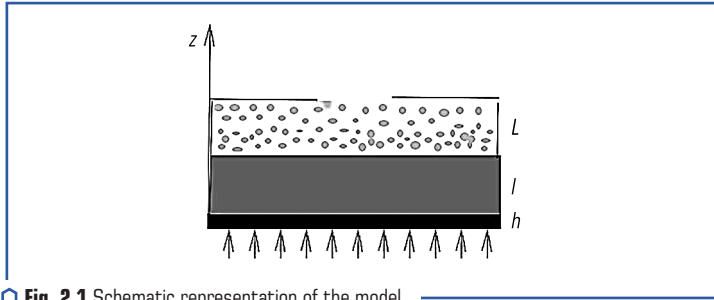


Fig. 2.1 Schematic representation of the model

Conductive contact drying takes place in a steam-air (gas) environment by transferring heat to the material when it is in contact with heated surfaces. The plate has an area  $s$ , thickness  $h_w$ , its material is characterized by density  $\rho_w$ , specific heat capacity  $C_w$ . A layer of capillary-porous moisture-saturated material of the thickness  $l$  is placed on this plate. The capillary-porous material has the porosity  $\Pi$ , density  $\rho_0^0$ , specific heat capacity  $C_0$ , and thermal conductivity coefficient in the dry state  $\lambda_0$ .

From the open side of the capillary-porous material, the moisture evaporates into the cavity of the volume  $V$  and the depth  $L = V/S$ . There is an outlet in the cavity through which the steam-air mixture flows into the environment under pressure  $P_e$ . The cavity is thermally insulated. It is possible to neglect the heat capacity of its walls. Such an installation can serve as an example of a drying chamber for conductive drying.

The system of heat and mass transfer equations is described as follows:

$$T / T_0 \frac{d}{d\tau} \left[ \rho_0 C_{ef} T + r_0 \Pi (1 - \alpha) \rho_v^0 \right] = \nabla \left[ \lambda_{ef} \nabla T - r_0 J_v - \sum_{i=l,v,a} C_{pi} T J_i \right], \quad (2.50)$$

$$P_g = \left( \frac{\rho_v^0}{M_v} + \frac{\rho_a^0}{M_a} \right) R T,$$

$$\Pi \frac{\partial \left[ (\rho_l^0 - \rho_v^0) \alpha + \rho_v^0 \right]}{\partial \tau} + \nabla J_m = 0, \quad (2.51)$$

$$J_l + J_v = J_m,$$

$$\Pi \frac{\partial \left[ (1 - \alpha) \rho_a^0 \right]}{\partial \tau} + \nabla J_a = 0, \quad (2.52)$$

$$\rho_v^0 = 133 \frac{M_v}{R T} \exp \left( 18,681 - \frac{4105}{T - 35} \right). \quad (2.53)$$

Here  $\Pi$ ,  $\alpha$ ,  $r_0$ ,  $\lambda_{ef}$ ,  $J_i$  are the porosity, relative moisture saturation, specific heat of vaporization, effective thermal conductivity, and moisture, steam, and air flows, respectively. If the evaporation is not strong, then it can be roughly assumed that the steam pressure in the cavity is equal to the saturation pressure. In this system of equations, the temperature  $T$ , moisture saturation  $\alpha$ , and air density  $\rho_a^0$  are unknown. At the initial moment, there can be moisture, air, steam in the pores. It is possible to assume that the steam-air mixture is a mixture of ideal gases and in the wet state, when the capillary-porous material is saturated with moisture  $\alpha > 0$ , the density of steam-air mixture is a function of temperature only. The equation does not include the phase transition criterion, the dependence of which on the parameters is complex. The equations remain valid in the dry zone, where there is no moisture, and  $\alpha = 0$ ,  $J_v = 0$  in this domain, equation (2.52) serves to determine the moisture density.

The boundary conditions are formulated as follows: at the initial moment of time, the pressure of the steam-air mixture in the capillary-porous material and in the cavity is equal to the external atmospheric pressure  $P_e$ :  $P_g = P_e(0) = P_0$ .

The initial temperature:

$$T(x, 0) = T_0. \quad (2.54)$$

The moisture saturation  $\alpha(x, 0) = \alpha_0 \leq 1$ .

The air density  $\rho_a^0(x, 0) = \frac{P_0 - P_{vs}}{R T_0} M_a$ .

The boundary conditions on the side of the heated plate are as follows:

$$q_e = -\lambda \nabla T + \rho_w C_w h_w \frac{\partial T}{\partial \tau} + r^* J_v, \quad r^*(T) = r_0 - (C_L - C_{pv})T. \quad (2.55)$$

The moisture and air flows at the interface from the side of the plate are zero:

$$J_m = 0, \quad J_a = 0.$$

The boundary conditions on the surface of the capillary-porous material from the side of the cavity with the opening for  $x = l$  are as follows:

$$-\lambda \nabla T = r^* J_L + V / S (\rho_a^0 C_{va} + \rho_v^0 C_{vv}) \frac{\partial T}{\partial t} + \frac{V}{S} \left[ R_a \frac{\partial \rho_a^0}{\partial t} + R_v \frac{\partial \rho_v^0}{\partial t} \right] T, \quad (2.56)$$

where the first term  $\lambda \nabla T$  characterizes the heat flow that penetrates inside the body; the second term is equal to the product of the specific heat of vaporization multiplied by the density of the moisture flow that evaporates; the third term is the power spent on heating the surface; the fourth term is the flow of heat transmitted by the movement of the steam-air mixture.

The total flow of vaporized moisture should be equal to the flow rate of the moisture flowing out through the hole, to estimate which let's use the formula for adiabatic output from the cavity [36]. To determine the flow of moisture, the equation of conservation of moisture mass in the cavity is used:

$$SJ_m = Q_e \frac{\rho_v^0}{\rho_g^0} + V \frac{\partial \rho_v^0}{\partial t}, \quad (2.57)$$

the air flow:

$$SJ_a = Q_e \frac{\rho_a^0}{\rho_g^0} + V \frac{\partial \rho_a^0}{\partial t}, \quad \rho_v^0 = \rho_{vs}(T_c). \quad (2.58)$$

The vapor density is equal to the saturated vapor density. The movement of gas in the cavity into which evaporation occurs is neglected. The gas temperature in the cavity is assumed to be the same throughout the volume.

The flow of the steam-air mixture through the drainage hole is determined by the formulae of output from the cavity:

$$Q_e = s \left[ \gamma \left( \frac{2}{\gamma + 1} \right)^{\frac{\gamma + 1}{\gamma - 1}} \right]^{1/2} Q(\epsilon_p) P_c (R_g T_c)^{-1/2}, \quad \epsilon_p = P_e / P_c, \quad (2.59)$$

$$Q(\varepsilon_p) = \begin{cases} \left[ \frac{\gamma+1}{2} \right]^{\frac{1}{\gamma-1}} \varepsilon_p^{1/\gamma} \left[ \frac{\gamma+1}{\gamma-1} \left( 1 - \varepsilon_p^{\frac{\gamma-1}{\gamma}} \right) \right]^{-1/2}, & \varepsilon_p > \left[ \frac{2}{\gamma+1} \right]^{\frac{\gamma}{\gamma-1}}, \\ 1, & \varepsilon_p \leq \left[ \frac{2}{\gamma+1} \right]^{\frac{\gamma}{\gamma-1}}. \end{cases}$$

Here  $T_c, P_c$  are temperature and pressure in the cavity,  $Q_e$  is the gas flow through the drainage hole [37],  $\gamma$  is the adiabatic index,  $R_g$  is a gas constant. The boundary conditions are obtained under the assumption that the gradients of temperature, pressure, and concentration across the cavity are negligible, and the vapor pressure in the cavity is close to the saturation pressure for the cavity temperature.

Let's write the system of nonlinear differential equations (2.1)–(2.3) in a matrix form:

$$\frac{\partial}{\partial T} [E(u)] + \frac{\partial}{\partial x} \bar{J} = 0, \quad (2.60)$$

where  $u = (T, \alpha, \rho_a^0)$ ;  $\bar{E}$  is a vector, the components of which are the total content of enthalpy, moisture, and air in a unit volume of the material;  $\bar{J}$  is a vector composed of heat, moisture,

and air flows, it is linearly related to the gradients  $T, \alpha, P$ ;  $c_a = \rho_a^0 / \rho_g^0$ ;  $J(u) = -A(u) \frac{\partial F(u)}{\partial x}$ ;

$F = F(T, \alpha, P, c_a)$ ;  $A(u)$  is the  $3 \times 4$  matrix, and the  $3 \times 5$  matrix (if capillary pressure is taken into account) [38–40]:

$$A = [a_{ij}], \quad i = \overline{1, 4}, \quad j = \overline{1, 3},$$

where  $a_{11} = \lambda$ ,  $a_{12} = 0$ ;  $a_{13} = \frac{\tilde{K}}{\mu_{eff}} (1 - \alpha) (r_0 \rho_v^0 + TC_{pa} \rho_a^0 + TC_{pv} \rho_v^0)$ ;

$$a_{14} = \Pi D_{ef} (1 - \alpha) (\rho_v^0 + \rho_a^0) (r_0 - C_{pa} T - C_{pv} T); \quad a_{21} = a_l \rho_0 \delta; \quad a_{22} = D_L \Pi \rho_L^0;$$

$$a_{23} = \alpha \frac{\tilde{K} \rho_L^0}{\mu_L} + \frac{\tilde{K} (1 - \alpha)}{\mu_{ef}} \rho_v^0; \quad a_{24} = \Pi D_{ef} (1 - \alpha) (\rho_v^0 + \rho_a^0); \quad a_{31} = 0;$$

$$a_{32} = 0; \quad a_{33} = \frac{\tilde{K} (1 - \alpha)}{\mu_{ef}} \rho_a^0; \quad a_{34} = -\Pi D_{ef} (1 - \alpha) (\rho_v^0 + \rho_a^0).$$

Here  $D_{ef}, C_{pa}, C_{pv}$  are the coefficients of effective diffusion, specific heat capacities of air and steam at a constant pressure, respectively;  $\lambda$  is the coefficient of effective thermal conductivity:

$$E(T, \alpha, \rho_v^0) = \frac{\left[ T \left\{ \rho_0 C_0 + \Pi \left[ \rho_l^0 C_l \alpha + (1 - \alpha) (\rho_v^0 C_v + \rho_a^0 C_a) \right] + r_0 \Pi (1 - \alpha) \rho_v^0 \right\} \right]}{\Pi \left[ (\rho_l^0 - \rho_v^0) \alpha + \rho_v^0 \right] \Pi (1 - \alpha) \rho_v^0};$$

$$A = \begin{vmatrix} \lambda & 0 & \frac{\tilde{K} K_g}{\mu_{ef}} (r_0 \rho_v^0 + T (C_{pa} \rho_a^0 + C_{pv} \rho_v^0)) & \Pi D_{ef} (1 - \alpha) \rho_g^0 (r_0 - (C_{pa} + C_{pv}) T) \\ D_l \rho_0 \delta & D_l \rho_l^0 \Pi & \left[ \frac{\tilde{K} K_l \rho_l^0}{\mu_l} + \frac{\tilde{K} K_g \rho_v^0}{\mu_{ef}} \right] + & \Pi D_{ef} (1 - \alpha) (\rho_v^0 + \rho_a^0) \\ 0 & 0 & \frac{\tilde{K} K_g \rho_a^0}{\mu_{ef}} & -\Pi D_{ef} (1 - \alpha) (\rho_v^0 + \rho_a^0) \end{vmatrix};$$

where  $K_g = 1 - \alpha$  is a relative gas permeability;  $r_0$  is the heat of vaporization for  $T = 0$  K;

$$F = \begin{vmatrix} T \\ \alpha \\ \left( \frac{\rho_v^0}{M_v} + \frac{\rho_a^0}{M_a} \right) RT \\ \frac{\rho_v^0}{\rho_v^0 + \rho_a^0} \end{vmatrix}.$$

The system of equations has to satisfy the boundary conditions:

$$J|_{x=0}(u) = Q_0, \quad J|_{x=1}(u) = Q_1,$$

and the initial conditions:  $(0 \leq (x) \leq l, t = 0), T = T_0, \alpha = \alpha_0 < 1,$

$$\rho_a^0 = [P_0 - P_{vs}(T)] M_a / RT_0, \quad (2.61)$$

$$Q_0 = \begin{vmatrix} q_e - \rho_p C_p h \partial T / \partial t \\ 0 \\ 0 \end{vmatrix} \quad \text{is the gas flow from the side of the plate,}$$



$$Q_1 = \left| \begin{array}{l} \frac{V}{S} \left\{ \left( \frac{\partial \rho_a^0}{\partial t} C_{va} + \frac{\partial \rho_v^0}{\partial T} \frac{\partial T}{\partial t} C_{vv} \right) T + \left( \rho_a^0 C_{va} + \rho_v^0 C_{vv} \right) \frac{\partial T}{\partial t} + r_0 \frac{\partial \rho_v^0}{\partial T} \frac{\partial T}{\partial t} \right\} + \\ + \frac{Q_a}{S} \frac{(\rho_a^0 C_{va} + \rho_v^0 C_{vv}) T + r_0 \rho_v^0}{\rho_a^0 + \rho_v^0} \\ \frac{1}{S} \frac{Q_a \rho_v^0}{\rho_a^0 + \rho_v^0} + \frac{V}{S} \frac{\partial \rho_v^0}{\partial T} \frac{\partial T}{\partial t} \\ \frac{1}{S} \frac{Q_a \rho_v^0}{\rho_a^0 + \rho_v^0} + \frac{V}{S} \frac{\partial \rho_a^0}{\partial T} \end{array} \right|.$$

The nonlinear problem is solved by two methods for comparing the results.

**Construction of a difference scheme.**

Let's integrate the matrix Eq. (2.60) with respect to  $x$  over the interval  $x_n - \frac{\Delta x}{2}, x_n + \frac{\Delta x}{2}$

for  $t = t_k = k\Delta t$ . Let's obtain:

$$- \int_{x_n - \frac{\Delta x}{2}}^{x_n + \frac{\Delta x}{2}} \frac{\partial E^k}{\partial t} dx + J_{n+\frac{1}{2}}^k - J_{n-\frac{1}{2}}^k = 0. \quad (2.62)$$

Equation (2.62) after the difference approximation is reduced to the difference scheme. A three-point approximation of the spatial variables is used. The system of nonlinear algebraic equations is solved by Newton's method.

**The linearization method.**

In order to solve the boundary value problem, in addition, an iterative process is built, at each step of which a linear boundary value problem is solved for the next approximation, which uses the information of the previous one. A small-time step is used to ensure convergence of iterations.

If an approximation  $u_i = \begin{pmatrix} T \\ \alpha \\ \rho_a^0 \end{pmatrix}$  of the problem solution is known, then the exact solution  $u^*$  can

be presented as follows  $u^* = u_i + \Delta u_i^*$ .

Put  $u^* = u_{i+1}$ .

Based on the Lagrange formula:

$$\dot{E}[u_{i+1}(t, x)] = \dot{E}[u_i(t, x)] + \left\{ \left[ \dot{E}[u_i(t, x)] \right]' \right\}_T \left[ \dot{E}[u_i(t, x)] \right]'_{\alpha} \left[ \dot{E}[u_i(t, x)] \right]'_{\rho_a} \times$$

$$\times \begin{bmatrix} T_{i+1} - T_i \\ \alpha_{i+1} - \alpha_i \\ \rho_{ai+1} - \rho_{ai} \end{bmatrix} + \left\{ \left[ \dot{E}[u_i(t, x)] \right]'_{T'} \left[ \dot{E}[u_i(t, x)] \right]'_{\alpha'} \left[ \dot{E}[u_i(t, x)] \right]'_{\rho_a} \right\} \begin{bmatrix} \dot{T}_{i+1} - \dot{T}_i \\ \dot{\alpha}_{i+1} - \dot{\alpha}_i \\ \dot{\rho}_{ai+1} - \dot{\rho}_{ai} \end{bmatrix}, \quad (2.63)$$

$$J(t, x, u_{i+1}) = -A(t, x, u_{i+1}) \frac{\partial F}{\partial X}(t, x, u_{i+1}, \dot{u}_{i+1}) = J[u_i(t, x)] + \left\{ J[u_i(t, x)]'_{T'} J[u_i(t, x)]'_{\alpha'}, \right.$$

$$\left. J[u_i(t, x)]'_{\rho_a} \right\} \begin{bmatrix} T_{i+1} - T_i \\ \alpha_{i+1} - \alpha_i \\ \rho_{ai+1} - \rho_{ai} \end{bmatrix} + \left\{ J[u_i(t, x)]'_{T'} J[u_i(t, x)]'_{\alpha'}, J[u_i(t, x)]'_{\rho_a} \right\} \begin{bmatrix} T'_{i+1} - T'_i \\ \alpha'_{i+1} - \alpha'_i \\ \rho'_{ai+1} - \rho'_{ai} \end{bmatrix}. \quad (2.64)$$

Using quadrature formulae of the interpolation type according to the 3/8 rule [38], let's obtain the difference scheme:

$$1/8 \left( \frac{\Delta E_{n-1}^k}{\Delta t} + 6 \frac{\Delta E_n^k}{\Delta t} + \frac{\Delta E_{n+1}^k}{\Delta t} \right) + \frac{1}{\Delta X} (J_{n+1/2}^k - J_{n-1/2}^k) = 0, \quad (2.65)$$

$$\text{where } \frac{\Delta E_n^k}{\Delta t} = \frac{1}{\Delta t} [E_n^k - E_{n-1}^{k-1}], \quad E_n^k = E(u_n^k),$$

$$\{J\}'_{T/\alpha/\rho_a} = - \left\{ [A]'_{T/\alpha/\rho_a} \left[ \frac{\partial F}{\partial X} \right] + [A] \left[ \frac{\partial F}{\partial X} \right]'_{T/\alpha/\rho_a} \right\},$$

$$\{J\}'_{T'/\alpha'/\rho'_a} = - \left\{ [A] \left[ \frac{\partial F}{\partial X} \right]'_{T'/\alpha'/\rho'_a} \right\}, \quad (2.66)$$

by  $[ ]'_{T, \alpha, \rho_a}$  the differentiations with respect to  $T, \alpha, \rho_a$  are denoted.

Denote

$$\left[ \frac{\partial E}{\partial t}(u, t, x) \right]_{u_j, t_k, x_n} = [\dot{E}_m^k], \quad [J(u, t, x)]_{u_j, t_k, x_n} = [J_m^k], \quad (2.67)$$

$$J_i(t^k, x_{n+1/2}) = -\frac{1}{2} \left[ (A_n^k + A_{n+1}^k) \frac{F_{n+1}^k - F_n^k}{\Delta X} \right]_i.$$

Taking into account Eqs. (2.63), (2.64) and the boundary conditions:

$$\begin{aligned} 1/8 \left( 3 \frac{\Delta E_0^k}{\Delta t} + \frac{\Delta E_1^k}{\Delta t} \right) + \frac{1}{\Delta x} (J_{1/2}^k - Q_0) &= 0, \\ 1/8 \left( 3 \frac{\Delta E_N^k}{\Delta t} + \frac{\Delta E_{N-1}^k}{\Delta t} \right) + \frac{1}{\Delta x} (Q_1 - J_{N-1/2}^k) &= 0, \end{aligned} \quad (2.68)$$

arrive at the iterative scheme of linear equations. If the  $i$ -th iteration of the solution  $u_m^k$  is known, then using Lagrange's formula  $E_{i+1,n}^k = E_{in}^k + E_{1in}^k (u_{i+1,n}^k - u_{in}^k)$ , let's obtain:

$$I_{i+1,n+1/2}^k = I_{i,n+1/2}^k + I_{1in+1/2}^k (u_{i+1,n+1}^k - u_{in+1}^k) + I_{2i,n+1/2}^k (u_{i+1,n}^k - u_{in}^k).$$

Here  $E_{in}^k$ ,  $I_{i,n+1/2}^k$  are values of the vectors  $\bar{E}_i$ ,  $\bar{I}_i$  at the points  $(n, k)$ ,  $(n+1/2, k)$ .

To verify the result, let's apply a slightly modified method of linearization, which is less time-consuming for the difference scheme. It is possible to proceed from equations (2.60), (2.61), (2.65)–(2.68), where  $Q_0 = (q_{h0}, q_{m0}, q_{a0})$  are the flows of enthalpy, moisture, and air through the surface  $x = 0$ . Then  $q_{m0} = 0$ ,  $q_{a0} = 0$ ,  $q_{h0} = q_1 - \rho_p c_p h \Delta T_0^k / \Delta t$ ,  $N$  is the number of nodes on  $x$ ;  $Q_1 = (q_{h1}, q_{m1}, q_{a1})$  are flows through the surface  $x = l$ :

$$\begin{aligned} q_{h1} &= \frac{V}{S} \frac{\Delta}{\Delta t} \left[ (\rho_{aN} c_{va} + \rho_{vN} c_{vv}) T_N + r_0 \rho_{vN} \right] + \frac{Q_\theta}{S(1 + X_N)} \left[ (X_N c_{p\theta} + c_{pv}) T_N + r_0 \right]; \\ q_{m1} &= \frac{V}{S} \frac{\Delta}{\Delta t} \rho_{vN} + \frac{Q_\theta}{S(1 + X_N)}; \\ q_{a1} &= \frac{V}{S} \frac{\Delta}{\Delta t} \rho_{aN} + \frac{Q_\theta X_N}{S(1 + X_N)}. \end{aligned} \quad (2.69)$$

Based on Lagrange's formula, let's present

$$E_{i+1,n}^k = E_{in}^k + E_{1in}^k (u_{i+1,n}^k - u_{in}^k), \quad (2.70)$$

$$J_{i+1,n+1/2}^k = J_{in+1/2}^k + J_{1in+1/2}^k (u_{i+1,n+1}^k - u_{in+1}^k) + J_{2in+1/2}^k (u_{i+1,n}^k - u_{in}^k),$$

where  $E_{in}^k$ ,  $J_{in+1/2}^k$  the values of the vectors  $\bar{E}_i$ ,  $\bar{J}_i$  at the points  $(n, k)$ ,  $(n+1/2, k)$ , respectively.  $E_{1in}^k$ ,  $J_{1in+1/2}^k$ ,  $J_{2in+1/2}^k$  are matrices formed as follows:

$$\begin{aligned}
 E_{im}^k &= \left[ \frac{\partial E_n^k}{\partial T_n^k}, \frac{\partial E_n^k}{\partial \alpha_n^k}, \frac{\partial E_n^k}{\partial \rho_{an}^k} \right]_i, \quad J_{im+1/2}^k = \left[ \frac{\partial J_{n+1/2}^k}{\partial T_{n+1}^k}, \frac{\partial J_{n+1/2}^k}{\partial \alpha_{n+1}^k}, \frac{\partial J_{n+1/2}^k}{\partial \rho_{an+1}^k} \right]_j, \\
 J_{2m+1/2}^k &= \left[ \frac{\partial J_{n+1/2}^k}{\partial T_n^k}, \frac{\partial J_{n+1/2}^k}{\partial \alpha_n^k}, \frac{\partial J_{n+1/2}^k}{\partial \rho_{an}^k} \right]_i.
 \end{aligned} \tag{2.71}$$

By analogy:

$$J_{i+1,n-1/2}^k = J_{in-1/2}^k + J_{im-1/2}^k (u_{i+1,n-1}^k - u_{i,n-1}^k) + J_{2in-1/2}^k (u_{i+1,n}^k - u_{i,n}^k),$$

where

$$J_{in-1/2}^k = [J_{in-1/2}^k],$$

$$J_{in+1/2}^k = [J_{in+1/2}^k],$$

$$J_{im-1/2}^k = \left[ \frac{\partial J_{n-1/2}^k}{\partial T_{n-1}^k}, \frac{\partial J_{n-1/2}^k}{\partial \alpha_{n-1}^k}, \frac{\partial J_{n-1/2}^k}{\partial \rho_{an-1}^k} \right]_j,$$

$$J_{2in-1/2}^k = \left[ \frac{\partial J_{n-1/2}^k}{\partial T_n^k}, \frac{\partial J_{n-1/2}^k}{\partial \alpha_n^k}, \frac{\partial J_{n-1/2}^k}{\partial \rho_{an}^k} \right]_j,$$

where

$$\begin{aligned}
 \frac{\partial J_{n+1/2}^k}{\partial T_{n+1}^k / \alpha_{n+1}^k / \rho_{an+1}^k} &= -\frac{1}{2} \left\{ \frac{\partial A(u_{n+1}^k)}{\partial T_{n+1}^k / \alpha_{n+1}^k / \rho_{an+1}^k} \left[ \frac{F_{n+1}^k - F_n^k}{\Delta x} \right] - [A_n^k + A_{n+1}^k] \frac{1}{\Delta x} \frac{\partial F_n^k}{\partial T_{n+1}^k / \alpha_{n+1}^k / \rho_{an+1}^k} \right\}, \\
 \frac{\partial J_n^k}{\partial T_n^k / \alpha_n^k / \rho_{an}^k} &= -\frac{1}{2} \left\{ \frac{\partial A(u_n^k)}{\partial T_n^k / \alpha_n^k / \rho_{an}^k} \left[ \frac{F_{n+1}^k - F_n^k}{\Delta x} \right] - [A_n^k + A_{n+1}^k] \frac{1}{\Delta x} \frac{\partial F_n^k}{\partial T_n^k / \alpha_n^k / \rho_{an}^k} \right\}, \\
 \frac{\partial J_{n-1/2}^k}{\partial T_{n-1}^k / \alpha_{n-1}^k / \rho_{an-1}^k} &= -\frac{1}{2} \left\{ \frac{\partial A(u_{n-1}^k)}{\partial T_{n-1}^k / \alpha_{n-1}^k / \rho_{an-1}^k} \left[ \frac{F_{n+1}^k - F_n^k}{\Delta x} \right] - [A_n^k + A_{n-1}^k] \frac{1}{\Delta x} \frac{\partial F_n^k}{\partial T_{n-1}^k / \alpha_{n-1}^k / \rho_{an-1}^k} \right\}, \\
 \frac{\partial J_{n-1/2}^k}{\partial T_n^k / \alpha_n^k / \rho_{an}^k} &= -\frac{1}{2} \left\{ \frac{\partial A(u_n^k)}{\partial T_n^k / \alpha_n^k / \rho_{an}^k} \left[ \frac{F_n^k - F_{n-1}^k}{\Delta x} \right] - [A_n^k + A_{n-1}^k] \frac{1}{\Delta x} \frac{\partial F_n^k}{\partial T_n^k / \alpha_n^k / \rho_{an}^k} \right\}.
 \end{aligned}$$

The variables  $Q_0, Q_1$  are presented in the form:

$$\begin{aligned} [Q_0]_{i+1,0}^k &= [Q_0]_{i,0}^k + [Q_0^1]_{i,0}^k (u_{i+1,0}^k - u_{i,0}^k) + [Q_0^2]_{i,0}^k (u_{i+1,0}^{k-1} - u_{i,0}^{k-1}), \\ [Q_0]_{i+1,N}^k &= [Q_0]_{i,N}^k + [Q_1]_{i,N}^k (u_{i+1,N}^k - u_{i,N}^k) + [Q_1^2]_{i,N}^k (u_{i+1,N}^{k-1} - u_{i,N}^{k-1}), \end{aligned} \quad (2.72)$$

where

$$\begin{aligned} [Q_0^1]_{i,0}^k &= \left[ \frac{\partial [Q_0]_{i,0}^k}{\partial T_0^k}, 0, 0 \right]_i, \\ [Q_0^2]_{i,0}^k &= \left[ \frac{\partial [Q_0]_{i,0}^k}{\partial T_0^{k-1}}, 0, 0 \right]_i, \\ [Q_1^1]_{i,N}^k &= \left[ \frac{\partial [Q_1]_{i,N}^k}{\partial T_N^k}, \frac{\partial [Q_1]_{i,N}^k}{\partial \alpha_N^k}, \frac{\partial [Q_1]_{i,N}^k}{\partial p_{aN}^k} \right]_i, \\ [Q_1^2]_{i,N}^k &= \left[ \frac{\partial [Q_1]_{i,N}^k}{\partial T_N^{k-1}}, \frac{\partial [Q_1]_{i,N}^k}{\partial \alpha_N^{k-1}}, \frac{\partial [Q_1]_{i,N}^k}{\partial p_{aN}^{k-1}} \right]_i. \end{aligned}$$

Taking into account these ratios, equations (2.65)–(2.68) are written as follows:

$$\begin{aligned} & \left[ \frac{3}{8\Delta t} E_{i/0}^k + \frac{1}{\Delta x} \left[ J_{2i\frac{1}{2}}^k - (Q_0^1)_{i/0}^k \right] \right] (u_{i+1,0}^k - u_{i,0}^k) - \left[ \frac{3}{8\Delta t} E_{i/0}^{k-1} + \frac{1}{\Delta x} \left[ (Q_0^2)_{i/0}^k \right] \right] (u_{i+1,0}^{k-1} - u_{i,0}^{k-1}) + \\ & + \left[ \frac{1}{8\Delta t} E_{i/1}^k + \frac{1}{\Delta x} J_{i\frac{1}{2}}^k \right] (u_{i+1,1}^k - u_{i,1}^k) - \frac{1}{8\Delta t} E_{i/1}^{k-1} (u_{i+1,1}^{k-1} - u_{i,1}^{k-1}) = - \frac{1}{8\Delta t} \left[ 3(E_{i/0}^k - E_{i/0}^{k-1}) + \right. \\ & + (E_{i/1}^k - E_{i/1}^{k-1}) \left. \right] - \frac{1}{\Delta x} \left[ J_{i\frac{1}{2}}^k - (Q_0^1)_{i/0}^k \right]; \\ & \left[ \frac{1}{8\Delta t} E_{i+1n-1}^k - \frac{1}{\Delta x} J_{i+1n-1}^k \right] (u_{i+1n-1}^k - u_{i-1n-1}^k) - \frac{1}{8\Delta t} E_{i+1n-1}^{k-1} (u_{i+1n-1}^{k-1} - u_{i-1n-1}^{k-1}) + \\ & + \left[ \frac{6}{8\Delta t} E_{i+1n}^k + \frac{1}{\Delta x} \left[ J_{2i+1n+1}^k - J_{2i+1n-1}^k \right] \right] (u_{i+1n}^k - u_{i-1n}^k) - \frac{6}{8\Delta t} E_{i+1n}^{k-1} (u_{i+1n}^{k-1} - u_{i-1n}^{k-1}) + \end{aligned}$$

$$\begin{aligned}
 & + \left[ \frac{1}{8\Delta t} E_{in+1}^k + \frac{1}{\Delta x} J_{in+\frac{1}{2}}^k \right] (u_{i+1n+1}^k - u_{in+1}^k) - \frac{1}{8\Delta t} E_{in+1}^{k-1} (u_{i+1n+1}^{k-1} - u_{in+1}^{k-1}) = \\
 & = -\frac{1}{8\Delta t} \left[ 6(E_{in}^k - E_{in}^{k-1}) + (E_{in-1}^k - E_{in-1}^{k-1}) + (E_{in+1}^k - E_{in+1}^{k-1}) \right] - \frac{1}{\Delta x} \left[ J_{in+\frac{1}{2}}^k - J_{in-\frac{1}{2}}^k \right]; \quad (2.73)
 \end{aligned}$$

where

$$[Q_0]_0^k = \begin{vmatrix} q_e - \rho_p c_p h \frac{T_0^k - T_0^{k-1}}{\Delta t} \\ 0 \\ 0 \end{vmatrix}_i,$$

$$Q_1 = [b_i], \quad i = \overline{1,3},$$

$$\begin{aligned}
 b_1 = & \frac{V}{S} \left\{ \left( \frac{\partial \rho_a^0}{\partial t} C_{va} + \frac{\partial \rho_v^0}{\partial T} \frac{\partial T}{\partial t} C_{vw} \right) T + (\rho_a^0 C_{va} + \rho_v^0 C_{vw}) \frac{\partial T}{\partial t} + r_0 \frac{\partial \rho_v^0}{\partial T} \frac{\partial T}{\partial t} \right\} + \\
 & + \frac{Q_e}{S} \frac{(\rho_a^0 C_{va} + \rho_v^0 C_{vw}) T + r_0 \rho_v^0}{(\rho_a^0 + \rho_v^0)};
 \end{aligned}$$

$$b_2 = \frac{1}{S} \frac{Q_e \rho_v^0}{\rho_v^0 + \rho_a^0} + \frac{V}{S} \frac{\partial \rho_v^0}{\partial T} \frac{\partial T}{\partial t};$$

$$b_3 = \frac{1}{S} \frac{Q_e \rho_a^0}{\rho_v^0 + \rho_a^0} + \frac{V}{S} \frac{\partial \rho_a^0}{\partial t};$$

$$[Q_1]_N^k = \begin{vmatrix} \frac{V}{S} \left\{ C_{va} T_N^k \frac{\rho_{aN}^{0k} - \rho_{aN}^{0k-1}}{\Delta t} + \left[ (C_{vw} T + r_0) \frac{\partial \rho_v^0}{\partial T} + (\rho_a^0 C_{va} + \rho_v^0 C_{vw}) \right]_N^k \frac{T_N^k - T_N^{k-1}}{\Delta t} \right\} + \\ + \frac{Q_e}{S} \frac{(\rho_a^0 C_{va} + \rho_v^0 C_{vw}) T + r_0 \rho_v^0}{(\rho_a^0 + \rho_v^0)} \Big|_N^k \\ \frac{Q_e}{S} \frac{\rho_v^0}{(\rho_a^0 + \rho_v^0)} \Big|_N^k + \frac{V}{S} \frac{\partial \rho_v^0}{\partial T} \Big|_N^k \frac{T_N^k - T_N^{k-1}}{\Delta t} \\ \frac{Q_e}{S} \frac{\rho_a^0}{(\rho_a^0 + \rho_v^0)} \Big|_N^k + \frac{V}{S} \frac{\rho_{aN}^{0k} - \rho_{aN}^{0k-1}}{\Delta t} \end{vmatrix}_i,$$

$$\left. \begin{aligned} & \frac{V}{S} \left\{ \mathcal{C}_{va} \frac{\rho_{aN}^{0k} - \rho_{aN}^{0k-1}}{\Delta t} + \left[ (\mathcal{C}_w T + r_0) \frac{\partial \rho_v^0}{\partial T} + (\rho_a^0 \mathcal{C}_{va} + \rho_v^0 \mathcal{C}_w) \right]_N^k \frac{1}{\Delta t} \right\} + \\ & + \frac{T_N^k - T_N^{k-1}}{\Delta t} \left[ \frac{\partial^2 \rho_v^0}{\partial T^2} (\mathcal{C}_w T + r_0) + 2 \mathcal{C}_{vv} \frac{\partial \rho_v^0}{\partial T} \right]_N^k + \frac{Q_e}{S} \left\{ \left[ \frac{(\rho_a^0 \mathcal{C}_{va} + \rho_v^0 \mathcal{C}_w) T + r_0 \rho_v^0}{(\rho_a^0 + \rho_v^0)^2} + \right. \right. \\ & \left. \left. \frac{\partial Q_{1N}^k}{\partial T_N^k} + \frac{(\mathcal{C}_{pv} T + r_0)}{(\rho_a^0 + \rho_v^0)} \right] \frac{\partial \rho_v^0}{\partial T} \right|_N^k + \frac{(\rho_a^0 \mathcal{C}_{pa} + \rho_v^0 \mathcal{C}_{pv})}{(\rho_a^0 + \rho_v^0)} \Big|_N^k \left\} \right. \\ & \left. \frac{Q_e}{S} \frac{\rho_v^0}{(\rho_a^0 + \rho_v^0)^2} \frac{\partial \rho_v^0}{\partial T} \right|_N^k + \frac{V}{S} \frac{\partial \rho_v^0}{\partial T} \Big|_N^k \frac{1}{\Delta t} + \frac{T_N^k - T_N^{k-1}}{\Delta t} \left( \frac{\partial^2 \rho_v^0}{\partial T^2} \right)_N^k \right. \\ & \left. - \frac{Q_e}{S} \frac{\rho_a^0}{(\rho_a^0 + \rho_v^0)^2} \frac{\partial \rho_v^0}{\partial T} \Big|_N^k \right. \end{aligned} \right|_i$$

$$\frac{\partial Q_{1N}^k}{\partial T_N^{k-1}} = 0, \quad \frac{\partial Q_{1N}^k}{\partial \alpha_N^{k-1}} = 0,$$

$$\frac{\partial Q_{1N}^k}{\partial T_N^{k-1}} = \left. \begin{aligned} & - \frac{V}{S} \left[ (\mathcal{C}_w T + r_0) \frac{\partial \rho_v^0}{\partial T} + (\rho_a^0 \mathcal{C}_{va} + \rho_v^0 \mathcal{C}_w) \right]_N^k \frac{1}{\Delta t} \\ & - \frac{V}{S} \frac{\partial \rho_v^0}{\partial T} \Big|_N^k \frac{1}{\Delta t} \end{aligned} \right|_0;$$

$$\frac{\partial Q_{1N}^k}{\partial \rho_{aN}^k} = \left. \begin{aligned} & \frac{V}{S} \left\{ \mathcal{C}_{va} T_N^k \frac{1}{\Delta t} + \mathcal{C}_{va} \frac{T_N^k - T_N^{k-1}}{\Delta t} \right\} + \frac{Q_e}{S} \left[ \frac{(\mathcal{C}_{pa} T)}{(\rho_a^0 + \rho_v^0)} - \frac{(\rho_a^0 \mathcal{C}_{pa} + \rho_v^0 \mathcal{C}_{pv}) T + r_0 \rho_v^0}{(\rho_a^0 + \rho_v^0)^2} \right]_N^k \\ & - \frac{Q_e}{S} \frac{\rho_v^0}{(\rho_a^0 + \rho_v^0)^2} \Big|_N^k \\ & - \frac{Q_e}{S} \frac{\rho_v^0}{(\rho_a^0 + \rho_v^0)^2} \Big|_N^k + \frac{V}{S} \frac{1}{\Delta t} \end{aligned} \right|;$$

$$\frac{\partial Q_{aN}^k}{\partial \rho_{aN}^{k-1}} = \begin{vmatrix} -\frac{V}{S} C_{va} T_N \frac{1}{\Delta t} \\ 0 \\ \frac{1}{\Delta t} \end{vmatrix};$$

$$\frac{\partial Q_{00}^k}{\partial T_0^k} = \begin{vmatrix} -\rho_p C_p h \frac{1}{\Delta t} \Big|_0^k \\ 0 \\ 0 \end{vmatrix}_i; \quad \frac{\partial Q_{00}^k}{\partial T_0^{k-1}} = \begin{vmatrix} \rho_p C_p h \frac{1}{\Delta t} \Big|_0^{k-1} \\ 0 \\ 0 \end{vmatrix};$$

$$\frac{\partial Q_{00}^k}{\partial \alpha_0^k} = 0; \quad \frac{\partial Q_{00}^k}{\partial \alpha_0^{k-1}} = 0; \quad \frac{\partial Q_{00}^k}{\partial \rho_{a0}^k} = 0; \quad \frac{\partial Q_{00}^k}{\partial \rho_{a0}^{k-1}} = 0;$$

$$\frac{\partial E_N^k}{\partial \alpha_N^k} = \begin{vmatrix} \left\{ T \Pi \left[ C_L \rho_L - (\rho_a^0 C_{va} + \rho_v^0 C_{vw}) \right] - r_0 \Pi \rho_v^0 \right\}_N^k \\ -\Pi (\rho_L^0 - \rho_v^0) \Big|_N^k \\ -\Pi \rho_a^0 \Big|_N^k \end{vmatrix},$$

$$\frac{\partial E_N^k}{\partial T_N^k} = \begin{vmatrix} \left\{ \rho_0 C_0 + \Pi \left[ C_L \rho_L \alpha + (1-\alpha) (\rho_a^0 C_{va} + \rho_v^0 C_{vw}) \right] \right\}_N^k + \Pi (1-\alpha) (TC_{vw} + r_0) \frac{\partial \rho_v^0}{\partial T} \Big|_N^k \\ \Pi (1-\alpha) \frac{\partial \rho_v^0}{\partial T} \Big|_N^k \\ 0 \end{vmatrix},$$

$$\frac{\partial E_N^k}{\partial \rho_{aN}^k} = \begin{vmatrix} T \Pi (1-\alpha) C_{va} \Big|_N^k \left\{ \rho_0 C_0 + \Pi \left[ C_L \rho_L \alpha + (1-\alpha) (\rho_a^0 C_{va} + \rho_v^0 C_{vw}) \right] \right\}_N^k + \\ + \Pi (1-\alpha) (TC_{vw} + r_0) \frac{\partial \rho_v^0}{\partial T} \Big|_N^k \\ 0 \\ \Pi (1-\alpha) \Big|_N^k \end{vmatrix},$$



$$F = \left( \frac{\rho_v^0}{\rho_v^0 + \rho_a^0} \right) \cdot \left( \frac{\rho_v^0}{\rho_v^0 + \rho_a^0} \right)$$

$$\frac{\partial A_N^k}{\partial T_N^k} = \begin{vmatrix} 0 & 0 & \frac{\tilde{K}}{\mu_{eff}}(1-\alpha) \left[ (r_0 \rho_v^0 + T C_{pa} \rho_a^0 + T C_{pv} \rho_v^0) + \right. \\ & & \left. + C_{pa} \rho_a^0 + C_{pv} \rho_v^0 + (T C_{pv} + r_0) \frac{\partial \rho_v^0}{\partial T} \right]_N^k & \Pi D_{ef} (1-\alpha) (\rho_v^0 + \rho_a^0) (C_{pv} - C_{pa}) + \\ & & & + \frac{\partial \rho_v^0}{\partial T} (r_0 - C_{pa} T + C_{pv} T) \Big|_N^k \\ \frac{\partial D_L}{\partial T} \rho_0 \delta & \frac{\partial D_L}{\partial T} \rho_L & \frac{\tilde{K}}{\mu_{eff}}(1-\alpha) \frac{\partial \rho_v^0}{\partial T} \Big|_N^k & \Pi D_{ef} (1-\alpha) \frac{\partial \rho_v^0}{\partial T} \Big|_N^k \\ 0 & 0 & 0 & \Pi D_{ef} \frac{\tilde{K}}{\mu_{eff}} (1-\alpha) \rho_v^0 \Big|_N^k - \end{vmatrix};$$

$$\frac{\partial A_N^k}{\partial \alpha_N^k} = \begin{vmatrix} \frac{\partial \lambda}{\partial \alpha} & 0 & -\frac{\tilde{K}}{\mu_{eff}} \left[ (r_0 \rho_v^0 + T C_{pa} \rho_a^0 + T C_{pv} \rho_v^0) + \right. \\ & & \left. + C_{pa} \rho_a^0 + C_{pv} \rho_v^0 + (T C_{pv} + r_0) \frac{\partial \rho_v^0}{\partial T} \right]_N^k & -\Pi D_{ef} (\rho_v^0 + \rho_a^0) (r_0 - C_{pa} T + C_{pv} T) \\ & & & + \frac{\partial \rho_v^0}{\partial T} (r_0 - C_{pa} T + C_{pv} T) \Big|_N^k \\ \left( \frac{\partial D_L}{\partial \alpha} \rho_0 \delta + \frac{\partial D_L}{\partial \alpha} \Pi \rho_L \right. & \frac{\tilde{K} \rho_L}{\mu_L} - \frac{\tilde{K} \rho_v^0}{\mu_{ef}} \Big|_N^k & & -\Pi D_{ef} (\rho_v^0 + \rho_a^0) \Big|_N^k \\ & & & \left. + a_L \rho_0 \frac{\partial \delta}{\partial \alpha} \frac{\partial a_L}{\partial \alpha} \right) \Big|_N^k \\ 0 & 0 & -\frac{\tilde{K} \rho_a^0}{\mu_{ef}} \Big|_N^k & \Pi D_{ef} (\rho_v^0 + \rho_a^0) \Big|_N^k \end{vmatrix};$$

$$\frac{\partial A_N^k}{\partial \rho_N^k} = \begin{vmatrix} 0 & 0 & -\frac{\tilde{K}}{\mu_{eff}} (1-\alpha) T C_{pa} & -\Pi D_{ef} (1-\alpha) (r_0 - C_{pa} T + C_{pv} T) \\ 0 & 0 & 0 & \Pi D_{ef} (1-\alpha) \\ 0 & 0 & \frac{\tilde{K}}{\mu_{ef}} (1-\alpha) \Big|_N^k & -\Pi D_{ef} (1-\alpha) \Big|_N^k \end{vmatrix};$$

$$\begin{aligned}
 & \left[ \frac{3}{8\Delta t} E_{iN}^k - \frac{1}{\Delta x} \left[ J_{2iN-\frac{1}{2}}^k - (Q_1^k)_{iN} \right] \right] (u_{i+1N}^k - u_{iN}^k) - \left[ \frac{3}{8\Delta t} E_{iN}^{k-1} + \frac{1}{\Delta x} \left[ (Q_1^k)_{iN} \right] \right] (u_{i+1N}^{k-1} - u_{iN}^{k-1}) + \\
 & + \left[ \frac{1}{8\Delta t} E_{iN-1}^k - \frac{1}{\Delta x} J_{iN-\frac{1}{2}}^k \right] (u_{i+1N-1}^k - u_{iN-1}^k) - \frac{1}{8\Delta t} E_{iN-1}^{k-1} (u_{i+1N-1}^{k-1} - u_{iN-1}^{k-1}) = \\
 & = -\frac{1}{8\Delta t} \left[ 3(E_{iN}^k - E_{iN}^{k-1}) + (E_{iN-1}^k - E_{iN-1}^{k-1}) \right] - \frac{1}{\Delta x} \left[ J_{iN-\frac{1}{2}}^k + (Q_1^k)_{iN} \right].
 \end{aligned}$$

The transfer coefficients are taken from the Lykov's work [32]. This model describes mass transfer processes under moderate heat loads.

The capillary-porous material for which:

$$\lambda = \begin{cases} \lambda_0 + (\lambda_L - \lambda_0) \sin \frac{\pi \alpha}{2\alpha_\lambda}, & \alpha \leq \alpha_\lambda, \\ \lambda_L, & \alpha > \alpha_\lambda. \end{cases}$$

Here  $\lambda_L = 0.06 \text{ W/(m K)}$ ,  $\alpha_\lambda = 0.1$ ;

$$\frac{\partial \lambda}{\partial \alpha} = \begin{cases} \frac{\pi}{2\alpha_\lambda} (\lambda_L - \lambda_0) \cos \frac{\pi \alpha}{2\alpha_\lambda}, & \alpha < \alpha_\lambda, \\ 0, & \alpha > \alpha_\lambda; \end{cases}$$

$$D_L(T, \alpha) = \begin{cases} \left[ D_{L0} + (D_{LL} - D_{L0}) \sin \frac{\pi \alpha}{2\alpha_\alpha} \right] (T / 273)^{20}, & \alpha < \alpha_D, \\ D_{LL} (T / 273)^{20}, & \alpha > \alpha_D; \end{cases}$$

$$\frac{\partial D_L(T, \alpha)}{\partial T} = \begin{cases} \left[ D_{L0} + (D_{LL} - D_{L0}) \sin \frac{\pi \alpha}{2\alpha_\alpha} \right] (20T^{19} / 273^{20}), & \alpha < \alpha_D, \\ D_{LL} (20T^{19} / 273^{20}), & \alpha > \alpha_D; \end{cases}$$

$$\frac{\partial D_L(T, \alpha)}{\partial \alpha} = \begin{cases} \frac{\pi}{2\alpha_\alpha} (D_{LL} - D_{L0}) \cos \frac{\pi \alpha}{2\alpha_\alpha} (T / 273)^{20}, & \alpha < \alpha_D, \\ 0, & \alpha > \alpha_D; \end{cases}$$

$$\delta(\alpha) = \delta_0 \left[ 1 - 4(\alpha - 0.5)^2 \right],$$

$$\frac{\partial \delta(\alpha)}{\partial \alpha} = \delta_0(4 - 8\alpha);$$

$$\frac{\partial \rho_v^0}{\partial T} = 133 \frac{M_v}{RT} \exp\left(18.681 - \frac{4105}{T - 35}\right) \left[ \frac{4105}{(T - 35)^2} - \frac{1}{T} \right],$$

$$\frac{\partial^2 \rho_v^0}{\partial T^2} = 133 \frac{M_v}{RT} \exp\left(18.681 - \frac{4105}{T - 35}\right) \left[ \left( \frac{4105}{(T - 35)^2} - \frac{1}{T} \right)^2 - \left( \frac{2 \cdot 4105}{(T - 35)^3} - \frac{1}{T^2} \right) \right];$$

$$P_c = \left( \frac{\rho_v^0}{M_v} + \frac{\rho_a^0}{M_a} \right) RT, \quad \frac{\partial P_c}{\partial \rho_v^0} = \frac{RT}{M_v}, \quad \frac{\partial P_c}{\partial \rho_a^0} = \frac{RT}{M_a}, \quad \frac{\partial P_c}{\partial T} = \left( \frac{\rho_v^0}{M_v} + \frac{\rho_a^0}{M_a} \right) R.$$

Calculations are made for an aluminum plate and a capillary-porous material of different porosity (cork tree). The flow of the continuous phase is assumed to be slow. Inertial terms are neglected. Transfer coefficients are considered to be known functions of saturation and temperature.

$T_0 = 290$  K,  $h = 2 \cdot 10^{-3}$  m,  $D_{L0} = 1.5 D_{L0}$ ,  $\alpha_0 = 0.2$ ,  $R = 1.01325 \cdot 10^5$  Pa,  $T_0 = 8.31$  J/Kmol,  $M_v = 1.8 \cdot 10^{-3}$  kg/mol,  $M_a = 2.9 \cdot 10^{-3}$  kg/mol,  $c_{pa} = 1.006 \cdot 10^3$  J/(kg·K),  $c_{pv} = 1.103 \cdot 10^3$  J/(kg·K),  $C_{pa} = 718$  J/(kg·K),  $C_{pv} = 862$  J/(kg·K),  $\alpha_t = 9.5 \cdot 10^{-1}$ ,  $r_0^* = 2.3 \cdot 10^6$  J/kg,  $P_g = 10$  Pa,  $l = 5 \cdot 10^{-2}$  m,  $L = 3 \cdot 10^{-2}$  m,  $\Pi = 9 \cdot 10^{-1}$ ,  $C_L = 4.190 \cdot 10^3$  J/(kg·K),  $C_0 = 10^3$  J/(kg·K),  $K = 10^{-14}$  m<sup>2</sup>,  $\mu_L = 5 \cdot 10^{-4}$  kg/(m·s),  $\mu_{ef} = \mu_g = 10^{-5}$  kg/(m·s),  $D_{ef} = 5 \cdot 10^{-5}$  m<sup>2</sup>/s,  $\lambda_0 = 6 \cdot 10^{-2}$  W/(m·K),  $\lambda_L = 6 \cdot 10^{-1}$  W/(m·K),  $\alpha_g = 8.5 \cdot 10^{-1}$ ,  $\alpha_a = \alpha_s = 10^{-1}$ ,  $\rho_0 = 6 \cdot 10^{-2}$  kg/m<sup>3</sup>,  $\rho_L = 10^3$  kg/m<sup>3</sup>,  $\delta_0 = 10^{-3}$  1/K,  $D_{L0} = 10^{-3}$  m<sup>2</sup>/s,  $T_c = 327$  K,  $s/S = 10^{-4}$ ,  $V/S = 3 \cdot 10^{-2}$  m.

As an example, porous materials with the porosity  $\Pi = 0.4, 0.6$ , and  $0.8$  heated by heat flows  $q = 3 \cdot 10^3, 5 \cdot 10^3, 10^4$  are considered and the influence of various parameters on drying processes is investigated. The results of the calculations are shown in **Fig. 2.2–2.7**.

The solutions of the problem are obtained by finite-difference and iterative methods, and the comparison of the results of these solutions is used to study their accuracy. Calculations have shown that, depending on the magnitude of the heat flux, porosity, and initial saturation of the capillary-porous material, evaporation proceeds differently. The temperature (dependent on porosity) under the action of the flow  $q = 3 \cdot 10^3, 5 \cdot 10^3, 10^4$  W/m<sup>2</sup> with the porosity  $\Pi = 0.4, 0.6$  during 500 s is monotonically increasing function of time, but for  $q = 10^4$  W/m<sup>2</sup> and  $\Pi = 0.8$ , this dependence is no longer monotonous either inside or on the surfaces of the material. With a heat flux  $q = 10^4$  W/m<sup>2</sup> and the porosity  $\Pi = 0.8$ , already at the 150<sup>th</sup> second of drying, a moisture of a certain mass is released from the material (condensation caused by oncoming warm and cold flows), while the temperature first decreases slightly and then increases with time slower than in a material with the same characteristics but with less porosity. In this case, the lower the porosity, the greater the gradient of temperature rise. This property is used in problems of thermal protection of materials. With the same porosity and heat flow at the beginning of the evaporation process, the temperature increases faster with a lower initial moisture content of the material.

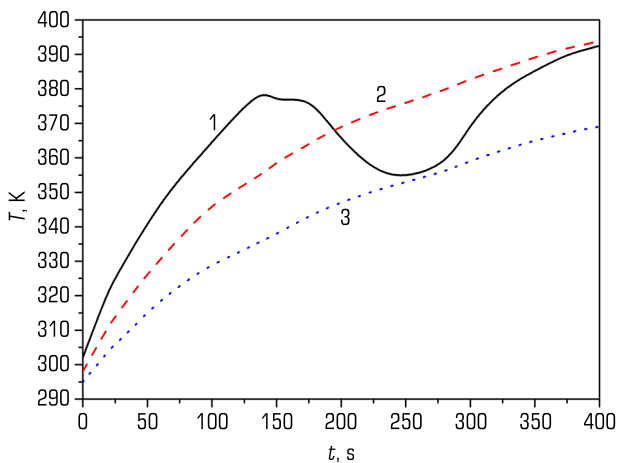


**Fig. 2.2** Temperature variations in time for  $II = 0.9$  and  $\alpha_0 = 0.8$ .  
The curves 1, 2, 3 correspond to the  $q = 10^4, 5 \cdot 10^3, 3 \cdot 10^3$ , respectively

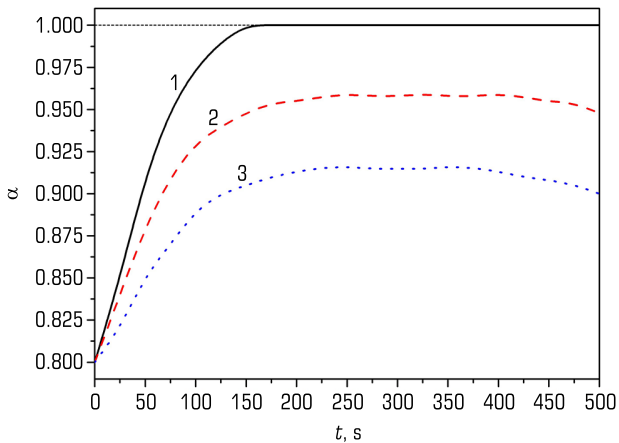


**Fig. 2.3** Change in volumetric saturation in time on the outer surface for  $\alpha_0 = 0.8$ .  
The curves 1, 2, 3 correspond to the  $q = 3 \cdot 10^3, 5 \cdot 10^3, 10^4$ , respectively

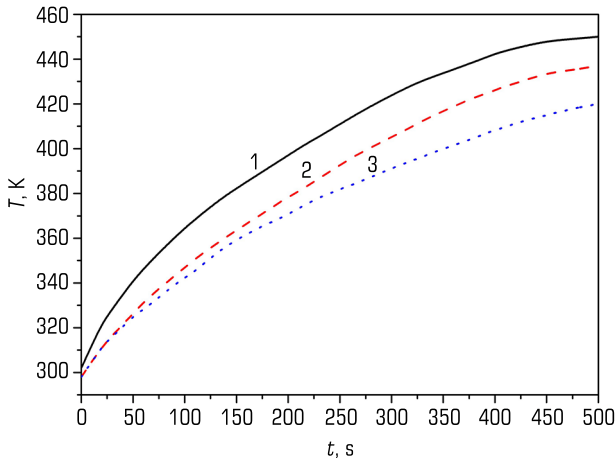


**Fig. 2.4** Temperature variations in time under the action of the flow  $q = 5 \cdot 10^3$ . The curves 1, 2, 3 correspond to the porosity  $\Pi = 0.4, 0.6, 0.8$ , respectively

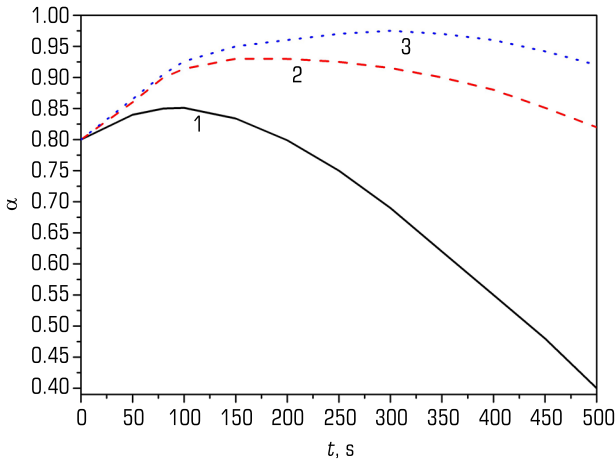


**Fig. 2.5** Change in volumetric saturation in time on the outer surface for  $q = 5 \cdot 10^3$ ,  $\alpha_0 = 0.8$ . The curves 1, 2, 3 correspond to the porosity  $\Pi = 0.4, 0.6, 0.8$ , respectively

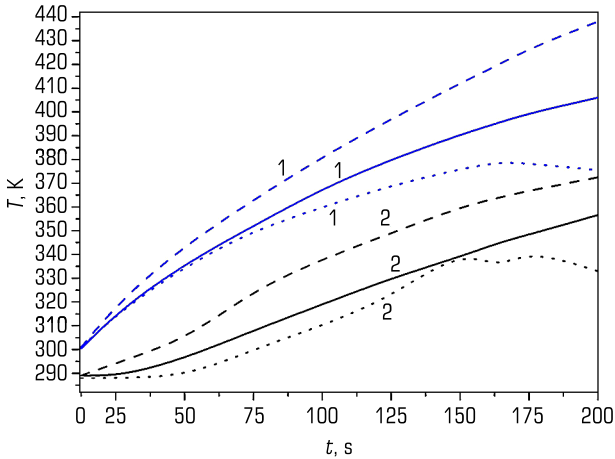


**Fig. 2.6** Temperature variations in time on the heating surface (curves 1); external surface (curves 2) for  $q = 10^4$ ,  $\alpha_0 = 0.8$  for different values of porosity (dashed curves for  $II = 0.4$ ; solid curves for  $II = 0.6$ , dotted curves for  $II = 0.8$ )

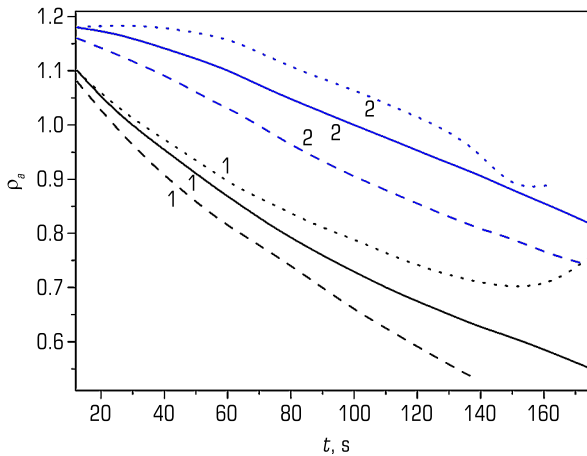


**Fig. 2.7** Change in air density in time on the heating surface (curves 1); external surface (curves 2) for  $q = 10^4$ ,  $\alpha_0 = 0.8$  for different values of porosity (dashed curves for  $II = 0.4$ ; solid curves for  $II = 0.6$ , dotted curves for  $II = 0.8$ )

## CONCLUSIONS

The basic statements are formulated and fundamental thermodynamic relations for moisturized capillary-porous deformable systems are obtained when describing them using continuum representations. Possible methods of choosing the parameters of the local thermodynamic state of a solid deformable multi-component system are presented, being consistent with their choice of the liquid (gaseous) phase. A complete system of equations is constructed to describe the drying process of dense packing of capillary-porous materials, based on the approaches of the theory of the mixtures of porous and dense packing of disperse materials of multicomponent three-phase media. There have been analyzed the influence of the external heat flow, the initial volumetric moisture saturation on changes in temperature, volumetric moisture saturation, and air density in body pores in time by the example of conductive drying. The magnitude of the heat flows of the external environment and the initial relative moisture saturation during contact drying of the material affects the behavior in time of both the temperature and the saturation of the porous solid. These characteristics are especially important in the first drying stage when the influence of the initial conditions is important. Therefore, the phenomena that occur at the heating stage with a large initial moisture content were considered.

## REFERENCES

1. Burak, Ya., Chaplia, Ye., Nahirnyi, T. et al. (2004). *Fyzyko-matematychne modeliuвання skladnykh system*. Lviv: SPOLOM, 264.
2. Haivas, B. I. (2004). Pro vplyv elektroosmosu na dvostoronnie konvektyvne osushennia porystoho sharu. *Volynskiy matematychniy visnyk. Seriya prykladna matematika*, 2 (11), 74–85.
3. Chaplya, Ye., Hayvas, B., Torsky, A. (2015). Construction of the solution of the thermal-convective drying problem for porous solids in drying plants. *Mathematical Modeling and Computing*, 2 (1), 1–15. <https://doi.org/10.23939/mmc2015.01.001>
4. Sokolovskyy, Y., Drozd, K., Samotii, T., Boretska, I. (2024). Fractional-Order Modeling of Heat and Moisture Transfer in Anisotropic Materials Using a Physics-Informed Neural Network. *Materials*, 17 (19), 4753. <https://doi.org/10.3390/ma17194753>
5. Hachkevych, O., Musii, R., Melnyk, N. (2023). Problems of Thermomechanics of Multilayered Electroconductive Bodies Under the Action of the Pulsed Electromagnetic Fields with Modulation of Amplitude. *Advances in Mechanics*, 185–206. [https://doi.org/10.1007/978-3-031-37313-8\\_11](https://doi.org/10.1007/978-3-031-37313-8_11)
6. Zhuravchak, L. M. (2007). *Matematychne modeliuвання protsesiv poshyrennia teplovoho ta elektromagnitnoho poliv u neodnorodnykh seredovyschakh metodamy pryhranychnykh elementiv ta skinchenykh riznyts*. [Extended abstract of doctors thesis].
7. Dukhin, S. S. (1975). *Elektroprovodnost y elektrokynetycheskiye svoistva dyspersnykh system*. Kyiv: Naukova dumka, 246.

8. Decker, Ž., Tretjakovas, J., Drozd, K., Rudzinskas, V., Walczak, M., Kilikevičius, A. et al. (2023). Material's Strength Analysis of the Coupling Node of Axle of the Truck Trailer. *Materials*, 16(9), 3399. <https://doi.org/10.3390/ma16093399>
9. Tokarchuk, M. V. (2024). Kinetic coefficients of ion transport in a porous medium based on the Enskog – Landau kinetic equation. *Mathematical Modeling and Computing*, 11 (4), 1013–1024. <https://doi.org/10.23939/mmc2024.04.1013>
10. Sokolovskyy, Ya. I., Boretska, I. B., Gayvas, B. I., Kroshnyy, I. M., Nechepurenko, A. V. (2021). Mathematical modeling of convection drying process of wood taking into account the boundary of phase transitions. *Mathematical Modeling and Computing*, 8 (4), 830–841. <https://doi.org/10.23939/mmc2021.04.830>
11. Borovytskyi, M. Y., Lysenko, L. L., Rynda, O. F., Mishchuk, N. O. (2014). Rehuliuвання властивостей дисперсії для електрокінетичної обробки. *Naukovi visti NTUU “KPI”*, (3), 100–106.
12. Barinova, N. O. (2016). Neliniini elektroforez ta elektroosmos dla odynnykh chastynok ta skladnykh system. [Extended abstract of Candidate's thesis; Institute of Colloid Chemistry and Water Chemistry, NAS of Ukraine].
13. Malyarenko, V. V., Makarov, A. S. (2000). Elektropoverkhnostnye svoystva vspenennykh kontsentririvannykh suspenziy kremnezema i uglya. *Ukrainskyi khimichnyi zhurnal*, 66 (9-10), 84–87.
14. Myshchuk, N. A., Lysenko, L. L., Kornilovych, B. Y., Barinova, N. O. (2002). Teoreticheskiy analiz zakonomernostey elektroosmoticheskogo transporta zhidkosti cherez diafragmu. *Khimia i tekhnologiya vody*, 24 (4), 328–351.
15. Bereznia, O. O. (1999). Zastosuvannya yavyshcha elektroosmosu pry znevodnenni kaolinu. *Zbahachennia korys. kopalyn*, 4 (45), 100–104.
16. Lysenko, L. L. (2002). Intensyfikatsiia masoperenosu pry elektrokinetichnii ochystsi hruntu. [Extended abstract of Candidate's thesis; Institute of Colloid Chemistry and Water Chemistry, NAS of Ukraine].
17. Shevchenko, R. O. (2012). Upravlinnia elektrokinetichnyimi protsesami dla poperedzhennia i podolannia avarii pry burinni sverdllovyn na naftu ta haz [Extended abstract of Candidate's thesis; National Technical University “Kharkiv Polytechnic Institute”].
18. Pushkarov, O., Zubko, O., Sevruk, I., Dolin, V. (2022). Use of mineral proton-conductive membranes for electroosmotic fractionation of the hydrogen isotopes. *Geochemistry of Technogenesis*, 35, 65–68. <https://doi.org/10.32782/geotech2022.35.12>
19. Musii, R., Melnyk, N., Dmytruk, V. (2024). Thermal stresses in bimetallic plate under induction heating by nonstationary electromagnetic field. *Journal of Thermal Stresses*, 47 (11), 1539–1551. <https://doi.org/10.1080/01495739.2024.2415030>
20. Musii, R., Dmytruk, V., Oryshchyn, O., Kushka, B., Shayner, H., Huk, L. (2024). Analysis of Thermal Modes of a Bimetallic Tube Under Short-Term Induction Heating. 2024 IEEE 19th International Conference on the Perspective Technologies and Methods in MEMS Design (MEMSTECH), 16–19. <https://doi.org/10.1109/memstech63437.2024.10620050>



21. Musii, R., Dmytruk, V., Voloshyn, M. M., Kushka, B., Nakonechny, R., Huk, L. (2023). Computer Analysis of Nonstationary Thermoelastic Processes in an Electrically Conductive Plate during Pulse Electromagnetic Treatment. 2023 IEEE XXVIII International Seminar/Workshop on Direct and Inverse Problems of Electromagnetic and Acoustic Wave Theory (DIPED), 221–224. <https://doi.org/10.1109/diped59408.2023.10269468>
22. Gayvas, B., Burak, Y., Kondrat, V. (2005). Do matematychnoho modeliuвання ta vyvchennia protsesu osushennia porystykh til. Fiz.-mat. modeliuвання ta inform. tekhnolohii, 1, 20–29.
23. Gayvas, B. I., Markovych, B. M., Dmytruk, A. A., Havran, M. V., Dmytruk, V. A. (2023). Numerical modeling of heat and mass transfer processes in a capillary-porous body during contact drying. Mathematical Modeling and Computing, 10(2), 387–399. <https://doi.org/10.23939/mmc2023.02.387>
24. Severyn, O. A. (2008). Rozrobka protsesu ta aparaturnoho osnashchennia kombinovanoho heliosushinnia plodovoi syrovyny z avtonomnym enerhopostachanniam. [Extended abstract of Candidate's thesis; Kharkiv State University of Food and Trade].
25. Fariseev, A. G. (2014). Rozrobka aparata dlia zharenia miasa v umovakh elektroosmosu. [Extended abstract of Candidate's thesis; Kharkiv State University of Food and Trade].
26. Drachov, V. I. (2000). Tekhnolohiia zbahachennia ta kompleksnoho vykorystannia vidkhodiv staleplavlynoho vyrobnytstva. [Extended abstract of Candidate's thesis; Kryvyi Rih Technical University].
27. Kostyuk, G. Ya., Kostyuk, O. G., Burkov, M. V., Golubovsky, I. A., Bulko, M. P., Bandura, L. O. et al. (2020). Pancreatic secretion and pressure biomechanics in pancreatic acinus. Clinical Anatomy and Operative Surgery, 19 (1), 6–12. <https://doi.org/10.24061/1727-0847.19.1.2020.1>
28. Kheifitc, L. I., Neimark, A. V. (1982). Mnogofaznye protsessy v poristyykh sredakh. Moscow: Khimiia, 320.
29. Gayvas, B. I., Dmytruk, V. A. (2022). Investigation of drying the porous wood of a cylindrical shape. Mathematical Modeling and Computing, 9 (2), 399–415. <https://doi.org/10.23939/mmc2022.02.399>
30. Burak, Ya., Kondrat, V., Haivas, B. (2002). Do matematychnoho modeliuвання protsesiv sushky porystykh til. Informatychno-matematychno modeliuвання skladnykh system – MIMUZ2002. Lviv: TsMM IPPMM im. Ya. S. Pidstryhacha NAN Ukrainy, Vyd-vo Akhil, 153–159.
31. Gayvas, B. I., Dmytruk, V. A., Semerak, M. M., Rymar, T. I. (2021). Solving Stefan's linear problem for drying cylindrical timber under quasi-averaged formulation. Mathematical Modeling and Computing, 8 (2), 150–156. <https://doi.org/10.23939/mmc2021.02.150>
32. Kondrat, V. F., Kubik, Yu., Chaplia, Ye. Ya. (2000). Vzaiemodiia mekhanotermoelektrodyfuziinykh protsesiv v porystomu nasychenomomu seredovyshchi. Mashynoznavstvo, 8, 3–9.
33. Gayvas, B., Dmytruk, V., Kaminska, O., Pastyrska, I., Dmytruk, A., Nezgoda, S. (2020). Simulation of Crack Resistance of Mustard in Pulsed Drying Mode. 2020 IEEE 15th International Conference on Computer Sciences and Information Technologies (CSIT), 91–94. <https://doi.org/10.1109/csit49958.2020.9321941>

34. Gayvas, B., Markovych, B., Dmytruk, A., Dmytruk, V., Kushka, B., Senkovych, O. (2023). Study of Contact Drying Granular Materials in Fluidized Bed Dryers. 2023 IEEE XXVIII International Seminar/Workshop on Direct and Inverse Problems of Electromagnetic and Acoustic Wave Theory (DIPED). Tbilisi, 238–241. <https://doi.org/10.1109/diped59408.2023.10269464>
35. Gayvas, B. I. (2004). On the influence of electroosmosis on two-sided convective drying of a porous layer. *Volyn Mathematical Bulletin*, 2 (11), 74–85.
36. Gayvas, B., Markovych, B., Dmytruk, A., Havran, M., Dmytruk, V. (2024). The methods of optimization and regulation of the convective drying process of materials in drying installations. *Mathematical Modeling and Computing*, 11 (2), 546–554. <https://doi.org/10.23939/mmc2024.02.546>
37. Polos, A. V. (2006). *Pidvyschennia efektyvnosti konvektivnoho sushinnia pylomaterialiv (na prykladi umovnoho material)*. [Dissertation].
38. Dmytruk, A. (2024). Modeling mass transfer processes in multicomponent capillary-porous bodies under mixed boundary conditions. *Mathematical Modeling and Computing*, 11 (4), 978–986. <https://doi.org/10.23939/mmc2024.04.978>
39. Gayvas, B. I. (2003). *Dynamika vologosti porystogo sharu pry osushuvanni z odniyeyi pov-erkhni*. Konferentsiia profesorsko-vykladatskoho skladu DU “Lvivska politekhnika”. Lviv, 7–9.
40. Grinchik, N. N. (1991). *Protcesy perenosa v poristyykh sredakh, elektrolitakh i membranakh*. Minsk: ITMO im. A.V. Lykova AN BSSR, 310.

## CHAPTER 3

## MATHEMATICAL MODELING OF DRYING PROCESSES IN POROUS MATERIALS CONSIDERING CAPILLARY PROPERTIES

## ABSTRACT

The Chapter aims to provide a detailed understanding of the drying kinetics and to identify conditions under which drying is most efficient, considering external factors such as airflow and electric fields. The model aims to predict the distribution of liquid and gas phases within the porous structure and the resulting mechanical stresses, contributing to optimizing drying processes in industrial applications. A particular focus is on the capillary properties of the porous medium being dried. Moreover, a sustainable mathematical model is proposed for analyzing the moisture and temperature distribution, radial displacements, and stresses within a multicomponent dispersed material of the capillary-porous structure. By solving the key system of differential equations for mass and heat transfer, and incorporating the mechanical properties of the material, the model predicts the changes in moisture concentration, temperature, and mechanical stresses in a material at any point in time and its placement within the layer. The work results provide insights into the drying kinetics and mechanical behavior of the grain under different drying conditions.

## KEYWORDS

Drying, porous materials, capillary properties, phase transition, mass transfer, diffusion, drying kinetics, mathematical modeling, structural model.

In modern conditions, sustainability is the primary requirement for developing all technologies used in the national economy. The field of agricultural product processing, specifically drying, is no exception. Since drying is an extremely energy-intensive process, one of the main requirements for its implementation is saving energy resources. Therefore, engineering tasks aimed at reducing energy consumption in the drying of agricultural products are urgent and relevant.

The application of mathematical modeling is one of the effective ways to solve engineering problems due to the accessibility of its tools and their powerful capabilities. Specifically, mathematical modeling is widely used to develop new drying technologies.

The problem under consideration is the convective-heat drying of a layer of wet dispersed material with a capillary-porous structure. It is possible to consider the stage of falling drying, when the grain is already heated to the desired temperature and is dried for a certain period of time. The heating of the drying agent stops, i.e., the grain is blown by the drying agent of an ambient temperature. This will provide an opportunity for crucial savings on energy resources.

Models of drying are typically based on the thermodynamics of irreversible processes. The hypothesis of local thermodynamic equilibrium is accepted, which, for small deviations from the equilibrium position in continuous media, is justified in the works of S. de Groot, I. D'yarmati, A. Kovalenko, and others.

Along with internal energy, the existence of a state function, entropy, is postulated. The concept of entropy is introduced to distinguish between reversible and irreversible processes. The acceptance of the hypothesis of local equilibrium, considering the equations of state, entropy balance, energy, mass, and momentum in many cases allows for the determination of all parameters characterizing the irreversible process.

Drying models must consider the actual mechanisms of heat and moisture transfer depending on the drying method, the impact of kinetic and geometric characteristics of the body, the controlling parameters of the drying agent, and their impact on the stress-strain state and stability of body shapes, maintaining their quality during the drying process. They are based on specific macroscopic physico-mathematical models of heat and mass transfer and require effective analytical-numerical methods for solving the corresponding boundary value problems of mathematical physics.

For the physico-mathematical modeling of processes in solid bodies, thermodynamic methods have been developed in the works of Y. Burak, E. Chaplya, O. Chernukha, and others [1]. Special attention is required for the mathematical description of the material structure. From the perspective of significance for the agro-industrial and food sectors of Ukraine's economy, special attention is deserved by the modeling of drying processes of dispersed bodies with capillary-porous structures, which are multiphase and heterogeneous.

The mathematical model of drying capillary-porous bodies, as a special case of the heat and mass transfer model in an  $n$ -component three-phase deformable porous moist medium with phase transitions and chemical reactions, studies the evolution of temperature, moisture content, pressure, kinematic characteristics of the process, sensitivity to parameter influences and boundary conditions. A moist porous body is generally considered as a three-phase medium containing a skeleton (porous or granular structure), liquid, and gas (homogeneous steam-air mixture), filling the pores or gaps between the grains, although the material is generally treated with chemically active mixtures before drying, interacting both among themselves and with the material, forming  $n$ -phase structures.

For reflecting multiphase nature, approaches of mixture theory and methods of multi-velocity system mechanics, capillary models of the porous body, and combined methods are used. When modeling heat and mass transfer processes, capillary models are used, and when solving mechanics problems, methods of homogenizing the heterogeneous structure are employed, obtaining physical

relationships for the body as a whole based on certain assumptions about the nature of temporal and spatial changes in the studied fields.

The continuum-thermodynamic approach to building physico-mathematical models of solid solution mechanics, describing interconnected mechanical, thermal, and diffusion processes, considering local state changes of the components, was developed in the works of Y. Burak, E. Chaplya, O. Chernukha, B. Gayvas, B. Gera, and others. This approach is based on the following propositions: for spatially inhomogeneous and non-equilibrium systems, the hypothesis of local thermodynamic equilibrium is accepted, implying that the state of physically small subregions of the system is determined by conjugated physical parameters describing the equilibrium state. For describing mechanical, physical, and chemical processes, the conjugated parameters are pressure and volume; stress tensor and strain tensor; thermal conductivity – absolute temperature and entropy; diffusion – chemical potential and particle concentration. To determine the change in mass, energy, and momentum, balance and kinetic relationships and equations of state are used.

The description of interconnected thermal, mechanical, and diffusion processes in porous multi-continuum media was considered by B. Gayvas, O. Hachkevych, L. Khoroshun, Y. Kubik, R. Kushnir, R. Terlets'kyi, V. Chekurin and other scientists. If the characteristic distances over which the system parameters change are greater than the characteristic dimensions of the inhomogeneities, the principle of homogenizing the heterogeneous structure is used. Then the macroscopic parameters are taken as the average effective coefficients over elementary volumes, satisfying the classical equations of thermoelasticity. The effective coefficients for granular, fibrous, and layered media were determined based on stochastic equations for micro-inhomogeneous bodies.

For building models of finely dispersed media, the approach of multi-phase media mechanics is also used, developed in the works of A. Neimark, L. Heifets, R. Nigmatulin, V. Nikolaevsky, and other scientists.

Mathematical models of drying porous bodies are based on the laws of conservation of mass, momentum, and energy, as well as known experimental dependencies, on the basis of which equations of heat and mass transfer of moisture in the body are constructed. The possibility of quantitative estimation of heat passing inside the body due to thermal conductivity is based on Fourier's hypothesis. At the same time, diffusion flows are considered based on Fick's laws, and filtration flows on Darcy's law. The similarity of heat and mass transfer processes is considered in the works of A. Kutz, V. Mustyats, M. Razin, and others. When building models of convective mass transfer, both conditions of convective mass exchange and conjugated problems using boundary layer theory are considered. In addition, the drying model includes the basics of the theory of thermoelasticity of viscoelastic bodies, considering the anisotropy of the structure and the basics of the theory of shape stability [2].

The formulation of drying problems is based on models describing interconnected phenomena and processes of heat and mass transfer and deformation occurring during drying. The drying process is not only a thermophysical one but also a technological one, where the forms of moisture bonding with the material, the regularities of heat and moisture transfer in wet materials during the interaction of porous bodies with hot surfaces, heated gases, and electric fields play

a significant role. During drying, the technological, biological, and structural-mechanical properties of the material change, due to the change in the forms of moisture bonding with the material and its partial removal by evaporation. The science of the forms of moisture bonding with the material was developed by P. Rebinder and further developed in the works of S. Lipatov, G. Maksimov.

P. Kostrobij's research in the field of thermodynamic potentials, diffusion processes, and simulation of interactions in a semi-infinite medium is related to the mechanisms of heat and mass transfer and reaction-diffusion processes in porous materials during drying and can be successfully applied to such problems. B. Markovych, M. Tokarchuk, I. Ryzha and others suggest using non-integer integral-differentiation to model systems, which are characterized by "memory" effects, structural heterogeneity, spatial non-locality, deterministic chaos, and self-organization.

A large number of works are devoted to the mathematical description and quantitative study of drying porous materials in stationary and non-stationary modes. Among them, the works of A. Bomba, N. Grinchik, O. Lykov, P. Lutsyk, Y. Sokolovsky, describe the processes in porous media based on the principle of homogenizing the heterogeneous structure of the body. The basics of this theory for describing moisture transfer within the material are formulated based on the classical theory of diffusion by P. Kosovich, A. Lebedev, Y. Miniovich, U. Lewis, and T. Sherwood.

In his research, O. Lykov introduced the concept of mass transfer potential, which serves as the driving force for the fluid flow under isothermal conditions and is based on experimental laws of heat and moisture conductivity [3]. The quasi-homogeneous approximation was used to analyze transfer processes, assuming the replacement of the real dispersed medium with a continuous medium with effective coefficients. The heat and moisture transfer equations included empirical coefficients dependent on temperature and pressure. Drying processes of capillary-porous bodies were studied within the framework of the single-continuum approach and based on the thermodynamics of irreversible processes. For modeling the vapor source, the phase transition criterion was introduced. This parameter is generally considered a function of moisture content but depends on all process parameters and can be arbitrarily assigned by different authors.

Also, O. Lykov obtained a system of differential equations of heat and mass transfer in capillary-porous materials in the region of hygroscopic moisture content. In particular, it is assumed that the non-equilibrium state of the system at any moment of the drying process is caused by the inhomogeneous distribution of temperature, moisture content, excess pressure, and deformations. The increase in entropy in systems is associated with irreversible processes of thermal conductivity, molecular and convective diffusion, phase transition, moisture-thermal deformation, and irreversible cross-processes (Dufour and Soret effects).

T. Sherwood proposed the hypothesis of deepening the surface of moisture evaporation during drying. The walls of the porous body skeleton absorb water, causing the body to swell when moistened and shrink when dried. To simplify the analysis of transfer processes in finely dispersed bodies, it is advisable to use averaged characteristics, whose use in models, as experiments show, gives results close to measured ones. The optimal control for the element functional properties under heating and the methodology for predicting its behavior is realized in [4].

In the views on the mathematical modeling of heat and mass transfer in the non-stationary case, significant differences arose among scientists. For example, L. Heifets and A. Neimark believed that the formal introduction of the mass transfer potential obscures the real mechanisms of mass transfer [5]. Since the relationship between the evaporated liquid flow and the specific saturation is nonlinear, determined by geometric characteristics, the use of thermodynamics of irreversible processes and Onsager's relationships, which assume a linear dependence of flows on thermodynamic forces, is unfounded. Their mathematical modeling methods for the drying process are based on the description of multiphase processes in porous media. The mutual distribution of phases in the pore space is one of the main characteristics of multiphase heterogeneous processes in porous media. In the case of processes with phase transitions, the mutual distribution of phases is established as a result of one phase transitioning into another and the redistribution of phases within the porous body due to the difference in capillary properties.

Recently, for modeling filtration processes in porous media, it has been proposed to use differential equations with fractional-order derivatives both in time and coordinates (O. Lopatiev, Y. Pyanylo, A. Torsky and others) [6].

A large number of works are devoted to the interaction of the body with the drying agent. Heat and mass exchange between the material being dried and the environment (drying agent) is one of the determining factors of the process. Heat exchange coefficients can be obtained directly from experiments, analytically using boundary layer theory and statistical methods, as well as from criterion equations.

The heat exchange coefficient during forced movement of the environment is obtained from the Nusselt criterion based on the criterion equation  $Nu = f(Re, Pr)$ , constructed empirically from experimental data.

Experimental studies by I. Fedorov, F. Polonskaya, and others have shown that the heat exchange coefficient in the drying process is greater than the pure heat exchange coefficient under the same conditions. In works of O. Lykov, P. Lebedev, V. Frolov and G. Shubin, it is shown that the heat exchange coefficient is constant only during the period of constant drying rate. In the period of falling drying rate, it continuously decreases, approaching the value of dry body heat exchange.

An important component of optimization the modeling drying processes is determining the effect of porosity change on the stress state of the body [7]. The stress-strain state of the body can change, and the body can lose its stability under the action of various physico-chemical processes (mechanical action, drying, phase transitions, etc.). Due to the need for a more detailed study of the mutual influences of stresses on mass transfer and mass transfer on stresses in a porous layer, many studies are conducted. It is considered appropriate when describing mass transfer processes to proceed from capillary models of the porous body, and when describing strength characteristics from homogenized models considering distortion caused by heat and mass transfer processes. Inhomogeneous deformations lead to the appearance of residual stresses, which are superimposed on the stresses caused by mechanical actions and can cause instability of the equilibrium shape.

### 3.1 MATHEMATICAL MODELING OF THE DRYING PROCESS

Mathematical modeling of the drying process is based on the selection of a model for the structure of the porous material; taking into account the specifics of multiphase mass transfer (interaction of phases with each other; considering phase and capillary forces that determine the mutual distribution of phases in the elementary physical volume of the porous body on one hand, and on the other are the driving forces of the process); formulation of boundary value problems that reflect the interaction of the external environment with the porous material under characteristic methods of drying intensification.

The movement of moisture under the influence of temperature (thermo-moisture conductivity) includes phenomena [3]:

- molecular diffusion of moisture, in the form of molecular leakage of steam, which occurs due to different velocities of molecules in the heated and cold layers of the material;
- capillary conductivity, due to the change in capillary potential, which depends on surface tension, which decreases with increasing temperature, and since the capillary pressure over the concave meniscus is negative, the decrease in pressure increases the suction force, resulting in moisture in the form of liquid moving from the heated layers of the body to the colder ones;
- movement of liquid in the porous body in the direction of the heat flow caused by the presence of trapped air. When the material is heated, the pressure of the trapped air increases and air bubbles expand. As a result, the liquid in the capillary pore is pushed in the direction of the heat flow (trapped air pushes the liquid to layers with a lower temperature).

The influence of trapped air, porosity, temperature, and material saturation with moisture on the process of conductive drying of a capillary-porous body is considered in [8, 9].

Since real porous materials have an irregular and random structure, stochastic structural models can claim adequacy [10, 11]. Statistical analysis of the distribution of liquid and gas in hydrophilic porous media is based on representing the pore space as a system of channels with variable cross-sections, which create a stochastic spatial lattice with a certain coordination number [5]. This representation allows the problem of liquid and gas distribution to be reduced to the problem of the mutual distribution of liquid and gas pores in a random lattice with certain statistical properties. Using the apparatus of penetration theory (percolation), it is shown that in the pore space during drying, moisture forms three characteristic configurations: a connected system of gas-filled pores that exits to the outer surface; a two-phase system (a set of unconnected liquid inclusions blocked by gas); and a liquid pore system. For each specific porous structure, there is a critical moisture content, at which the connectivity of the liquid phase is completely disrupted, and all moisture is localized in isolated inclusions. The value of the critical moisture content is a structural characteristic of the porous medium and can be used for a comparative analysis of different porous structures [12].

The mutual distribution of phases in the pore space has a significant impact on the processes occurring in the body. It determines the effective transfer coefficients across phases, the magnitudes of interphase surfaces [13]. Capillary forces are responsible for the phase distribution.



Changes in the liquid content in the porous body occur through liquid evaporation and capillary absorption [5]. The heat and mass transfer processes occurring in the pores, the properties of liquids and gases in the pores, and the methods of their modeling are covered in [13]. Experimental studies of diffusion, capillary, and film transfer mechanisms [5] indicate the decisive influence of capillary and surface forces on the mass transfer process and drying intensity. An overview of research results on heat and mass transfer in porous media is provided in [13, 14].

To account for the influence of geometric factors, it is possible to use a statistical consideration of the process in an elementary physical volume based on a certain structural-metric model. One type of capillary model is systems of parallel capillaries of different radii. The statistical average can be represented using the distribution function. The capillary radius distribution function correlates with the functions of pore size distribution measured by various methods. This correlates with the method of studying the filtration of cement stone, wood, and other porous materials based on their averaged characteristics, which allows not to account for fluid movement along winding paths and interflows and to consider the porous body as a material with homogeneous properties for the chosen filtration direction. The reproduction of the mass transfer pattern using capillary models based on the description of the sizes and shapes of pores in porous bodies is proposed in work [5].

### 3.1.1 HEAT AND MASS TRANSFER WITH THE EXTERNAL ENVIRONMENT

A significant number of works are devoted to the interaction of the body with the drying agent. Heat and mass transfer between the dried material and the medium (drying agent) is one of the determining factors of the process. The heat transfer coefficients can be obtained directly from experiments, analytically using the boundary layer theory [15], and statistical methods, as well as from criterial equations [3]. The boundary layer theory [15] provides solutions to various problems of the hydrodynamic boundary layer. Based on experimental studies, N. Mikheev and B. Smolsky indicated the influence of internal mass transfer on the field of partial pressures at the beginning of the drying process and concluded that the heat transfer coefficient must be calculated based on the solution of the conjugation problem.

To generalize experimental data when describing the drying process, the theory of similarity is also used, which allows combining physical quantities that characterize the process into dimensionless complexes. The obtained criteria are considered as new variables that reflect the influence of both individual factors and their combination [3].

The heat transfer coefficient during forced movement of the surrounding medium is obtained from the Nusselt criterion based on the empirical criterial equation constructed from experimental data.

Experimental studies by I. Fedorov, F. Polonskaya, and others showed that the heat transfer coefficient during drying is higher than the pure heat transfer coefficient under the same conditions. In the works of O. Lykov, P. Lebedev, and G. Shubin, it is shown that the heat transfer coefficient is constant only during the period of constant drying rate. During the period of falling

drying rate, it continuously decreases, approaching the heat transfer value of the dry body. The driving force of moisture exchange during moisture evaporation is considered to be the difference in partial pressures between the surface layer and the surrounding medium, although in the environment of superheated steam, the difference in partial pressures is absent. O. Lykov believed that molecular-molecular mass exchange on the surface is determined by the gradient of the chemical potential and the total pressure. Calculations in this case showed that the necessary mass transfer can be ensured only under the condition of a slight overheating of the surface of the wet sample relative to the saturation temperature at a given pressure.

There is also an opinion that mass exchange during drying in a stationary environment is determined by the chemical potential difference between the surface of the body and the heat carrier. This explains the significance of the medium temperature, higher than 1400 °C, if drying of thin material in the environment of superheated steam exceeds the drying rate in the air environment. Experiments on geometrically identical samples with different initial moisture contents at a constant Reynolds number showed a decrease in the heat transfer coefficient with decreasing initial moisture content. Reducing the hydraulic radius increases the heat transfer coefficient. To determine the mass transfer coefficient, it is considered advisable to use the analogy between heat transfer and mass transfer.

Within the framework of the capillary approach, for porous bodies with small dispersion of the transverse dimensions of pores in the quasi-stationary approximation, complete systems of relations for describing the processes of natural or stimulated by blowing or external constant electric field drying are formulated.

In the works [16, 17], the problems of isothermal two-sided drying of an initially moisture-saturated porous layer under the action of an external constant electric field are solved by adopting the model of cylindrical capillaries of a porous material. The law of phase boundary movement in time is determined for problems of enhancing natural two-sided drying of a porous layer, and the influence of electroosmosis on the drying of a porous layer under both natural and convective drying of one of the surfaces is investigated. Quantitative studies of the change in relative humidity over time due to the magnitude of the electric field intensity are conducted.

It is shown that with the increase in the intensity of the electric field, the drying process intensifies. The dependence of the critical time and the corresponding moisture content on the characteristics of the material and the intensity of the electric field is established. The curves of the relative moisture content over time during two-sided drying have a characteristic kink. Quantitative studies of the dynamics of the relative humidity of the layer indicate a reduction in drying time compared to the case when electroosmosis is absent.

In the work [19], a system of equations for the electrodynamics of a hereditary electroconductive nonferromagnetic porous body, taking into account the dependence of its characteristics on moisture and temperature, is formulated. The problem of high-frequency heating for such bodies is considered. The dependence of the heating intensity on the distance from the electrodes to the surface of the body being heated is studied. The absorption of heat and moisture by the solid body

leads to an increase in its volume, which, being non-uniform, creates stress. In particular, cyclic changes in the external conditions in which the material is located create variable stresses that can lead to the growth of defects of dangerous sizes.

Advancements in science and engineering have been significantly driven by the observed similarities between heat and mass transfer processes and the universality of diffusion equations. By leveraging common principles and mathematical descriptions, scientists and engineers can develop more efficient and effective solutions across a wide range of applications.

Recent investigations into complex systems have utilized heat and mass transfer models to achieve various outcomes. For instance, in [21] there is proposed an innovative approach for image restoration and contrast enhancement using a nonlinear reaction-diffusion model. This model simulates the behavior of a heat equation in low-gradient areas while halting diffusion in high-gradient regions to preserve edges. Their algorithm employs a divide-and-conquer technique coupled with a reaction-diffusion system. Similarly, a novel numerical approach using the Lattice Boltzmann method for a Gray-Scott-based reaction-diffusion model was introduced in [22], effectively handling noisy images by comparing pixel motion to fluid motion.

Further contributions include [23], which proposed a spatio-temporal dynamics model for a tritrophic reaction-diffusion system, offering methodologies for optimal system control. In [24], the spatio-temporal dynamics using a fractional order SEIR model, relevant for understanding drying processes, are explored. The work [25] developed a nonlinear fractional partial differential equation for image inpainting, applying nonlinear diffusive filters. Stability analysis techniques for reaction-diffusion systems with delay, essential for drying process models, are provided in [26]. In [27], a diffusive phytoplankton–zooplankton–nanoparticle model with a density-dependent predator death rate is formulated, as well as the analysis of its local stability. A time-fractional diffusion equation for image and signal smoothing is used in [28], demonstrating the use of anomalous diffusion behaviors in image processing.

In the context of catalytic reactions, in [29] it is provided a statistical description of catalytic hydrogen oxidation, incorporating both the diffusion of reactants and the magnetic properties of ions and atoms involved. A generalized Cattaneo-type diffusion equation in time-fractional derivatives was developed for electrons, accounting for the complexity of relaxation electromagnetic diffusion processes in layered nanostructures in [30]. In [31], it is suggested a discrete solution for nonlinear parabolic equations with diffusion terms, proving the existence and uniqueness of weak solutions using an internal approximation combined with the backward Euler scheme. A DDFV scheme for nonlinear parabolic reaction-diffusion problems on general meshes, applicable to complex geometries in capillary-porous structures is developed in [32]. In [16], solving Stefan's linear problem for drying cylindrical timber is addressed, proposing solutions for phase change problems in drying.

In [33], identification of diffusion scattering parameters for a modified viral infection model is proposed, while in [34] the examination of the dynamics of a diffusive SARS-CoV-2 model using fractional Laplacian operators is carried out. In [35], kinetic and hydrodynamic approaches in the theory of dense gases and liquids far from equilibrium are unified, under arbitrary Knudsen number

conditions, with insights into liquid and gas interactions. In [36], it is discussed coupled compressible two-phase flow, providing further insights into these interactions. In [37], focus is made on impurity diffusion processes, essential for accurately describing mass transfer equations.

In finance, it is proposed a penalty approach for pricing the American-style Asian option under the Merton model, capturing the skewness and kurtosis features of return distributions [38]. In [39], the diffusion of money income, providing methodologies for solving financial diffusion problems, is modeled. Calcium profiles in neuronal cells are studied in [40], allowing insights into the dependency of calcium concentration on variable diffusion coefficients.

The problem of optimizing the drying time of porous bodies is still relevant, determining the most efficient operation mode of the drying installation [7]. The optimization problem formulation includes a functional that should be minimized and a set of admissible solutions. As a rule, the objective function is a function of many variables. The objective functional is minimized on a set from the functional space. Given the environmental parameters, based on the solution of the direct drying problem of an initially moisture-saturated porous layer, the problem of minimizing the total drying time by temperature  $T$  and pressure  $P$  on the layer surface is formulated. The problem is reduced to the problem of minimizing the temperature on the moving phase transition front under certain constraints. The optimal pressure on the layer surface and the minimum temperature on the phase transition boundary that minimize the total drying time are found, given the known parameters of vapor and air densities (or relative humidity) and the temperature of the atmospheric environment, as well as the geometric parameters of the body and the boundary layer. If an analytical solution to the drying problem is found, choosing the necessary optimization criterion, one can optimize the drying regime of the material.

### 3.1.2 EQUATIONS OF THERMO-HYGRO-MECHANICAL PROCESSES IN A POROUS BODY IN THE HOMOGENEOUS APPROXIMATION (GENERALIZED COORDINATES: TEMPERATURE, DEFORMATION, MOISTURE CONTENT)

Consider a porous body in which the phase transition of liquid to vapor occurs, resulting in a vapor flow. The reduction of moisture in the body and its heating can cause shrinkage and thermal expansion of the material. Additionally, intensive drying generates additional pressure in the vapor-air mixture. Consequently, stresses arise in the body, the magnitudes of which, as studies show, can cause deformation and destruction of the body. In formulating the equations of thermo-mechanical-mass transfer, it is possible to follow the works [3, 11].

Assume that the primary physical processes occurring in the body during drying are mass and heat transfer and deformation. Let's consider these processes in the homogeneous approximation. Under the hypothesis of local equilibrium, the thermomechanical state of a physically small element of the body will be characterized by the parameters: stress tensor  $\hat{\sigma}$  – strain tensor  $\hat{e}$ ; temperature  $T$  – entropy  $S$ ; chemical potential  $\mu$  – moisture content  $W$ . The corresponding Gibbs

equation for free energy is written as [11]  $dF = \hat{\sigma} : d\hat{e} - SdT - \rho_0 \mu dW$ , where  $\rho_0$  is the density

of the absolutely dry body. The state equations in terms of moisture content are:  $\hat{\sigma} = \frac{\partial F}{\partial \hat{e}} \Big|_{T,W}$ ,  
 $S = -\frac{\partial F}{\partial T} \Big|_{\hat{e},W}$ ,  $\rho_0 \mu = -\frac{\partial F}{\partial W} \Big|_{T,\hat{e}}$ .

If the free energy of an elastic isotropic body is represented as a Taylor series expansion in terms of the components of the tensor  $\hat{e}$  and retaining terms no higher than second-order smallness [11]:

$$F(I_1, I_2, T, W) = F_0 + \frac{\partial F}{\partial I_1} I_1 + \frac{\partial F}{\partial I_2} I_2 + \frac{\partial^2 F}{\partial I_1^2} \frac{I_1^2}{2},$$

where  $F_0(0,0,T,W)$  is the free energy per unit volume in the absence of deformations;  $I_1 = e$  is the first invariant of the strain tensor;  $I_2 = e_{ij}e_{ij}$  is the second invariant of the strain tensor, then the components of the stresses can be expressed as:

$$\hat{\sigma} = \frac{\partial F}{\partial I_1} \frac{\partial I_1}{\partial \hat{e}} + \frac{\partial F}{\partial I_2} \frac{\partial I_2}{\partial \hat{e}} + \frac{\partial^2 F}{\partial I_1^2} \frac{\partial I_1}{\partial \hat{e}} I_1,$$

$$S = -\frac{\partial F_0}{\partial T} - \frac{\partial^2 F}{\partial I_1 \partial T} I_1 - \frac{\partial^2 F}{\partial I_2 \partial T} I_2 - \frac{\partial^3 F}{\partial I_1^2 \partial T} \frac{I_1^2}{2},$$

$$\rho_0 \mu = -\frac{\partial F_0}{\partial W} - \frac{\partial^2 F}{\partial W \partial I_1} I_1 - \frac{\partial^2 F}{\partial I_2 \partial W} I_2 - \frac{\partial^3 F}{\partial I_1^2 \partial W} \frac{I_1^2}{2}. \quad (3.1)$$

In the absence of deformations  $\hat{e}$  the change in free energy  $F_0$  due to changes in temperature and moisture content and the averaged specific heat capacity in the isochoric process can be represented as follows:

$$F_0 = \int_{T_0}^T \left( \frac{\partial F_0}{\partial T} \right)_{W,e=0} dT + \int_{W_0}^W \left( \frac{\partial F_0}{\partial W} \right)_{T,e=0} dW,$$

$$\rho_0 C_{W,e} = T \left( \frac{\partial S}{\partial T} \right)_{W,e} = -T \left( \frac{\partial^2 F}{\partial T^2} \right)_{W,e}.$$

Then  $\left( \frac{\partial F}{\partial T} \right)_{W,e} = -\int_{T_0}^T \frac{\rho_0 C_{W,e}}{T} dT$ , where  $C_{W,e}$  is the specific heat capacity in the absence of

deformation and at constant moisture content.

If  $U$  is the internal energy of the body, then in an isothermal-isochoric process ( $T = \text{const}, \hat{e} = 0$ ):

$$\left( \frac{\partial F_0}{\partial W} \right)_{T, \hat{e}=0} = \left( \frac{\partial U}{\partial W} \right)_{T, \hat{e}} - T \left( \frac{\partial S}{\partial W} \right)_{T, \hat{e}},$$

where  $\left( \frac{\partial U}{\partial W} \right)_{T, \hat{e}}$  is the heat of the phase transition;  $T \left( \frac{\partial S}{\partial W} \right)_{T, \hat{e}}$  is the heat due to the irreversible transfer of the absorbed substance (Dufo effect).

At low temperatures  $T \left( \frac{\partial S}{\partial W} \right)_{T, \hat{e}} \ll \left( \frac{\partial U}{\partial W} \right)_{T, \hat{e}}$ , thus  $\left( \frac{\partial F_0}{\partial W} \right)_{T, \hat{e}} = \left( \frac{\partial U}{\partial W} \right)_{T, \hat{e}} = \rho_0 \varepsilon_\Phi r^*$ , where  $r^*$

is the specific heat of the phase transition;  $\varepsilon_\Phi$  is the degree of completeness of the phase transition, similar to the phase transformation criterion introduced by O. Lykov [3].

Taking into account that:

$$\frac{\partial F}{\partial l_1} = -K \left[ \alpha_{TW} (T - T_0) + \beta_{TW} (W - W_0) + \frac{1}{K} (P - P_0) \right] = -\frac{K}{3} \varepsilon, \quad (3.2)$$

$$\frac{\partial F}{\partial l_2} = G = \frac{E}{2(1+\nu)}, \quad \frac{\partial^2 F}{\partial l_1^2} = \frac{1}{3} (K - 2G) = \lambda = \frac{E\nu}{(1+\nu)(1-2\nu)},$$

where  $\nu$  is the Poisson's ratio;  $\lambda$  is the Lamé coefficient;  $E = \frac{(1+\nu)(1-2\nu)}{3\nu} (K - 2G)$  is the

Young's modulus;  $K$  is the bulk modulus;  $G$  is the shear modulus;  $\varepsilon$  is the resulting change in the unit volume of the body in the absence of stresses;  $T_0$  is the initial temperature;  $T$  is the actual temperature;  $P$  is the pore pressure;  $P_0$  is the atmospheric pressure;  $\alpha_{TW}$  is the coefficient of linear thermal expansion;  $\beta_{TW}$  is the coefficient of linear shrinkage.

The free energy of an elastic isotropic body can now be written as [3]:

$$F(\hat{e}, T, W) = Gl_2 + \frac{1}{6} (K - 2G) e^2 - Ke \left[ \alpha_{TW} (T - T_0) + \beta_{TW} (W - W_0) + \frac{1}{E} (P - P_0) \right] - \int_{T_0}^T dT \int_{T_0}^T \frac{\rho_0 C_{W, \hat{e}}}{T} dT + \rho_0 r^* \int_{W_0}^W \varepsilon_\Phi dW, \quad (3.3)$$

where  $e = \vec{\nabla} \cdot \vec{u}$  is the relative volume change of the body;  $\vec{u}$  is the displacement vector.

Then the state equations (3.1) take the form [3]:

$$S = -l_2 \frac{\partial G}{\partial T} - \frac{e^2}{6} \frac{\partial}{\partial T} (K - 2G) + e \frac{\partial}{\partial T} \left[ K \left( \alpha_T (T - T_0) + \beta_w (W - W_0) + \frac{1}{K} (P - P_0) \right) \right] + \int_{T_0}^T \frac{\rho_0 C_{W,\varepsilon}}{T} dT + \frac{\partial}{\partial T} \left( \rho_0 r^* \int_{W_0}^W \varepsilon_\Phi dw \right); \quad (3.4)$$

$$\rho_0 \mu = -l_2 \frac{\partial G}{\partial W} - \frac{e^2}{6} \frac{\partial}{\partial W} (K - 2G) + e \frac{\partial}{\partial W} \left[ K \left( \alpha_T (T - T_0) + \beta_w (W - W_0) + \frac{1}{K} (P - P_0) \right) \right] - \rho_0 \varepsilon_\Phi r^*; \quad (3.5)$$

$$\hat{\sigma} = 2G\hat{e} + \frac{1}{3} (K - 2G)\hat{e} - K \left( \alpha_T (T - T_0) + \beta_w (W - W_0) + \frac{1}{K} (P - P_0) \right) \hat{l}. \quad (3.6)$$

For small changes in moisture content and temperature, the equations (3.4)–(3.6) can be linearized by perturbations of these quantities:

$$S = \left( K\alpha_T + \frac{\partial P}{\partial T} \right) e + \rho_0 C_{W,\varepsilon} \frac{(T - T_0)}{T_0};$$

$$\rho_0 \mu = \left( K\beta_w + \frac{\partial P}{\partial W} \right) e - \rho_0 \varepsilon_\Phi r^*. \quad (3.7)$$

To derive the heat conduction equations, it is possible to use the entropy balance equation [3]:

$$T \frac{\partial S}{\partial t} = -\vec{\nabla} \cdot j_q - \mu \frac{\partial P}{\partial t} + l, \quad (3.8)$$

where  $\rho = \rho_0 (1 + W)$  is the density of the wet system;  $l$  is the total power of the heat sources;  $t$  is time;  $j_q = -\lambda_q \vec{\nabla} T$  is the heat flux.

Using the state equations, equation (3.8) is reduced to the heat conduction equation of the deformed system during drying:

$$\frac{\partial T}{\partial t} = a_q \nabla^2 T - \frac{K\beta_w e - \rho_0 \varepsilon_\Phi r^*}{\rho_0 C_{W,\varepsilon}} \frac{\partial W}{\partial t} - \frac{e}{\rho_0 C_{W,\varepsilon}} \frac{\partial P}{\partial t} - T_0 \frac{K\alpha_T + \alpha_p}{\rho_0 C_{W,\varepsilon}} \frac{\partial e}{\partial t}, \quad (3.9)$$

where  $a_q = \frac{\lambda_q}{\rho_0 C_{W,\varepsilon}}$  is the thermal diffusivity coefficient;  $\alpha_p = \frac{\partial P}{\partial T}$  is the temperature coefficient

of excess water vapor pressure, such that  $\frac{1}{\alpha_p}$  is the change in the phase transition temperature

due to the emergence of excess pressure.

The linearized equation of diffusion-convective mass transfer, according to [11], is written as:

$$\frac{\partial W}{\partial t} = \vec{\nabla} \cdot \left( a_m \vec{\nabla} W + a_m \delta \vec{\nabla} T + \frac{K_p}{\rho_0} \vec{\nabla} P \right); \quad (3.10)$$

$$\frac{\partial P}{\partial t} = \vec{\nabla} \cdot (a_p \vec{\nabla} P) - \frac{\varepsilon_\phi}{C_{W,\varepsilon}} \frac{\partial W}{\partial t}, \quad (3.11)$$

where  $a_m$  is the coefficient of molecular diffusion of substance absorption;  $a_p$  is the coefficient of convective diffusion;  $\delta$  is the coefficient of thermogradient mass transfer;  $K_p$  is the permeability of the system.

The equations of motion for a deformable system, neglecting the convective velocity component, are given by:

$$\vec{\nabla} \cdot \hat{\sigma} + \vec{F} = \rho \frac{\partial^2 \vec{u}}{\partial t^2}. \quad (3.12)$$

Here  $\vec{F}$  is the external force vector per unit volume. The components of the stress tensor  $\hat{\sigma}$  are determined by the relations (3.6). The relations (3.6), (3.7), (3.10)–(3.12) form a complete system and are used in the practice of investigating interconnected mechanical processes and heat-mass transfer processes. Considering the quasi-stationarity of the system's process, inertial forces in the equations of motion can be neglected. Then the equations of motion (3.12) can be written as:

$$\vec{\nabla} \cdot \hat{\sigma} + \vec{F} = 0. \quad (3.13)$$

When formulating problems of moisture-thermomechanics, it is necessary to add the appropriate boundary conditions to the equations (3.10)–(3.13). Initial conditions can be taken in the form:

$$T = T_0, \quad W = W_0, \quad P = P_0, \quad \vec{u} = \vec{u}_0, \quad \frac{\partial \vec{u}}{\partial t} = \vec{v}_0 \quad \text{at } t = t_0. \quad (3.14)$$

The boundary conditions for mechanical quantities involve specifying displacements or forces:

$$\vec{u} = \vec{u}_z \quad \text{or} \quad \hat{\sigma} \cdot \vec{n} = \vec{\sigma}_z \quad \text{for } \vec{r} \in (\Sigma). \quad (3.15)$$

The surface conditions for thermal quantities can be of the first, second, or third kind, i.e.:



$$T = T_\Sigma \text{ or } \vec{q} \cdot \vec{n} = q_\Sigma \text{ or } \frac{\partial T}{\partial n} - \lambda_T (T - T_0) = 0, \quad (3.16)$$

where  $\vec{n}$  is the normal to the surface ( $\Sigma$ ). Similar conditions can be set for moisture content  $W$ :

$$W = W_\Sigma \text{ or } \vec{j}_w \cdot \vec{n} = j_\Sigma \text{ or } \frac{\partial W}{\partial n} - \lambda_w (W - W_0) = 0. \quad (3.17)$$

The boundary conditions for pressure  $P$  on the surface ( $\Sigma$ ) typically reflect the equality of this pressure to the atmospheric pressure or the pressure in the boundary layer [5]:

$$P = P_\Sigma. \quad (3.18)$$

When considering semi-infinite regions, it is necessary to add appropriate conditions (boundedness of the solution) at infinity. For cylindrical or spherical regions using cylindrical or spherical coordinate systems, it is also necessary to formulate boundedness conditions on the cylinder axis or at the sphere center.

For isothermal processes, equation (3.9) is not considered, and equations (3.10), (3.11) are reduced to the system:

$$\begin{aligned} \frac{\partial W}{\partial t} &= \vec{\nabla} \cdot \left( a_m \vec{\nabla} W + \frac{K_p}{\rho_0} \vec{\nabla} P \right); \\ \frac{\partial P}{\partial t} &= \vec{\nabla} \cdot \left( a_p \vec{\nabla} P \right) - \frac{\varepsilon_\phi}{C_{w,\varepsilon}} \frac{\partial W}{\partial t}. \end{aligned} \quad (3.19)$$

This allows the moisture mechanics problem to be solved sequentially. In the first stage, it is necessary to find the solutions of the mass transfer problem (3.14), (3.17)–(3.19) with subsequent determination of the stress-strain state of the body from the mechanics equations (3.6), (3.13), (3.15). When solving the mechanics problem, the solutions of the mass transfer problem are used. Experimental studies show that the equilibrium distribution of liquid in the pore space

during evaporation is determined by the relative vapor pressure  $\chi = \frac{P}{P_s}$ , or the related capillary pressure  $P_k = \frac{RT}{V_L} \ln \chi$ . As  $\chi$  increases, the porous body is saturated with capillary condensate,

and as  $\chi$  decreases, evaporation occurs and the porous body is saturated with gas by moving the meniscus along the pore. This means that under nonequilibrium conditions, gradients of capillary and surface forces are the driving forces of mass transfer in the gas and liquid phases and have a decisive influence on the intensity of mass transfer. Gradients of partial and disjoining pressures arise

due to the uneven moisture content during drying. During drying, the amount of liquid decreases due to the release of pores from condensate, thinning of films, and reduction of relative vapor pressure. Since the amount of liquid in films and in the gas phase is small compared to bulk liquid, it makes sense to only track changes in saturation. The space freed from the liquid is occupied by air. Since the molar volume of air is greater than the molar volume of the liquid, the air flow is much smaller than the liquid flow and can be neglected. The equations of motion during evaporation represent filtration equations complicated by diffusion in the gas phase.

### 3.1.3 MATHEMATICAL MODELING OF THE DRYING PROCESS OF POROUS BODIES CONSIDERING CAPILLARY PROPERTIES

To describe the mutual distribution of phases in a porous medium, structural models of porous media, particularly with irregular and random structures, are used. In this regard, it is necessary to use stochastic structural models [5]. The pore space is treated as a statistical ensemble of interconnected structural elements (pores), whose distribution is probabilistic. The most suitable model should be a simple statistical model that adequately describes the structure. To establish effective transfer coefficients for each phase, their connections as functions of macrovariables, conditions of the process in an individual pore, and geometric characteristics of the porous structure, the choice of an appropriate averaging technique is crucial. The necessary characteristics to describe the kinetics of the process in an individual pore are obtained based on mathematical models, the results of which are confirmed by experimental studies in capillaries [14].

The construction of capillary models is based on comparing known literature data on the sizes of the conductive elements of the material obtained through microscopic studies of the body's structure with the corresponding data obtained using capillary conductivity kinetics [5].

In real materials, whose pores represent a complex system of heterogeneous elements, capillary equilibrium is established, and the filling of an individual pore by a particular phase depends on the characteristics of the pore and its connections with other pores. The properties of the mutual distribution of phases are determined both by the distribution function of the structure characteristics of individual elements and by parameters reflecting the interconnection of these elements. The influence of the porous structure is taken into account by introducing effective coefficients of binary interaction into the Stefan-Maxwell equations [16]. Effective transfer coefficients are determined by the random geometry of the pore space, the nature of microinhomogeneities, or empirical dependencies that relate them to the parameters of the porous structure. In a quasi-homogeneous approximation, macroscopic transfer equations are applied, the structure of which coincides with the structure of equations valid in an individual elementary pore, in most cases in a straight cylindrical capillary.

The simplest model of the pore space of a polydisperse porous body is a system of cylindrical capillaries with ideal connections. In such a model, if the pores of radius  $r_f$  are filled with wetting

liquid, then the pores of smaller radius are necessarily filled as well. This implies that each saturation value  $\alpha_m = \bar{z}_m = \frac{L_m}{L}$  corresponds to a critical radius  $r_f(\bar{z}_m)$  of the filled pores, where  $L_m$  is the

moving phase transition coordinate. The walls of other pores with a radius  $r > r_f$  are covered with equilibrium polymolecular films. The film flow equation in the porous medium can be represented as

$$j_{pl} = -\frac{[K_{pl}(\chi)]}{\mu_l V_L} \nabla P_L, \text{ where } [K_{pl}(\chi)] = \Pi \int_{r_f}^{r_{\max}} \frac{h^3(r, \chi)}{r} \phi(r) dr \text{ is the effective permeability coefficient of the films, which depends on the relative vapor pressure } \chi; r_f(\chi) \text{ is the boundary radius of the filled pores at relative vapor pressure } \chi \text{ (in the gas zone } r_f(\chi) = r_{\min}); \Pi \text{ is the porosity; } \mu_l \text{ is the viscosity.}$$

The equilibrium film thickness  $h$  is determined by the relation  $\frac{A}{6\pi h^3} = \frac{RT}{V_L} \ln \frac{P}{P_n}$ . For water,

$A = 7 \cdot 10^{-21}$  J;  $V_L$  is the molar volume;  $h$  is the equilibrium film thickness;  $R$  is the gas constant;  $T$  is the absolute temperature. The relative pressure of saturated vapor  $\chi$  over the curved surface

of the meniscus is determined by the Kelvin equation:  $\chi = \frac{P}{P_n} = \exp \left\{ -\frac{2\sigma_{lg} \cos \theta V_L}{RT r} \right\}$ , where  $P_n$  is

the saturated vapor pressure over a free surface;  $\sigma_{lg}$  is the surface tension;  $r$  is the radius. In the framework of the "well-mixed pores" model, the averaging operations for the gas phase are integration operations over  $r$  with a weighting function  $\phi(r)$  within the limits  $[r_f(r); r_{\max}]$ , for example

$$K_{pl}(r) = \frac{2A r_f(r)}{\mu \sigma_{lg}} \int_{r_f(r)}^{r_{\max}} \frac{\phi(r) dr}{2r - r_f(r)}.$$

Experimental studies show, and theoretical ones confirm, that polymolecular films should be taken into account only when  $\chi > 0.96$ . In capillaries with a radius of  $r < 10$  nm, which are filled with capillary condensate at  $\chi > 0.96$ , film flow is not observed. In wide pores with molecular diffusion mode ( $r > 500$ – $1000$  nm), vapor flow prevails, while in narrow capillaries with a radius of  $10 < r < 50$  nm,  $\chi > 0.96$ , film flow must be considered. In transitional pores ( $50 < r < 500$  nm), the contributions of both mechanisms to mass transfer are comparable [3]. In pores with molecular diffusion mode, film flow can be neglected. In [3], it is argued that film transport of liquid due to the gradient of disjoining pressure and thermosmosis at temperatures of the wet zone  $60$ – $70$  °C can also be neglected. These assumptions are justified for intensive drying, where the heating of the wet zone occurs quickly, and the processes of internal evaporation and redistribution of film moisture have much less impact than the processes of moisture removal due to phase transitions.

The pressure in the gas zone consists of the partial pressures of vapor and air. In the case of a gas pore (a pore free of capillary condensate), the transfer is carried out both by convection and diffusion of the vapor-air mixture and by film flow under the influence of the disjoining pressure gradient.

The averaged flow in the gas zone is as follows:

$$\langle J(r) \rangle = \langle j_v \rangle + \langle j_{pl} \rangle + \langle j_D \rangle = -\rho_v \frac{K_g(r)}{\mu_g} \nabla P_g(r) + \rho_l \frac{K_{pl}(r)}{\mu_l} \nabla P_{kap}(r) + D_{1va} \nabla \rho_g,$$

where  $K_g$  and  $K_{pl}(r)$  are the effective permeability coefficients for the gas zone and film filtration;

$D_{1va}$  and  $\rho_g$  are the effective diffusion coefficient and gas density, respectively, and  $P_{kap}(r) = \frac{2\sigma_{lg} \cos \theta}{r_f}$ ,

where  $r_f$  is the critical radius. In the presence of a partial pressure gradient in the gas phase, vapor flow is observed in the capillary. The nature of gas movement in a straight cylindrical capillary is

determined by the parameter  $Kn = \frac{\lambda}{2r}$  (the Knudsen number, which represents the ratio of the

number of molecular collisions with the walls to the number of intermolecular collisions), where  $\lambda$  is the mean free path length of the molecules, which depends on the gas composition and the total pressure of the mixture, and  $r$  is the radius. Depending on the Knudsen number, there are three characteristic regions of gas flow: Knudsen flow ( $Kn \rightarrow \infty$ ), transitional flow ( $Kn = 1$ ), and molecular flow ( $Kn \rightarrow 0$ ).

The use of the “dusty gas” model allows the identification of the structure of binary interaction coefficients in the Stefan-Maxwell system of equations. Within this model, interpolation formulas for effective diffusion coefficients in the transitional region between Knudsen and molecular diffusion are derived. They are also applied when the linear dimensions of the pores are so small that they are comparable to the mean free path length of the molecules. The generalized gas-kinetic binary diffusion coefficients, obtained in the first approximation of the Chapman-Enskog method, have the form:

$$D_{ij} = \left( \frac{3}{8} \pi R T / 2 m_{ij} \right)^{\frac{1}{2}} \left( c \pi \sigma_{ij}^2 \Omega_{ij} \right)^{-1},$$

where  $\sigma_{ij}^2$  is the effective collision cross-section for the pair  $(i, j)$ ;  $m_{ij} = \frac{M_i M_j}{(M_i + M_j)}$  is the reduced

molecular mass;  $M_i$  is the molecular mass of the  $i$ -th component of the mixture;  $\Omega_{ij}$  is the collision integral;  $R$  and  $T$  are the universal gas constant and the temperature of the mixture;  $c = \sum c_i$ ;  $c_i$  is the number of moles of the  $i$ -th component per unit volume.

To describe the molecular flow of a binary gas mixture in a porous medium with micro- and

macropores, the relation  $j_i = D_{ij} \frac{d\rho_i}{dz}$  is used. In this case, the effective diffusion coefficient can

be taken as:

$$D_{1va} = D_{1av} = \left(1/D_{va}^\infty + 1/D_{va}\right)^{-1} = \left\{1/D^\infty + 1/D\right\}^{-1},$$

where  $D$  and  $D^\infty$  are the molecular and Knudsen diffusion coefficients. At low Knudsen numbers, there is a viscous flow regime, in which the interaction of the gas with the capillary walls leads to

slip with velocity  $u_{sl}$ . In this case, the average gas flow velocity is  $\bar{v}_i = -\frac{r^2}{8\mu_i} \left(1 + 8\xi^* Kn_i\right) \frac{dP}{dz}$ ,

where the second term expresses the slip effect;  $\xi^*$  is the dimensionless slip coefficient, which varies in the range of 0.67–1.43 [12].

The total convective flow of the gas mixture in the range from purely viscous flow to the transitional regime with  $\xi^*_i = \frac{2}{3}$  is determined from the Weber equation  $j_i = -\left\{\left(\frac{r^2}{8\mu}\right)P + D_i^\infty \frac{\pi/4 + Kn}{1 + Kn}\right\} \frac{dP}{dz}$ .

This interpolation formula provides accurate results for Knudsen, purely viscous, and transitional flows. The slip velocity is comparable to the average velocity even in capillaries whose radius exceeds the mean free path by tens of times. Only when  $Kn \rightarrow 0$  can the slip effect be neglected. The mass flows  $J_i$  are related to the molar ratios  $J_i = M_j$ .

At the phase transition boundary, the moisture density equals the critical density corresponding to the maximum negative pressures of the capillary moisture, which is in a bound state, causing moisture migration to the boundary. At this boundary, there is an energy jump equal to the amount of heat needed to convert the liquid to vapor. It should be noted that the phase transition temperature in a porous body also depends on the curvature of the interface. An analysis of stresses considering pore size dispersion and in the equivalent pore model [14] suggests that liquid evaporation occurs in a narrow zone separating areas occupied by liquid and gas.

A characteristic feature of describing the drying of capillary-porous bodies is the need to consider their capillary properties as fully as possible at the continuum level [5]. Note that the approach based on using the mass transfer potential [3] does not allow for this sufficiently.

In theoretical studies of heat and mass transfer processes, approaches are used where complex transfer processes in porous bodies are reduced to the Stefan problem with a moving phase boundary. In this approach, the evaporation conditions are recorded differently. The moisture content at the phase boundary can be taken as the initial moisture content, assuming that there is a moist area with the initial moisture content and a dry area where the moisture content is zero. In other studies, the moisture content at the phase boundary is taken as the average integral moisture content of the moist area located in the first half of the material's thickness behind the dry area.

In this regard, when describing the drying process, let's base it on the approach of [5], where the driving forces of mass transfer in the pores are taken to be the gradients of the partial pressures of the components of the pore gas and the capillary pressure. On this basis, it is possible to formulate a complete system of relations for the drying of porous bodies for characteristic

methods of modeling external influences on them, neglecting the pore size dispersion. Let's separately consider the possibility of the drying process under the influence of an external constant electric field (electroosmotic drying).

### 3.1.4 CAPILLARY MODEL OF A POROUS BODY. PROBLEM STATEMENT

Let's consider a capillary-porous body occupying the region ( $V$ ) of Euclidean space and bounded by a smooth surface ( $S$ ). Let's assume that the porosity is open. At the initial moment of time, the body is saturated with liquid. Let's consider a class of materials whose transverse pore size is characterized by a small dispersion, which it is possible to neglect. The body on the surface ( $S$ ) is in contact with a gas medium, which is a mixture of dry air and water vapor. Provided that the water vapor in the surrounding air relative to the body is unsaturated, the process of moisture evaporation from the pore space of the body and the gradual drying of the pores from the surface ( $S$ ) into the body will occur. Due to the uniform transverse pore sizes, this process will proceed equally across the entire cross-section of the body, parallel to the surface ( $S$ ). As a result, two zones will form – dried pores and liquid-filled pores, with the boundary of these zones in each pore being the meniscus of the liquid, the convexity or concavity of which is determined by the properties of the pore surface (its hydrophilicity or hydrophobicity). The surface enveloping the meniscus vertices will be denoted as ( $S^*$ ).

Let's note that pore drying is never complete. In hydrophilic pores, water remains in the form of a wall layer (bound water). In the zone of dried pores, air and water vapor are present. It is possible to assume that the transverse pore size is significantly larger than the mean free path of the molecules present. This allows the expressions for the flows  $\vec{j}_a$  and  $\vec{j}_v$  of air and vapor in the dried zone to be written as [5]:

$$\vec{j}_k = \rho_k \vec{v} - D' \vec{\nabla} \rho_k, \quad k = a, v,$$

where  $\rho_a$  and  $\rho_v$  are the densities of air and vapor, respectively;  $D'$  is an effective coefficient of binary diffusion in pores. The flow of air inside the body is quantitatively much smaller than the flow of steam outside, generated as a result of the water-steam phase transition. In this regard, in the future it is possible to neglect the air flow  $\vec{j}_a$  putting  $\vec{j}_a = 0$ .

Let's also neglect the local change in vapor density  $\rho_v$ , assuming [5]:

$$\frac{\partial \rho_v}{\partial t} = 0,$$

which leads to the following vapor mass balance equation:

$$\vec{\nabla} \cdot \vec{j}_v = 0. \quad (3.20)$$

From these assumptions follow the isothermal Stefan-Maxwell equations for the binary gas mixture in the dried zone:

$$\rho_a \vec{v} - D' \vec{\nabla} \rho_a = 0, \quad \vec{\nabla} \cdot (\rho_v \vec{v} - D' \vec{\nabla} \rho_v) = 0. \quad (3.21)$$

The average mass velocity  $\vec{v}$  satisfies the Darcy equation [13]:

$$\vec{v} = -\frac{K_g}{\mu_g} \vec{\nabla} P_g. \quad (3.22)$$

It is possible to assume that the ideal gas law applies to the gas mixture  $P_g = \left( \frac{\rho_a}{M_a} + \frac{\rho_v}{M_v} \right) RT$ ,

where  $P_g$  is the gas pressure in the pores;  $M_a$  is the molar mass of air;  $M_v$  is the molar mass of vapor;  $R$  is the gas constant.

Using the state equation for the gas mixture and Darcy's law (3.22), it is possible to write the Stefan-Maxwell equations in terms of the key functions  $\rho_a$  and  $\rho_v$  (the densities of air and vapor):

$$\begin{aligned} \rho_a \frac{K_g}{\mu_g} \vec{\nabla} \left( \frac{\rho_a}{M_a} + \frac{\rho_v}{M_v} \right) RT + D' \vec{\nabla} \rho_a &= 0, \\ \vec{\nabla} \cdot \left[ \rho_v \frac{K_g}{\mu_g} \vec{\nabla} \left( \frac{\rho_a}{M_a} + \frac{\rho_v}{M_v} \right) RT + D' \vec{\nabla} \rho_v \right] &= 0, \end{aligned} \quad (3.23)$$

where  $K_g$  is the permeability coefficient dependent on the radius and shape of the pores;  $\mu_g$  is the dynamic viscosity coefficient of the gas.

The written equations are valid in the region of dried pores, which is bounded by the surfaces (S) and (S\*). Note the non-linearity of the differential equation system (3.23).

On the moving surface (S\*), the vapor density can be taken as the saturated vapor density [5]:

$$\rho_v = \rho_{v*}. \quad (3.24)$$

The form of the boundary conditions on the surface (S) depends on the method of modeling the interaction of the body with the environment.

In the considered case of the body's surface (S) contacting with a medium that is a mixture of air and vapor, under natural drying conditions, it is possible to assume that at a distance from the surface (S), the densities  $\rho_{ve}$  of vapor and  $\rho_{ae}$  of air reach constant values  $\rho_{v1}$ ,  $\rho_{a1}$ , respectively, which are characteristic of atmospheric air, i.e.:

$$\lim_{r \rightarrow \infty} \rho_{ve} = \rho_{v1}, \quad \lim_{r \rightarrow \infty} \rho_{ae} = \rho_{a1}, \quad (3.25)$$

where  $r$  is the distance from the surface (S).

In the region outside the body, mass transfer processes will be described by the Stefan-Maxwell equations under the condition of constant atmospheric pressure:

$$\vec{\nabla} \rho_{ae} - \frac{\rho_{ae}}{D'_e} \vec{v}_e = 0,$$

$$\vec{\nabla} \cdot \left( \vec{\nabla} \rho_{ve} - \frac{\rho_{ve}}{D'_e} \vec{v}_e \right) = 0, \quad (3.26)$$

$$P_{ge} = \left( \frac{\rho_{ae}}{M_a} + \frac{\rho_{ve}}{M_v} \right) RT = \text{const.} \quad (3.27)$$

On the surface (S), the normal component of the vapor flow from the drying body must be continuous, i.e.:

$$\vec{n} \cdot \vec{j}_v = \left( \vec{\nabla} \rho_{ve} - \frac{\rho_{ve}}{D'_e} \vec{v}_e \right) \cdot \vec{n}, \quad (3.28)$$

and the densities of the mixture components must be equal, which follows from the equality of the partial pressures on the surface (S):

$$\rho_{ae} = \rho_a, \quad \rho_{ve} = \rho_v. \quad (3.29)$$

Equations (3.23)–(3.29) constitute the complete system of relations and can be used to describe mass transfer during the natural drying of a porous body [5].

Often, when studying the drying process, especially under intensified blowing conditions, the external problem is posed only for the boundary layer of some finite thickness  $\delta$  [5]. In this case, mass transfer in the boundary layer is described by the equations (3.23), (3.24). On the surface (S) of the body, the conjugation condition (3.29) holds, and on the outer surface ( $S^{**}$ ) of the boundary layer, the condition:

$$\rho_{ae} = \rho_{a1}, \quad \rho_{ve} = \rho_{v1}. \quad (3.30)$$

It is possible to note that a number of authors [5] do not consider the boundary layer near the body surface, instead placing a Newton-type mass transfer condition on the surface (S):

$$\vec{n} \cdot \vec{j}_v = \beta(\rho_v - \rho_{v1}), \quad (3.31)$$

as well as the condition:

$$\rho_a = \rho_{a1}. \quad (3.32)$$



Here  $\beta$  is the mass transfer coefficient of the body with the environment. In this case, the mass transfer parameter depends on the conditions of the impact (blowing) on the surface ( $S$ ) of the body.

In this case, it is not possible to pose an external mass transfer problem and will describe the drying of the body with the system of relations (3.21)–(3.24).

To characterize the moisture content of the body, it is advisable to introduce the quantity:

$$\alpha_m = \frac{m_l}{m_{0L}}, \quad (3.33)$$

where  $m_l$ ,  $m_{0L}$  are the current and initial masses of the liquid in the body, respectively. The rate of change of the liquid mass will be determined from the equation:

$$\frac{dm_l}{dt} = - \int_{(S)} (\vec{n} \cdot \vec{j}) dS, \quad (3.34)$$

under the initial condition:

$$m_l = m_{0L} \text{ at } t = 0. \quad (3.35)$$

The vector  $\vec{j}_v$  of the vapor flux density from the body is the solution of the above-formulated problems (3.30); or (3.23), (3.24), (3.26); or (3.23), (3.35).

In terms of relative humidity, the equations (3.23), (3.35) have the form:

$$\frac{d\alpha_m}{dt} = - \frac{1}{m_{0L}} \int_{(S)} (\vec{n} \cdot \vec{j}) dS, \quad (3.35)$$

$$\alpha_m = 1 \text{ at } t = 0. \quad (3.36)$$

The values of moisture content in the zones of dried and liquid-saturated pores are determined as follows:

$$W_v = \frac{\int_{(V_v)} \rho_v dV}{\rho_s V_s}; \quad (3.37)$$

in the zone of dried pores:

$$W_L = \frac{\rho_L V_L}{\rho_s V_s}, \quad (3.38)$$

in the zone of liquid-saturated pores, where ( $V_v$ ) is the region of dried pores;  $V_v$ ,  $V_l$ ,  $V_s$  are the volumes of the regions of dried and liquid-filled pores and the volume of the skeleton.

It is possible to note that in general, due to the nonlinearity of the equations (3.23), (3.26), finding exact solutions to the drying problem constitutes a significant mathematical challenge. Approximate solutions to problems for canonical regions of a layer and a sphere are given, in particular, in the works [5].

Now proceed to Section 3.2 of our study, namely the mathematical model for analyzing the moisture and temperature distribution, radial displacements, and stresses within an individual particle of a multicomponent dispersed material of the capillary-porous structure during its convective drying.

### 3.2 MATHEMATICAL MODELING AND COMPUTATIONAL ANALYSIS OF MOISTURE, TEMPERATURE, AND STRESS DISTRIBUTION IN GRAIN IN CONVECTIVE DRYING. PROBLEM FORMULATION AND KEY SYSTEM OF EQUATIONS

Let's consider a layer of thickness  $L$ , which is blown by a drying agent (gas) with the convective transfer velocity in the intergranular medium for the falling-rate drying stage. The layer is composed in a certain way from identical wet grains, which we assume be of a  $R$ -radius spheres and is referenced to the Cartesian coordinate system so that the  $Oz$  axis is perpendicular to its surfaces.

The movement of gas in the stationary layer of dispersed particles is characterized by the flow around the particles that make up the layer and the flow in the channels between them. Each grain is considered a two-component solid solution (consisting of the main substance and moisture) of the so-called equivalent volume, which is referenced to the spherical coordinate system with the origin at its center ( $r = 0$ ).

The drying process of the grain occurs through its outer surface of contact  $r = R$  with the intergranular medium. The moisture concentration  $c_z$  at the location of the selected grain across the layer thickness  $z$  is determined from the solution of the mass transfer problem in the intergranular space, where the steam-air mixture is uniformly filtered in the complete displacement regime.

Under isothermal conditions, let's accept temperature  $T$ , the vector of radial displacements of the grain  $u_r$ , and moisture concentration  $c$  as the defining functions [3].

Based on the criterion of similarity of heat and mass transfer processes, the equations for the moisture concentration  $c_z$  and temperature  $T_z$  in the intergranular space of the layer are as follows [13]:

$$\frac{\partial c_z}{\partial \tau} + v \frac{\partial c_z}{\partial z} = D_z \frac{\partial^2 c_z}{\partial z^2} + J, \quad \frac{\partial T_z}{\partial \tau} + v \frac{\partial T_z}{\partial z} = \lambda_{tz} \frac{\partial^2 T_z}{\partial z^2} + J_T, \quad (3.39)$$

where  $\partial T$  is the diffusion coefficient of moisture in the pore space;  $a_T$  is the thermal diffusivity;  $J$ ,  $J_T$  are the intensities of the local sources of moisture and heat resulting from evaporation from individual grains;  $\tau$  is time;  $z$  is the coordinate.

To determine the intensity of the local moisture source  $J$ , it is necessary to study the moisture diffusion in a separate grain.

It is possible to consider the grain substance as a two-component solid solution consisting of the main substance and moisture. The local thermodynamic state of such an isotropic system is determined by the values of the conjugate thermodynamic parameters: absolute temperature  $T$ , entropy  $S$ , components of the Cauchy stress tensor  $\sigma$ , strain  $\varepsilon$ , and chemical potentials of the solution components  $\mu'_k$ , concentrations  $C_k (k = 1, 2)$ .

Then, applying the approaches of the theory of solid solutions [1] and choosing temperature  $T$ , displacement  $\vec{u}$ , and moisture concentration  $C_2$  as the solving functions, under certain physical assumptions in the linear approximation, let's obtain:

1. Equation of state:

$$\sigma_{\alpha\beta} = \left[ \left( K - \frac{2}{3}G \right) \varepsilon - K(\beta c + \alpha t) \right] \hat{I} + 2G\varepsilon. \quad (3.40)$$

2. Equilibrium equations and compatibility conditions:

$$\begin{aligned} \vec{\nabla} \cdot \hat{\sigma} &= 0, \quad \text{Ink } \hat{\varepsilon} = \vec{\nabla} \times (\vec{\nabla} \times \hat{\varepsilon})^T = 0, \\ \hat{\varepsilon} &= \left[ \vec{\nabla} \otimes \vec{u} + (\vec{\nabla} \otimes \vec{u})^T \right] / 2. \end{aligned} \quad (3.41)$$

3. Balance equation of concentration and thermal conductivity equation:

$$\begin{aligned} \frac{\partial c}{\partial \tau} &= D\Delta c - D_\varepsilon \Delta \varepsilon, \\ \vec{J} &= -D\vec{\nabla} c + D_\varepsilon \vec{\nabla} \varepsilon, \quad \frac{\partial t}{\partial \tau} = a_t \Delta t. \end{aligned} \quad (3.42)$$

Here,  $K$  is the bulk modulus;  $G$  is the shear modulus;  $\varepsilon = Tr\varepsilon$  is the first invariant of the strain tensor  $\varepsilon$ ;  $\beta, \alpha$  are the concentration and temperature coefficients of volumetric expansion;  $c = C_2 - C_2^{(0)}$  and  $t = T - T^{(0)}$  are deviations of moisture concentration and temperature from their values  $C_2^{(0)}$  and  $T^{(0)}$  in the initial state;  $\hat{I}$  is the unit tensor;  $\vec{\nabla} \cdot$  is the Hamiltonian operator;  $D$  is the diffusion coefficient;  $D_\varepsilon$  is the coefficient of the influence of the volumetric strain gradient on the mass flow;  $a_t$  is the thermal diffusivity coefficient;  $\vec{J}$  is the moisture diffusion flux;  $\Delta = \vec{\nabla} \cdot \vec{\nabla}$  is the Laplace operator; the symbols “ $\cdot$ ”, “ $\nabla$ ”, “ $\otimes$ ” denote the scalar, vector, and tensor products, respectively.

It should be noted that for the so-called “soft regimes” of drying, it is possible to assume that  $(T - T_0) / T_0 \ll 1$ .

A separate grain in the geometric approximation of a spherical particle is referenced to the spherical coordinate system with the origin at its center ( $r = 0$ ). The drying process occurs through the surface  $r = 0$  of contact with the intergranular air medium, whose characteristics depend on the coordinate  $z$  in the layer. Then, for the grain, the displacement vector has only a radial component  $u_r$  and accordingly:

$$\varepsilon_{rr} = \frac{du_r}{dr}, \quad \varepsilon_{\varphi\varphi} = \varepsilon_{\theta\theta} = \frac{u_r}{r},$$

$$\Delta c = \frac{1}{r} \frac{\partial^2 (rc)}{\partial r^2}, \quad \vec{\nabla} \cdot \vec{\sigma} = \frac{\partial \sigma_{rr}}{\partial r} + \frac{1}{r} (2\sigma_{rr} - \sigma_{\theta\theta} - \sigma_{\varphi\varphi}). \quad (3.43)$$

From the equilibrium conditions (3.41), the state equations (3.40) [13], and the formulas (3.43), it is possible to obtain the relations of the volumetric strain gradients with the concentration expansion gradient.

From the equations (3.42) and (3.43), it is possible to obtain the key system of equations for a single sphere in the form of the displacement equation and the moisture concentration balance equation:

$$\frac{\partial}{\partial r} \left[ \frac{1}{r^2} \frac{\partial (r^2 u_r)}{\partial r} \right] - \xi \left( \beta \frac{\partial c}{\partial r} + \alpha \frac{\partial t}{\partial r} \right) = 0, \quad \frac{\partial (rc)}{\partial \tau} = D \frac{\partial^2 (rc)}{\partial r^2} - \xi \beta D_\varepsilon \frac{\partial^2 (rc)}{\partial r^2}, \quad (3.44)$$

where  $\xi = 3K / (3K + 4G)$  is the mechanical constant;  $\varepsilon = \partial u_r / \partial r + 2u_r / r$ .

At the initial moment of time ( $\tau = 0$ ):

$$u_r = 0, \quad c = c_0 = \text{const}. \quad (4.45)$$

On the surface of the sphere  $r = R$ , which is free from external loads, the condition  $\vec{\sigma} \cdot \vec{n} = 0$  is written as:

$$\sigma_{rr} = \left( K + \frac{4}{3} G \right) \frac{\partial u_r}{\partial r} + 2 \left( K - \frac{2}{3} G \right) \frac{u_r}{r} - K (\beta c + \alpha t) = 0. \quad (3.46)$$

It is possible to assume that the moisture flow on this surface is proportional to the concentration difference on the surface of the grain and the intergranular medium  $c_z$ :  $c_R(\tau) \equiv c(R, \tau)$  [13]:

$$-D \frac{\partial c}{\partial r} + D_\varepsilon \frac{\partial \varepsilon}{\partial r} = k (c_R - c_z), \quad (3.47)$$

where  $k$  is the mass transfer constant on the surface of the sphere.

It is possible to assume that the sought functions and their derivatives at the center of the sphere ( $r = 0$ ) are limited, in particular:

$$c(0, \tau) \neq \infty, \quad \left. \frac{\partial c}{\partial r} \right|_{r=0} = 0. \quad (3.48)$$

Since in the centrosymmetric problem, the relations hold:

$$\frac{\partial}{\partial r} \left[ \frac{1}{r^2} \frac{\partial (r^2 u_r)}{\partial r} \right] = \frac{\partial \varepsilon}{\partial r}, \quad \frac{\partial \varepsilon}{\partial r} = \xi \left( \beta \frac{\partial c}{\partial r} + \alpha \frac{\partial t}{\partial r} \right), \quad (3.49)$$

the moisture balance equation (3.44) in the grain is written as:

$$\frac{\partial (rc)}{\partial \tau} = \tilde{D} \frac{\partial^2 (rc)}{\partial r^2}, \quad (3.50)$$

and the boundary condition (3.47) is:

$$-\tilde{D} \left. \frac{\partial c}{\partial r} \right|_{r=R} = k(c_R - c_z) \text{ or } - \left. \frac{\partial c}{\partial r} \right|_{r=R} + H(c_z - c_R) = 0, \quad (3.51)$$

where  $\tilde{D} = D - \xi \beta D_\varepsilon$  is the effective moisture diffusion coefficient;  $H = k / \tilde{D}$  is the reduced mass transfer coefficient.

The heat conduction equation for temperature can be written as:

$$\frac{\partial (rt)}{\partial \tau} = a_r \frac{\partial^2 (rt)}{\partial r^2}, \quad (0 < r < R). \quad (3.52)$$

The initial and boundary conditions for temperature are as follows:

$$-\left. \frac{\partial t}{\partial r} \right|_{r=R} + H_T(t_z - t_R) = 0, \quad \left. \frac{\partial t}{\partial r} \right|_{r=0} = 0,$$

$$t(0, \tau) \neq \infty, \quad t(r, 0) = f_T(r). \quad (3.53)$$

### 3.3 DEVELOPMENT OF SOLUTION ALGORITHMS FOR MOISTURE CONTENT AND STRESS-STRAIN STATE OF THE GRAIN

During the analysis of the moisture diffusion process in the grain, the moisture concentration in the intergranular space of the layer can be considered independent of time, i.e.,  $c_z = c_z(z)$ . The function  $c_z$  is found from the solution of equation (3.39) under the corresponding boundary conditions in the quasi-stationary approximation (neglecting the partial derivative with respect to time, but the time dependence remains in the source). The solution of the problem is sought by the method of separation of variables [3]. Let's outline new functions:

$$\vartheta(r, z, \tau) = c_z(z) - c(r, z, \tau), \quad \vartheta_r(r, z, \tau) = T_z(z) - T(r, z, \tau), \quad (2.54)$$

for which the problem (3.50)–(3.53) takes the form:

$$\frac{\partial(r\vartheta)}{\partial\tau} = \tilde{D} \frac{\partial^2(r\vartheta)}{\partial r^2}, \quad \frac{\partial(r\vartheta_r)}{\partial\tau} = \alpha_r \frac{\partial^2(r\vartheta_r)}{\partial r^2}, \quad (3.55)$$

$$\left. \frac{\partial\vartheta}{\partial r} \right|_{r=R} + H\vartheta_R = 0; \quad \vartheta(0, \tau) \neq \infty, \quad \left. \frac{\partial\vartheta}{\partial r} \right|_{r=0} = 0, \quad (3.56)$$

$$\vartheta(r, 0) = c_{z0} - c_0, \quad \left. \frac{\partial\vartheta_r}{\partial r} \right|_{r=R} + H_r\vartheta_{rR} = 0, \quad (3.57)$$

where  $\vartheta_R(\tau) \equiv \vartheta(R, \tau)$ ,  $\vartheta_{rR}(\tau) \equiv \vartheta_r(R, \tau)$ .

Then the solution of the problem (3.55)–(3.57) is written as [1]:

$$\vartheta(r, z, \tau) = 2\delta c \sum_{n=1}^{\infty} A_n(\tau) \frac{\sin r_n}{r_n}, \quad \vartheta_r(r, z, \tau) = 2\delta T \sum_{n=1}^{\infty} A_{rn}(\tau) \frac{\sin r_{rn}}{r_{rn}}, \quad (3.58)$$

where

$$\delta c = c_{z0}(z) - c_0, \quad A_n(\tau) = \frac{(\sin \mu_n - \mu_n \cos \mu_n) e^{-\mu_n^2 \tilde{D} \tau / R^2}}{\mu_n - \sin \mu_n \cos \mu_n}, \quad r_n = \mu_n r / R,$$

$$\delta T = t_{z0}(z) - t_0, \quad A_{rn}(\tau) = \frac{(\sin \mu_{rn} - \mu_{rn} \cos \mu_{rn}) e^{-\mu_{rn}^2 \alpha_r \tau / R^2}}{\mu_{rn} - \sin \mu_{rn} \cos \mu_{rn}}, \quad r_{rn} = \mu_{rn} r / R,$$

$\mu_n, \mu_{Tn}$  are the roots of the characteristic equations:

$$\tan \mu = -\frac{\mu}{Fo - 1}, \quad \tan \mu_T = -\frac{\mu_T}{Fo_T - 1}, \quad (3.59)$$

where  $Fo = HR$ ,  $Fo_T = H_T R$  are the Fourier numbers.

According to the relation (3.54), for the moisture concentration and temperature in the grain, let's find:

$$c(r, z, \tau) = c_z(z, \tau) - 2\delta c \sum_{n=1}^{\infty} A_n(\tau) \frac{\sin r_n}{r_n}, \quad T(r, z, \tau) = T_z(z, \tau) - 2\delta T \sum_{n=1}^{\infty} A_{Tn}(\tau) \frac{\sin r_{Tn}}{r_{Tn}}. \quad (3.60)$$

For the moisture and temperature fluxes  $J_R, J_{TR}$  through the surface of the sphere:

$$J_R = -\tilde{D} \frac{\partial c}{\partial r} \Big|_{r=R} = -\frac{2\tilde{D}(\delta c)}{R} \sum_{n=1}^{\infty} \frac{A_n(\tau)}{\mu_n} (\sin \mu_n - \mu_n \cos \mu_n), \quad (3.61)$$

$$J_{TR} = -\lambda_T \frac{\partial T}{\partial r} \Big|_{r=R} = -\frac{2\lambda_T(\delta T)}{R} \sum_{n=1}^{\infty} \frac{A_{Tn}(\tau)}{\mu_{Tn}} (\sin \mu_{Tn} - \mu_{Tn} \cos \mu_{Tn}).$$

Then the intensity of the local sources of moisture and temperature in the case of evaporation from individual grains  $J, J_T$ , which appear in the original equation (3.39), will be:

$$J = \tilde{\alpha}(J_R + \delta_T J_{TR}), \quad J_T = \tilde{\alpha}_T J_{TR}, \quad (3.62)$$

where  $\tilde{\alpha}, \tilde{\alpha}_T$  are coefficients that depend on the size of the spheres (radius) and their packing (simple cubic, body-centered cubic, or face-centered cubic, etc.),  $\delta_T$  is the thermo-gradient coefficient.

Given the accepted assumptions, the process of convective diffusion in the intergranular space of a layer of thickness  $z = L$ , composed of identical grains, is a fast process compared to the process of moisture diffusion from the volume of the grain to its surface. Therefore, further analysis of the drying process will be performed based on the equations:

$$D_z \frac{d^2 c_z}{dz^2} - v \frac{dc_z}{dz} + J = 0, \quad \lambda_{Tz} \frac{d^2 t_z}{dz^2} - v \frac{dt_z}{dz} + J_T = 0, \quad (3.63)$$

where the function  $J$  is determined by expression (3.62). Considering that  $J, J_T$  can be written in the form (3.62), the equations (3.63) will be written as:

$$D_z \frac{d^2 c_z}{dz^2} - v \frac{dc_z}{dz} + c_z J_0(\tau) = c_0 J_0(\tau), \quad (3.64)$$

$$\lambda_{tz} \frac{d^2 t_z}{dz^2} - v \frac{dt_z}{dz} + t_z J_{T0}(\tau) = t_0 J_{T0}(\tau).$$

Here,

$$J_0(\tau) = -\alpha \frac{2\tilde{D}}{R} \sum_{n=1}^{\infty} \frac{A_n(\tau)}{\mu_n} (\sin \mu_n - \mu_n \cos \mu_n),$$

$$J_{T0}(\tau) = -\alpha_{\tau} \frac{2a_{\tau}}{R} \sum_{n=1}^{\infty} \frac{A_{\tau n}(\tau)}{\mu_{\tau n}} (\sin \mu_{\tau n} - \mu_{\tau n} \cos \mu_{\tau n}).$$

Equations (3.64) will be solved under first-kind boundary conditions:

$$c_z|_{z=0} = 0, \quad c_z|_{z=L} = c_z^n, \quad t_z|_{z=0} = 0, \quad t_z|_{z=L} = t_z^n;$$

and third-kind boundary conditions:

$$\begin{aligned} -D_z \frac{\partial c_z(0, \tau)}{\partial z} &= \beta_z (c_z(0, \tau) - c_c), \quad c_z|_{z=L} = c_z^n, \\ -\lambda_z \frac{\partial t_z(0, \tau)}{\partial z} &= \beta_{tz} (t_z(0, \tau) - t_c), \quad t_z|_{z=L} = t_z^n, \end{aligned} \quad (3.65)$$

where  $c_z^n$  is the concentration of saturated vapor,  $c_c$  is the concentration of the steam-air mixture in the external environment,  $t_z^n$  is the temperature corresponding to vapor saturation.

The solution of the problem (3.64), (3.65) is sought by the method of variation of constants [3]. After the corresponding calculations for the first case of boundary conditions, let's obtain:

$$c_z(z, \tau) = -K_1 e^{\lambda_1 z} + K_2 e^{\lambda_2 z} + c_0, \quad (3.66)$$

$$t_z(z, \tau) = -K_{\tau 1} e^{\lambda_{\tau 1} z} + K_{\tau 2} e^{\lambda_{\tau 2} z} + t_0,$$

where

$$K_1 = [c_0 e^{\lambda_2 L} + c_z^n - c_0] / \Delta, \quad K_2 = [c_0 e^{\lambda_1 L} + c_z^n - c_0] / \Delta,$$



$$\Delta = e^{\lambda_{2L}} - e^{\lambda_{1L}};$$

$$K_{T1} = [t_0 e^{\lambda_{T2}L} + t_z^n - t_0] / \Delta_T, K_{T2} = [t_0 e^{\lambda_{T1}L} + t_z^n - t_0] / \Delta_T,$$

$$\Delta_T = e^{\lambda_{T2}L} - e^{\lambda_{T1}L};$$

$$\lambda_{1/2} = v \pm \sqrt{v^2 - 4D_z J_0(\tau) / (2D_z)},$$

$$\lambda_{T1/2} = v \pm \sqrt{v^2 - 4\alpha_{Tz} J_{T0}(\tau) / (2\alpha_{Tz})}.$$

Further, it is possible to use the dimensionless coordinate  $\bar{z} = z / L$ . Then:

$$c_z(\bar{z}, \tau) = -K_1 e^{\bar{\lambda}_1 \bar{z}} + K_2 e^{\bar{\lambda}_2 \bar{z}} + c_0, \quad (3.67)$$

$$t_z(\bar{z}, \tau) = -K_{T1} e^{\bar{\lambda}_{T1} \bar{z}} + K_{T2} e^{\bar{\lambda}_{T2} \bar{z}} + t_0,$$

where  $\bar{\lambda}_i = L\lambda_i$ ,  $\bar{\lambda}_{Ti} = L\lambda_{Ti}$ ,  $i = 1, 2$ .

In the case of third kind boundary conditions, the sought functions  $c_z$  and  $t_z$  are also determined by formulas (3.67), in which:

$$K_1 = \left[ \frac{\beta L}{D_z} (c_0 - c_c) e^{\bar{\lambda}_2} - (c_z^n - c_0) \left( \bar{\lambda}_2 + \frac{\beta L}{D_z} \right) \right] / \tilde{\Delta},$$

$$K_2 = \left[ \frac{\beta L}{D_z} (c_0 - c_c) e^{\bar{\lambda}_1} + (c_z^n - c_0) \left( \bar{\lambda}_1 + \frac{\beta L}{D_z} \right) \right] / \tilde{\Delta},$$

$$\tilde{\Delta} = \left( \bar{\lambda}_1 + \frac{\beta L}{D_z} \right) e^{\bar{\lambda}_2} - \left( \bar{\lambda}_2 + \frac{\beta L}{D_z} \right) e^{\bar{\lambda}_1}.$$

Integrating the second equation (3.49), for the volumetric strain it is possible to obtain:

$$\varepsilon = \xi(\beta c + \alpha t) + L, \quad (3.68)$$

where the function  $L(z, \tau)$ , the “integration constant”, is determined from the condition of zero strain at its center, i.e.:

$$L(z, \tau) = -\xi[\beta c(0, z, \tau) + \alpha t(0, z, \tau)].$$

From here:

$$\varepsilon(r, z, \tau) = \xi \left\{ \beta \left[ c(r, z, \tau) - c(0, z, \tau) \right] + \alpha \left[ t(r, z, \tau) - t(0, z, \tau) \right] \right\},$$

and accordingly:

$$\varepsilon(r, z, \tau) = -2\xi \left\{ \beta \delta c \sum_{n=1}^{\infty} A_n(\tau) \left( \frac{1}{r_n} \sin r_n - 1 \right) + \alpha \delta t \sum_{n=1}^{\infty} A_{In}(\tau) \left( \frac{1}{r_{In}} \sin r_{In} - 1 \right) \right\}. \quad (3.69)$$

The displacement  $u_r$  is found from the condition of zero radial stresses (3.46) on the surface of the sphere  $r = R$ . There is:

$$u_r(R, z, \tau) = -\frac{KR}{4G} \left\{ \beta c(0, z, \tau) + \alpha t(0, z, \tau) \right\}. \quad (3.70)$$

To determine the radial displacement at an arbitrary point of the grain, it is possible to integrate the first expression (3.49). As a result, taking into account its limitation for  $r = 0$  and the expression (3.70) for  $r = R$ , let's obtain:

$$\begin{aligned} u_r(r, z, \tau) = & \frac{\xi \beta}{r^2} \left[ c_z \frac{r^3}{3} - 2R^3 \delta c \sum_{n=1}^{\infty} \frac{A_n(\tau)}{\mu_n^3} (\sin r_n - r_n \cos r_n) \right] + \frac{r}{3} L_1(z, \tau) + \\ & + \frac{\xi \alpha}{r^2} \left[ t_z \frac{r^3}{3} - 2R^3 \delta t \sum_{n=1}^{\infty} \frac{A_{In}(\tau)}{\mu_{In}^3} (\sin r_{In} - r_{In} \cos r_{In}) \right]. \end{aligned} \quad (3.71)$$

Here from formula (3.68):

$$\begin{aligned} L_1(z, \tau) = & \left\{ \frac{3K\beta}{4G} \left[ -c_z + 2\delta c \sum_{n=1}^{\infty} A_n(\tau) \right] - 3\xi \beta \left[ \frac{c_z}{3} - 2\delta c \sum_{n=1}^{\infty} \frac{A_n(\tau)}{\mu_n^3} (\sin \mu_n - \mu_n \cos \mu_n) \right] + \right. \\ & \left. + \frac{3K\alpha}{4G} \left[ -t_z + 2\delta t \sum_{n=1}^{\infty} A_{In}(\tau) \right] - 3\xi \alpha \left[ \frac{t_z}{3} - 2\delta t \sum_{n=1}^{\infty} \frac{A_{In}(\tau)}{\mu_{In}^3} (\sin \mu_{In} - \mu_{In} \cos \mu_{In}) \right] \right\}. \end{aligned}$$

In our case, the following components of the stress tensor are non-zero:

$$\sigma_{rr} = 2G \frac{\partial u_r}{\partial r} + \left[ \left( K - \frac{2}{3}G \right) \varepsilon - K(\beta c + \alpha t) \right], \quad (2.34)$$

$$\sigma_{\phi\phi} = \sigma_{\theta\theta} = 2G \frac{u_r}{r} + \left[ \left( K - \frac{2}{3}G \right) \varepsilon - K(\beta c + \alpha t) \right].$$

Based on the determined moisture concentration  $c$  and temperature  $t$  (formulas (3.66), (3.67)), displacement  $u_r$  (formula (3.71)), strain  $\varepsilon$  (formula (3.69)), let's obtain the stresses  $\sigma_{rr}$ ,  $\sigma_{\theta\theta}$ ,  $\sigma_{\varphi\varphi}$  (formula (3.72)).

Thus, based on the proposed model, it is possible to calculate the stress-strain state of an individual grain, which depends on its location in the layer, the characteristics of the grain material and the intergranular space, the size and packing of the grains under different regimes of convective-diffusive moisture transfer.

## CONCLUSIONS

Well-known mathematical models are typically based on quasi-homogeneous approximations. This approach is successfully applied to describe processes in which products and reactants form a single phase that uniformly fills the pore space. However, the application of interpenetrating continua methods is unjustified when studying processes with phase transformations and interphase boundaries. The interaction of phases determines capillary transport mechanisms. Capillary properties and phase transformation processes regulate the distribution of phases in the pore space and the magnitudes of interphase surfaces where heterogeneous transformations occur. Therefore, the use of capillary models, especially in the second stage of drying when phase transitions deepen, and the use of structural stochastic models are necessary.

Thus, the development of approaches and methods for mathematical modeling of heat and mass transfer processes in multiphase, multicomponent bodies, taking into account the sizes and nature of the phases, is relevant. In drying tasks, the efficiency of the process and the quality of the dried product are also important issues. This necessitates the study of the stress-strain state and the stability of the shape of thin-walled flat objects.

## REFERENCES

1. Burak, Ya. Y., Chaplia, Ye. Ya., Chernukha, O. Yu. (2006). Kontynualno-termodynamichni modeli mekhaniky tverdykh rozchyniv. Kyiv: Naukova dumka, 272.
2. Sokolovskyy, Y., Levkovich, M., Mysyk, M. (2023). Matrix Approach to Numerical Modeling of Heat-and-Moisture Transfer Processes in a Medium with a Fractal Structure. 2023 17th International Conference on the Experience of Designing and Application of CAD Systems (CADSM), 44–48. <https://doi.org/10.1109/cadsm58174.2023.10076519>
3. Lykov, A. V. (1968). Teoriia sushki. Moscow: Energiia, 472.
4. Hachkevych, O. R., Kushnir, R. M., Terletskii, R. F. (2022). Mathematical Problems of Thermomechanics for Deformable Bodies Subjected to Thermal Irradiation. Ukrainian Mathematical Journal, 73 (10), 1522–1536. <https://doi.org/10.1007/s11253-022-02011-7>

5. Kheifitc, L. I., Neimark, A. V. (1982). *Mnogofaznye protsessy v poristyykh sredakh*. Moscow: Khimiia, 320.
6. Pyanylo, Y. (2022). Analysis of Filtration Processes in Porous Environments Taking Into Account the Movement of Capillaries. 2022 12th International Conference on Advanced Computer Information Technologies (ACIT), 9–12. <https://doi.org/10.1109/acit54803.2022.9913087>
7. Gayvas, B., Markovych, B., Dmytruk, A., Havran, M., Dmytruk, V. (2024). The methods of optimization and regulation of the convective drying process of materials in drying installations. *Mathematical Modeling and Computing*, 11 (2), 546–554. <https://doi.org/10.23939/mmc2024.02.546>
8. Hayvas, B., Dmytruk, V., Torsky, A., Dmytruk, A. (2017). On methods of mathematical modeling of drying dispersed materials. *Mathematical Modeling and Computing*, 4 (2), 139–147. <https://doi.org/10.23939/mmc2017.02.139>
9. Baranovsky, S. V., Bomba, A. Ya. (2024). The diffusion scattering parameters identification for a modified model of viral infection in the conditions of logistic dynamics of immunological cells. *Mathematical Modeling and Computing*, 11 (1), 59–69. <https://doi.org/10.23939/mmc2024.01.059>
10. Mozhaev, A. P. (2001). Chaotic homogeneous porous media. 1. Theorems about structure. *Engineering-Physical Journal*, 74 (5), 196–201.
11. Lutcyk, P. P. (1988). *Issledovanie protsessov teplomassopere nosa pri sushke kapillarno-poristyykh tel s uch etom vnutrennikh napriazhenii. Teplomassoobmen*. Minsk: Institut teplo-i massoobmena im. A. V. Lykova, 184–197.
12. Khoroshun, L. P., Maslov, B. P., Leshchenko, P. V. (1989). *Prognozirovanie effektivnykh svoistv pezoaktivnykh kompozitsionnykh materialov*. Kyiv: Naukova dumka, 208.
13. Burak, Y., Kondrat, V., Gayvas, B. (2002). On the mathematical modeling of drying processes of porous bodies. *Informational-Mathematical Modeling of Complex Systems*. Lviv: CMM IPPMM named after Y. S. Pidstryhach NAS of Ukraine, Akhil Publishing House, 153–159.
14. Dibagar, N., Kowalski, S. J., Chayjan, R. A., Figiel, A. (2020). Accelerated convective drying of sunflower seeds by high-power ultrasound: Experimental assessment and optimization approach. *Food and Bioproducts Processing*, 123, 42–59. <https://doi.org/10.1016/j.fbp.2020.05.014>
15. Shlikhting, G. (1974). *Teoriia pogranichnogo sloia*. Moscow: Nauka, 690.
16. Gayvas, B. I., Dmytruk, V. A., Semerak, M. M., Ry mar, T. I. (2021). Solving Stefan’s linear problem for drying cylindrical timber under quasi-averaged formulation. *Mathematical Modeling and Computing*, 8 (2), 150–156. <https://doi.org/10.23939/mmc2021.02.150>
17. Gayvas, B. I., Dmytruk, V. A. (2022). Investigation of drying the porous wood of a cylindrical shape. *Mathematical Modeling and Computing*, 9 (2), 399–415. <https://doi.org/10.23939/mmc2022.02.399>
18. Gayvas, B. I., Markovych, B. M., Dmytruk, A. A., Havran, M. V., Dmytruk, V. A. (2023). Numerical modeling of heat and mass transfer processes in a capillary-porous body during

- p contact drying.
- Mathematical Modeling and Computing*
- , 10 (2), 387–399.
- <https://doi.org/10.23939/mmc2023.02.387>
19. Gera, B., Kovalchuk, V., Dmytruk, V. (2022). Temperature field of metal structures of transport facilities with a thin protective coating. *Mathematical Modeling and Computing*, 9 (4), 950–958. <https://doi.org/10.23939/mmc2022.04.950>
  20. Gayvas, B., Markovych, B., Dmytruk, A., Dmytruk, V., Kushka, B., Senkovych, O. (2023). Study of Contact Drying Granular Materials in Fluidized Bed Dryers. 2023 IEEE XXVIII International Seminar/Workshop on Direct and Inverse Problems of Electromagnetic and Acoustic Wave Theory (DIPED), 238–241. <https://doi.org/10.1109/diped59408.2023.10269464>
  21. Alaa, K., Atounti, M., Zirhem, M. (2021). Image restoration and contrast enhancement based on a nonlinear reaction-diffusion mathematical model and divide & conquer technique. *Mathematical Modeling and Computing*, 8 (3), 549–559. <https://doi.org/10.23939/mmc2021.03.549>
  22. Alaa, H., Alaa, N. E., Aqel, F., Lefraich, H. (2022). A new Lattice Boltzmann method for a Gray–Scott based model applied to image restoration and contrast enhancement. *Mathematical Modeling and Computing*, 9 (2), 187–202. <https://doi.org/10.23939/mmc2022.02.187>
  23. Baala, Y., Agmour, I., Rachik, M. (2022). Optimal control of tritrophic reaction–diffusion system with a spatiotemporal model. *Mathematical Modeling and Computing*, 9 (3), 647–662. <https://doi.org/10.23939/mmc2022.03.647>
  24. Bounkaicha, C., Allali, K., Tabit, Y., Danane, J. (2023). Global dynamic of spatio-temporal fractional order SEIR model. *Mathematical Modeling and Computing*, 10 (2), 299–310. <https://doi.org/10.23939/mmc2023.02.299>
  25. Gouasnouane, O., Moussaid, N., Boujena, S., Kabli, K. (2022). A nonlinear fractional partial differential equation for image inpainting. *Mathematical Modeling and Computing*, 9 (3), 536–546. <https://doi.org/10.23939/mmc2022.03.536>
  26. Najm, F., Yafia, R., Aziz Alaoui, M. A., Aghriche, A., Moussaoui, A. (2023). A survey on constructing Lyapunov functions for reaction-diffusion systems with delay and their application in biology. *Mathematical Modeling and Computing*, 10 (3), 965–975. <https://doi.org/10.23939/mmc2023.03.965>
  27. Suganya, G., Senthamarai, R. (2022). Mathematical modeling and analysis of Phytoplankton–Zooplankton–Nanoparticle dynamics. *Mathematical Modeling and Computing*, 9 (2), 333–341. <https://doi.org/10.23939/mmc2022.02.333>
  28. Ben-Loghfry, A., Hakim, A. (2022). Time-fractional diffusion equation for signal and image smoothing. *Mathematical Modeling and Computing*, 9 (2), 351–364. <https://doi.org/10.23939/mmc2022.02.351>
  29. Kostrobij, P. P., Markovych, B. M., Ryzha, I. A., Tokarchuk, M. V. (2021). Statistical theory of catalytic hydrogen oxidation processes. Basic equations. *Mathematical Modeling and Computing*, 8 (2), 267–281. <https://doi.org/10.23939/mmc2021.02.267>

30. Kostrobij, P. P., Ivashchyshyn, F. O., Markovych, B. M., Tokarchuk, M. V. (2021). Microscopic theory of the influence of dipole superparamagnetics (Type  $\langle \beta\text{-CD(FeSO}_4 \rangle \rangle$ ) on current flow in semiconductor layered structures (type gas, inse). *Mathematical Modeling and Computing*, 8 (1), 89–105. <https://doi.org/10.23939/mmc2021.01.089>
31. Aberqi, A., Elmassoudi, M., Hammoui, M. (2021). Discrete solution for the nonlinear parabolic equations with diffusion terms in Museilak-spaces. *Mathematical Modeling and Computing*, 8 (4), 584–600. <https://doi.org/10.23939/mmc2021.04.584>
32. Bazirha, Z., Azrar, L. (2024). DDFV scheme for nonlinear parabolic reaction-diffusion problems on general meshes. *Mathematical Modeling and Computing*, 11 (1), 96–108. <https://doi.org/10.23939/mmc2024.01.096>
33. Baranovsky, S., Bomba, A., Lyashko, S., Pryshchepa, O. (2024). Diffusion Perturbations in Models of the Dynamics of Infectious Diseases Taking into Account the Concentrated Effects. *Computational Methods and Mathematical Modeling in Cyberphysics and Engineering Applications* 1, 273–303. <https://doi.org/10.1002/9781394284344.ch11>
34. El Hassani, A., Bettoui, B., Hattaf, K., Achtaich, N. (2024). Global dynamics of a diffusive SARS-CoV-2 model with antiviral treatment and fractional Laplacian operator. *Mathematical Modeling and Computing*, 11 (1), 319–332. <https://doi.org/10.23939/mmc2024.01.319>
35. Tokarchuk, M. V. (2023). Unification of kinetic and hydrodynamic approaches in the theory of dense gases and liquids far from equilibrium. *Mathematical Modeling and Computing*, 10 (2), 272–287. <https://doi.org/10.23939/mmc2023.02.272>
36. Belhachmi, Z., Mghazli, Z., Ouchtout, S. (2022). A coupled compressible two-phase flow with the biological dynamics modeling the anaerobic biodegradation process of waste in a landfill. *Mathematical Modeling and Computing*, 9 (3), 483–500. <https://doi.org/10.23939/mmc2022.03.483>
37. Pukach, P. Y., Chernukha, Y. A. (2024). Mathematical modeling of impurity diffusion process under given statistics of a point mass sources system. I. *Mathematical Modeling and Computing*, 11 (2), 385–393. <https://doi.org/10.23939/mmc2024.02.385>
38. Laham, M. F., Ibrahim, S. N. I. (2023). Penalty method for pricing American-style Asian option with jumps diffusion process. *Mathematical Modeling and Computing*, 10 (4), 1215–1221. <https://doi.org/10.23939/mmc2023.04.1215>
39. Dmytryshyn, L. I., Dmytryshyn, M. I., Olejnik, A. (2023). Model of money income diffusion in the European integration context. *Mathematical Modeling and Computing*, 10 (2), 583–592. <https://doi.org/10.23939/mmc2023.02.583>
40. Patil, J. V., Vaze, A. N., Sharma, L., Bachhav, A. (2021). Study of calcium profile in neuronal cells with respect to temperature and influx due to potential activity. *Mathematical Modeling and Computing*, 8 (2), 241–252. <https://doi.org/10.23939/mmc2021.02.241>

## CHAPTER 4

# DRYING OF A POROUS LAYER IN AN EXTERNAL CONSTANT ELECTRIC FIELD (ELECTROSMOTIC DRYING)

## ABSTRACT

In this Chapter, mathematical modeling of the drying process of a porous layer under the influence of an external constant electric field is presented, taking into account the electroosmotic effects on mass and heat transfer. A mathematical model of electroosmotic drying is formulated based on the coupled equations of moisture transport, electrokinetic flow, and thermal effects. The analysis considers both natural and convective drying conditions, incorporating the impact of electroosmotic forces on moisture migration within the porous medium.

In the study, the fundamental mechanisms governing electroosmotic moisture removal are explored, including the formation of a double electric layer at the interface between the pore liquid and the solid skeleton, the competition between electroosmotic and capillary forces, and the transition between different drying regimes. A system of governing equations, including modified Stefan-Maxwell relations and generalized Darcy's law, is derived to describe the transport processes in the porous domain.

Numerical simulations are carried out. The experiments have demonstrated the effect of key parameters, such as electric field intensity, moisture content, temperature, and mass transfer coefficients, on drying kinetics. Results indicate that increasing the electric field intensity significantly accelerates moisture removal, particularly during the initial drying stage when electroosmotic forces dominate.

## KEYWORDS

Electroosmotic drying, porous media, moisture transport, external electric field, capillary effects, ponderomotive force, convective drying, unilateral drying, bilateral drying, boundary layer properties, isothermal drying, electrokinetic flow, sustainable technology, numerical methods.

In drying processes, external mass transfer can be intensified through an active hydrodynamic regime in the near-wall layer, induced by the action of external physical fields of various

natures [1–10]. Thus, the application of physical fields can stimulate efficient moisture removal from wet materials.

The works [11–14] explore the feasibility of using electroosmosis for moisture removal from various dispersed systems. These studies emphasize the role of electrokinetic properties in the process of liquid transport and separation under an applied electric field. The study by O. Bereznik [15] presents an experimental investigation of electroosmotic dewatering of kaolin, highlighting the potential practical application of this drying method.

The possibility of using electroosmosis for mass transfer intensification is associated with the existence of a double electric layer at the interface between the pore liquid and the solid skeleton. This concept has been explored in theoretical and experimental studies [16–18], demonstrating how electrokinetic effects influence moisture movement in porous media and complex dispersed systems. To the issues of intensification of heat and mass transfer processes under the influence of an external electric field are devoted the works [19–21]. They have demonstrated the role of electromagnetic fields in controlling thermal stresses and optimizing heating modes in electrically conductive materials.

In [16], L. Lysenko has analyzed electrokinetic soil purification, which shares fundamental principles with electroosmotic drying.

Mathematical modeling has played an important role in understanding electroosmotic drying processes. The works [22, 23] have focused on the mathematical representation of moisture transport in porous bodies, considering phase transition kinetics and deformations.

Additionally, research on applied electroosmosis has extended to diverse fields, including industrial drying and food processing. Studies such as those by O. Severyn and A. Fariseev [24, 25] investigated drying systems enhanced by electroosmotic effects, demonstrating their potential in improving energy efficiency and process control.

Moreover, electroosmosis has been studied for its influence on multiphase systems and reactive environments [26, 27]. The interplay between electrokinetic forces and fluid dynamics in these systems suggests promising applications for controlling moisture distribution and enhancing separation processes.

The possibility of using electroosmosis for moisture removal from a body is associated with the existence of a double electric layer at the interface between the pore liquid and the solid skeleton. The presence of electric forces alters the nature of the drying process.

At the initial stage, a dried zone forms within the body only near a portion ( $S_1$ ) of the surface ( $S$ ) on the side of the acting forces (dried Zone 1). The other part ( $S_2$ ) of the body's surface remains moist, and if the electric force exceeds the capillary force caused by the curvature of the liquid-gas contact surface, electroosmotic liquid outflow will occur through this region. The liquid-gas phase transition surface is denoted by  $S^*$ .

As the dried zone expands, its electrical resistance and voltage drop increase. Consequently, the voltage and the electric field intensity in the liquid-filled region will decrease. The reduction in liquid content during drying will also lead to a decrease in its total electric charge. The ponderomotive force  $\rho_q \vec{E}$  ( $\rho_q$  is the average charge density of the diffuse layer,  $\vec{E}$  is the electric field



intensity in the pores) acting on the liquid due to the electric field will diminish throughout the drying process. Meanwhile, the capillary force remains nearly unchanged at this stage.

Once these forces reach equilibrium, the electroosmotic liquid outflow through the surface ( $S_2$ ) ceases, and a dried zone also begins to form there. From this moment, the dried zones propagate inward from the surfaces ( $S_1$ ) and ( $S_2$ ), moving toward each other. Thus, the drying process occurs in two stages:

*The 1<sup>st</sup> stage of drying.*

The mass transfer equations in the dried zone and the boundary conditions will be assumed under the following formulation:

$$\vec{\nabla} \cdot \left[ \rho_v \frac{K_g}{\mu_g} \vec{\nabla} \left( \frac{\rho_a}{M_a} + \frac{\rho_v}{M_v} \right) RT + D' \vec{\nabla} \rho_v \right] = 0, \quad (4.1)$$

where  $\rho_v$  is water vapor density;  $\rho_a$  is air density;  $K_g$  is permeability coefficient of the porous medium, depending on the radius and shape of the pores;  $\mu_g$  is dynamic viscosity coefficient of the gas;  $M_a$  is molar mass of air;  $M_v$  is molar mass of water vapor;  $R$  is universal gas constant;  $T$  is temperature;  $D'$  is effective binary diffusion coefficient in the pores.

On the moving surface ( $S^*$ ), the vapor density can be assumed to be equal to the saturated vapor density [28, 29]:

$$\rho_v = \rho_{v*}. \quad (4.2)$$

The form of the boundary conditions on the surface ( $S$ ) depends on the method of modeling the interaction between the body and the surrounding environment.

In the case under consideration, where the body is in contact with an environment consisting of an air-vapor mixture on the surface ( $S$ ) under natural drying conditions, it can be assumed that at a sufficient distance from the surface ( $S$ ), the vapor density  $\rho_{ve}$  and air density  $\rho_{ae}$  reach constant values  $\rho_{v1}$  and  $\rho_{a1}$ , respectively, which are characteristic of atmospheric air, i.e. [3, 12, 35, 36]:

$$\lim_{r \rightarrow \infty} \rho_{ve} = \rho_{v1}, \quad \lim_{r \rightarrow \infty} \rho_{ae} = \rho_{a1}, \quad (4.3)$$

where  $r$  is the distance from the surface ( $S$ ).

In the region external to the body, mass transfer processes will be described by the Stefan-Maxwell equations under the assumption of constant atmospheric pressure:

$$\vec{\nabla} \rho_{ae} - \frac{\rho_{ae}}{D'_e} \vec{v}_e = 0,$$

$$\vec{\nabla} \cdot \left( \vec{\nabla} \rho_{ve} - \frac{\rho_{ve}}{D'_e} \vec{v}_e \right) = 0, \quad (4.4)$$

$$P_{ge} = \left( \frac{\rho_{ae}}{M_a} + \frac{\rho_{ve}}{M_v} \right) RT = \text{const.} \quad (4.5)$$

On the surface ( $S$ ), the normal component of the vapor flux from the drying body must be continuous, i.e.:

$$\vec{n} \cdot \vec{j}_v = \left( \vec{\nabla} \rho_{ve} - \frac{\rho_{ve}}{D'_e} \vec{v}_e \right) \cdot \vec{n}, \quad (4.6)$$

as well as the component densities of the mixture, which follow from the equality of partial pressures at the surface ( $S$ ):

$$\rho_{ae} = \rho_a, \rho_{ve} = \rho_v. \quad (4.7)$$

Equations (4.1)–(4.7) form a complete system of relations and can be used to describe mass transfer under natural drying of a porous body [30, 31].

At the first stage, the liquid moves under the influence of electric forces toward the surface ( $S_2$ ) with velocity (Generalized Darcy's law):

$$\vec{v}_l = \frac{K_L}{\mu_L} \left( \rho_q \vec{E} - \vec{\nabla} P_k \right),$$

where  $K_L$  is the permeability coefficient of the body relative to the liquid;  $\mu_L$  is its dynamic viscosity;  $P_k$  is the pressure induced by the curvature of the liquid-gas contact surface. It is possible to assume that the liquid freely exits the pores. At this stage, the phase transition of liquid to vapor near the surface ( $S_2$ ) will not be considered.

Thus, the amount of liquid in the body will decrease both due to drying from the surface ( $S_1$ ) and due to electroosmotic removal of moisture through the surface ( $S_2$ ). The mass balance equation in this case takes the form:

$$\frac{dm}{dt} = - \int_{(S_1)} (j_{v1} \cdot \vec{n}_1) dS_1 - \int_{(S_2)} (j_{v2} \cdot \vec{n}_2) dS_2, \quad (4.8)$$

where  $\vec{n}_1, \vec{n}_2$  are the outward normals to the surfaces ( $S_1$ ) and ( $S_2$ ), respectively;  $\vec{j}_{v1}$  is the vapor flux through the surface ( $S_1$ );  $\vec{j}_l$  is the liquid flux through the surface ( $S_2$ ):

$$j_L = \Pi \gamma_L \bar{V}_L. \quad (4.9)$$

The 2<sup>d</sup> stage of drying.

At the moment when the electrical and capillary forces balance each other, i.e.:

$$\int_{(V_l)} \rho_q \bar{E} dV_L - P_k S_1^* = 0, \quad (4.10)$$

the liquid outflow ceases, and a second dried zone (Zone 2) emerges, which will expand from surface ( $S_2$ ) into the depth of the material. In (4.10) ( $V_L$ ) represents the region of the body occupied by the liquid;  $V_L$  is its volume, and  $S_1^*$  is the area of the gas-liquid contact surface.

The problem of drying Zone 2 is formulated similarly to the drying problem for Zone 1. The mass balance equation for the moisture in the material now takes the form:

$$\frac{dm_L}{dt} = - \int_{(S_1)} (j_{v1} \cdot \bar{n}_1) dS_1 - \int_{(S_2)} (j_{v2} \cdot \bar{n}_2) dS_2. \quad (4.11)$$

#### **Determination of electrical quantities.**

The electric field intensity is determined from the corresponding electrostatics problems. For the first stage, the governing equation is given as:

$$\Delta \phi_j = 0, \quad \bar{E}_j = -\bar{\nabla} \phi_j, \quad (j = 1, 2), \quad (4.12)$$

which applies to the region ( $V_1$ ) ( $j = 1$ ), bounded by surfaces ( $S_1$ ) and ( $S_1^*$ ), and the region ( $V_L$ ) ( $j = 2$ ), occupied by liquid, with the boundary conditions:

$$\phi_1 = \phi_{01} \text{ on the surface } (S_1), \quad \phi_2 = \phi_{02} \text{ on the surface } (S_2), \quad (4.13)$$

and the conjugation conditions at the interface:

$$\phi_1 = \phi_2, \quad \bar{n}_1 \cdot (\bar{j}_1 - \bar{j}_2) = 0, \text{ on the surface } (S_1^*), \quad (4.14)$$

where

$$\bar{j}_j = \sigma_j \bar{E}_j, \quad (j = 1, 2). \quad (4.15)$$

Here,  $\bar{j}_1, \bar{j}_2$  are the current density vectors, while  $\sigma_1, \sigma_2$  denote the electrical conductivity coefficients in regions ( $V_1$ ) and ( $V_L$ ), respectively. The vector  $\bar{n}_1$  represents the normal to the interface ( $S_1^*$ ).

For the second stage of drying, the electrostatics problem is formulated as:

$$\Delta\phi_m = 0, \vec{E}_m = -\vec{\nabla}\phi_m, \quad (m = 1, 2, 3), \quad (4.16)$$

for the regions  $(V_1)$  ( $m = 1$ ),  $(V_2)$  ( $m = 2$ ), and  $(V_3)$  ( $m = 3$ ), bounded by surfaces  $(S_1^*)$  and  $(S_2)$ , under the boundary conditions:

$$\phi_1 = \phi_{01} \text{ on the surface } (S_1), \quad \phi_3 = \phi_{02} \text{ on the surface } (S_2), \quad (4.17)$$

and the conjugation conditions:

$$\begin{aligned} \phi_1 &= \phi_2, \quad \vec{n}_1 \cdot (\vec{j}_1 - \vec{j}_2) = 0, \text{ on the surface } (S_1^*), \\ \phi_2 &= \phi_3, \quad \vec{n}_2 \cdot (\vec{j}_2 - \vec{j}_3) = 0, \text{ on the surface } (S_2^*), \end{aligned} \quad (4.18)$$

where  $\vec{n}_2$  is the normal to the surface  $(S_2^*)$ .

The average charge density of the diffuse layer for a binary electrolyte solution, based on the theory of the double electric layer and works [1, 32, 33], is determined by the formula:

$$\rho_q = \sqrt{\frac{2\varepsilon_f C \Pi}{fRTk_p}} \frac{zF\phi_1}{T_r}, \quad (4.19)$$

where  $\varepsilon_f$  is the average absolute dielectric permittivity of the liquid phase;  $T_r$  is the tortuosity factor;  $k_p$  is the permeability coefficient of the porous medium;  $\phi_1$  is the surface potential at the closest approach of ions [7];  $z = z_+ = -z_-$ , where  $z_+$  and  $z_-$  are the valencies of cations and anions;  $F_f$  is the Faraday constant;  $C$  is the electrolyte concentration;  $\Pi$  is the porosity of the material.

Thus, the problem of electroosmotic drying of a porous body includes the relationships given by (4.1)–(4.9).

It should also be noted that the use of an *isothermal model* for describing electroosmotic drying requires imposing appropriate restrictions on the magnitude of the external electric field.

## 4.1 ELECTROOSMOSIS DRYING A POROUS LAYER

Let's consider the problem of the influence of electroosmosis influence on drying a porous layer, where free evaporation occurs on one of its surfaces into the external environment, while the other surface is supplied with moisture from a well-permeable wet medium. This problem can model the drying of basements after floods.

A porous layer initially saturated with moisture is examined, with one of its surfaces (Surface 1) in contact with an environment that is a mixture of air and vapor, while Surface 2 borders a well-permeable wet medium.

The air and layer temperatures are assumed to be equal.

Since the vapor in the pores is saturated at the liquid surface, while the surrounding environment is unsaturated, vapor outflow occurs from Surface 1. As a result, a region of dried pores filled with a mixture of air and vapor is formed within the body, where these components are considered separate constituents of the filling gas. During the drying process, this zone expands deeper into the material. The coordinate of the moving boundary is denoted as  $z = L_m$ .

To intensify the drying process via electroosmotic moisture removal from the porous layer, a constant potential difference is applied between Surfaces 1 and 2. Due to the influence of the electric field on the charge of the diffuse part of the electrical double layer at the solid skeleton-pore liquid interface, an additional (ponderomotive) force arises, inducing an electroosmotic moisture flux  $j_3$  toward Surface 2. Under the action of the electric field, a directed movement of electric charges in the diffuse part of the electrical double layer occurs, accompanied by the movement of the liquid layer along the pore surfaces (electroosmosis) [34, 35].

If a well-permeable wet medium is present on the side of Surface 2, a significant portion of moisture is absorbed into the porous layer through capillary imbibition. Capillary imbibition, driven by the gradient of capillary pressure, results in the formation of a filtration flux  $j_2$ .

As a result of the combined action of these fluxes, changes in the relative moisture content of the porous layer occur. Notably, if the dispersion of pore sizes in the porous body model is neglected, the relative moisture content  $\alpha_m$ , defined as before, coincides with the phase interface boundary:

$$\bar{z}_m = \frac{L_m}{L_0}.$$

The mass of liquid lost during the drying process is given by:

$$\Delta m = m_{L_n} - m_L = \Pi S \rho_L L_0 (1 - \bar{z}_m),$$

where  $S$  is the pore area;  $\rho_L$  is the density of water;  $\Pi$  is the porosity of the material. Given that the rate of change of liquid mass in the layer is determined by the vapor and liquid flux  $j$  from the layer, let's arrive at the differential equation governing the relative moisture content  $\alpha_m$  in the layer, which can also be interpreted as the equation of motion for the phase interface:

$$\frac{d\alpha_m}{dt} = \frac{d\bar{z}_m}{dt} = -\frac{j(\bar{z}_m)}{\Pi \rho_L L_0},$$

where  $j(\bar{z}_m)$  is the total flux acting in the porous medium, which is the sum of the vapor flux, the electroosmotic flux, and the flux induced by capillary pressure, counteracting the electroosmotic flow.

The phase transition from liquid to vapor at the gas-liquid interface is accounted for by specifying the density of the saturating vapor on this surface, which depends on the temperature and is given by the formula:

$$\rho_n(T) = 133e^{\left[18.681 - \frac{4105}{(T-35)}\right]} \frac{M_v}{RT} \quad (\text{kg/m}^3). \quad (4.20)$$

As a result of solving the nonlinear boundary problem, the dependence of the convective-diffusive vapor flux on the parameters of the porous and boundary layers is determined in the form [30, 39]:

$$j_1(\bar{z}_m) = \frac{\Omega}{B - \Gamma_0 \bar{z}_m}, \quad (4.21)$$

where  $\Omega$  is a parameter characterizing the intensity of moisture transfer, which depends on the physical properties of the medium and the drying conditions;  $B$  is a coefficient that depends on the effective diffusion and permeability characteristics of the porous medium;  $\Gamma_0$  is a parameter characterizing the influence of the electric field on the mass transfer process [2].

#### 4.11 CAPILLARY MOISTURE FLOW

The transfer caused by capillary imbibition is considered. The capillary pressure is determined by the Laplace equation:

$$P_k = P_L - P_g = \frac{-2\sigma_{lg} \cos\theta}{\bar{R}},$$

where  $\theta$  is the angle formed by the meniscus surface with the solid surface;  $P_L$ ,  $P_g$  are the pressures in the liquid and gas phases, respectively;  $\sigma_{lg}$  is the surface tension coefficient at the liquid-gas interface.

In the Laplace equation,  $\bar{R}$  represents the equivalent Kelvin radius. The flux  $j_2$  caused by capillary imbibition is determined using Poiseuille's equation:

$$j_2 = \Pi \rho_L \frac{K_L}{\mu_L} \frac{P_K}{L_0 \bar{z}_m}, \quad (4.22)$$

where  $K_L$  is the permeability of the liquid;  $\mu_L$  is the dynamic viscosity of the liquid.

## 4.1.2 ELECTROOSMOTIC LIQUID FLOW

The liquid flow caused by the action of an external constant electric field is considered under the condition of the presence of a dried pore zone. The effect of the electric field on the pore liquid is associated with the presence of a double electric layer near the pore surface. The skeleton material is assumed to be hydrophilic, and the minimum transverse pore size is significantly larger than the thickness of the diffuse part of the double electric layer  $\delta_e = 1/K_e$ , where for a symmetric binary electrolyte solution [1, 32]:

$$K_e = \sqrt{2\pi F_f^2 Z^2 C_0 / \varepsilon^{(1)} RT},$$

where  $F_f$  is Faraday's constant;  $Z$  is valence of ions considering their charge sign;  $C_0$  is electrolyte solution concentration;  $\varepsilon^{(1)}$  is absolute dielectric permeability of the liquid.

Then, on average, the charge density  $\rho_e$  in the diffuse part of the double electric layer is determined as [1]:

$$\rho_e = \rho_{e0} e^{-K_e(\bar{R}-r)}, \quad (4.23)$$

where  $\rho_{e0}$  is charge density value on the surface of capillaries;  $r$  is running radial coordinate.

For the assumed condition of the smallness of the double electric layer thickness compared to the capillary radius,  $K_e \bar{R} \gg 1$ .

The force density across the capillary section:

$$f_e = \rho_e E_L,$$

where  $E_L = U_L/L_m$  is electric field intensity;  $U_L$  is voltage applied to the liquid-filled part of the capillary.

The average force density:

$$\bar{f}_e = \frac{2\rho_{e0} E_L}{K_e \bar{R}} - \frac{2\rho_{e0} E_L}{(K_e \bar{R})^2} (1 - e^{-K_e \bar{R}}).$$

For the earlier assumption  $\bar{R} K_e \gg 1$ , let's obtain:

$$\bar{f}_e \approx \frac{2\rho_{e0} E_L}{K_e \bar{R}} = \frac{2\bar{\eta} E_L}{\bar{R}},$$

where  $\bar{\eta} = \rho_{e0} / K_e$ .

The force acting on the charge in the capillary:

$$\bar{F}_e = \bar{f}_e SL_m.$$

The average pressure caused by electrical forces:

$$\bar{P}_e = \bar{F}_e / S = \bar{f}_e L_m.$$

The gradient of this pressure:

$$\bar{\nabla} \bar{P}_e = \left( d\bar{P}_e / dz \right) \bar{e}_z, \quad d\bar{P}_e / dz = -\bar{P}_e / L_m = -\bar{F}_e / SL_m = -\bar{f}_e.$$

Considering that the current forces  $I_g$  and  $I_L$  in the dried and liquid-saturated pore regions are equal, i.e.,  $I_g = I_L$ , according to Ohm's law:

$$I_g = U_g / R_g, \quad I_L = U_L / R_L,$$

let's obtain  $U_g / U_L = R_g / R_L$ .

Here

$$R_g = \rho_g^* (L_0 - L_m) / S, \quad R_L = \rho_L^* L_m / S,$$

where  $\rho_g^*, \rho_L^*$  are the specific resistances of these regions.

As the voltage  $U$  between the layer surfaces is  $U = U_g + U_L$ , then:

$$\frac{U}{U_L} = 1 + \frac{\rho_g^* (1 - \bar{z}_m)}{\rho_L^* \bar{z}_m} = 1 + \frac{(1 - \bar{z}_m)}{\varepsilon_p \bar{z}_m}. \quad (4.24)$$

Here  $\varepsilon_p = \rho_L^* / \rho_g^*$  is the ratio of specific resistances in the liquid and dried zones, and  $\bar{z}_m = L_m / L_0$ . From (4.24), it follows that:

$$U_L = \varepsilon_p U \bar{z}_m / \left[ (1 - \bar{z}_m) + \varepsilon_p \bar{z}_m \right].$$

Then the electric field intensity in the liquid zone is:

$$E_L = U_L / L_m = \varepsilon_p U / L_0 \left[ (1 - \bar{z}_m) + \varepsilon_p \bar{z}_m \right].$$

The formulas for determining the pressure gradient and the magnitude of the electroosmotic flow  $j_3$  are given as follows:



$$\begin{aligned}\frac{d\bar{P}_e}{dz} &= -\bar{f}_e = -\frac{2\bar{\eta}}{\bar{R}} \frac{\varepsilon_p U}{L_0 [\varepsilon_p \bar{z}_m + (1 - \bar{z}_m)]}; \\ j_3 &= \Pi \rho_L v_3; \\ v_3 &= \frac{K_L}{\mu_L} \frac{dP_e}{dz} = -\frac{K_L}{\mu_L} \frac{2\bar{\eta}}{\bar{R}} \frac{\varepsilon_p U}{L_0 [\varepsilon_p \bar{z}_m + (1 - \bar{z}_m)]}.\end{aligned}\quad (4.25)$$

#### 4.1.3 SOLUTION OF THE PROBLEM AND RESULTS OF QUANTITATIVE ANALYSIS

The determination of the change in relative moisture content during the drying process is reduced to the Cauchy problem, where the convective-diffusion flow is determined from (4.21), and the capillary and electroosmotic flows are determined from (4.22) and (4.23), respectively:

$$\begin{aligned}\frac{d\bar{z}_m}{dt} &= -\frac{\Omega}{B - \Gamma_0 \bar{z}_m} + \frac{\tilde{K}}{\bar{z}_m} + \frac{\tilde{K}_1}{(1 - \bar{z}_m) + K_2 \bar{z}_m}, \quad \bar{z}_m(0) = 1; \\ \tilde{K} &= \frac{K_L}{\mu_L \bar{R}} \frac{2\sigma_{lg}}{L_0^2}, \quad \tilde{K}_1 = \frac{K_L}{\mu_L} \frac{2\bar{\eta} \varepsilon_p E}{\bar{R} L_0}.\end{aligned}\quad (4.26)$$

Equation (4.26) can be written as follows:

$$\frac{a_{32} \bar{z}_m^3 + a_{22} \bar{z}_m^2 + a_{12} \bar{z}_m}{a_{21} \bar{z}_m^2 + a_{11} \bar{z}_m + a_{01}} \frac{d\bar{z}_m}{dt} = 1;$$

where

$$a_{21} = \Omega(1 - K_2) + \tilde{K} \Gamma_0 (1 - K_2) - \tilde{K}_1 \Gamma_0;$$

$$a_{11} = -\Omega - \tilde{K} B (1 - K_2) - \tilde{K} \Gamma_0 + \tilde{K}_1 B;$$

$$a_{01} = \tilde{K} B; \quad a_{32} = \Gamma_0 (1 - K_2);$$

$$a_{22} = -B(1 - K_2) - \Gamma_0;$$

$$a_{12} = B;$$

or

$$\left[ \frac{a_{32}}{a_{21}} \frac{\bar{z}_m}{2} + \frac{a_{42} \bar{z}_m^2 + a_{41} \bar{z}_m}{a_{21} \bar{z}_m^2 + a_{11} \bar{z}_m + a_{01}} \right] d\bar{z}_m = dt;$$

$$a_{42} = a_{22} - \frac{a_{32}a_{11}}{a_{21}};$$

$$a_{41} = a_{12} - \frac{a_{32}a_{01}}{a_{21}}.$$

The solution of (4.26) using the initial condition  $\bar{z}_m(0) = 1$  has the form:

$$\frac{1}{2} \frac{a_{32}}{a_{21}} (\bar{z}_m^2 - 1) + \frac{a_{42}}{a_{21}} (\bar{z}_m - 1) + \left( -\frac{a_{42}a_{11}}{2a_{21}^2} + \frac{a_{41}}{2a_{21}} \right) \ln |f_2(\bar{z}_m)| + f(\bar{z}_m) = t, \quad (4.27)$$

where

$$f(\bar{z}_m) = \left( \frac{a_{42}(a_{11}^2 - 2a_{21}a_{01})}{2a_{21}^2} - \frac{a_{41}a_{11}}{2a_{21}} \right) f_1(\bar{z}_m);$$

$$f_1(\bar{z}_m) = \frac{2}{\sqrt{4a_{21}a_{01} - a_{11}^2}} \left( \arctan \frac{2a_{21}\bar{z}_m + a_{11}}{\sqrt{4a_{21}a_{01} - a_{11}^2}} - \arctan \frac{2a_{21} + a_{11}}{\sqrt{4a_{21}a_{01} - a_{11}^2}} \right);$$

$$|f_2(\bar{z}_m)| = \left| \frac{a_{21}\bar{z}_m^2 + a_{11}\bar{z}_m + a_{01}}{a_{21} + a_{11} + a_{01}} \right|, \text{ if } 4a_{21}a_{01} > a_{11}^2.$$

Otherwise,

$$f_1(\bar{z}_m) = \frac{1}{\sqrt{a_{11}^2 - 4a_{21}a_{01}}} \ln |f_3(\bar{z}_m)|,$$

where

$$f_3(\bar{z}_m) = \frac{2a_{21}\bar{z}_m + a_{11} - \sqrt{a_{11}^2 - 4a_{21}a_{01}}}{2a_{21}\bar{z}_m + a_{11} + \sqrt{a_{11}^2 - 4a_{21}a_{01}}} \frac{2a_{21} + a_{11} + \sqrt{a_{11}^2 - 4a_{21}a_{01}}}{2a_{21} + a_{11} - \sqrt{a_{11}^2 - 4a_{21}a_{01}}}, \text{ if } a_{11}^2 > 4a_{21}a_{01}.$$

The formulas obtained above are the basis for a quantitative analysis of the influence of geometric and physical parameters on the drying a porous layer of cement stone.

**Table 4.1** shows the dependence of relative moisture content at a fixed point in time on temperature and boundary layer thickness during capillary infiltration under natural drying (without an electric field). The influence of an external constant electric field is illustrated by the data given in **Tables 4.2** and **4.3** for different boundary layer thicknesses.

#### 4 DRYING OF A POROUS LAYER IN AN EXTERNAL CONSTANT ELECTRIC FIELD (ELECTROOSMOTIC DRYING)

● **Table 4.1** Consideration of capillary imbibition ( $t = 10^4$  s,  $L_0 = 0.1$  m)

	$\delta, \text{ m}$	$T_1 = 300 \text{ K}$	$T_2 = 310 \text{ K}$	$T_3 = 320 \text{ K}$	$T_4 = 330 \text{ K}$
$\alpha_m = \bar{z}_m$	0.0001	0.573	0.428	0.254	0.082
	0.001	0.591	0.445	0.27	0.091
	0.01	0.727	0.59	0.416	0.209
	0.1	0.967	0.933	0.875	0.784

● **Table 4.2** Influence of electric field intensity on relative moisture content at  $E = 200$  V/m

	$\delta, \text{ m}$	$T_1 = 300 \text{ K}$	$T_2 = 310 \text{ K}$	$T_3 = 320 \text{ K}$	$T_4 = 330 \text{ K}$
$\alpha_m = \bar{z}_m$	0.0001	0.561	0.415	0.242	0.075
	0.001	0.577	0.432	0.257	0.083
	0.01	0.705	0.569	0.396	0.193
	0.1	0.914	0.873	0.81	0.718

● **Table 4.3** Influence of electric field intensity on relative moisture content at  $E = 400$  V/m

	$\delta, \text{ m}$	$T_1 = 300 \text{ K}$	$T_2 = 310 \text{ K}$	$T_3 = 320 \text{ K}$	$T_4 = 330 \text{ K}$
$\alpha_m = \bar{z}_m$	$10^{-4}$	0.524	0.377	0.206	0.059
	$10^{-2}$	0.647	0.511	0.343	0.149

In **Fig. 4.1** and **4.2**, the dynamics of relative moisture content dependence on time are shown for  $\delta = 0.001$  m and  $\delta = 0.1$  m, respectively (curves 1, 2, 3, 4) for  $T = 300$  K, 310 K, 320 K, and 330 K.

From the provided quantitative data, it follows that the intensity of drying significantly depends on the thickness of the boundary layer. When the thickness of the boundary layer increases by a factor of 100, the relative moisture content may increase by a factor of 10 or more. At a boundary layer thickness of  $\delta = 0.1$  m and temperatures of 300 K, 310 K, and 320 K, the relative moisture content decreases by no more than 10 % over approximately 3 hours.

An electric field intensity of  $E = 200$  V/m and  $E = 400$  V/m (these are not high fields) counteracts liquid infiltration through wall 2, leading to a resultant reduction in relative moisture content of up to 40 %.

Let's investigate the influence of electroosmosis on the drying process of a porous layer under convective mass transfer on one of its surfaces. Let's consider a porous layer initially saturated with moisture, where one surface (Surface 1) is in contact with a gaseous environment (air), while the other surface (Surface 2) is in contact with a moisture-saturated, highly permeable

wet medium. It is assumed that gas flow can be applied to Surface 1 and a constant difference in electric potential can be created between Surfaces 1 and 2. This allows to explore the possibility of stimulating and controlling the drying process through air blowing on Surface 1 and electroosmotic moisture removal. The transport of air and vapor in the dried region is described by the Stefan-Maxwell equations [31] with boundary conditions on Surface 1.

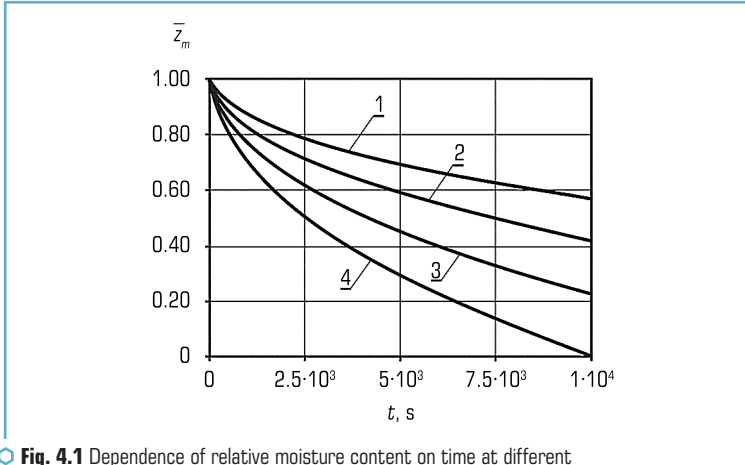


**Fig. 4.1** Dependence of relative moisture content on time at different temperatures for  $\delta = 0.001$  m

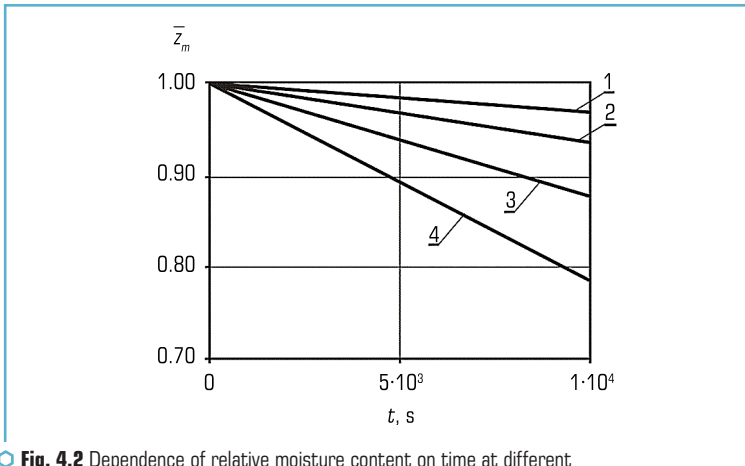


**Fig. 4.2** Dependence of relative moisture content on time at different temperatures for  $\delta = 0.1$  m

## 4.2 ENHANCEMENT OF CONVECTIVE DRYING OF A POROUS LAYER SURFACE BY ELECTROOSMOSIS

Solving the nonlinear boundary value problem, let's determine the vapor density at the wall  $\eta_1$  and the vapor flux magnitude  $j_1$ :

$$\eta_1 = -\left(A + B\bar{z}_m^*\right) + \sqrt{U + S\bar{z}_m^* + B^2\bar{z}_m^{*2}}, \quad (4.28)$$

$$j_1 = H\left[-\left(a_1 + B\bar{z}_m^*\right) + \sqrt{U + S\bar{z}_m^* + B^2\bar{z}_m^{*2}}\right]. \quad (4.29)$$

Due to the pressure effect under the meniscus of the water surface in the pores at the gas-liquid contact boundary, capillary moisture inflow occurs from the medium in contact with the layer at Surface 2. The competition between drying and moisture inflow may lead to a steady-state moisture content level in the layer. To further reduce moisture, a constant electric field generated by an external source can be used. The action of the field on the electric charge in the diffuse part of the double electric layer at the solid-liquid interface creates an additional (ponderomotive) force that reduces moisture inflow or drives electroosmotic moisture flux toward Surface 2. The vapor outflow conditions through Surface 1 of the drying body are modeled using third-kind mass transfer conditions (4.29). The mass transfer coefficient is related to the nature of the air blowing on Surface 1, which intensifies the drying process.

The total flux  $j$  consists of the diffusion-convective flux  $j_1$ , the flux due to capillary imbibition  $j_2$ , and the electroosmotic liquid flux  $j_3$ , caused by the force with which the electric field acts on the charged liquid.

For partial filling of the capillary with liquid, surface forces act at the three-phase liquid-gas-solid interface, forming a meniscus — a curved gas-liquid boundary surface.

The flux  $j_2$  due to capillary imbibition, according to Poiseuille's equation, is defined as:

$$j_2 = \Pi \rho_l \nu_l = \Pi \rho_l \frac{K_l}{\mu_l} \frac{P_k}{L_0 (1 - \bar{z}_m^*)}. \quad (4.30)$$

The electroosmotic flux is given in the form:

$$j_3 = \rho_l \nu_{osm} \Pi = \frac{\rho_l K_l \Pi}{\mu_l} \frac{2\bar{\eta} \epsilon_p E}{\bar{R} \left[ (1 - \bar{z}_m) + \epsilon_p \bar{z}_m \right]}. \quad (4.31)$$

Thus, the problem reduces to the following Cauchy problem:

$$\frac{d\bar{z}_m^*}{dt} = H \left[ f(\bar{z}_m^*) + \frac{\tilde{K}}{1 - \bar{z}_m^*} + \frac{\tilde{K}_1}{K_2(1 - \bar{z}_m^*) + K_3\bar{z}_m^*} \right], \quad H = -\frac{\beta\rho_n}{\Pi\rho_0\rho_l}; \quad (4.32)$$

$$f(\bar{z}_m^*) = -(a_1 + B\bar{z}_m^*) + \sqrt{U + S\bar{z}_m^* + B^2\bar{z}_m^{*2}}, \quad (4.33)$$

under the initial condition  $\bar{z}_m^*(0) = 0$ ,

$$\text{where } \tilde{K} = \frac{\rho_l K_l P_k}{\mu_l L_0 \beta \rho_n}; \quad P_k = -\frac{2\sigma}{R}; \quad K_2 = \varepsilon_p; \quad K_3 = 1; \quad \tilde{K}_1 = \frac{2K_l \rho_l \Pi \varepsilon_p \bar{\eta} E}{\beta \rho_n \mu_l \bar{R}}.$$

By substituting the variables  $\sqrt{U + S\bar{z}_m^* + B^2\bar{z}_m^{*2}} = \chi + \bar{z}_m^* B$ , (4.33) transforms into:

$$-\frac{2(B\chi^2 - S\chi + BU)}{(S - 2B\chi)^2} \frac{d\chi}{dt} = H(\chi - a_1)f_2(\chi), \quad (4.34)$$

$$f_2(\chi) = \frac{(\tilde{a}\chi^4 + \tilde{b}\chi^3 + c\chi^2 + \tilde{d}\chi + \tilde{e})}{(\chi^2 + 2\chi B - \omega_1)(\Omega_2\chi^2 + \Omega_1\chi + \Omega_0)}, \quad (4.35)$$

where

$$\omega_1 = S + U;$$

$$\Omega_2 = K_2 - K_3;$$

$$\Omega_1 = 2K_2B;$$

$$\Omega_0 = -K_2\omega_1 + K_3U;$$

$$\tilde{a} = 1;$$

$$\tilde{b} = \frac{\Omega_1 + 2B\Omega_2}{\Omega_2};$$

$$\tilde{c} = \frac{\Omega_0 + 2B\Omega_1 - \Omega_2\omega_1 + 2\tilde{K}B\Omega_2 + 2\tilde{K}_1B}{\Omega_2};$$

$$\tilde{e} = \frac{2\tilde{K}B\Omega_0 - \Omega_0\omega_1 - 2\tilde{K}_1B\omega_1}{\Omega_2};$$

$$\tilde{d} = \frac{2B\Omega_0 - \Omega_1\omega_1 + 2\tilde{K}B\Omega_1 + 4\tilde{K}_1B^2}{\Omega_2}. \quad (4.36)$$

Equation (4.34) can be rewritten as:

$$-\frac{2(B\chi^2 - S\chi + BU)f_3(\chi)}{(S - 2B\chi)^2(\chi - a_1)f_4(\chi)} \frac{d\chi}{dt} = H\Omega_2, \quad (4.37)$$

$$f_3(\chi) = (\chi^2 + 2\chi B - \omega_1)(\Omega_2\chi^2 + \Omega_1\chi + \Omega_0),$$

$$f_4(\chi) = (\chi - c_1)(\chi - c_2)(\chi - c_3)(\chi - c_4),$$

where  $c_i = \chi_i$ ,  $i = \overline{1, 4}$  are the roots of the fourth-order polynomial appearing in the numerator of equation (4.35).

The solution to this equation, considering the initial condition  $\bar{Z}_m^*(0) = 0$ , is given by:

$$\begin{aligned} D_1 \ln \left| \frac{S - 2B\chi}{S - 2B\sqrt{U}} \right| + D_2 \left[ \frac{1}{S - 2B\chi} - \frac{1}{S - 2B\sqrt{U}} \right] + \\ + D_3 \left[ \frac{1}{(S - 2B\chi)^2} - \frac{1}{(S - 2B\sqrt{U})^2} \right] + R_3 \ln \left| \frac{\chi - c_1}{\sqrt{U} - c_1} \right| + R_4 \ln \left| \frac{\chi - c_2}{\sqrt{U} - c_2} \right| + \\ + R_5 \ln \left| \frac{\chi - c_3}{\sqrt{U} - c_3} \right| + R_6 \ln \left| \frac{\chi - c_4}{\sqrt{U} - c_4} \right| = H\Omega_2 t, \end{aligned} \quad (4.38)$$

where  $D_1 = -\frac{R_2}{8B^3}$ ;  $D_2 = -\frac{1}{4B^2} \left( \frac{R_2 S}{B} + R_1 \right)$ ;  $D_3 = \frac{1}{4B} \left( \frac{R_2 S^2}{4B^2} + \frac{R_1 S}{2B} + R_0 \right)$ ; and coefficients  $R_0$ ,

$R_1, \dots, R_6$  are solutions of the algebraic system:

$$\sum_{i=0}^2 d_{i,6-j} R_i + \sum_{i=3}^6 b_{i-2,6-j} R_i = 4B\Omega_{1,6-j} \quad (j = \overline{0,6}),$$

$$d_{0,6} = d_{1,6} = d_{0,5} = 0; \quad d_{2,6} = d_{1,5} = d_{0,4} = 1; \quad d_{2,5} = d_{1,4} = d_{0,3} = \tilde{b};$$

$$d_{2,4} = d_{1,3} = d_{0,2} = \tilde{c}; \quad d_{2,3} = d_{1,2} = d_{0,1} = \tilde{d}; \quad d_{2,2} = d_{1,1} = d_{0,0} = \tilde{e};$$

$$b_{1,6} = 8B^3 a_{i+2,3};$$

$$b_{1,5} = 8B a_{i+2,2} + 12B^2 S a_{i+2,3}, \dots, b_{1,4} = 8B^3 a_{i+2,1} + 12B^2 S a_{i+2,2} - 6BS^2 a_{i+2,3};$$

$$b_{1,3} = 8B^3 a_{i+2,0} + 12B^2 S a_{i+2,1} - 6BS^2 a_{i+2,2} + S^3 a_{4,3};$$

$$b_{i,2} = 12B^2Sa_{i+2,0} - 6BS^2a_{i+2,1} + S^3a_{4,2}, \quad b_{i,1} = -6BS^2a_{i+2,0} + S^3a_{4,1};$$

$$b_{i,1} = S^3a_{4,0}, \quad a_{3,2} = -(c_4 + c_2 + c_3), \quad a_{3,1} = (c_2 + c_3)c_4 + c_2c_3;$$

$$a_{3,0} = -c_2c_3c_4, \quad a_{4,2} = -(c_4 + c_1 + c_3), \quad a_{i+2,1} = 1, \quad a_{4,1} = (c_1 + c_3)c_4 + c_1c_3;$$

$$a_{4,0} = -c_1c_3c_4;$$

$$a_{5,2} = -(c_2 + c_1 + c_4); \quad a_{5,1} = (c_1 + c_2)c_4 + c_1c_2; \quad a_{5,0} = -c_1c_4c_2;$$

$$a_{6,2} = -(c_2 + c_1 + c_3); \quad a_{6,1} = (c_1 + c_2)c_3 + c_1c_2; \quad a_{6,0} = -c_1c_3c_2;$$

$$a_{0,4} = B; \quad a_{0,3} = 2B^2 - S; \quad a_{0,2} = \omega_1B - 2BS + BU; \quad a_{0,1} = \omega_1S + 2B^2U;$$

$$a_{0,0} = -BU\omega_1; \quad \Omega_{16} = a_{0,4}\Omega_2; \quad \Omega_{15} = a_{0,4}\Omega_1 + a_{0,3}\Omega_2;$$

$$\Omega_{14} = a_{0,4}\Omega_0 + a_{0,3}\Omega_1 + a_{0,2}\Omega_2, \quad \Omega_{13} = a_{0,3}\Omega_0 + a_{0,2}\Omega_1 + a_{0,1}\Omega_2,$$

$$\Omega_{12} = a_{0,2}\Omega_0 + a_{0,1}\Omega_1 + a_{0,0}\Omega_2, \quad \Omega_{11} = a_{0,1}\Omega_0 + a_{0,0}\Omega_1, \quad \Omega_{10} = a_{0,0}\Omega_0.$$

The transcendental equation (4.38) establishes the relationship between the relative moisture content in the porous layer and time, depending on the system parameters, as presented in **Tables 4.4, 4.5**, and **Fig. 4.3–4.5**.

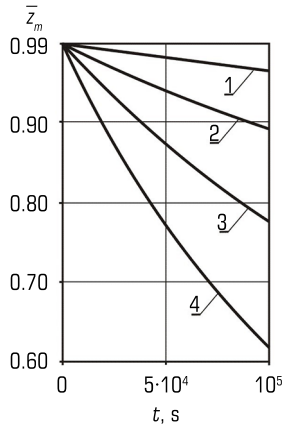


**Fig. 4.3** Time variation of relative moisture content for different temperature values in the absence of an external electric field



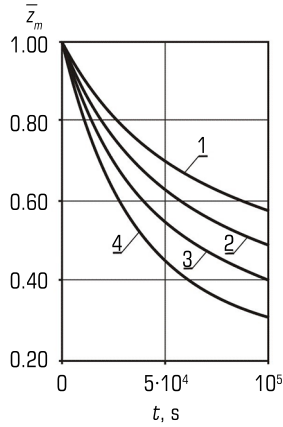


**Fig. 4.4** Time variation of relative saturation as a function of temperature at a given electric field strength  $E = 200$  V/m

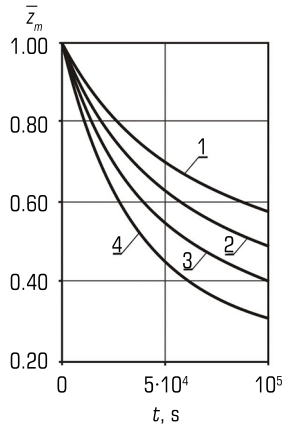


**Fig. 4.5** Time dependence of relative moisture content for different values of the mass transfer coefficient at  $E = 200$  V/m

#### 4.2.1 NUMERICAL ANALYSIS OF PARAMETER INFLUENCE ON CONVECTIVE ELECTROSMOTIC DRYING

**Fig. 4.3–4.5** show the time dependence of relative moisture content considering capillary imbibition in the absence and presence of an external electric field. In **Fig. 4.3** and **4.4**, curves 1

correspond to a temperature of 300 K; curves 2 correspond to 310 K; curves 3 correspond to 320 K; curves 4 correspond to 330 K. The calculations were performed using  $\beta = 0.01$  and  $L_0 = 0.1$  m. The analysis of the results indicates that at  $T = 300$  K, an electric field intensity of  $E = 200$  V/m reduces the relative moisture content of the layer from 0.960 to 0.574 for  $t = 10^6$  s, whereas at  $T = 330$  K, it decreases from 0.620 to 0.313, nearly by a factor of two.

● **Table 4.4** Dependence of relative moisture content  $\bar{Z}_m = 1 - \bar{Z}_m^*$  on temperature at a mass transfer coefficient  $b = 0.01$  for  $E = 200$  V/m, and  $E = 400$  V/m

E, V/m	T, K			
	300	310	320	330
200	0.574	0.488	0.397	0.312
400	0.395	0.319	0.261	0.222

● **Table 4.5** Dependence of relative moisture content  $\bar{Z}_m$  on the mass transfer coefficient  $b$  at  $T = 300$  K,  $E = 200$  V/m, and  $E = 400$  V/m

E, V/m	$\beta$					
	0.01	0.005	0.0025	0.001	0.0005	0.0001
200	0.574	0.594	0.617	0.646	0.656	0.664
400	0.349	0.395	0.429	0.455	0.462	0.47

In **Fig. 4.4 and 4.5**, curves 1–6 correspond to the values of the mass transfer coefficient  $\beta = 0.0001, 0.0005, 0.001, 0.0025, 0.005$ , and  $0.01$ . In **Fig. 4.4**, curves 1–4 almost coincide with the abscissa axis, indicating that the relative moisture content corresponding to these curves is approximately equal to one, meaning that the moisture content of the layer remains nearly unchanged over the studied time interval. In the presence of an external constant electric field (**Fig. 4.5**), the drying process of the layer becomes significantly more effective. The drying rate also increases with higher mass transfer coefficients and temperature.

### 4.3 INFLUENCE OF AN EXTERNAL CONSTANT ELECTRIC FIELD ON BILATERAL NATURAL DRYING OF A POROUS LAYER

A porous layer, initially saturated with moisture, is considered within a Cartesian coordinate system  $(x, y, z)$  and occupies the region  $0 < z < L_0$ . The layer undergoes mass exchange with the surrounding environment from both sides, while the temperature of the medium and the layer remains the same. A constant difference in electric potential is maintained between the surfaces

of the layer. Due to the action of the field on the electric charge within the diffuse part of the electrical double layer near the solid matrix–pore liquid interface, an additional (ponderomotive) force arises, inducing an electroosmotic moisture flow within the body. The surface from which the electroosmotic flow is directed will be referred to as the first surface (Surface 1), while the other surface (toward which the flow is directed) will be referred to as Surface 2. The coordinate system is chosen such that Surface 1 coincides with  $z = L_0$  and Surface 2 with  $z = 0$ .

As a result of liquid evaporation from the pores and vapor outflow to the external environment, a zone of dried pores forms on the side of Surface 1, filled with a mixture of air, vapor, and residual liquid bound to the pore surfaces, which remains stable against drying at a given temperature. During the drying process, this zone expands deeper into the material. Let's consider a class of materials with low permeability to liquids, where the influence of a two-phase zone can be neglected [1]. Therefore, the formation of two distinct zones is assumed: dried pores and liquid-filled pores. The boundary between these zones within each pore is marked by a liquid meniscus, the convexity or concavity of which is determined by the properties of the pore surface (its hydrophilicity or hydrophobicity).

### 4.3.1 MASS TRANSFER IN THE SURROUNDING GAS

When formulating the mass transfer problem in the surrounding gas, it is assumed that changes in the density of its components – air and vapor – occur only within a certain layer of thickness  $\delta_i$ , ( $i=1,2$ ), which occupies the regions  $L_0 < z < L_0 + \delta_1$ ,  $0 > z > -\delta_2$ . At the surfaces  $z = L_0 + \delta_1$ ,  $z = -\delta_2$ , the air and vapor densities are equal to their values in atmospheric air. Thus, the mass transfer problem in the surrounding gas includes:

– the Stefan-Maxwell equations [31]:

$$\frac{\partial p_{ae}}{\partial z} - \frac{p_{ae}}{D_1} v = 0, \quad \frac{\partial}{\partial z} \left( \frac{\partial p_{ve}}{\partial z} - \frac{p_{ve}}{D_1} v \right) = 0, \quad \frac{p_{ae}}{M_a} + \frac{p_{ve}}{M_v} = \frac{P_{g1}}{RT}, \quad (4.39)$$

in the regions  $L_0 + \delta_1 > z > L_0$ ,  $0 > z > -\delta_2$ ;

– the boundary conditions:

$$\frac{p_{ve1}}{M_v} v - \frac{D_1}{M_v} \frac{\partial p_{ve1}}{\partial z} = j_1(L_0, t) \quad \text{on the surface } z = L_0; \quad (4.40)$$

$$p_{ve} = p_{v1}, \quad p_{ae} = p_{a1}, \quad p_{a1} = \frac{M_a P_{g1}}{RT} - \frac{M_a}{M_v} p_{v1} \quad \text{on the surface } z = L_0 + \delta; \quad (4.41)$$

$$\frac{p_{ve2}}{M_v} v_2 - \frac{D_1}{M_v} \frac{\partial p_{ve2}}{\partial z} = j_2(0, t) \quad \text{on the surface } z = 0; \quad (4.42)$$

$$\rho_{ve2} = \rho_{v2}, \quad \rho_{ae2} = \rho_{a2}, \quad \rho_{a2} = \frac{M_a P_{g1}}{RT} - \frac{M_a}{M_v} \rho_{v2} \quad \text{on the surface } z = -\delta_2, \quad (4.43)$$

where  $\rho_{vei}$ ,  $\rho_{aei}$  are the vapor and air densities, respectively;  $\rho_{vi}$ ,  $\rho_{ai}$  are the vapor and air densities at the surfaces  $z = L_0 + \delta_1$ ,  $z = -\delta_2$ ;  $v_i$  is the mass-averaged velocity;  $j_1$ ,  $j_2$  are the vapor fluxes at the surfaces.

### 4.3.2 MASS TRANSFER IN THE ZONE OF DRIED PORES

Mass transfer in the gas zone within the porous layer will also be described using the Stefan-Maxwell equations [31]. However, the gas pressure  $P$  in the pores depends on the coordinate, and the mass-averaged velocity  $v$  satisfies Darcy's law. Then, the transport equations in the region  $L_0 > z > L_{\max}$  take the form:

$$\rho_a \frac{K_g}{\mu_g} \frac{\partial P}{\partial z} + D \frac{\partial \rho_a}{\partial z} = 0, \quad \frac{\partial}{\partial z} \left( \rho_v \frac{K_g}{\mu_g} \frac{\partial P}{\partial z} + D \frac{\partial \rho_v}{\partial z} \right) = 0, \quad (4.44)$$

where  $L_{\max}$  is the coordinate of the gas-liquid contact boundary within the porous layer.

The boundary conditions at the surfaces  $z = L_0$  and  $z = L_{\max}$  in the gas zone are given as follows:

$$\rho_v \frac{K_g}{\mu_g} \frac{\partial P}{\partial z} + D \frac{\partial \rho_v}{\partial z} = -j_1 \quad \text{on the surface } z = L_0; \quad (4.45)$$

$$\rho_v = \rho_n \quad \text{on the surface } z = L_{\max}. \quad (4.46)$$

When a zone of dried pores forms near Surface 2, the mass transfer in this region is described by equation (4.44) with the following boundary conditions:

$$\rho_v \frac{K}{\mu_g} \frac{\partial P}{\partial z} + D \frac{\partial \rho_v}{\partial z} = j_2 \quad \text{on the surface } z = 0,$$

$$\rho_v = \rho_n \quad \text{on the surface } z = L_{\min}. \quad (4.47)$$

Equations (4.39)–(4.48) form a complete system of relationships for determining the convective-diffusive vapor flux in the given porous layer. The expression for this flux is obtained in the form:

$$j_1(\bar{z}_m) = \frac{\Omega}{B - \Gamma_0 \bar{z}_m}, \quad (4.48)$$

where  $\bar{z}_m$  is relative moisture content of the porous layer;  $B$  is a coefficient characterizing the convective-diffusive transfer equation, which includes material and transport properties;  $\Gamma_0$  is a coefficient accounting for the influence of relative moisture content  $\bar{z}_m$  on mass transfer;

$C_0$  is initial concentration of moisture;  $\eta_0 = \frac{\rho_{v1}}{\rho_n}$  is a dimensionless parameter expressing the ratio

of vapor density  $\rho_{v1}$  to a reference density  $\rho_n$ ;  $a$ ,  $b$  are coefficients of porosity and diffusion properties, respectively.

The electroosmotic flow is described by equation (4.25):

$$j_3 = \Pi \rho_L v_3, \quad v_3 = \frac{K_L}{\mu_L} \frac{dP_e}{dz} = -\frac{K_L}{\mu_L} \frac{2\bar{\eta}}{\bar{R}} \frac{\varepsilon_p U}{L_0 [\varepsilon_p \bar{z}_m + (1 - \bar{z}_m)]}. \quad (4.49)$$

### 4.3.3 LIQUID FLOW UNDER THE INFLUENCE OF CAPILLARY FORCES

Let the electric forces be sufficiently strong so that the liquid flows out through Surface 2. In this case, the capillary pressure  $P_k = P_L - P = 2\sigma L g \cos \theta / \bar{R}$  induces a flow of liquid  $j_4$  in the direction opposite to the electroosmotic flow:

$$j_4 = \Pi \rho_L v_4, \quad v_4 = \frac{K_L}{\mu_L} \frac{P_k}{L_{\max}} = \frac{K_L}{\mu_L} \frac{P_k}{L_0 \bar{z}_m}. \quad (4.50)$$

The total liquid flux  $j_L$  is determined as the sum of fluxes  $j_3$  and  $j_4$ :

$$j_L = j_3 + j_4 = \Pi \rho_L \left( \frac{K_L}{\mu_L} \left( \frac{P_k}{L_0 \bar{z}_m} - \frac{2\bar{\eta}}{\bar{R}} \frac{\varepsilon_p U}{L_0 [\varepsilon_p \bar{z}_m + (1 - \bar{z}_m)]} \right) \right). \quad (4.51)$$

During electroosmotic displacement of liquid through Surface 2 (i.e., reduction of parameter  $\bar{z}_m$ ), the magnitude of the first term in equation (4.52) will increase, while the second term changes weakly due to the smallness of parameter  $\varepsilon_p$ , or even decreases (Stage 1). The total liquid flux through Surface 2 will decrease until it reaches zero. At this moment, the electric field can be switched off. The capillary pressures at surfaces  $z = L_{\max}$  and  $z = 0$  will equalize, and the pore liquid will reach equilibrium. Drying of the layer through Surface 2 will then commence, governed by equations (4.39), (4.42), (4.45), (4.47), and (4.48).

Thus, the acceleration of the drying process due to electroosmosis will be observed only during the first stage.

Setting the total liquid flux  $j_L$  to zero in equation (4.51), let's obtain the following expression for the parameter  $\bar{z}_m^*$ , which defines the thickness of the saturated layer at the transition from the first to the second drying stage:

$$\bar{z}_m^* = \frac{\sigma}{\sigma(1 - \varepsilon_p) + \bar{\eta}\varepsilon_p U}. \quad (4.51)$$

Expression (4.51) is written for a zero wetting angle.

#### 4.3.4 MASS BALANCE EQUATION FOR LIQUID

The rate of liquid reduction in the layer is determined by the fluxes of liquid and vapor from the body. For the first drying stage, the mass balance equation for the liquid can be written as:

$$\frac{dm}{dt} = -\Pi(j_1 - j_L)S. \quad (4.52)$$

Considering that for the first drying stage  $m = \Pi S \rho_L L_m = \Pi S \rho_L L_0 \bar{z}_m$ , equation (4.54) can be rewritten in terms of the parameter  $\bar{z}_m$  as:

$$\frac{d\bar{z}_m}{dt} = -\frac{1}{L_0 \rho_L}(j_1 - j_L), \quad (4.53)$$

with the initial condition:

$$\bar{z}_m = 1 \text{ at } t = 0. \quad (4.54)$$

The final value of the parameter  $k_m = k_m^*$  corresponds to the first drying stage.

It is noteworthy that the relative moisture content  $\alpha_m = m_z / m_0$  of the porous layer ( $m_z$  being the residual moisture mass in the layer after drying, and  $m_0$  the initial moisture mass) during the first stage is determined by the parameter  $\bar{z}_m$ , i.e.:

$$\alpha_m = \bar{z}_m. \quad (4.55)$$

Indeed, using the definitions  $m_z = \Pi S \rho_L L_{\max} = \Pi S \rho_L L_0 \bar{z}_m$  and  $m_0 = \Pi S \rho_L L_0$ , let's obtain the expression  $\alpha_m = m_z / m_0$  for relative moisture content.

For the second drying stage, the mass balance equation takes the form:

$$\frac{dm}{dt} = -\Pi(j_1 - j_2)S, \quad (4.56)$$

with the initial condition:

$$m = \Pi S \rho_L L_0 \bar{z}_m^* \text{ at } t = t^*. \quad (4.57)$$

Here,  $t^*$  represents the time at which the parameter  $\bar{z}_m$  reaches its final value  $\bar{z}_m^*$  in the first drying stage.

The relative moisture content in this stage is given by:

$$\alpha_m = \frac{(L_{\max} - L_{\min})}{L_0} = (\bar{z}_m - \bar{z}_{m1}), \quad (4.58)$$

where  $L_{\min} = L_0 \bar{z}_{m1}$  is the coordinate of the boundary between the dried and saturated zones on Surface 2 of the porous layer. Since the change in the moisture mass of the layer is now determined by:

$$\Delta m = \Delta m_1 + \Delta m_2, \quad \Delta m_1 = \Pi S \rho_L (\bar{z}_m^* - \bar{z}_m), \quad \Delta m_2 = \Pi S \rho_L \bar{z}_{m1}, \quad (4.59)$$

where the change  $\Delta m_1$  (change in  $\bar{z}_m$ ) is governed by the vapor flux  $j_1$ , and  $\Delta m_2$  (change in  $\bar{z}_{m1}$ ) is governed by the flux  $j_2$ , the problem (4.56), (4.57) can be formulated as two Cauchy problems:

$$\frac{d\bar{z}_m}{dt} = -\frac{j_1}{L_0 \rho_L}, \quad (4.60)$$

under the initial condition:

$$\bar{z}_m = \bar{z}_m^* \text{ at } t = t^*; \quad (4.61)$$

and

$$\frac{d\bar{z}_{m1}}{dt} = \frac{j_2}{L_0 \rho_L}, \quad (4.62)$$

under the initial condition:

$$\bar{z}_{m1} = 0 \text{ at } t = t^*. \quad (4.63)$$

The relative moisture content is now determined by the formula  $\alpha_m = \bar{z}_m - \bar{z}_{m1}$ , and the drying process is completed when the condition  $\bar{z}_m = \bar{z}_{m1}$  is met (i.e.,  $\alpha_m = 0$ ).

### 3.5 SOLUTION OF THE PROBLEM AND ANALYSIS OF THE OBTAINED RESULTS

The convective-diffusive fluxes  $j_1$  and  $j_2$  are determined from the solutions of problems (4.39)–(4.41), (4.44)–(4.46) and (4.39), (4.42)–(4.44), (4.47), (4.48) and are given by [40]:

$$j_1(\bar{z}_m) = \frac{\Omega_1}{B_1 - \Gamma_{01}\bar{z}_m}, \quad j_2(\bar{z}_{m1}) = \frac{\Omega_2}{B_2 - \Gamma_{02}\bar{z}_{m1}}, \quad (4.64)$$

where for  $i = 1, 2$ :

$$\Omega_i = \left\{ b_i \left[ 1 + \frac{b_i}{2(1+a_i)} \right] - (C_{0i} - 1) \left[ 1 + \frac{C_{0i} - 1}{2(1+a_i)} \right] \right\} \frac{DM_v P}{RT \delta_i},$$

$$B_i = 1 + \frac{C_{0i} - 1}{1 + a_i} + \Gamma_{0i},$$

$$C_{0i} = \frac{P_{g1}}{RT} \frac{M_a}{\rho_{ai}} = 1 + \frac{\rho_{vi}}{M_v} \frac{M_a}{\rho_{ai}}, \quad a_i = \frac{D' M_a}{\left( \frac{K_g}{\mu_g} \right) \rho_{ai} RT}, \quad b_i = \frac{\rho_v M_a}{\rho_{ai} M_v}, \quad \Gamma_{0i} = C_{0i} \frac{L_0}{\delta_i} \frac{D'_1}{D'}.$$

Using expression (4.52) for the liquid flux in the layer and formula (4.64) for the flux  $j_1$ , the Cauchy problem (4.55), (4.56) for the first drying stage is formulated as:

$$\frac{d\bar{z}_m}{dt} = -\frac{\Omega_1}{B_1 - \Gamma_{01}\bar{z}_m} + \frac{\tilde{K}}{\bar{z}_m} + \frac{\tilde{K}_1}{(1 - \bar{z}_m) + K_2 \bar{z}_m} \text{ at } \bar{z}_m(0) = 1, \quad (4.65)$$

where

$$\tilde{K} = \frac{K_L}{\mu_L R} \frac{2\sigma_{lg}}{L_0}, \quad \tilde{K}_1 = \frac{K_L}{\mu_L} \frac{2\bar{\eta}\varepsilon_p F}{R}, \quad K_2 = \varepsilon_p.$$

Equation (4.65) can be rewritten as:

$$\frac{a_{32}\bar{z}_m^3 + a_{22}\bar{z}_m^2 + a_{12}\bar{z}_m}{a_{21}\bar{z}_m^2 + a_{11}\bar{z}_m + a_{01}} \frac{d\bar{z}_m}{dt} = 1, \quad (4.66)$$

where

$$a_{21} = \Omega_1(1 - K_2) + \tilde{K}\Gamma_{01}(1 - K_2) - \tilde{K}_1\Gamma_{01}, \quad a_{11} = -\Omega_1 - \tilde{K}B_1(1 - K_2) - \tilde{K}\Gamma_{01} + \tilde{K}_1B_1,$$



$$a_{32} = \Gamma_{01}(1 - K_2), \quad a_{22} = -B_1(1 - K_2) - \Gamma_{01}, \quad a_{12} = B_1.$$

The solution of equation (4.65) with the initial condition (3.18) is given by:

$$\frac{1}{2} \frac{a_{32}}{a_{21}} (\bar{z}_m^2 - 1) + \frac{a_{42}}{a_{21}} (\bar{z}_m - 1) + \left( -\frac{a_{42}a_{11}}{2a_{21}^2} + \frac{a_{41}}{2a_{21}} \right) \ln |\phi(\bar{z}_m)| + f(\bar{z}_m) = t, \quad (4.7)$$

where

$$a_{42} = a_{22} - \frac{a_{32}a_{11}}{a_{21}}, \quad a_{41} = a_{12} - \frac{a_{32}a_{01}}{a_{21}}, \quad \phi(\bar{z}_m) = \frac{a_{21}\bar{z}_m^2 + a_{11}\bar{z}_m + \bar{z}_{01}}{a_{21} + a_{11} + a_{01}},$$

$$f(\bar{z}_m) = \left( \frac{a_{42}(a_{11}^2 - 2a_{21}a_{01})}{2a_{21}^2} - \frac{a_{41}a_{11}}{2a_{21}} \right) f_1(\bar{z}_m),$$

$$f_1(\bar{z}_m) = \frac{2}{\sqrt{4a_{21}a_{01} - a_{11}^2}} \left( \arctg \frac{2a_{21}\bar{z}_m + a_{11}}{\sqrt{4a_{21}a_{01} - a_{11}^2}} - \arctg \frac{2a_{21} + a_{11}}{\sqrt{4a_{21}a_{01} - a_{11}^2}} \right), \text{ if } 4a_{21}a_{01} > a_{11}^2;$$

$$f_1(\bar{z}_m) = \frac{1}{\sqrt{a_{11}^2 - 4a_{21}a_{01}}} \ln \left| \frac{f_3(\bar{z}_m)}{f_3(1)} \right|, \text{ if } a_{11}^2 > 4a_{21}a_{01};$$

$$f_3(\bar{z}) = \frac{2a_{21}\bar{z} + a_{11} - \sqrt{a_{11}^2 - 4a_{21}a_{01}}}{2a_{21}\bar{z} + a_{11} + \sqrt{a_{11}^2 - 4a_{21}a_{01}}}.$$

The transcendental Eq. (4.67) provides the dependence of relative moisture content in the porous layer on time during the first drying stage. The final moment  $t^*$  of the first stage is given by:

$$t^* = \frac{1}{2} \frac{a_{32}}{a_{21}} \left[ (\bar{z}_m^*)^2 - 1 \right] + \frac{a_{42}}{a_{21}} (\bar{z}_m^* - 1) + \left( -\frac{a_{42}a_{11}}{2a_{21}^2} + \frac{a_{41}}{2a_{21}} \right) \ln |\phi(\bar{z}_m^*)| + f(\bar{z}_m^*), \quad (4.68)$$

where  $\bar{z}_m^*$  is given by Eq. (4.53).

The solution of the problem (4.67), (4.68) of the drying at Stage 2 has the form:

$$\bar{z}_m = \frac{B_1}{\Gamma_{01}} \pm \sqrt{\left( \frac{B_1}{\Gamma_{01}} \right)^2 + \frac{2}{\Gamma_{01}} \left[ -B_1\bar{z}_m^* + \Gamma_{01} \frac{\bar{z}_m^{*2}}{2} + \frac{1}{l_0\rho_l} \Omega_1(t - t^*) \right]},$$

and of the problem (4.68), (4.69):

$$\bar{z}_{m1} = \frac{B_2}{\Gamma_{02}} \pm \sqrt{\left(\frac{B_2}{\Gamma_{02}}\right)^2 + \frac{2}{\Gamma_{02}} \left[ \frac{1}{L_0 \rho_L} \Omega_2 (t - t^*) \right]}.$$

The relative moisture content at Stage 2 of drying ( $t > t^*$ ) is determined by the expression:

$$\alpha_m = \frac{B_1}{\Gamma_{01}} - \sqrt{\left(\frac{B_1}{\Gamma_{01}}\right)^2 + \frac{2}{\Gamma_{01}} \left[ -B_1 \tilde{z}_m^* + \Gamma_{01} \frac{\tilde{z}_m^{*2}}{2} + \frac{1}{L_0 \rho_L} \Omega_1 (t - t^*) \right]} - \frac{B_2}{\Gamma_{02}} + \sqrt{\left(\frac{B_2}{\Gamma_{02}}\right)^2 + \frac{2}{\Gamma_{02}} \left[ \frac{1}{L_0 \rho_L} \Omega_2 (t - t^*) \right]}.$$

Let's proceed to the quantitative analysis of the obtained correlations.

Based on the obtained formulas, a quantitative analysis is conducted. The study examines the variation of relative moisture content  $\alpha_m$  over time for different temperatures and external electric field intensities. Results are presented in **Fig. 4.6–4.7**.

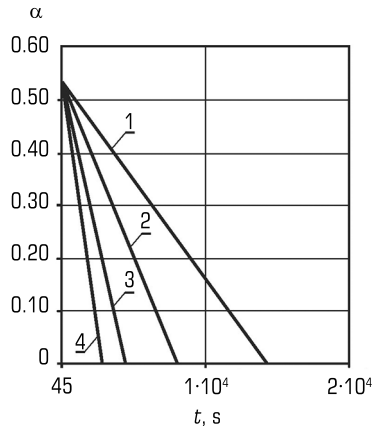


**Fig. 4.6** Temporal dependence of the relative moisture content of the layer during the second stage of drying at  $E = 200$  V/m for temperatures of 300 K, 310 K, 320 K, and 330 K

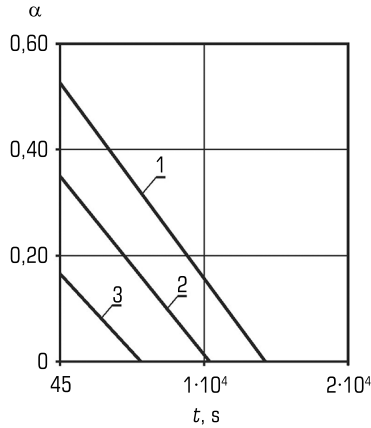


**Fig. 4.7** Temporal dependence of the relative moisture content of the layer during the second stage of drying for a temperature of 300 K at  $E = 200$  V/m, 400 V/m, and 1000 V/m

**Fig. 4.6** and **4.7** illustrate the nature of the temporal dependence of relative moisture content for different temperatures (**Fig. 4.6**) and different intensities of the external electric field applied during the first stage of drying (**Fig. 4.7**). It follows that this dependence is linear. The drying rate (slope of the curve) during the second stage is determined by the temperature. The initial humidity level in the second stage of drying is lower for higher field intensities applied during the first stage.

#### 4.3.6 ESTIMATION OF TEMPERATURE CHANGE IN THE LAYER DUE TO THE INFLUENCE OF THE ELECTRIC FIELD

In this work, the change in temperature due to Joule heating, caused by the action of the electric field in the first stage of drying, is neglected. Let's substantiate this by estimating such a change for the maximum electric field intensity ( $E = 1000$  V/m).

The heat generation density in the liquid according to Joule-Lenz's law is given by:

$$Q = \sigma E^2 t,$$

where  $\sigma$  is the electrical conductivity coefficient. This heat is used to heat the liquid and the skeleton. It is possible to assume that the heating time is significantly greater than the heat transfer time from the liquid to the skeleton, meaning that the heating of the layer is considered uniform.

The thermal balance equation is:

$$\Pi \sigma E^2 t = [\rho_s C_s (1 - \Pi) + \rho_l C_l \Pi] \Delta T,$$

where  $C_s$  and  $C_l$  are the specific heat capacities of the dry material and liquid, respectively. From this equation, let's obtain:

$$\Delta T = \frac{\Pi \sigma E^2 t}{\rho_s C_s (1 - \Pi) + \rho_l C_l \Pi}.$$

Let  $E = 1000$  V/m, the density of dry pine wood  $\rho_s = 500 \text{ kg/m}^3$ , water  $\rho_l = 1000 \text{ kg/m}^3$ , porosity  $\Pi = 0.291$ , specific heat capacities  $C_s = 1.604 \text{ kJ/(kg}\cdot\text{K)}$ ,  $C_l = 4.19 \text{ kJ/(kg}\cdot\text{K)}$ , and  $\sigma = 10^{-3} \text{ S/m}$  [37].

A quantitative estimate for the rate of temperature change gives:

$$\frac{\Delta T}{t} \approx 10^{-4} \text{ K/s}.$$

For the above-mentioned durations of the first stage of drying, this results in a temperature change of fractions of a degree, which can be neglected.

#### 4.4 THE INFLUENCE OF ELECTROOSMOSIS ON BILATERAL CONVECTIVE DRYING OF A POROUS LAYER

Let's consider the formulation and solution of the problem of drying a porous layer that is in contact with an environment consisting of a mixture of air and vapor, under the influence of convective airflow and the enhancement of this process by an external electric field.

The objective here is to formulate and solve the problem of drying an initially moisture-saturated porous layer, stimulated by convection and electroosmosis. As in previous sections, the quasi-homogeneous approximation is used, based on the application of macroscopic equations analogous to those in an individual pore, but with effective transport coefficients, while neglecting film transport.

##### 4.4.1 OBJECT OF STUDY AND PROBLEM FORMULATION

Let's consider an initially moisture-saturated porous layer, referenced to a Cartesian coordinate system  $(x, y, z)$ , occupying the region  $0 < z < L_0$ . Let's investigate the effect of electroosmosis

on the drying process of the porous layer under convective mass exchange at one of the surfaces (Surface 1). The temperature of the air and the layer is assumed to be equal. Since the vapor at the pore surface is saturated, while the surrounding medium is unsaturated, vapor flows outward. As a result, a zone of dried pores filled with a mixture of air and vapor forms in the material, with air and vapor considered as separate components of the gas phase. During the drying process, this zone expands deeper into the material. The coordinate of the moving boundary is denoted as  $z = L_m$ .

To intensify the drying process by electroosmotic moisture removal from the porous layer, a constant potential difference is applied between Surfaces 1 and 2. Due to the action of the field on the electric charge of the diffuse part of the double electric layer near the solid-liquid interface, an additional (ponderomotive) force arises, inducing an electroosmotic moisture flow  $j_3$  toward Surface 2. In opposition to the osmotic pressure, capillary forces arise, leading to a filtration flow  $j_2$ .

On Surface 2, moisture removal occurs via convective evaporation of the saturated vapor. Due to the displacement of the moving boundary and neglecting film transport, the vapor at the opposite side (Surface 2) of the porous layer remains saturated. The vapor flux from Surface 2 is given by [1, 38, 39]:

$$j_4 = \beta_2 (\rho_n - \rho_0) \text{ at } z = 0. \quad (4.69)$$

As a result of the combined effects of the forces that arise during drying, the relative moisture content in the porous layer changes. Using the notations adopted in Section 2, the transport of dry air and vapor in the dried region  $L_0 < z < L_m$  under a quasi-stationary process, while neglecting the flow of dry air into the pores, is described by the nonlinear Stefan-Maxwell differential equation (4.43) [31].

The convective mass transfer conditions at the surface  $z = L_0$  are:

$$\rho_v \frac{K}{\mu_g} \frac{\partial P}{\partial z} + D \frac{\partial \rho_v}{\partial z} = -j, \quad \rho_s = \rho_{s0}, \quad (4.70)$$

where  $j = \beta(\rho_{v1} - \rho_0)$ .

The phase transition from liquid to vapor at the gas-liquid interface  $z = L_m$  is accounted for by prescribing the density of the saturated vapor at this surface, which depends on temperature and is determined by equation (4.20). At the phase transition surface  $z = L_m$ :

$$\rho_v = \rho_n, \quad (4.71)$$

where  $\rho_n$  is the density of the saturated vapor.

#### 4.4.2 SOLUTION AND QUANTITATIVE ANALYSIS OF THE PROBLEM

From the solution of the problem about convective-diffusive vapor transport [2], the vapor density  $\eta_1$  at the wall  $k=1$  is determined as follows:

$$\eta_1 = -\left(A + B\bar{z}_m^*\right) + \sqrt{U + S\bar{z}_m^* + B^2\bar{z}_m^{*2}}, \quad (4.72)$$

where

$$\begin{aligned} A &= \frac{(1+a)}{b}, \quad B = -\beta' A, \quad U = (A+1)^2, \quad S = 2B(A+\eta_0), \quad \eta_0 = \frac{\rho_0}{\rho_n}, \\ a &= \frac{D'M_a}{\left(\frac{K_g}{\mu_g}\right)\rho_{a0}RT}, \quad b = \frac{\rho_n}{\rho_{a0}} \frac{M_a}{M_v}, \quad \beta' = \frac{L_0\beta}{D'}, \quad \bar{z}_m^* = 1 - \bar{z}_m, \end{aligned} \quad (4.73)$$

$$\rho_a = \rho_a \xi, \quad \rho_v = \rho_n \eta, \quad z = L_0 \bar{z}, \quad \eta_1 = \eta|_{\bar{z}=1}.$$

The convective-diffusive flux  $j_1$ :

$$j = H \left[ -\left(a_1 + B\bar{z}_m^*\right) + \sqrt{U + S\bar{z}_m^* + B^2\bar{z}_m^{*2}} \right], \quad a_1 = A + \eta_0. \quad (4.74)$$

Since the moisture reserve in the porous layer is limited, drying occurs in two stages. In the first stage, a filtration-osmotic regime is established, which lasts until the electroosmotic and filtration fluxes equalize. The capillary pressure forces induce the flow  $j_2$  equation (4.22):

$$j_2 = \Pi \rho_l v_l = \rho_l \frac{K_l}{\mu_l} \frac{P_K}{L_0 (1 - \bar{z}_m^*)} \Pi. \quad (4.75)$$

To determine the electroosmotic flow, let's use the quasi-homogeneous approximation for the porous body. The electroosmotic liquid flow in the porous layer is given by equation (4.25):

$$j_3 = \gamma_l v_{osm} \Pi = \frac{\gamma_l K_l \Pi}{\mu_l} \frac{2\bar{\eta} \varepsilon_p E}{\bar{R} \left[ (1 - \kappa_m) + \varepsilon_p \kappa_m \right]}. \quad (4.76)$$

The critical relative moisture content at which the liquid flows balance and the second drying regime begins is determined from equation (4.27). Since the rate of liquid mass change in the

drying process is defined by the vapor and liquid fluxes from the layer, let's arrive at the following Cauchy problem:

$$\frac{dz_m}{dt} = H \left[ -\left(a_1 + Bz_m^*\right) + \sqrt{U + Sz_m^* + B^2 z_m^{*2}} + \frac{\tilde{K}}{1 - z_m^*} + \frac{\tilde{K}_1}{K_2(1 - z_m^*) + K_3 z_m^*} \right], \quad (4.77)$$

under the initial condition:

$$z_m^*(0) = 0, \quad (4.78)$$

where

$$\tilde{K} = \frac{\rho_L K_L P_k}{\mu_L L_0 \beta \rho_n} \Pi, \quad \tilde{K}_1 = \frac{2K_L \rho_L \Pi \varepsilon_p \bar{\eta} E}{\beta \rho_n \mu_L \bar{R}}, \quad K_2 = \varepsilon_p, \quad K_3 = 1, \quad \bar{\eta} = ZF\psi_1 \sqrt{2\varepsilon \frac{C}{RT}}, \quad \varepsilon = \varepsilon_0 \varepsilon_r.$$

By substituting variables  $\sqrt{U + Sz_m^* + B^2 z_m^{*2}} = \chi + z_m^* B$ , Eq. (4.77) transforms into:

$$-\frac{2(B\chi^2 - S\chi + BU)}{(S - 2B\chi)^2} \frac{d\chi}{dt} = H \frac{(\chi - a_1)(\tilde{a}\chi^4 + \tilde{b}\chi^3 + c\chi^2 + \tilde{d}\chi + \tilde{e})}{(\chi^2 + 2\chi B - \omega_1)(\Omega_2\chi^2 + \Omega_1\chi + \Omega_0)}, \quad (4.79)$$

where

$$\begin{aligned} \omega_1 &= S + U, \quad \Omega_2 = K_2 - K_3, \quad \Omega_1 = 2K_2 B, \quad \Omega_0 = -K_2 \omega_1 + K_3 U, \quad \tilde{a} = 1, \quad \tilde{b} = \frac{\Omega_1 + 2B\Omega_2}{\Omega_2}, \\ \tilde{c} &= \frac{\Omega_0 + 2B\Omega_1 - \Omega_2 \omega_1 + 2\tilde{K}B\Omega_2 + 2\tilde{K}_1 B}{\Omega_2}, \quad \tilde{e} = \frac{2\tilde{K}B\Omega_0 - \Omega_2 \omega_1 - 2\tilde{K}_1 B\omega_1}{\Omega_2}, \\ \tilde{d} &= \frac{2B\Omega_0 - \Omega_1 \omega_1 + 2\tilde{K}B\Omega_1 + 4\tilde{K}_1 B^2}{\Omega_2}. \end{aligned} \quad (4.80)$$

Equation (4.79) is written in the form:

$$-\frac{2(B\chi^2 - S\chi + BU)(\chi^2 + 2\chi B - \omega_1)(\Omega_2\chi^2 + \Omega_1\chi + \Omega_0)}{(S - 2B\chi)^2(\chi - a_1)(\chi - c_1)(\chi - c_2)(\chi - c_3)(\chi - c_4)} \frac{d\chi}{dt} = H\Omega_2, \quad (4.81)$$

where  $c_i = \chi_i$ ,  $i = \overline{1,4}$  are roots of Eq.  $(\tilde{a}\chi^4 + \tilde{b}\chi^3 + c\chi^2 + \tilde{d}\chi + \tilde{e}) = 0$ . The solution of Eq. (4.81) has the form:

$$D_1 \ln \left| \frac{S - 2B\chi}{S - 2B\sqrt{U}} \right| + D_2 \left[ \frac{1}{S - 2B\chi} - \frac{1}{S - 2B\sqrt{U}} \right] + D_3 \left[ \frac{1}{(S - 2B\chi)^2} - \frac{1}{(S - 2B\sqrt{U})^2} \right] + R_3 \ln \left| \frac{\chi - c_1}{\sqrt{U} - c_1} \right| + R_4 \ln \left| \frac{\chi - c_2}{\sqrt{U} - c_2} \right| + R_5 \ln \left| \frac{\chi - c_3}{\sqrt{U} - c_3} \right| + R_6 \ln \left| \frac{\chi - c_4}{\sqrt{U} - c_4} \right| = H\Omega_2 t, \quad (4.82)$$

where  $D_1 = -\frac{R_2}{8B^3}$ ,  $D_2 = -\frac{1}{4B^2} \left( \frac{R_2 S}{B} + R_1 \right)$ ,  $D_3 = \frac{1}{4B} \left( \frac{R_2 S^2}{4B^2} + \frac{R_1 S}{2B} + R_0 \right)$ ,  $R_0, R_1, \dots, R_6$  are solutions of the following system of algebraic equations:

$$\sum_{i=0}^2 d_{i,6-j} R_i + \sum_{i=3}^6 b_{i-2,6-j} R_i = 4B\Omega_{1,6-j} \quad (j = \overline{0,6}), \quad (4.83)$$

$$d_{0,6} = d_{1,6} = d_{0,5} = 0, \quad d_{2,6} = d_{1,5} = d_{0,4} = 1, \quad d_{2,5} = d_{1,4} = d_{0,3} = \tilde{b}, \\ d_{2,4} = d_{1,3} = d_{0,2} = \tilde{c}, \quad d_{2,3} = d_{1,2} = d_{0,1} = \tilde{d}, \quad d_{2,2} = d_{1,1} = d_{0,0} = \tilde{e},$$

$$b_{1,6} = 8B^3 a_{i+2,3}, \quad b_{1,5} = 8B a_{i+2,2} + 12B^2 S a_{i+2,3}, \quad b_{1,4} = 8B^3 a_{i+2,1} + 12B^2 S a_{i+2,2} - 6BS^2 a_{i+2,3}, \\ b_{1,3} = 8B^3 a_{i+2,0} + 12B^2 S a_{i+2,1} - 6BS^2 a_{i+2,2} + S^3 a_{4,3}, \quad b_{1,2} = 12B^2 S a_{i+2,0} - 6BS^2 a_{i+2,1} + S^3 a_{4,2}, \\ b_{1,1} = -6BS^2 a_{i+2,0} + S^3 a_{4,1}, \quad b_{1,0} = S^3 a_{4,0},$$

$$a_{i+2,1} = 1, \quad a_{3,2} = -(c_4 + c_2 + c_3), \quad a_{3,1} = (c_2 + c_3)c_4 + c_2 c_3, \quad a_{3,0} = -c_2 c_3 c_4, \\ a_{4,2} = -(c_4 + c_1 + c_3), \quad a_{4,1} = (c_1 + c_3)c_4 + c_1 c_3, \quad a_{4,0} = -c_1 c_3 c_4, \\ a_{5,2} = -(c_2 + c_1 + c_4), \quad a_{5,1} = (c_1 + c_2)c_4 + c_1 c_2, \quad a_{5,0} = -c_1 c_4 c_2, \\ a_{6,2} = -(c_2 + c_1 + c_3), \quad a_{6,1} = (c_1 + c_2)c_3 + c_1 c_2, \quad a_{6,0} = -c_1 c_3 c_2, \\ a_{0,4} = B, \quad a_{0,3} = 2B^2 - S, \quad a_{0,2} = \omega_1 B - 2BS + BU, \quad a_{0,1} = \omega_1 S + 2B^2 U, \quad a_{0,0} = -BU\omega_1,$$

$$\Omega_{16} = a_{0,4}\Omega_2, \quad \Omega_{15} = a_{0,4}\Omega_1 + a_{0,3}\Omega_2, \quad \Omega_{14} = a_{0,4}\Omega_0 + a_{0,3}\Omega_1 + a_{0,2}\Omega_2, \\ \Omega_{13} = a_{0,3}\Omega_0 + a_{0,2}\Omega_1 + a_{0,1}\Omega_2, \quad \Omega_{12} = a_{0,2}\Omega_0 + a_{0,1}\Omega_1 + a_{0,0}\Omega_2, \\ \Omega_{11} = a_{0,1}\Omega_0 + a_{0,0}\Omega_1, \quad \Omega_{10} = a_{0,0}\Omega_0.$$



The transcendental equation (4.83) establishes the relationship between the relative moisture content in the porous layer and time in the first drying regime. When the relative moisture content reaches the value  $\bar{z}_m = \bar{z}_{kr}$ , the evaporation regime begins, where the change in relative moisture content is determined by the following Cauchy problem:

$$\frac{d\bar{z}_m^*}{dt} = H \left[ -\left(a_1 + B\bar{z}_m^*\right) + \sqrt{U + S\bar{z}_m^* + B^2\bar{z}_m^{*2}} - \frac{\beta_2}{\beta} (1 - \eta_{02}) \right], \quad (4.84)$$

under the condition that at  $t = t_{kr}$ ,  $\bar{z}_m^* = 1 - \bar{z}_{kr}$ .

By introducing  $a_2 = a_1 + (1 - \eta_{02})\beta_2 / \beta$ , let's obtain the equation:

$$\frac{d\bar{z}_m^*}{dt} = H \left[ -\left(a_2 + B\bar{z}_m^*\right) + \sqrt{U + S\bar{z}_m^* + B^2\bar{z}_m^{*2}} \right], \quad (4.18)$$

which, upon introducing the variable  $\chi$ , transforms into:

$$\frac{2(\chi S - BU - B\chi^2)}{(2B\chi - S)^2 (\chi - a_2)} \frac{d\chi}{dt} = H, \quad (4.85)$$

under the initial condition:

$$t = t_{kr} \quad \chi = \chi_{kr}, \quad (4.86)$$

where

$$\chi_{kr} = \sqrt{U + S\bar{z}_{kr}^* + B^2\bar{z}_{kr}^{*2}} - \bar{z}_{kr}^* B, \quad \bar{z}_{kr}^* = 1 - \bar{z}_{kr},$$

and  $t_{kr}$  is determined from the solution of the Cauchy problem (4.75), (4.76).

Integration of equation (4.85) under condition (4.86) leads to the following transcendental equation for  $\chi$ :

$$\begin{aligned} & \frac{C_1}{4B^2} \ln \left| \frac{2B\chi - S}{2B\chi_{kr} - S} \right| - \frac{1}{2B} \left( \frac{C_1 S}{4B^2} + C_2 \right) \left[ \frac{1}{S - 2B\chi} - \frac{1}{S - 2B\chi_{kr}} \right] + \\ & + C_3 \ln \left| \frac{\chi - a_2}{\chi_{kr} - a_2} \right| = H(t - t_{kr}), \end{aligned} \quad (4.87)$$

where

$$C_1 = \frac{2B(-S^2 + 4B^2U)}{(S - 2a_2B)^2}, \quad C_2 = \frac{2(Ba_2 - S)(-S^2 + 4B^2U)}{(S - 2a_2B)^2}, \quad C_3 = \frac{-2BU - 2Ba_2^2 + 2Sa_2}{(S - 2a_2B)^2}.$$

Equation (4.87) establishes the relationship between relative moisture content and time over the range  $\bar{z}_{kr} - 0$ . Graphs of the dependence of the layer's relative moisture content on the mass transfer coefficient, electric field intensity, and temperature are presented in **Fig. 4.8–4.11**. Calculations were performed for a coarse-porous material, where  $D'$  represents the molecular diffusion of the vapor-air mixture, which is a function of temperature.

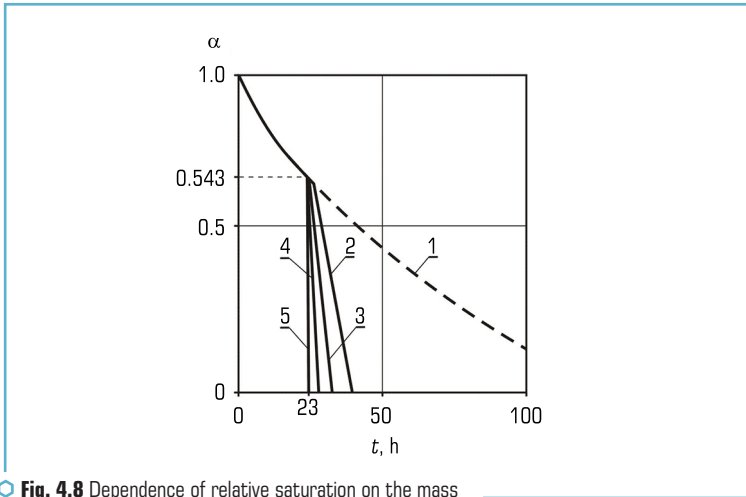


**Fig. 4.8** Dependence of relative saturation on the mass transfer coefficient  $\beta_2$

In **Fig. 4.8**, the mass transfer coefficients  $\beta_2 = 0.01; 0.05; 0.1; 0.5; 1$  (curves 1–5, respectively), with  $E = 200$  V/m ( $\beta = 0.1$ ;  $T = 300$  K,  $L_0 = 0.1$  m,  $\bar{z}_{kr} = 0.543$ ,  $t_{kr} = 23$  h), correspond to complete dehydration times of 139; 39.751; 31.305; 23.733; and 23.244 hours, respectively.

In **Fig. 4.9**, curves 1 and 2 correspond to the electric field intensities of  $E = 200$  V/m and  $E = 400$  V/m. Here,  $L_0 = 0.5$  m,  $T = 300$  K, and  $\beta = 0.1$ . The points where curve branching occurs correspond to the critical values of  $\bar{z}_m = \bar{z}_{kr}$  for humidity. The curve branches after the branching point, from right to left, correspond to mass transfer coefficient values of  $\beta_2 = 0.01; 0.05; 0.1; 0.5$ ; and 1.

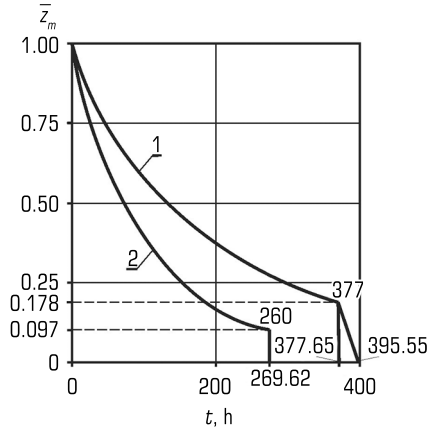


Fig. 4.9 The effect of electric field intensity on humidity variation over time

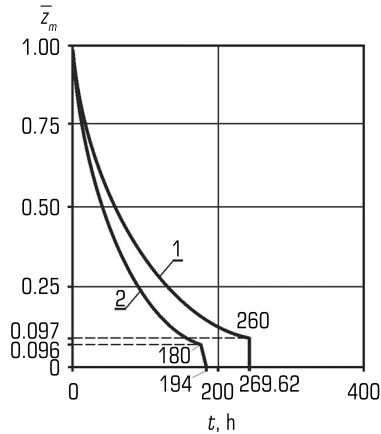


Fig. 4.10 Time dependence of relative moisture content for different temperatures

Thus, at  $E = 200$  V/m,  $\bar{z}_{kr} = 0.178$ ,  $t_{kr} = 377$  hours, the total dehydration time for  $\beta_2 = 0.01$  is 395.552 hours, and for  $\beta_2 = 1$  it is 377.65 hours.

For  $E = 400$  V/m,  $\kappa_{kr} = 0.097$ ,  $t_{kr} = 260$  hours, the total dehydration time for  $\beta_2 = 0.01$ ; 0.05; 0.1; 0.5; 1 is 269.62; 261.11; 260.555; 260.185; 260.185 hours, respectively.

Quantitative calculations, the graphical results of which are shown in **Fig. 4.10**, were conducted for  $E = 400$  V/m,  $\beta = 0.1$ ;  $L_0 = 0.5$  m. At  $\bar{z}_{kr} = 0.097$ ,  $t_{kr} = 260$  hours, and temperature  $T = 300$  K, the corresponding total dehydration times for mass transfer coefficient values of  $\beta_2 = 0.01$ ; 0.05; 0.1; 0.5; 1 are 269.62; 261.11; 260.555; 260.185; 260.185 hours.

For  $\bar{z}_{kr} = 0.096$ ,  $t_{kr} = 180$  hours, and temperature  $T = 310$  K, the total dehydration times for the same  $\beta_2$  values are 185.74; 180.82; 180.205; 180; 180 hours, respectively.

## CONCLUSIONS

Based on the electroosmotic drying model, a series of problems have been solved regarding the influence of external constant electric field parameters on moisture mass transfer in pores. The effects of the following parameters have been investigated:

- a) boundary layer properties;
- b) electric field intensity in unilateral natural drying;
- c) moisture exchange coefficients in convective drying when the second side is saturated with moisture (a process relevant to basement flooding);
- d) bilateral drying.

It has been demonstrated that in bilateral drying the electric field affects the process primarily during the first stage of drying, when the ponderomotive force dominates over the capillary force. As a result, the relative moisture content curve exhibits a breakpoint, both in natural and convective drying. It has been shown that the temperature change induced by a constant electric field in a moist body can be neglected. Increasing the intensity of the electric field enhances the drying process. Numerical results are provided for cement stone material.

## REFERENCES

1. Burak, Ya., Chaplia, Ye., Nahirnyi, T. et al. (2004). Fizyko-matematychne modeliuвання skladnykh system. Lviv: SPOLOM, 264.
2. Haivas, B. I. (2004). Pro vplyv elektroosmosu na dvostoronne konvektyvne osushennia porystoho sharu. Volynskiy matematychnyi visnyk. Seriya prykladna matematyka, 2 (11), 74–85.
3. Chaplya, Ye., Hayvas, B., Torskyi, A. (2015). Construction of the solution of the thermal-convective drying problem for porous solids in drying plants. Mathematical Modeling and Computing, 2 (1), 1–15. <https://doi.org/10.23939/mmc2015.01.001>
4. Sokolovskyy, Y., Drozd, K., Samotii, T., Boretska, I. (2024). Fractional-Order Modeling of Heat and Moisture Transfer in Anisotropic Materials Using a Physics-Informed Neural Network. Materials, 17 (19), 4753. <https://doi.org/10.3390/ma17194753>

5. Hachkevych, O., Musii, R., Melnyk, N. (2023). Problems of Thermomechanics of Multilayered Electroconductive Bodies Under the Action of the Pulsed Electromagnetic Fields with Modulation of Amplitude. *Advances in Mechanics*, 185–206. [https://doi.org/10.1007/978-3-031-37313-8\\_11](https://doi.org/10.1007/978-3-031-37313-8_11)
6. Zhuravchak, L. M. (2007). Matematychni modeliuvannya protsesiv poshyrennia teplovoho ta elektromagnitnoho poliv u neodnorodnykh seredovyschakh metodamy pryhranychnykh elementiv ta skinennykh riznyts. [Extended abstract of doctors thesis].
7. Dukhin, S. S. (1975). *Elektroprovodnost y elektrokynetycheskye svoistva dyspersnykh system*. Kyiv: Naukova dumka, 246.
8. Decker, Ž., Tretjakovas, J., Drozd, K., Rudzinskas, V., Walczak, M., Kilikevičius, A. et al. (2023). Material's Strength Analysis of the Coupling Node of Axle of the Truck Trailer. *Materials*, 16(9), 3399. <https://doi.org/10.3390/ma16093399>
9. Tokarchuk, M. V. (2024). Kinetic coefficients of ion transport in a porous medium based on the Enskog – Landau kinetic equation. *Mathematical Modeling and Computing*, 11 (4), 1013–1024. <https://doi.org/10.23939/mmc2024.04.1013>
10. Sokolovskyy, Ya. I., Boretska, I. B., Gayvas, B. I., Kroshnyy, I. M., Nechepurenko, A. V. (2021). Mathematical modeling of convection drying process of wood taking into account the boundary of phase transitions. *Mathematical Modeling and Computing*, 8 (4), 830–841. <https://doi.org/10.23939/mmc2021.04.830>
11. Borovytskyi, M. Y., Lysenko, L. L., Rynda, O. F., Mishchuk, N. O. (2014). Rehuliuвання vlasty-vostei dyspersii dlia yikh elektrokinyetichnoi obrobky. *Naukovi visti NTUU “KPI”*, (3), 100–106.
12. Barinova, N. O. (2016). Nelineini elektroforez ta elektroosmos dlia odynychnykh chastynok ta skladnykh system. [Extended abstract of Candidate's thesis; Institute of Colloid Chemistry and Water Chemistry, NAS of Ukraine].
13. Malyarenko, V. V., Makarov, A. S. (2000). Elektropoverkhnostnye svoystva vspenennykh kont-sentrirovannykh suspenziy kremnezema i uglya. *Ukrainskyi khimichnyi zhurnal*, 66 (9-10), 84–87.
14. Myshchuk, N. A., Lysenko, L. L., Kornilovych, B. Y., Barinova, N. O. (2002). Teoreticheskii analiz zakonomernostey elektroosmoticheskogo transporta zhidkosti cherez diafragmu. *Khim-ia i tekhnologiya vody*, 24 (4), 328–351.
15. Bereznia, O. O. (1999). Zastosuvannya yavyshcha elektroosmosu pry znevodnenni kaolinu. *Zbahachennia korys. kopalyn*, 4 (45), 100–104.
16. Lysenko, L. L. (2002). Intensyfikatsiia masoperenosu pry elektrokinyetichnii ochystsi hruntu. [Extended abstract of Candidate's thesis; Institute of Colloid Chemistry and Water Chemistry, NAS of Ukraine].
17. Shevchenko, R. O. (2012). Upravlinnia elektrokinyetichnymy protsesamy dlia poperedzhennia i podolannia avarii pry burinni sverdlovyn na naftu ta haz [Extended abstract of Candidate's thesis; National Technical University “Kharkiv Polytechnic Institute”].
18. Pushkarov, O., Zubko, O., Sevruk, I., Dolin, V. (2022). Use of mineral proton-conductive membranes for electroosmotic fractionation of the hydrogen isotopes. *Geochemistry of Tech-nogenesis*, 35, 65–68. <https://doi.org/10.32782/geotech2022.35.12>

19. Musii, R., Melnyk, N., Dmytruk, V. (2024). Thermal stresses in bimetallic plate under induction heating by nonstationary electromagnetic field. *Journal of Thermal Stresses*, 47 (11), 1539–1551. <https://doi.org/10.1080/01495739.2024.2415030>
20. Musii, R., Dmytruk, V., Oryshchyn, O., Kushka, B., Shayner, H., Huk, L. (2024). Analysis of Thermal Modes of a Bimetallic Tube Under Short-Term Induction Heating. 2024 IEEE 19th International Conference on the Perspective Technologies and Methods in MEMS Design (MEMSTECH), 16–19. <https://doi.org/10.1109/memstech63437.2024.10620050>
21. Musii, R., Dmytruk, V., Voloshyn, M. M., Kushka, B., Nakonechny, R., Huk, L. (2023). Computer Analysis of Nonstationary Thermoelastic Processes in an Electrically Conductive Plate during Pulse Electromagnetic Treatment. 2023 IEEE XXVIII International Seminar/Workshop on Direct and Inverse Problems of Electromagnetic and Acoustic Wave Theory (DIPED), 221–224. <https://doi.org/10.1109/diped59408.2023.10269468>
22. Gayvas, B., Burak, Y., Kondrat, V. (2005). Do matematychnoho modeliuвання ta vyvchennia protsesu osushennia porystykh til. *Fiz.-mat. modeliuвання ta inform. tekhnolohii*, 1, 20–29.
23. Gayvas, B. I., Markovych, B. M., Dmytruk, A. A., Havran, M. V., Dmytruk, V. A. (2023). Numerical modeling of heat and mass transfer processes in a capillary-porous body during contact drying. *Mathematical Modeling and Computing*, 10(2), 387–399. <https://doi.org/10.23939/mmc2023.02.387>
24. Severyn, O. A. (2008). Rozrobka protsesu ta aparaturnoho osnashchennia kombinovanoho heliosushinnia plodovoi syrovyny z avtonomnym enerhopostachanniam. [Extended abstract of Candidate's thesis; Kharkiv State University of Food and Trade].
25. Fariseev, A. G. (2014). Rozrobka aparata dlia zharenia miasa v umovakh elektroosmosu. [Extended abstract of Candidate's thesis; Kharkiv State University of Food and Trade].
26. Drachov, V. I. (2000). Tekhnolohiia zbahachennia ta kompleksnoho vykorystannia vidkhodiv stale-playvynoho vyrobnytstva. [Extended abstract of Candidate's thesis; Kryvyi Rih Technical University].
27. Kostyuk, G. Ya., Kostyuk, O. G., Burkov, M. V., Golubovsky, I. A., Bulko, M. P., Bandura, L. O. et al. (2020). Pancreatic secretion and pressure biomechanics in pancreatic acinus. *Clinical Anatomy and Operative Surgery*, 19 (1), 6–12. <https://doi.org/10.24061/1727-0847.19.1.2020.1>
28. Kheifitc, L. I., Neimark, A. V. (1982). *Mnogofaznye protsessy v poristyykh sredakh*. Moscow: Khimiia, 320.
29. Gayvas, B. I., Dmytruk, V. A. (2022). Investigation of drying the porous wood of a cylindrical shape. *Mathematical Modeling and Computing*, 9 (2), 399–415. <https://doi.org/10.23939/mmc2022.02.399>
30. Burak, Ya., Kondrat, V., Haivas, B. (2002). Do matematychnoho modeliuвання protsesiv sushky porystykh til. *Informatychno-matematychno modeliuвання skladnykh system – MIMUZ2002*. Lviv: TsMMP IPPMM im. Ya. S. Pidstryhacha NAN Ukrainy, Vyd-vo Akhil, 153–159.
31. Gayvas, B. I., Dmytruk, V. A., Semerak, M. M., Ryamar, T. I. (2021). Solving Stefan's linear problem for drying cylindrical timber under quasi-averaged formulation. *Mathematical Modeling and Computing*, 8 (2), 150–156. <https://doi.org/10.23939/mmc2021.02.150>

32. Kondrat, V. F., Kubik, Yu., Chaplia, Ye. Ya. (2000). Vzaiemodiiia mekhanotermoelektrodyfuziinykh protsesiv v porystomu nasychenomu seredovyshchi. *Mashynoznavstvo*, 8, 3–9.
33. Gayvas, B., Dmytruk, V., Kaminska, O., Pastyrska, I., Dmytruk, A., Nezgoda, S. (2020). Simulation of Crack Resistance of Mustard in Pulsed Drying Mode. 2020 IEEE 15th International Conference on Computer Sciences and Information Technologies (CSIT), 91–94. <https://doi.org/10.1109/csit49958.2020.9321941>
34. Gayvas, B., Markovych, B., Dmytruk, A., Dmytruk, V., Kushka, B., Senkovych, O. (2023). Study of Contact Drying Granular Materials in Fluidized Bed Dryers. 2023 IEEE XXVIII International Seminar/Workshop on Direct and Inverse Problems of Electromagnetic and Acoustic Wave Theory (DIPED). Tbilisi, 238–241. <https://doi.org/10.1109/diped59408.2023.10269464>
35. Gayvas, B. I. (2004). On the influence of electroosmosis on two-sided convective drying of a porous layer. *Volyn Mathematical Bulletin*, 2 (11), 74–85.
36. Gayvas, B., Markovych, B., Dmytruk, A., Havran, M., Dmytruk, V. (2024). The methods of optimization and regulation of the convective drying process of materials in drying installations. *Mathematical Modeling and Computing*, 11 (2), 546–554. <https://doi.org/10.23939/mmc2024.02.546>
37. Polos, A. V. (2006). Pidvyschennia efektyvnosti konvektivnoho sushinnia pylomaterialiv (na prykladi umovnoho material). [Dissertation].
38. Dmytruk, A. (2024). Modeling mass transfer processes in multicomponent capillary-porous bodies under mixed boundary conditions. *Mathematical Modeling and Computing*, 11 (4), 978–986. <https://doi.org/10.23939/mmc2024.04.978>
39. Gayvas, B. I. (2003). Dynamika vologosti porystogo sharu pry osushuvanni z odniyeyi pov-erkhni. Konferentsiia profesorsko-vykladatskoho skladu DU “Lvivska politekhnika”. Lviv, 7–9.
40. Grinchik, N. N. (1991). Protcesy perenosa v poristyykh sredakh, elektrolitakh i membranakh. Minsk: ITMO im. A.V. Lykova AN BSSR, 310.

## CHAPTER 5

ON THE ISSUES OF OPTIMIZATION AND REGULATION OF  
THE CONVECTIVE DRYING PROCESS OF MATERIALS IN  
DRYING UNITS

## ABSTRACT

The Chapter presents the main approaches to optimizing and regulating the drying process of materials, taking into account the structural characteristics and operating principles of drying equipment. An essential factor in optimizing such processes is the consideration of the drying object and the mathematical methods used to describe drying problems. To this end, widely applied practical methods of mathematical modeling of capillary-porous and dispersed materials are analyzed, along with the specific features of models that describe heat and mass transfer in such materials.

Particular attention is given to the role of diffusion and thermo-diffusion mechanisms in moisture transfer regulation. Optimization strategies are developed using fundamental drying principles, where the Kirpichov criterion provides a quantitative assessment of moisture transport dynamics, while Nusselt numbers serve as key parameters for controlling temperature gradients and ensuring efficient moisture removal. Additionally, the Postnov criterion is used as a means of evaluating the balance between temperature gradients and moisture content distribution, helping to prevent excessive stress accumulation that may lead to cracking. The study further explores empirical relationships between these criteria and essential process parameters, including moisture content, temperature, and airflow velocity, to enhance drying efficiency and maintain structural integrity.

The study investigates the peculiarities of constructing mathematical models of non-isothermal moisture transfer and deformation during the drying of capillary-porous, dispersed, and fractal-structured materials from the perspective of continuum mechanics, mixture theory, and statistical approaches. This allows for the broadest possible range of model implementations, accounting for the anisotropy of thermomechanical properties, elastic and viscoelastic behavior, material shrinkage, and other relevant factors.

## KEYWORDS

Mathematical modeling, drying, capillary-porous body, dispersed materials, gas-suspended state, fluidization, relative moisture content, stress, optimization, heat and mass transfer, deformation, anisotropy, numerical methods.



The effective resolution of several significant scientific and technical problems related to the drying processes of capillary-porous bodies requires consideration of the material's structure, real mechanisms of heat and moisture transfer depending on the drying method, the influence of kinetic and geometric characteristics of the body, and the control parameters of the drying agent. Additionally, these factors affect the stress-strain state and the stability of the body's shape. The preservation of material quality during the drying process is based on specific macroscopic physico-mathematical models of heat and mass transfer and necessitates efficient analytical and numerical methods for solving the corresponding boundary value problems of mathematical physics. These models are constructed using the fundamental principles of continuum mechanics and the thermodynamics of non-equilibrium processes.

However, capillary-porous bodies are multiphase and heterogeneous during the drying process. To represent multiphase characteristics approaches from mixture theory and methods from the mechanics of multi-velocity systems are utilized alongside capillary models of porous media and combined methods. These approaches incorporate capillary models for heat and mass transfer modeling while employing homogenization methods for solving mechanical problems, deriving physical relationships for the body as a whole based on specific assumptions about the temporal and spatial variations of the studied fields.

To account for the material's structure, the interaction of heat and mass transfer processes within the body, and the impact of heat and mass exchange between the body's surface and the drying agent on phase transition processes, methods of effective properties and stochastic approaches are applied.

## 5.1 FUNDAMENTALS OF HETEROGENEOUS MEDIA DESCRIPTION

In multiphase systems, structural effects and their changes, interphase interactions – particularly capillary effects – phase transitions, particle rotation, and collisions occur [1]. Colloidal mixtures occupy an intermediate position between heterogeneous and homogeneous mixtures. The solid particles in a dispersed mixture are referred to as dispersed, while the continuous carrier phase is called the dispersion medium.

The laws governing the motion of heterogeneous systems are essential, especially in processes involving a fixed granular layer through which a gas mixture is passed, processes with a granular layer suspended by a gas flow, and processes in a porous medium, which represents a heterogeneous system containing liquid or gas in its pores. When analyzing heterogeneous systems, it is assumed that the size of inclusions and inhomogeneities in the mixture is significantly larger than molecular-kinetic scales but smaller than the inhomogeneities at which the macroscopic or averaged parameters of the mixture change substantially.

These assumptions allow for the investigation of the behavior of individual inclusions and the processes occurring near them. This includes studies on heat exchange, phase transformations

around and within particles, deformations within the particles or the skeleton of capillary-porous bodies, and the behavior of mixtures in channels, among other aspects. Most materials undergo drying in a dispersed state, which has led to the increasing application of various hydrodynamic modes of fluidized beds for drying.

In each continuum, distinct macroscopic parameters are defined, such as velocity, density, pressure, and temperature. The results of microprocess studies are incorporated into continuum equations through averaged parameters describing interphase interactions.

### **Homogeneous mixture.**

In homogeneous mixtures (such as solutions and gas mixtures), the components interact at the molecular or atomic level, and their relative motion velocities are small. These velocities need to be considered only when determining the concentration of components. The diffusion approximation in mixture mechanics is associated with neglecting the dynamic and inertial effects of diffusion velocities.

The relative motion of components, described by diffusion velocities or diffusion fluxes, is determined by the diffusion mechanism, which establishes dependencies on concentration gradients, temperature gradients, and pressure gradients. In this approach, the inertia of the relative motion of the components is disregarded [2].

### **Model of a heterogeneous mixture.**

Unlike homogeneous mixtures, liquid-solid suspensions (e.g., slurries, water-saturated soils, etc.) are described by a multi-velocity model that accounts for dynamic effects due to velocity mismatches between the components (phases). In a heterogeneous mixture, each phase occupies only a fraction of the total volume. Therefore, volume fractions of the mixture are used, along with specific densities, in addition to the apparent densities.

The phases exist as macroscopic entities relative to molecular dimensions. Consequently, the deformation of each phase, which determines its state and response, is associated not only with the displacement of external boundaries – described by the velocity field  $\mathbf{v}$ , which may differ significantly from the mass-averaged velocity field  $\bar{\mathbf{v}}$  of the selected volume – but also with the displacement of interphase surfaces within the selected mixture volume.

For each phase, both the external deformation rate tensor and a set of tensors accounting for the displacement of the substance of phase  $i$  at interphase boundaries are considered. Thus, the

true deformation rate of a phase is determined by the tensor:  $\mathbf{e}_i^{*kl} = \mathbf{e}_i^{kl} + \sum_{j=1, j \neq i}^m \mathbf{e}_j^{*R}$ . The determi-

nation of  $\mathbf{e}_j^{*R}$  is associated with considering the conditions of joint deformation and motion of the phases, as well as the structural properties of the medium's components. When strength effects are negligible, such as in gas-suspended states or in solid bodies under high pressures, the conditions for joint motion are simpler than in the general case. They reduce to equations defining phase volume fractions, pressure equality conditions between phases, or incompressibility conditions for one of the phases.

If the temperature  $T_i$  of each phase can be determined at any arbitrary point in the mixture, then, unlike the homogeneous case, the equations of state take the form:  $\sigma_i^{kl} = \sigma_i^{kl}(\rho_i^0, e_i^{0mp}, T_i, \chi_i^1, \dots, \chi_i^r)$ ,  $u_i = u_i(\rho_i^0, T_i, \chi_i^1, \dots, \chi_i^r)$ . These equations are defined not by the average, but by the true densities of the components  $\rho_i^0$ .

Additionally, the laws governing the relative motion of the phases become more complex, as this motion is influenced not only by diffusion processes but also by phase interactions at the macroscopic level. For example, in a gas-suspended state, the influence of interphase forces must be taken into account, including phase inertia, mass exchange, force interactions, and energy interactions.

When the relative motion processes are insignificant compared to the phase-averaged velocity, and the dynamic and inertial effects of this motion are small, a diffusion approximation can be applied to describe heterogeneous mixtures, with some modifications due to the presence of a suspended phase. A notable example of a non-inertial diffusion law is Darcy's filtration law:  $\rho_i w_i = k \nabla P$ .

To close the system of equations, barotropic-type state equations are used:  $P = P_i = P_i(\rho_i^0)$ . This approach is valid when the size of inclusions significantly exceeds molecular dimensions.

### **Motion of a heterogeneous medium with phase transitions.**

The momentum exchange between phase  $i$  and phase  $j$  per unit time and per unit volume is expressed as  $P_{ij} = -P_{ji} = R_{ij} v_{ji}$ , ( $i, j = 1..m$ ), where  $R_{ij}$  is the interphase force per unit volume due to friction, pressure, and adhesion between phases, and  $v_{ji}$  represents the velocity or momentum of mass undergoing transformation from phase  $j$  to phase  $i$ .

If each phase is assumed to be homogeneous up to the phase boundary surface within an elementary volume of the mixture, and if the energy of each component is proportional to its mass, then the influence of the interfacial layer – on the order of the molecular interaction radius ( $10^{-9}$  m) – can be neglected. This assumption requires that all inclusion sizes be significantly larger than the thickness of this layer. Furthermore, the energy equation should not account for small-scale flow effects, such as micro-scale chaotic motion of inclusions. Under these conditions, the kinetic energy of the mixture, when represented homogeneously, is additive over the mass of the phases. The introduction of phase temperatures is linked to the hypothesis of local equilibrium.

Using averaging methods, the momentum equations, heat flux equations for phases, and energy equations for pulsational (small-scale) motion can be derived [26, 30].

### **Porous medium saturated with liquid or gas.**

In a two-phase mixture of a porous solid phase with liquid or gas, the total stress is determined by the fictitious stresses and the pressure exerted by the liquid or gas. Fictitious stresses are defined through directly measurable quantities and pressure and interpreted as part of the average stress tensor in the solid phase or skeleton. These stresses are caused by an independent force transmission mechanism through contacts between the grains, rather than by the liquid. The strength properties of the solid phase manifest in the fictitious stress tensor.

Studies [4, 5] have classified drying objects. A. Lykov divided all solid wet materials into three groups: capillary-porous, colloidal, and capillary-porous colloidal materials. Capillary-porous colloidal

materials are those in which liquid exhibits different forms of bonding, which are characteristic of both capillary-porous and colloidal bodies. In particular, in capillary-porous bodies, the liquid is bound by capillary forces. Upon dehydration, capillary-porous bodies become brittle. They exhibit low compressibility and high liquid absorption capacity. Capillary forces significantly exceed gravitational forces.

Colloidal materials are those in which moisture is primarily bound by adsorption and osmotic forces. When dried, colloidal bodies contract with maintaining elasticity [2]. When moistened, they absorb liquids that are most similar in polarity. These materials are quasi-capillary-porous bodies, where molecular sizes are comparable to microcapillary dimensions.

B. Sazhin [6] classified dispersed materials into four groups based on the decreasing critical pore radius: greater than 100 nm; from 100 to 6 nm; from 6 to 2 nm; 2 nm or less. Additionally, he introduced subgroups and classes considering the particle size of the material, its adhesion-cohesion properties, and drying duration.

A two-phase dispersed mixture that contains dispersed particles of uniform shape and size within an elementary macro volume is called monodisperse. If the particles vary in size, the mixture is polydisperse. The carrier phase is a spatially connected volume (the dispersion medium).

An essential characteristic of convective drying is the gas and vapor pressure in both the drying agent and the material being dried.

### **Models of corpuscular structure.**

Dispersion is a thermodynamic characteristic of a system that determines the magnitude of the phase interface. The degree of dispersion is the degree of fragmentation of the substance in the dispersed phase, which is inversely proportional to the particle size  $s = 1/l$ , where  $l$  is the linear dimension that determines the particle size. L. Frevel [7] studied the method of forming regular packings composed of identical spheres. The distance between spheres varied from  $\sqrt{3}R$ , corresponding to the densest packing, to  $\rho_M$ , corresponding to the vertical alignment of layer centers directly above one another. The porosity  $\varepsilon$  in such packings varies from 0.2595 to 0.3954, and the coordination number for the densest packing equals 8.

K. Schlichter [2] studied another method of forming regular packings in the form of layers. The centers of the spheres were arranged at the nodes of rhombohedral lattices defined by the acute angle  $\omega$  of the rhombus, with vertices at the centers of adjacent layers. An angle of  $\omega = 60^\circ$  corresponds to the densest packing with  $\varepsilon = 0.2595$ , while  $\omega = 90^\circ$  corresponds to simple cubic packing with  $\varepsilon = 0.4764$ . The coordination number for such packing is  $N = 12$ .

If regions around the voids are cut out such that the cutting planes pass through the narrowest cross-sections of pore necks, the porous body is divided into elementary cells – polyhedra. An elementary pore in such a cell represents a cavity bounded by spherical surfaces with several necks connecting it to other elementary pores. In cubic packing, the elementary pore cavity is bounded by eight spheres and connected to six square-shaped necks leading to neighboring cavities.

The sizes of elementary pores in framework packings are characterized by the radius  $\rho_{rop}$  of the sphere inscribed in the cavity and the equivalent radius  $\rho_{rop}$  of the circle inscribed in the neck.

According to V. Karnaukhov, for framework packings:  $\rho_{3\text{э}} \approx 0,45 \frac{\varepsilon}{1-\varepsilon} R$ . The shape and sizes of

pores in random sphere packings vary, but their qualitative appearance is similar to elementary pores in regular packings. The specific surface area of particles is given by:  $s_y = S/V_M$ , where  $S$  and  $V_M$  are the surface area and volume of the particles in the material.

### Drying of natural organic materials.

The process is accompanied by structural changes, physicochemical transformations, endothermic and exothermic reactions. Variations between isosteric and calorimetric values of specific heat of evaporation for starch and cellulose have been observed. These variations are caused by changes in the configurational entropy of solid components and the entropy of mixing due to interactions between solvent molecules (water) and macromolecules of high-molecular substances. However, during the removal of capillary and adsorbed moisture, an increase in the specific heat of evaporation is observed by only 3–5 % and 20 % relative to the evaporation heat of bulk liquid, respectively.

At low moisture contents, individual water molecules reside in micropores, comparable in size to the sorbate molecule, and interact via hydrogen bonds with the polar functional groups of the sorbent. If the pores are larger and not fully filled, translational motion of sorbate molecules may occur inside them. As the pores fill, mobility decreases. At high moisture contents, the material swells, and pore sizes increase. Water molecules in such conditions are more mobile, and as intermediate and macropores fill, their mobility approaches that of ordinary water molecules. The swelling process is analogous to the dissolution of water in a high-molecular substance. With increasing moisture content, water molecule clusters merge and form a continuous phase within the sorbent, defining the physical properties of the sorbate, which become similar to those of a typical liquid.

The sorption isotherm on swollen colloidal materials is described as  $1/W = n \ln(P_g/P) + a$ , where  $W$  is the moisture content,  $P_g/P$  is the relative vapor pressures of the sorbate, and  $a, p$  are constants. The primary indicator characterizing a material as a drying object is moisture resistance, which determines the limit of residual moisture in the dehydration process. Living cells exhibit high moisture sensitivity. Their physicochemical properties and responses to dehydration conditions vary significantly. Consequently, no consistent pattern has been found linking residual moisture to microbial cell viability, often resulting in a final product with a low count of viable cells.

When biological systems are dried, they enter a state of dry anabiosis, in which vital processes are suppressed, but a lethal state does not occur. Upon restoration of favorable conditions, normal metabolic processes can resume. Water acts as a regulator of essential metabolic processes between the cell and its external environment [7, 8].

Experimental data reveal a pattern for vegetative microbial cultures of various origins, showing a sharp loss of microbial cell viability within the moisture content range of 50–80 %. The effect of residual moisture on microbial viability exhibits a stepwise nature, where the primary lethal factor is the sudden rupture of the cell membrane. The critical moisture content, corresponding to

a drastic change in microbial viability, coincides with the maximum hygroscopic moisture content, and the viability decline region aligns with the sorption isotherm segment where moisture is primarily capillary-bound.

For a given relative air humidity, the average capillary radius is determined using the Thomson equation:

$$\bar{r} = \frac{2\rho_l \sigma \cos\Theta}{\rho_l P \ln(1/\varphi)}.$$

Thus, for  $\varphi = 0.96$ , the mean capillary radius is  $r = 10^{-5}$  cm. In this case, the capillary rise height is  $h = 150$  m, and the pressure of such a column is approximately 1.5 MPa. If the capillary height is less than  $h$ , a negative pressure is generated within the capillary, causing deformation of the elastic body skeleton (cell membranes). Liquid under negative pressure exists in an unstable metastable state. However, a metastable phase can persist indefinitely under unchanged thermodynamic conditions, which is associated with the stationary state of a dehydrated biological system – anabiosis. A necessary condition for anabiosis is the presence of a metastable liquid film around a living cell, forming part of the capillary-porous body structure.

In work [9], a model for unsteady processes of a single-component liquid was proposed, accounting for the mutual influence of vapor pressure, liquid pressure (determined by capillary and surface forces), temperature on phase mass exchange intensity, thermocapillary flows, and the conditions for mechanical and dynamic equilibrium of thin liquid layers on curved phase interfaces.

### Material permeability.

In work [10], a dependence of the permeability coefficient on the effective pore size was obtained based on the differential pore characteristics of the material and Darcy's law for different moisture contents. The permeability of dry materials is expressed through the linear dependence of gas flow through a porous medium on the gas pressure gradient.

As the liquid is removed from a material initially saturated to its maximum moisture capacity, it exits the largest pores and then the smaller ones. During this process, the effective porosity of the material and the permeability coefficient change. By maintaining a constant pressure difference under filtration conditions, the volumetric airflow rate  $J_0$  can be measured. Given the known sample thickness, filtering surface, and viscosity of the absorbed liquid, the material's permeability can be calculated as a function of the minimum diameter of open pores.

Since the applied air pressure compensates for the capillary pressure of the liquid in the material's pores, the minimum diameter of open pores is determined using Laplace's equation. A stepwise increase in pressure difference leads to the sequential displacement of liquid from progressively smaller pores, thereby altering the permeability coefficient. To determine the material's permeability and the minimum diameter of open pores, the moisture content of the sample must be measured at each pressure difference increment. Studies show that the effective radius of open pores significantly influences the permeability coefficient.

### **Drying process and product quality.**

The quality of the final product obtained through drying is determined by the heat-moisture conditions and the mechanism of heat and mass transfer. Studying diffusion and thermodiffusion processes enables a better understanding of substance movement within the material, the identification of effective ways to control mass transfer mechanisms, and the development of new drying technologies to enhance product quality.

If liquid moisture diffusion occurs during drying, water-soluble substances accumulate on the surface. In contrast, when vapor-phase moisture diffusion dominates, water-soluble components remain within the material.

### **Suspended-state grain drying.**

The method of drying grain in a suspended state involves a continuous alternation between heating and cooling processes. In intermittent drying, the surface layer of the grain cools more than the inner layers. In such cases, thermomoisture conductivity supports moisture transfer, and the heat flux aligns with the moisture flux. Moisture evaporation starts from the surface, causing water-soluble nutrients to remain near the surface and close to the germ, promoting its growth and improving the seed quality.

During drying, materials undergo shrinkage. High-quality material maintains uniform shrinkage throughout its thickness. Significant variations in moisture content and temperature during drying result in volumetric stress-strain states that exceed permissible limits, leading to cracking or complete structural failure. Materials may warp or develop pores. The surface with lower moisture content contracts more, causing the sample to warp toward the drier side. Ideally, the moisture transfer mechanism should ensure equal moisture removal rates from both surfaces.

Temperature gradients drive moisture movement inside the material. The moisture flux toward the surface decreases by an amount proportional to the thermodiffusion-induced moisture flux, which opposes the movement of moisture from the central layers to the surface. Thermodiffusion reduces the moisture gradient, decreases moisture transfer rates, and limits the accumulation of water-soluble substances on the surface. Changes in the temperature gradient's direction alter the material's physicochemical and biochemical properties. To retain water-soluble substances within the material, the most intense evaporation should occur inside the material rather than at the surface.

The temperature gradient increases with airflow velocity. In thick materials, an increase in temperature gradient results in a moisture content gradient, leading to internal stresses and crack formation.

### **Steam-heat treatment drying.**

In steam-heat drying, saturated steam is used as the heat carrier. Heat is transferred from the steam-air mixture to the solidifying material through convection. A temperature gradient is established in the material, generating internal stresses. Since the surface temperature is lower than that of the steam-air mixture, a condensate film forms on the surface, and moisture migrates from the surface layers to the center, leading to material reabsorption of moisture. The hydration

reaction occurring during this process can cause the material's temperature to exceed that of the surrounding environment. Intense evaporation at high moisture levels results in directed pore formation.

To control moisture transfer, it is essential to establish the relationship between diffusion and thermodiffusion coefficients with moisture content and temperature, particularly using stationary and non-stationary mass transfer methods.

### **Models based on continuum mechanics.**

Changes in the volume and shape of solid porous bodies during drying in the absence of external forces indicate the emergence and development of a stress-strain state caused by moisture-thermal effects [15]. Colloidal materials undergo dimensional changes during drying. The removal of moisture from the material requires energy, which corresponds to breaking the bonds between the moisture and the material.

Physico-mechanical bound moisture is present in large capillaries and on the external surface of the material. Removing this moisture requires energy equal to the heat of vaporization. Physico-chemical bound moisture is retained on the internal surface of pores by adsorption forces. The amount of adsorbed moisture depends on the temperature and humidity of the external environment.

As temperature increases and moisture content in the body decreases, two opposing processes occur: thermal expansion and contraction, which are governed by the physical properties of the material. These opposing deformations restrict each other, leading to the formation of nonstationary stresses, which can exceed the strength limit, resulting in crack formation and propagation.

Studying the stress-strain state in drying kinetics and comparing stress values with material strength characteristics allows optimization of drying processes based on strength parameters. In work [15], a mathematical drying model was developed that accounts for the stress-strain state of the material based on non-equilibrium thermodynamics and continuum mechanics.

It is assumed that the wet body is isotropic and undergoes small elastic, nonlinear elastic, and plastic deformations, where linear deformation theory holds. The capillary-porous body is considered as a local superposition of a solid porous or granular component and a fluid phase (in liquid and vapor states) filling the pores. During drying, the body is treated as a heterogeneous non-equilibrium system that exchanges energy and mass with the surrounding environment.

The principle of local equilibrium in non-equilibrium thermodynamics enables the description of the system using equilibrium state parameters. During drying, the temperature, volume, and composition of the system change. The composition changes only due to phase transitions of the liquid and vapor removal.

If evaporation occurs at temperature  $T$ , evaporation of liquid in the pores occurs, an excess vapor pressure arises in the system  $p = P - P_0$ , where  $P_0$  is the barometric pressure. This excess pressure causes tensile deformation  $p / E_0$ , which leads to convective mass transfer, alters the phase transition temperature, affects the mass transfer intensity, and influences material compression. At different drying stages, the intensities of these components vary, and the resulting deformation may manifest as either tensile or compressive deformation.



A mathematical model of capillary-porous material drying is formulated, including:

1. Equation of state.
2. Diffusion-convective mass transport equation.
3. Momentum equation.
4. Heat conduction equation.
5. Compatibility conditions for deformations.

A closed system of nonlinear equations describes the time-dependent processes of heat and mass transfer and deformation, considering the dependence of thermophysical, heat and mass transfer, and physico-mechanical properties on temperature and moisture content.

These equations, with initial and boundary conditions, define a nonstationary drying problem and establish the interrelation between heat and mass transfer and the stress-strain state.

In drying process formulation in displacements, the diffusion-convective mass transport equations in displacements are used along with the corresponding heat and mass exchange boundary conditions and mechanical boundary conditions ensuring deformation compatibility.

For drying technology applications, interest lies in the deformations and stresses induced by moisture-thermal effects. It is shown that in transport equations, the mechanical coupling terms can be omitted, while in equilibrium equations, hydro-barothermal field variations can be disregarded.

The continuum mechanics approach to studying the stress-strain state is detailed in work [16].

### **Stress and deformation relations.**

The stresses induced during drying lead to elastic-plastic deformations, which are determined by the relationship between the strain tensor  $\varepsilon_{ij}$  and the stress tensor  $\sigma_{ij}$ :

$$\sigma_{ij} = f(\varepsilon_{ij}).$$

Since drying-induced stresses have a negligible effect on the excess vapor-air mixture pressure within the body, the coupling effect is insignificant in problems concerning moisture-thermal stresses in drying materials.

In the heat conduction equation, the mechanical coupling terms can be neglected, and in the momentum equation, the inertial term can be omitted. The interaction between heat and mass transfer and the stress-strain state is also negligible in most cases.

On the boundary surface, the components of internal stresses must equal the external surface forces. In many drying cases, volume and surface force loads can be neglected.

As a result of heat and mass transfer through the material thickness, nonstationary temperature, moisture content, and pressure fields develop, which are determined from the heat and mass transfer equations.

To solve the drying problem, six stress tensor components  $\sigma_{ij}$  must be determined, satisfying:

- a) six equilibrium equations;
- b) deformation compatibility equations;

- c) boundary conditions;
- d) these relationships enable a comprehensive analysis of moisture-thermal stresses and deformations in drying processes.

### **Models based on mixture theory.**

In works [17, 18], the laws of non-equilibrium thermodynamics were applied to a three-phase medium consisting of a solid skeleton, liquid, and vapor-air mixture in a porous deformable system to analyze interphase interaction forces, considering phase transitions.

The porous body was treated as a thermodynamic system comprising solid, liquid, and gaseous phases. The solid particles were tightly packed into either a granular skeleton or a capillary-porous body. Initially, the pores were filled with moisture and air. Under the influence of external heat sources and pressure differences between the pores and the surrounding environment, interconnected heat and mass transfer and deformation processes occurred.

It was assumed that the gaseous phase is homogeneous. Due to capillary forces, pressure differences in the capillaries, and chemical activity of liquid and gaseous phase particles, chemical transformations and phase transitions of the components may occur in the capillaries.

Particles of the same chemical species, when in different aggregate states, exhibit different diffusion, filtration, and thermal conductivity coefficients. In a  $p$ -component three-phase system with chemically active elements, phase transitions of the components can occur.

Chemical transformation can be considered as a complex interaction of thermal, mechanical, mass, and electrical processes among the subsystems.

The mass balance equations for each component and the law of conservation of total energy of the system are postulated. Balance relations for the momentum of the total system mass, considering chemical transformations, potential, kinetic, and internal energies, entropy, and the Gibbs equation for free energy are obtained.

Assuming that the kinetic potential is a function of thermodynamic forces, kinetic relations for the thermodynamic system are derived [17, 18].

Thus, a complete nonlinear system of equations for the model is constructed, including:

- 1) the coupled heat conduction equation;
- 2) the equation of state (expressing the dependence of entropy, the total stress tensor, and chemical potential on temperature  $T$ ,  $\varepsilon_{\alpha\beta}$ ,  $C_k^{(j)}$ ;
- 3) equations for liquid and gas phase pressures;
- 4) the equation for the density of saturated vapor;
- 5) mass balance equations for the skeleton, air, vapor, and liquid;
- 6) relations for the liquid, vapor, and air fluxes in terms of gradients  $T$ ,  $\varepsilon_{\alpha\beta}$ ,  $C_k^{(j)}$ ;
- 7) invariants for the volume-averaged mixture related to skeleton dilation due to concentration differences;
- 8) the compatibility equation;
- 9) the momentum balance equation for the skeleton;
- 10) expressions for the components of the fictitious stress tensor;

- 11) the total stress tensor as a function of fictitious stresses and the stress tensor of the liquid and gas phases taking into account the viscosity effects;
- 12) the difference in pressure between the carrier and solid phases due to mechanical strength;
- 13) relations for volume-averaged velocities and skeleton deformations.

### **Application to engineering problems of conductive drying.**

Based on this model, the problem of conductive drying of a porous layer is formulated as follows:

A thin plane plate with surface area  $S$  and thickness  $h_w$  is exposed to an external heat flux  $q_e(t)$  on one side. The plate has density  $\rho_w$  and specific heat capacity  $c_w$ . A moisture-saturated capillary-porous material of thickness  $l$  is placed on the plate. The material has the porosity  $\Pi$ , density  $\rho_0^0$ , specific heat capacity  $c_0$ , thermal conductivity coefficient in the dry state  $\lambda_0$ . From the exposed surface of the capillary-porous material, liquid evaporates into a cavity with volume  $V$  and depth  $V/S$ . The thermally insulated cavity has an opening, through which the vapor-air mixture escapes into the ambient environment at pressure  $P_e$ . Heating of the material induces filtration flow of both liquid and gas. The liquid flow is driven by the gradients of relative saturation  $\alpha$  (the volume fraction of liquid in the pores), temperature  $T$ , and vapor-air mixture pressure  $P$ . The vapor and air fluxes are governed by pressure and mass concentration gradients of vapor in the mixture. The relative permeabilities of liquid and gas are proportional to their respective saturations. Appropriate initial and boundary conditions are formulated.

A model of convective-thermal drying of a layer in a drying system, considering the movement of the phase transition boundary, has also been developed.

In work [20], the drying problem was formulated for a non-stationary thermal regime of the drying agent in a drying system. The use of time-varying thermal regimes during drying can significantly reduce energy consumption and improve material quality.

When the temperature of the drying agent decreases, the temperature of the material's surface layers also decreases, creating an additional temperature gradient, which serves as a driving force for moisture migration within the material. This leads to an increase in relative humidity and moisture treatment of the material surface, reducing internal stresses.

The timing and duration of heat-moisture treatment are critical for different materials. Therefore, it is necessary to develop methods for:

- a) investigating heat and mass transfer processes;
- b) diagnosing the stress-strain state of materials;
- c) determining optimal drying agent parameters based on diagnostic results;
- d) formulation of the drying problem for a layer under a time-varying thermal regime.

To assess the influence of a time-dependent thermal regime in the drying system, the drying process is formulated for a layer  $(-L \leq z \leq L)$ , where moisture removal occurs through its surfaces under the influence of a convective-thermal non-stationary flow of the drying agent.

The problem is reduced to solving the Stefan problem, which includes the following system of equations in the dried zone:

1. Energy equation.
2. Mass transfer equation for the vapor-air mixture.

3. State equation for the binary vapor-air mixture.
4. Energy balance equation at the moving phase transition boundary.
5. Linearized state equation at the moving phase transition boundary  $z = L_m$ .
6. Equation of motion for the phase interface.
7. The boundary conditions at  $z = L$  express heat exchange between the material surface and the drying agent by the Newton's law.

At the phase transition boundary  $z = L_m$ , the transition temperature  $T_m$  is unknown and depends on the pressure  $P_n$  of the saturated vapor ( $T_m = f(P_n)$ ) is to be determined; the time-dependent temperature of the drying agent is represented as a Fourier series expansion.

The solution algorithm was validated using a wood drying model (pine). The problem was reduced to solving the Stefan-Maxwell system of equations. Given a specified vapor flux across the thickness, the relationship between the phase transition coordinate and time was constructed. By solving the heat and mass transfer equations under a non-stationary drying agent regime with three-stage temperature control [20, 21], it was shown that as the mass transfer coefficient and temperature increase, and as the vapor density decreases, the relative humidity of the layer decreases; numerical results demonstrate parabolic dependencies of relative saturation over time and linear dependencies on changes in mass transfer coefficients.

The temperature distribution across the material thickness was determined as a function of dimensionless coordinate  $\bar{z}$  and phase transition coordinate  $\bar{z}_m$ ; the phase transition temperature variation over time was analyzed; the change in the phase transition coordinate over time was evaluated in relation to the relative saturation of the drying agent; the relationship between drying time and the width of the dried zone  $z_m$  was studied as a function of the heat transfer coefficient, mass transfer coefficient, permeability, diffusion, and average temperature.

It was shown that in a non-stationary regime, drying time depends both on the equation of state at the phase transition boundary and the heat and mass transfer coefficients. In a gentle drying regime, the process can be controlled by increasing or decreasing airflow speed via heat or mass transfer coefficients; adjusting the drying agent humidity; modifying the temperature change intervals of the drying agent using the control function expansion coefficients  $u(\tau)$ . The study demonstrated the possibility of selecting and minimizing optimal drying criteria [17–21].

The drying of dispersed materials in a suspended state was studied in [22]. The external heat and mass transfer process was analyzed based on the simultaneous consideration of the equations of motion and continuity for the drying agent flow and the convective-diffusive transfer of vapor and heat in the moving drying agent.

Experimental data on the intensity of external heat and mass transfer were presented as dependencies between similarity criteria derived from the governing equations and corresponding uniqueness conditions. The mass transfer coefficient appears in the Nusselt criterion, whose value is a function of the Reynolds and Prandtl numbers.

For forced airflow along a wet surface, the criterion equations for heat and mass transfer were provided based on experimental studies on the intensity of heat and mass exchange between the

drying agent and the material, whose surface remains moist due to moisture supply from internal zones of the material.

Further, moisture undergoes phase transformation into vapor within the internal zones, causing the external surface temperature to increase and the heat and mass transfer coefficients to change. The variation in heat transfer coefficient due to decreasing moisture content was accounted for by the ratio of moisture content  $u$  to the critical value  $u_{kr}$ , at which the constant drying rate period ends, and the surface ceases to be wetted. An approximate formula was derived, incorporating the contributions of the frontal and rear sections of a spherical body in mass transfer.

It should be noted that the equations of motion for the drying medium are nonlinear, and for the numerical implementation of velocity, an alternative approach was developed in [23] through the phase state diagram of an infiltrated dispersed medium. This diagram includes not only the stationary bed and the boiling layer but also vertical pneumatic transport and the circulating fluidized bed. Expressions were derived for calculating an important characteristic of flow systems – the transport velocity; the critical point on the phase diagram was identified, which determines the velocity at the onset of fluidization.

The heat and mass transfer in a dispersed medium were studied in [24] as occurring in a homogeneous continuum or in multiple coexisting homogeneous continua within each point in space without considering microscopic transport phenomena near individual particles. Macroscopic heat or mass conservation equations were formulated for a continuous medium containing dispersed phase particles, neglecting the effect of random fluctuations of the medium and particles on the transport processes.

## 5.2 STATISTICAL METHODS FOR STUDYING THE DRYING OF CAPILLARY-POROUS BODIES

In works [25, 26], the problem of random pulsations in a coarse-disperse fluidized bed was formulated. Additionally, the problem of convective thermal conductivity or diffusion near an individual particle was posed. The problem was solved for low Péclet numbers, which characterize heat and mass transfer in the vicinity of an individual particle. It was assumed that the spatial scale  $L$  of temperature fields or impurity concentration in a dispersed system is significantly larger than the internal structure scale  $l$  of the system, such as the distance between neighboring particles. The dispersed system was considered as a superposition of coexisting continua, each characterized by its own average velocity and temperature. The variations of these quantities were described by averaged conservation equations. A system of conservation equations for mass, heat, momentum, and angular momentum of continua was developed, simulating the phases of a monodisperse suspension. If the phases of the dispersed medium are stationary, these equations describe transport processes in composite granular materials.

Using the mass conservation equations of the phases, a model was derived in which the dispersed medium is considered a superposition of two continua, each having different velocities and

temperatures. The equations contain unknown variables, such as concentration and temperature, averaged over the ensemble of particles. The problem of determining these variables in the form of functions or functionals of unknown variables and physical parameters is analogous to the problem of obtaining rheological equations of state for suspensions.

Averaged equations describing heat transfer in the continuous phase near a selected particle were formulated. Their solution allows for the calculation of the average temperature and heat flux on the particle surface. In the ensemble averaging process, it was assumed that particle placement is random and that the correlation weakening condition holds. This condition states that conditional averages, obtained by averaging over the particle distribution function, given that a certain fixed point is occupied by the center of a test particle, asymptotically approach the corresponding unconditional averages as the distance from this point increases.

Furthermore, the average temperature of the continuous phase at a given point approximately coincides with the value obtained by averaging the temperature only over those configurations in which the presence of a particle center at that point would be possible. By analyzing integral sums and neglecting terms quadratic in random deviations of local values from their averages, a differential heat transfer equation was derived for both the continuous and dispersed phases on average. The heat transfer in the continuous phase was represented as transport in a hypothetical medium that fills the entire space and contains distributed heat sources. The equation describing heat transfer near a particle with its center at  $r = 0$  was obtained similarly to the equation for the continuous phase, assuming conditional averaging only over configurations of all other particles that are compatible with the presence of a particle center at a fixed point. In such averaging, terms quadratic in fluctuations of values relative to their mean were neglected; a heat transfer equation was obtained in a coordinate system associated with the center of a particle in the continuous phase. The heat transfer inside a test particle was described, considering its rotation. On the surface at  $r = a$  of the test particle, continuity conditions for temperature and heat flux were imposed, defining the interaction between the particle and the continuous phase, which closes the heat conduction problem near the test particle.

The evaporation or condensation of moisture is accompanied by a sudden absorption or release of latent heat of vaporization, which is determined at the normal boiling temperature according to Trouton's rule  $r_{boil} = 88T_{boil}$ , since from the Clapeyron-Clausius equation  $dp/dT = r/T\Delta v$ , where  $dp/dT$  is the derivative of pressure with respect to temperature, which is determined from the phase equilibrium curve. If the phase transition data are missing,  $r_{boil} = (RT_{kp}T_{boil} \ln P_{kp}) / (T_{kp} - T_{boil})$  is put.

The structure of a body is influenced by the liquid contained within the porous medium. Swelling is a specific case of structural deformation caused by the interaction of the liquid with the material. In the absence of specific interactions between the body and the liquid, swelling pressure  $P_{swel}$  is proportional to the surface tension of the liquid.

To describe the distribution of phases within a porous medium, it is necessary to apply structural models of porous media [30]. Since real porous materials possess irregular and random structures, only stochastic structural models can claim adequacy. The pore space is represented

as a statistical ensemble of interconnected structural elements (pores), whose properties follow certain probabilistic laws.

In the elementary physical volume of the medium, a specific porous medium model must be selected. The most suitable statistical model should accurately describe the structure. To determine the effective transport coefficients for each phase, their interconnections as functions of macroscopic variables, the conditions governing the process within an individual pore, and the geometric characteristics of the porous structure, a key factor is the choice of an averaging method, which is determined by the selected porous medium model.

The principle of local equilibrium is applied to determine the characteristics of phase distribution. This principle considers the process in an elementary physical volume as occurring in an unbounded porous medium, neglecting transport phenomena and accounting only for the conditions of interphase boundary formation under capillary dynamic equilibrium between the phases. The distribution of phases in the pore space is governed by pressure differences between phases and capillary properties, considering electrochemical transformations, if present.

The statistical analysis of liquid and gas distribution in hydrophilic porous media is based on representing the pore space as a network of variable cross-section channels, forming a stochastic spatial lattice with a specific coordination number. This representation reduces the problem of liquid and gas distribution to that of the mutual arrangement of liquid-filled and gas-filled pores in a random lattice with certain statistical properties.

During drying, the gas phase in the pore space forms three characteristic configurations:

- a) a connected system of gas-filled pores that extends to the external surface;
- b) a two-phase system consisting of isolated liquid inclusions trapped by gas;
- c) a liquid-filled pore system.

For each specific porous structure, there exists a critical moisture content at which the connectivity of the liquid phase is completely disrupted, and all moisture is localized in isolated inclusions. The critical moisture content is a structural characteristic of the porous medium and can be used for comparative analysis of different porous structures.

The connectivity factor plays a key role in transport processes. The transport of any substance through either the gas or liquid phase is only possible within a connected network of gas (or liquid) pores, some of which are dead-end pores blocked by liquid (or gas) at one end. If a given pore belongs to an isolated inclusion, long-range transport is impossible. In the case of gas-filled pores, moisture transport occurs through: convection, vapor diffusion in the vapor-air mixture, film flow driven by the disjoining pressure gradient. As the moisture content changes during drying, the mechanisms of transport also change.

The mutual phase distribution in the pore space determines the effective transport coefficients for each phase and the interphase surface areas. The capillary forces are responsible for the distribution of phases. The liquid content in a porous body changes through evaporation and capillary absorption. In a capillary-porous body, vapor, filtration, and film mechanisms of moisture transfer operate, aiding in the establishment of capillary equilibrium.

The vapor mechanism follows the sequence: evaporation → vapor transport through the vapor-gas phase → condensation. The filtration mechanism occurs due to liquid flow under the capillary pressure gradient. During evaporation, the meniscus recedes only in a wide capillary, while in a narrow capillary, the recession begins only after the entire wide capillary has been dehydrated. Additionally, the volume of liquid evaporated from the narrow capillary is immediately replenished at the rate of evaporation by liquid from the wide capillary.

It can be lowered below the equalizing mechanisms' rate by artificially reducing the evaporation rate through external drying conditions. For example, reducing the external moisture transfer rate increases the moisture content, leading to a nearly uniform moisture distribution across the thickness of the porous body. Non-uniform moisture distribution causes undesirable deformation of porous materials.

Experimental data confirm that the distribution of pore volumes governs the equilibrium distribution of liquid within a porous body according to capillary pressures  $P^k$  and the influence of the temperature gradient on the moisture content gradient in the porous body. During drying, the mutual phase distribution is established through the interaction of two factors: the transition of one phase into another and the redistribution of phases in the porous material due to differences in capillary properties.

The control of heat and mass transfer processes in heterogeneous, fluidized, and vibro-circulating media has been extensively studied in works [23–29].

In the monograph [30], it is shown that during the drying process, three distinct zones are formed: the outer gas zone, where all pores are completely dried, and the gas distribution across the thickness is nearly uniform; the intermediate two-phase zone, where both dried pores and liquid-filled pores coexist; the inner liquid zone, where all pores remain filled with liquid. If the removal of vapor from the evaporation zone is rapid, and capillary inflow and recondensation cannot sufficiently replenish moisture in the dried pores near the surface, the two-phase zone disappears, leading to the formation of a spatial front inside the material. This front separates the liquid and gas zones and gradually moves deeper into the material. Conversely, if capillary inflow and recondensation are effective, but vapor removal is hindered, the phase boundary follows pores of a specific radius – one that depends on the amount of liquid present but not on spatial coordinates. In this case, the two-phase zone extends throughout the entire volume.

During evaporation, the connected liquid system undergoes fragmentation. Once a critical threshold is reached, the liquid phase connectivity breaks within the elementary volume of the porous medium. The connectivity of the liquid phase plays a key role in the mechanism of capillary moisture transfer. The redistribution of moisture in disconnected inclusions occurs through capillary recondensation. In diffusive or migratory transport within a connected liquid system, provided that this system remains connected to the outer surface, the effective diffusion or electrical conductivity coefficients depend on the amount of connected liquid. If liquid-phase transport becomes impossible due to the loss of connectivity at moisture content  $u < u_{kr}$ , it leads to a non-uniform concentration of liquid during evaporation. The connected liquid pore system is also heterogeneous



in terms of transport processes due to the presence of dead-end pores – pores that are blocked by gas at one end.

### **Model of intersecting variable-section capillaries.**

If pores are represented as circular cylinders with a radius  $r$  that varies along their length and does not intersect, then the serial model of the porous medium is applied. The liquid-gas interface at any given time is located within the critical pore and moves deeper into the material during evaporation. Pores with a radius larger than the critical value are referred to as supercritical pores. These supercritical pores can branch, which facilitates gas penetration into the porous medium.

### **Random process model.**

A randomly selected supercritical pore located at the surface of the material ( $y=0$ ) can, through branching and blocking, generate  $s$  supercritical pores with probability  $p_s(y)$ .

The pattern of pore filling with vapor depends on the relationship between the probabilities of blocking  $\lambda$  and branching  $\nu$ . If  $\lambda > \nu$ , the probability of blocking a supercritical pore near the surface is given by  $p_{s=0}(y) = F(y, a)$ . To determine  $\lambda$  and  $\nu$ , it is necessary to define the type of random process governing the radius variation along the pore length.

### **Random walk model.**

In a purely random process, the blocking probability does not depend on the pore radius. However, in reality, the blocking probability of a supercritical pore depends on its radius. Thus, in the random walk model, the blocking process of supercritical pores occurs stepwise: evaporation begins in the widest pores, then progresses to narrower supercritical pores, these pores transition to the subcritical class with higher probability as their radius decreases. This process resembles a random walk in the radius space of pores.

### **Serial model.**

In [31], a numerical solution to the two-dimensional problem of non-isothermal moisture transport in an anisotropic wood structure under convective drying was obtained by the serial model. Based on elasticity theory, internal thermohygroscopic stresses were determined.

The values for elastic modulus and strength limit were taken from the formulas derived by G. Shubin [32] for pine wood. The study showed that at the beginning of the drying process, internal stresses in the surface zone increase and later decrease. A stress drop was observed after the moisture content of the inner zone fell below the fiber saturation point, estimated at 25 %. The appearance of significant residual deformations leads, at the end of drying, to a change in the sign of stresses. In the dried board, residual compressive stresses remain in the surface layers, while tensile stresses are present in the inner zone. For initial moisture content below 25 %, stress relaxation was not observed.

### **Fractal models and fractional-order differential equations.**

In [33], a literature review on the mathematical modeling of non-isothermal moisture transport and viscoelastic deformation in capillary-porous materials with fractal structures was conducted. For describing unsteady processes in media with fractal structures, which exhibit: biological variability of rheological properties; structural heterogeneity; memory effects; self-organization; deterministic chaos; the mathematical apparatus of fractional-order differentiation was employed.

The Riemann-Liouville, Caputo, and Grünwald-Letnikov approaches, along with fractional integration operators, were applied.

Significant contributions to the development of mathematical models were made by B. Ugolev, G. Shubin, Ya. Sokolovskyy, I. Krechetov, and P. Biley.

The elastic and viscoelastic deformations have been extensively studied, whereas models incorporating fractal material structures remain underexplored.

#### **Advances in mathematical models.**

In [34], the mathematical model of non-isothermal moisture transport in capillary-porous drying materials was refined to account for their fractal structure and anisotropy of thermomechanical properties. The heat and mass transfer process during drying is described by a system of fractional-order partial differential equations based on the Riemann-Liouville formulation. The solution was implemented using the finite difference method.

The model accounts for:

- 1) elastic, viscoelastic, and residual deformations;
- 2) memory effects and self-organization;
- 3) the impact of wood species properties on moisture content variations;
- 4) the effect of fractal structure on the stress tensor distribution in wood.

Additionally, the Voigt, Maxwell, and Kelvin fractal models were considered.

The relationship between stress and strain components in wood drying, considering the fractal structure of the medium, is presented as a system of fractional-order differential equations. These equations were derived from the integral equations of viscoelasticity, which are based on the hereditary Boltzmann-Volterra theory.

To determine the criteria for selecting the relaxation kernel, the rheological behavior of wood and its fractal structure were taken into account. The kernel was chosen based on literature and experimental data. The solution was obtained using the predictor-corrector finite difference method. A two-dimensional viscoelastic deformation model of wood as a fractal medium was investigated under non-isothermal moisture transport conditions. The influence of drying process parameters on the distribution of temperature, moisture content, and stress-strain components was established.

### **5.3 DRYING PROCESS CONTROL AND OPTIMIZATION FOR ENERGY EFFICIENCY AND SUSTAINABILITY**

The issue of controlling drying processes is addressed in many works, emphasizing the importance of precise process regulation to ensure efficient moisture removal while minimizing material degradation. Given the complex dynamic nature of drying, achieving optimal control requires the application of advanced mathematical models and systematic process analysis [35].

To simplify the study of complex dynamic systems, various structural transformations and equation modifications have been suggested, including:

*Decomposition.* Dividing the complex system into weakly coupled subsystems by selecting inverse connections, allowing the system to be managed through simpler, autonomous subsystems, each controlled independently by local regulators.

*Aggregation.* Combining smaller components into larger functional blocks to prevent excessive system complexity and order increase.

*Transformation.* Converting the system into a standardized form without changing the equation order, ensuring a more structured representation of the control scheme.

While these methodological approaches improve the structural representation of drying processes, a key challenge remains: achieving energy-efficient drying without compromising product quality. The drying process is energy-intensive, and unoptimized control strategies can lead to excessive energy consumption, material defects, and operational inefficiencies.

Thus, optimizing drying processes has become a crucial factor in advancing sustainable industrial practices. Strategies such as real-time process monitoring, adaptive control algorithms, and heat recovery systems contribute to energy savings and reduced environmental impact. Moreover, incorporating sustainability principles into drying system design ensures that industrial drying aligns with global energy efficiency goals and eco-friendly production standards.

Addressing drying optimization from an energy-saving and sustainability perspective requires an integrated approach, balancing technical performance, economic feasibility, and environmental responsibility.

### 3.1 GENERAL INFORMATION ON CONVECTIVE DRYING OF POROUS MATERIALS IN DRYING INSTALLATIONS

To proceed with the optimization of drying processes, it is essential to first understand the fundamentals of technological processes occurring in industrial drying facilities. In particular, a comprehensive knowledge of the types of drying equipment used and their specific purposes is required. The selection of appropriate drying methods and operating conditions depends on the properties of the material, the target moisture content, and the efficiency of heat and mass transfer mechanisms.

The optimal process parameters – such as environmental temperature  $T_s$ , air humidity in the drying chamber  $\phi$ , and airflow velocity  $v$  – must be carefully chosen considering the technological characteristics of the material being dried.

Moisture removal under heating is constrained by the maximum allowable temperature for a given material and the permissible gradient of its change over time. The control of temperature and humidity in drying chambers is achieved by regulating the dry-bulb  $T_c$  and wet-bulb  $T_m$  temperatures of the drying agent.

In steam-based chamber drying installations, the drying process follows the characteristics of dry-bulb  $T_c$  and wet-bulb  $T_m$  temperature changes.

In **Fig. 5.1**, the relative change in drying duration is plotted along the x-axis, representing the ratio of actual drying time  $\tau$  to the standard drying cycle time  $\tau_{nom}$  of 48 hours. The y-axis shows the relative value of the dry-bulb temperature, where a reference temperature of 120 °C is taken as the unit value.

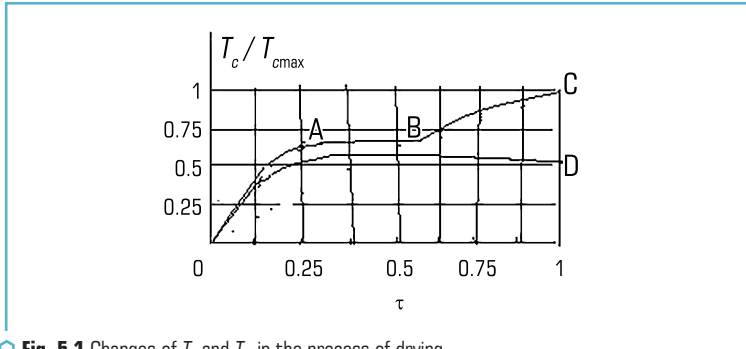


**Fig. 5.1** Changes of  $T_c$  and  $T_m$  in the process of drying

During the drying process, three main stages can be distinguished:

1. Material heating stage.
2. Isothermal heating stage throughout the cross-section.
3. Falling drying rate stage.

The dry-bulb temperature varies at different stages of the drying process:

a) during the material heating stage (segment OA), the temperature increases at its maximum rate;

b) during the isothermal heating stage throughout the cross-section (segment AB), the temperature rise slows down, allowing temperature equalization across different layers of the material's thickness;

c) in the final stage (segment BC), dry-bulb temperature changes, and intensive moisture removal occurs along with changes in the drying potential.

In the first two stages (heating and isothermal heating), the moisture loss per unit time (drying rate) remains constant. As long as the moisture supplied to the surface exceeds the amount that the surrounding medium can absorb, the surface moisture content remains constant, meaning the material's surface remains moisture-saturated. Consequently, the moisture removal rate stays unchanged. Throughout this period, the surface temperature of the material remains stable and equals the adiabatic saturation temperature of the air (i.e., the wet-bulb temperature). The central part of the material, in contrast, heats up more slowly compared to the surface and reaches the wet-bulb temperature somewhat later in the drying process.

During the isothermal heating stage, the surface temperature and the temperature at the material's core remain unchanged, meaning that the temperature gradient inside the material

is zero. At the same time, the temperature difference between the air and the material's surface remains constant. Under these conditions, with a constant heat transfer coefficient, the drying rate remains stable. This phase is referred to as the constant-rate drying period, characterized by an unchanging material temperature.

During this phase, moisture evaporates from the material's surface, as it is continuously supplied from the inner layers, keeping the surface moist. The material temperature closely approximates the wet-bulb temperature, and the drying rate reaches its maximum. This stage continues until the moisture content reaches a critical level, beyond which the surface temperature starts rising over time, and the drying rate begins to decline. The linear drying curve segment transitions into a curve that asymptotically approaches the equilibrium moisture content. The core temperature also rises, but its curve lags slightly behind the surface temperature curve. Consequently, a temperature gradient develops within the material, gradually diminishing until the equilibrium moisture content is reached, at which point the temperature gradient becomes zero. In this equilibrium state, moisture content no longer decreases, and the material temperature equals the air temperature.

The falling-rate drying period (segment BC for temperature increase, segment BD for drying rate decrease) is characterized by a gradual rise in material temperature and a decline in the drying rate.

Once all layers reach the same temperature, it becomes possible to lower the wet-bulb temperature by removing moisture-laden air from the drying chamber using an exhaust fan, increasing the dry-bulb temperature, and reducing steam humidification. This adjustment continues until the psychrometric difference (corresponding to a specific material moisture content) reaches a pre-defined value. The two-stage drying mode should be set according to material thickness, initial and final moisture content, and air velocity inside the chamber.

When temperature distribution is uniform, shrinkage does not induce critical stresses. However, shrinkage development is associated with the emergence of internal stresses. Preventing material cracking can be achieved by reducing tensile stresses through minimizing moisture gradients within the material's cross-section. This can be accomplished by softening the drying mode at the initial stage and applying thermal treatment in the middle and final stages.

In the two-stage drying process, during the constant-rate drying period, a high relative vapor pressure and a relatively low temperature are maintained. In the falling-rate drying period, the dry-bulb temperature increases to its maximum, while the relative vapor pressure decreases. The moisture content of the capillary-porous material at the transition from the first to the second stage should be equal to the fiber saturation point of the material.

For high-temperature drying modes, it is crucial to consider that the rate of moisture migration from the core to the surface is proportional to the moisture conductivity coefficient. The moisture conductivity coefficient increases with temperature, while the moisture content gradient increases as the relative humidity of the vapor decreases, due to the corresponding reduction in surface moisture. In high-speed, high-temperature hydrothermal treatment, controlling moisture gradients is critical for maintaining process rigidity, efficiency, and safety.

The rigidity of the drying regime is characterized by the magnitude of the psychrometric difference  $T_c - T_m$  and plays a critical role in high-temperature, high-speed drying. The rigidity must be adjusted continuously throughout the entire drying process when dealing with high initial moisture content and should be periodically regulated during low-temperature drying. The efficiency of the drying process is defined as the ratio of the normal drying time to the time spent in high-temperature mode. The safety of the process is determined by the ratio of the material's strength limit to the maximum stresses that develop under the given drying conditions.

One of the main obstacles to high-speed drying is cracking. The cause of cracks is the development of surface stress in the material, which exceeds the allowable limit. This stress state is created by unacceptable shrinkage, which occurs due to the uneven distribution of moisture content and temperature within the material. Cracking can be avoided by reducing tensile stresses through minimizing moisture gradients across the section. This can be achieved by softening the drying regime at the beginning and performing heat treatment in the middle and at the end of the process.

If to assume that local failure occurs in the elastic region under the action of normal tensile stresses, then in a plate of thickness  $2L$ , the moisture content gradient between the central and

surface layers, given by  $\frac{L}{3}(u_c - u_p)$ , where  $u_c$  is the moisture content at the central surface and

$u_p$  is the moisture content at the outer surface, can serve as a criterion for determining moisture content based on critical normal stresses.

However, in the work of Voronov, it is noted that the calculated stresses exceed experimental values by a factor of 5 to 10 [35]. The author attributes this discrepancy to the inapplicability of Hooke's law, as local failure occurs in an elastoplastic region. It is also indicated that the cause of crack formation is shear stress, and the failure conditions reduce to ensuring that the intensity of shear stresses at a given point in the specimen reaches critical values, whereas tensile stresses alone cannot be the cause of local rupture. In real materials, local ruptures occur due to defects, weak points, and pre-existing cracks.

The process of material failure consists of two stages: local failure and complete failure. Crack formation occurs in the elastoplastic region under the influence of plastic deformations, which arise before the appearance of cracks and, at the moment of their formation, account for 60–80 % of the total deformation, depending on the moisture content of the material. The values of fracture-inducing stresses and ultimate failure stresses depend on the loading rate, increasing with the intensity of stresses by a factor of 2 or more. At high moisture content, the ultimate shear stress and the crack-inducing stress are approximately the same. As the moisture content decreases, the ultimate failure stress increases more than the crack-inducing stress [5].

The optimal drying regimes for capillary-porous materials are influenced by the material's shrinkage due to moisture changes. The shrinkage process varies across different materials. For example, in cement stone, shrinkage increases only when the moisture content drops below 30 %. Some materials, such as clay, begin to shrink immediately upon moisture reduction. Let's consider

this effect in the case of wood. If the moisture content in a certain section falls below the hygroscopic limit, the fibers attempt to contract in size, but this is hindered by the fibers that still have a higher moisture content. As a result, internal stresses arise. The shrinking fibers, unable to contract, experience tensile stress, while adjacent fibers, influenced by the shrinking ones, are compressed.

As hygroscopic moisture is removed from the material, the shrinkage process gradually slows down. If a microscopic crack forms within the material, shrinkage may decelerate. If the internal cracking does not progress, shrinkage may resume at its previous rate and eventually stop after some time. This cessation occurs when the material reaches an average moisture content close to the equilibrium value corresponding to the given temperature and relative humidity of the drying agent. The shrinkage development law may follow various dependencies, such as an exponential decay. At the same time, it should be noted that wood is an anisotropic material, and shrinkage occurs below the fiber saturation point.

The dependence of the modulus of elasticity on moisture content is inversely proportional to moisture up to the fiber saturation point and can be approximated by straight lines with different slopes before and after this point. By maintaining the required surface moisture level, the desired values of permissible stresses can be ensured. The surface moisture is regulated by adjusting the moisture content of the drying agent.

According to [35], the moisture content distribution across the thickness of the material satisfies the expression  $\frac{u_c - u_y}{u_c - u_p} = \left(\frac{y}{L}\right)^n$ , where  $u_c, u_p, u_y$  are the moisture content values at

the center, on the surface, and at a distance  $y$  from the center, respectively, and  $n$  is an exponent characterizing the steepness of the relative moisture distribution across the thickness. At the beginning of the drying process,  $n \rightarrow \infty$ , while at the end,  $n \rightarrow 0$ . Shrinkage follows an exponential dependence on time  $\varepsilon = \varepsilon_k (1 - e^{-\tau/T})$ , where  $\varepsilon$  is the current shrinkage value,  $\varepsilon_k$  is the shrinkage at the end of the process, and  $T$  is the time constant.

At the beginning of the falling drying rate period, the moisture distribution across the thickness is parabolic ( $n = 2$ ).

For internal stresses in the layer at  $y$ , there is  $\sigma_y = \frac{A}{3} u_y (2u_c - u_p - 3u_y)$ . Further deepening of the evaporation zone is accounted for using a cosine-like distribution at  $n = 1.5$ :

$$\sigma_y = \frac{A}{2.5} u_y (1.5u_c - u_p - 2.5u_y).$$

At later stages, the distribution is assumed to follow a linear law ( $n = 1$ ):  $\sigma_y =$

$$= \frac{A}{2} u_y (u_c - u_p - 2u_y).$$

The coefficient  $A$  is determined by the material properties and the control system settings:

$$A = k \left[ \varepsilon_k \left( 1 - e^{-\tau/T} \right) + u_p \right].$$

Maintaining the desired surface moisture content ensures that the allowable stress limits are not exceeded. Thus, for a safe drying process, it is necessary to determine the optimal air velocity, relative humidity, drying agent temperature, and the timing of regulation phase transitions.

The change in moisture content with temperature variations inside the material over time depends on the interrelationship between internal moisture and heat transfer processes, as well as the heat and mass exchange at the material surface with the environment.

At low temperatures, thermodiffusion is minimal, and the resulting moisture flux coincides with the convective-diffusive vapor flux. During drying, moisture from the inner layers moves toward the surface, leading to a decrease in moisture not only at the surface but also in deeper regions. Evaporation occurs within the body at a specific zone or throughout the entire volume, depending on the pore size distribution density and the dispersion of pore sizes. In this case, moisture transport inside the material takes place in both liquid and vapor forms. The rate of moisture migration inside the material depends on the type of moisture binding.

Different approaches exist for optimizing the drying process. If the primary requirement is preventing cracks, the drying regime should be adjusted according to changes in the structural and mechanical properties of the material. If cracking occurs in the first drying period, the cracking criterion can be expressed as the relative moisture content gradient between the average moisture content  $\bar{u}$  and the local moisture content  $u$  with respect to the initial moisture content  $\bar{u}_0$ :

$$K = \frac{\bar{u} - u}{\bar{u}_0}.$$

If cracking occurs on the surface in the first drying period, then  $u = u_p$ . For a parabolic moisture distribution:  $K = \frac{2(u_c - u_p)}{3\bar{u}_0}$ , where  $u_c - u_p$  is the difference in moisture content between

the central and surface layers. The primary moisture transport criterion in the drying process is the Kirpichev criterion  $Ki'$ , defined as the ratio of the surface moisture gradient  $\nabla u_p$  to the initial moisture content  $\bar{u}_0$ , multiplied by the characteristic size of the material  $R$ . The obtained values of  $Ki'$  correspond to specific values of surface moisture content  $u_p$  and temperature  $t_p$ .

For the constant drying rate period with a parabolic moisture and temperature distribution, A. Lykov established that:

$$\frac{(u_c - u_p)}{\bar{u}_0} = \frac{1}{2} Ki' + \frac{t_p - t_c}{t_c} Pn,$$



where

$$Ki' = \frac{q'R}{a'\gamma_0\bar{u}_0} \text{ is the Kirpichev criterion for moisture transfer,}$$

and

$$Pn = \frac{\delta t_e}{u_0} \text{ is the Postnov criterion.}$$

Here,  $q'$  represents the evaporation rate,  $a'$  is the mass transfer potential conductivity coefficient  $a' = \frac{\lambda'}{c'\gamma_0}$ , where  $\gamma_0$  is the skeleton density,  $R$  is half of the material thickness for a plate, and  $\lambda'$ ,  $c'$  are the moisture conductivity and moisture capacity, respectively.

### Drying modes.

Under mild drying conditions, the temperature gradient in the first period is absent, and the relative moisture content gradient is directly proportional to the Kirpichev criterion. The criterion  $Ki'$  can be determined in various ways: by evaporation intensity  $q'$ , by the moisture content difference  $u_e - u_n$ , by the surface moisture gradient, or by the decrease in moisture content over time:

$$Ki' = \frac{q'R}{a'\gamma_0\bar{u}_0} = \frac{2(u_e - u_p)}{\bar{u}_0} = -\frac{R(\nabla u)_p}{\bar{u}_0} = \frac{(\bar{u}_0 - \bar{u})}{\bar{u}_0 Fo'},$$

where  $\bar{u}$  is the average moisture content corresponding to the Fourier criterion:

$$Fo' = \frac{a'\tau}{R^2}$$

in the constant drying rate period. The maximum allowable Kirpichev criterion depends on the material's moisture content; as the moisture content decreases, the criterion increases. This criterion is directly proportional to the drying intensity  $q'$  and inversely proportional to the potential conductivity coefficient  $a'$ . Other parameters included in the criterion are the dry material density  $\gamma_0$ , initial moisture content  $u_0$ , and characteristic size  $R$ .

At low drying intensities  $q'$ , it can be assumed to be equal to the evaporation rate of the liquid from a free surface. The evaporation rate is uniquely determined by the formula  $q' = Nu' \frac{\lambda'}{l} \Delta p_i$ ,

where  $\lambda'$  is the moisture conductivity coefficient. Heat and mass transfer coefficients under natural convection conditions are determined using Nesterov's formulas, which are provided later. Using these formulas, drying intensity is calculated at different air temperatures and humidity levels. During the constant drying rate period, the body temperature can be assumed equal to

the wet-bulb temperature. Thus, given the parameters  $T_s$  and  $\phi$ , the material's temperature and coefficient  $a'$  are uniquely determined.

With a graph of coefficient  $a'$  variations with temperature, a family of curves  $Ki' = f(T_s)$  can be constructed for different values of  $\phi$  at a constant air velocity and characteristic body size. If the maximum allowable Kirpichev criterion is known, and the dependence of  $Ki'$  on different moisture contents is plotted, an entire region of permissible drying modes is obtained, from which the mode with the highest drying intensity is selected. The drying apparatus should have minimal heat and electricity consumption. As the moisture content decreases, the maximum permissible criterion  $Ki'_{\max}$  increases, and the range of allowable drying regimes expands. Therefore, optimal drying regimes should be stepwise, with drying intensity increasing as drying progresses.

Increasing air velocity reduces the range of permissible process parameters  $T_s$  and  $\phi$  (the family of curves  $Ki' = f(T_s)$  shifts upward), so at the beginning of the drying process, air velocities should be low. The air velocity is chosen based on a joint analysis of the allowable drying regime area with the calculated energy consumption, temperature, and humidity gradients for selected regimes in the given drying chamber.

At high air humidity levels (low drying intensity), heat transfer coefficients are close to those of heat exchange without mass transfer. The greater the sample length along the airflow direction, the lower the drying intensity.

During gentle drying modes, in the constant-rate period, the partial pressure of vapor near the surface of the material equals the saturated vapor pressure at the wet-bulb temperature. This value remains constant, even though the moisture content at the surface of the material gradually decreases to the maximum hygroscopic moisture content. The decrease in moisture content follows a complex curve that asymptotically approaches the equilibrium moisture level. At this stage, the material temperature is equal to the wet-bulb temperature.

In intensive drying modes, the heat and mass transfer patterns change. The temperature at any given point in the material, starting from the surface, gradually increases, while the decrease in moisture content at any point follows a linear law. This means that the drying rate remains constant, while the temperature increases, including at the surface layer. A temperature gradient is observed. The temperature near the surface of the material initially equals the wet-bulb temperature, but then continuously rises. By the end of the process, the air temperature and the material temperature equalize. Near the surface, the temperature distribution follows a linear law, which then transitions into a curve, asymptotically approaching the ambient temperature.

At the very surface, heat transfer occurs via molecular mechanisms (vapor diffusion in an inert gas). As the distance from the surface increases, molecular heat transfer transitions into molar (convective) transfer, which gradually intensifies. The thickness of the conditional boundary layer remains constant in the first period of drying but then increases approximately according to a linear law.

In the temperature range of 0–150 °C, when heating a product (e.g., bricks), hygroscopic moisture is removed, accompanied by a significant release of water vapor. The vapor pressure

inside the product reaches high values even at 70 °C, increasing progressively as the temperature rises. If the rate of vapor generation inside the material exceeds the rate of vapor filtration through its thickness, the resulting internal pressure may lead to cracks and delamination. Furthermore, the surface of the material, having dried rapidly, continues to heat up significantly. Inside the material, the temperature quickly rises to 100 °C and remains at this level until complete moisture removal, creating significant temperature differences between the surface and the inner part of the product, leading to high stresses and crack formation.

Experiments show that if the final drying phase is carried out by increasing the gas flow rate with a moderate increase in temperature (50–80 °C per hour), the process occurs with high intensity, minimal temperature gradients across the material's thickness, and no damage to product quality. The temperature range of the drying process is critical: if it is narrow, a slow temperature rise and prolonged holding time are preferable. Holding the material at the maximum temperature ensures uniform temperature distribution throughout its thickness.

#### **Cooling of the product after maximum temperature holding.**

The cooling phase after holding the product at maximum temperature is just as critical in the drying process as the heating phase. In the initial stage of cooling, as the temperature decreases, materials undergo shrinkage and plastic deformations under minimal loads. During this phase, material cracking may occur. In each temperature range, the cooling intensity should be adjusted accordingly.

Let's consider, as an example, the intensification of chamber drying of lumber. The drying process is conducted under atmospheric pressure.

Evaporation occurs at any given temperature, but the higher the temperature, the more intense the evaporation. During evaporation, the molecules of liquid near the surface have higher velocity than others, and overcoming molecular cohesion forces, they escape into the surrounding environment. The process of evaporation is explained by the fact that the surface layer is heated slightly above the readings of the wet-bulb thermometer of a psychrometer placed in the surrounding environment. As a result, the vapor pressure of the liquid on the surface is higher than that in the drying agent. Boiling, on the other hand, occurs only at the saturation temperature. The vapor formed from boiling water is called wet saturated vapor. During boiling, the amount of water decreases until the last drop turns into vapor. Once the droplets have evaporated, the vapor becomes dry saturated. If the temperature of the dry saturated vapor increases without changing the pressure, it is referred to as superheated vapor.

Removing heat from superheated vapor leads to a decrease in its temperature and specific volume. Condensation of vapor occurs only when its temperature drops below the saturation temperature. These properties of vapor are widely used in drying technology.

Superheated steam, while expending part of its heat, can heat the material and evaporate moisture from it. As moisture evaporates from the material, the amount of vapor increases. To prevent a drop in pressure at the lower part of the chamber, a vapor outlet to the atmosphere or a heat exchanger must be installed. The saturation temperature of vapor depends only on pressure. Each specific vapor pressure corresponds to a saturation temperature. Knowing the water

vapor pressure, it is easy to determine the temperature and vice versa. When saturated vapor is cooled, it condenses into water. During condensation, the saturated vapor releases all of its latent heat of vaporization. This heat is used in dryers for heating heat exchangers. The heat exchangers then transfer this energy to the drying agent, which, through convection, heats the material and facilitates moisture evaporation.

### **Methods of lumber drying using superheated steam.**

Lumber drying using superheated steam can be achieved through the following methods:

1. Direct superheated steam supply: superheated steam from a boiler is introduced into a sealed drying chamber, where it is forcibly circulated through the stack of lumber. The used superheated steam, after mixing with the vaporized moisture from the wood, is expelled from the chamber. Closed-cycle drying with a vapor outlet pipe: A hermetically sealed chamber with a vapor outlet pipe is created. Inside the chamber, a heat exchanger with high thermal power and devices for circulating the drying agent are installed.

At the initial stage of drying, saturated steam is introduced into the chamber, which heats the wood and displaces air from the chamber. Simultaneously, the steam is circulated by fans through heat exchangers, where it becomes superheated. Once the introduced steam in the chamber turns superheated, it starts evaporating moisture from the wood, mixing with the vapor from the extracted moisture.

At this point, the steam supply to the chamber is stopped, as sufficient steam is generated from the moisture evaporated from the wood. The steam mixture is circulated by a fan through heat exchangers, increasing its degree of superheating, then passing through the lumber stack, and so on. Excess steam is removed through a vapor outlet pipe or directed to heat exchange systems.

2. The second method is more efficient than the first one because in hermetic chambers with vapor outlet pipes, heat losses associated with the intake of superheated steam from the boiler and its release into the atmosphere are eliminated.

At the beginning of the drying process, when the material has not yet heated up, the surface layers of the material, which are in contact with the hot chamber environment, have a higher temperature than the core. This creates a temperature gradient, which causes moisture movement toward lower temperatures, i.e., from the surface to the center. This phenomenon is known as thermo-hydroconductivity.

If wood is dried in an environment where the temperature exceeds 100 °C, an excess vapor-air mixture pressure may develop and persist inside the material for an extended period (compared to atmospheric pressure). This pressure induces a steady movement of water vapor (along with liquid water) from the center to the surface of the material, a process known as molar moisture transfer.

During drying, all driving forces act simultaneously, and their effects combine.

Drying concludes with the removal of moisture from the surface into the surrounding environment. The intensity of moisture removal depends on the difference in partial vapor pressures in the air layer above the wood surface and in the surrounding air, as well as on the velocity of the air

flowing around the wood. The greater the difference in partial pressures and the air velocity, the more intense the moisture evaporation from the material's surface.

The heat and mass transfer criteria are expressed through the Nusselt criteria:

$$Nu = \frac{\alpha l}{\lambda_g} = \frac{ql}{\lambda_g \Delta t}; \quad Nu' = \frac{\alpha' l}{\lambda'_g} = \frac{q' l}{\lambda'_g \Delta p}, \quad (5.1)$$

where  $l$  is the characteristic linear dimension.

If the complex transfer mechanism is replaced by an equivalent molecular transfer, a conditional boundary layer of thickness  $\delta$  is obtained. From experimental curves, the heat and mass transfer coefficients, as well as the Nusselt numbers, are determined using the following formulas:

$$\alpha = \frac{\lambda}{\delta_t}, \quad \alpha' = \frac{\lambda'}{\delta_p}, \quad Nu = \frac{l}{\delta_t}, \quad Nu' = \frac{l}{\delta_p}. \quad (5.2)$$

By extending the moisture distribution lines of the air to the horizontal axis, the conditional depth of the evaporation surface  $\xi$  can be determined [5].

In the *first drying period*, the drying intensity remains constant despite the continuous deepening of the evaporation surface. This phenomenon is explained by the increase in the mass transfer coefficient  $\lambda'$  due to the displacement of the diffusion transfer mechanism of vapor in the boundary layer by the effusion mechanism in the surface layer of the material (evaporation zone).

The drying intensity in the first period is given by  $q' = \frac{\lambda'_\phi}{\delta_\phi + \xi} (\phi - \phi_c)$ .

In the first approximation,  $\delta_\phi$  is constant and greater than  $\xi$ . The increase in the denominator due to the growth of  $\xi$  is compensated by an increase in  $\lambda'$ , thus maintaining a constant density of the drying flux. In the second drying period,  $\delta_\phi$  increases, leading to a reduction in drying intensity [36–40].

In the transition region from mild to intensive drying modes, the rate of evaporation front penetration remains constant during the first period, and evaporation occurs at a certain fixed depth, while the temperature distribution curves at different moments of the first period coincide with each other. The same applies to the humidity distribution curves of the air. In mild drying modes, during the first period, the evaporation front is close to the surface of the material. The Nusselt criteria, which characterize external heat and mass transfer, are inversely proportional to the thickness of the conditional boundary layer; therefore, they remain constant during the constant drying rate period and decrease over time during the falling drying rate period.

In intensive drying modes, the heat flux density can be determined as  $q = r_k q' + \bar{c} \gamma_0 \frac{V}{F} \frac{d\bar{T}}{d\tau}$ ,

where  $\frac{V}{F}$  is the volume-to-surface ratio of the material, and  $r_k$  is the specific heat of evaporation.

Due to auxiliary expenditures when calculating heat flux density, the Nusselt criterion is determined by the conditional boundary layer thickness. Experimental studies have shown that in the first period, the Nusselt number remains constant, while in the second period, it decreases with decreasing

moisture content. P. Lebedev obtained the empirical relationship  $\frac{Nu}{Nu_n} = \left( \frac{u}{u_{kr}} \right)^n$ , where  $u_{kr}$  is the critical moisture content, and  $Nu_n$  is the Nusselt number in the constant drying rate period, given

by  $Nu_n = A \left( \frac{T_c}{T_m} \right)^2 \left( \frac{T_u}{T_c} \right)^{0.4} Re^{0.5}$ . For wood,  $A = 0.5$ ,  $n = 0.3$ . Similar relationships hold for mass transfer:  $\frac{Nu'}{Nu'_n} = \left( \frac{u}{u_{kr}} \right)^{n'}$ , where the exponent  $n'$  is close to  $n$ . Thus, changes in heat and mass

transfer follow the same pattern.

Calculating the Nusselt number  $Nu'$  using formulas (5.1) and the conditional boundary layer thickness shows that the Nusselt number  $Nu'$  calculated using formulas (5.1) in the first period is significantly higher than  $Nu'$  calculated based on the boundary layer thickness. The difference between them decreases as the moisture content decreases [5].

This difference is greater at higher drying intensities. This is explained by the vapor transfer mechanism through the evaporation zone. During evaporation, the evaporation front penetrates deeper into the material. Transfer within the evaporation zone occurs not only through diffusion but also effusion (molecular flow) if the capillary radius of the material is smaller than  $10^{-5}$  cm and the pressure equals atmospheric pressure.

A distinguishing feature of molecular flow is the movement of gas from less heated regions of the capillary to more heated ones under the same pressure  $p$ . During drying, the surface of the material has a higher temperature compared to the evaporation zone surface. Thus, this temperature

gradient accelerates molecular flow, as the driving potential of effusion flow is  $\frac{p}{\sqrt{T}}$ . In the case

of diffusion transfer, the presence of a temperature gradient in the evaporation zone reduces transfer speed. If the material contains capillaries with radii greater than  $10^{-5}$  cm, then a combined diffusion-effusion transport mechanism takes place.

In the presence of macroscopic capillaries, diffusion vapor transfer is complicated by thermal creep, which works as follows: if a temperature gradient exists along the walls of a macroscopic capillary, then circulation currents of moist gas arise. Gas near the capillary wall moves against the heat flow, while along the capillary axis, it moves with the heat flow. Since the capillaries near the evaporation surface have a lower temperature compared to the capillaries in the surface layer of the material, thermal creep facilitates vapor transfer through the evaporation zone.

From the surface of the material to the surrounding environment, vapor transfer occurs primarily by molar transport. The mass conductivity coefficient  $\lambda'$  in the evaporation zone – boundary layer near the material surface underline{is significantly greater than the molecular mass conductivity coefficient}. Therefore, the Nusselt numbers calculated using standard formulas are overestimated compared to those determined by the boundary layer thickness, which provides more accurate results. This new mass transfer mechanism affects both heat transfer and the hydrodynamics of heat exchange. The increase in the Nusselt number during the drying process is explained as follows:

– as the evaporation front penetrates deeper, vapor passes through this zone via a diffusion-effusion mechanism, complicated by thermal creep and the presence of a general pressure gradient. Upon exiting the surface layer of the material, the overall pressure gradient immediately relaxes, acting as a turbulence-inducing factor for the laminar flow of the surface layer of the vapor-gas mixture. As a result, heat exchange intensifies, leading to an increase in  $Nu$ . As moisture is removed, drying intensity decreases, and the heat transfer coefficient decreases, approaching the coefficient of pure heat transfer. The relationship between the criteria  $Ki'$  and  $Nu'$  is

given by  $Ki' = Nu' \cdot \frac{R}{l} \cdot \frac{\lambda_g}{\alpha \lambda_0 \bar{u}_0} (p_{nm} - p_e)$ . The criterion  $Ki'$  is an analogue of the Biot criterion

$Bi = \frac{\alpha}{\lambda} R = Nu \frac{R}{l} \frac{\lambda_g}{\lambda}$  for heat transfer, where  $\lambda$  is the thermal conductivity coefficient of the

material, and  $R$  is the characteristic size of the material (for an infinite plate – half its thickness) or

the hydraulic radius  $R_v = \frac{V}{S}$ , which is the volume-to-surface ratio of the material.

Regulation of temperature and humidity in drying chambers is carried out by adjusting the temperature according to the dry-bulb  $T_c$  and wet-bulb  $T_m$  thermometers of the drying agent. The dry-bulb temperature takes different values at different stages of the drying process. During the heating stage of the material, the temperature changes at the maximum rate. In the stage of isothermal heating throughout the cross-section, the temperature increases slightly. Temperature equalization of individual layers across the material thickness occurs. At the final stage, changes in the dry-bulb temperature lead to intensive moisture removal and a shift in drying potential.

Evaporation of moisture from the wet-bulb thermometer surface occurs more intensively when the humidity of the drying agent is lower. Measuring humidity based on different readings of the dry and wet thermometers is reliable under the condition of hydrodynamic equilibrium, i.e., when  $S\alpha(T_c - \tilde{T}_m) = CS(P_m - P_v)r$ , where  $S$  is the evaporation surface of the wet-bulb thermometer,  $\alpha$  is the heat transfer coefficient,  $C$  is the evaporation intensity coefficient of moisture from the wet-bulb thermometer surface,  $P = 475$  mmHg is the total barometric pressure,  $P_v$  is the vapor pressure in the air, and  $r = 595$  cal/kg is the latent heat of evaporation. From this relationship:

$P_v = P_m - A(T_c - \tilde{T}_m)$ , where  $A = \frac{\alpha}{Gr}$ . By determining the partial pressure of vapor, the relative humidity of the drying agent can be found:  $\phi = \frac{P_v}{P_m}$ .

The coefficient  $A$  is determined by the empirical formula:

$$A = 0.00001 \left( 65 + \frac{6.75}{v} \right),$$

where  $v$  is the velocity of the vapor-air mixture in the chamber. Thus, the readings of the dry and wet thermometers determine the humidity and temperature of the drying agent, and information about its state is a necessary condition for high-quality drying. For the heating period, it is assumed that the wet-bulb temperature uniquely determines the humidity of the drying agent and, at constant  $T_c$ , does not depend on its temperature.

### Drying with heated gas.

In many cases, drying of wet materials is carried out using heated gas. The drying process also takes place in drying chambers. In these devices, the drying mode changes over time. The drying mode is characterized by three parameters: the gas temperature  $t_c$ , humidity  $\phi$ , and gas velocity  $v$ . These parameters affect both the drying time and the quality of the material. Therefore, it is necessary to find such a mode that, with minimal drying time and the lowest heat consumption, provides the best technological properties of the material. To understand the impact of the drying mode on duration, it is necessary to obtain drying kinetics curves depending on the parameters characterizing the mode. From practice, it is known that increasing the drying agent temperature increases the drying intensity and critical moisture content. Increasing the temperature from 15 to 45 degrees results in a 2.5-fold increase in drying intensity in the first period. Increasing air humidity sharply reduces drying intensity and critical moisture content. For example, increasing air humidity from 0.177 to 0.758 decreases the intensity by approximately 4.5 times. Increasing air velocity increases intensity in the first period and has significantly less effect at the end of the process. The ratio between capillary moisture and adsorptively bound moisture significantly affects drying intensity in the second period and the critical moisture content, while it has little effect on intensity in the first period [5]. As the amount of capillary water increases, the critical moisture content decreases. Therefore, the greater the amount of bound water, the higher the critical moisture content. The critical moisture content characterizes the end of the period with a constant drying rate, after which the drying intensity decreases.

At high gas temperatures, in the first period, the drying rate is constant, and the surface temperature of the material continuously increases and significantly exceeds the wet-bulb temperature. The drying intensity equals the mass transfer intensity:

$$q = \alpha(t_c - t_{p,m}) = Nu \frac{\lambda_g}{l} \Delta t,$$



$$q' = \alpha' (p_{p,m} - p_c) = Nu' \frac{\lambda'_g}{l} \Delta p,$$

where  $q$  and  $q'$  are the heat and mass flux densities, respectively,  $\Delta t = (t_c - t_{p,m})$  is the temperature difference between the gas and the body surface,  $\Delta p = (p_{p,m} - p_c)$  is the partial pressure difference of vapor at the body surface and in the surrounding environment.

In the humidity range of 50–70 %, the following formulas are proposed for water evaporation from a free surface:

$$Nu = 0,46Re^{0,53}, \quad Nu' = 0,63Re^{0,52} \quad \text{at } 3 \cdot 10^3 < Re < 3 \cdot 10^4.$$

The Reynolds number is defined as:

$$Re = \frac{vl}{\nu}.$$

Through the analysis of multiple heat and mass transfer experiments under forced convection of moist gas, the following relationships were established:

$$Nu = 2 + A \cdot Pr^{0,33} \cdot Re^n \cdot Gu^m,$$

where constants are provided in **Table 5.1**.

● **Table 5.1** Constants for relationships heat and mass transfer

<i>Re</i>	<i>A</i>	<i>n</i>	<i>m</i>	<i>A'</i>	<i>n'</i>	<i>m'</i>
1–2·10 <sup>2</sup>	1.07	0.48	0.175	0.83	0.53	0.135
3.15·10 <sup>3</sup> –2.2·10 <sup>4</sup>	0.51	0.61	0.175	0.49	0.61	0.135
2.2·10 <sup>4</sup> –3.15·10 <sup>5</sup>	0.027	0.90	0.175	0.0248	0.90	0.135

For  $Re > 200$ , the term 2 is omitted, and the formula simplifies to:

$$Nu = A \cdot Pr^{0,33} \cdot Re^n \cdot Gu^m, \left( Pr = \frac{\nu}{a} = \frac{\mu}{a\gamma} \right).$$

Similarly, for mass transfer:

$$Nu' = 2 + A' \cdot (Pr')^{0,33} \cdot Re^{n'} \cdot Gu^{m'}, \left( Pr' = \frac{\nu}{D} \right).$$

Here  $\nu$  is the viscosity coefficient, and  $D$  is the diffusion coefficient. For an ideal gas,  $Pr = Pr' = 1$ , for dry air  $Pr = 0.73$ , and for vapor transport in an inert gas  $Pr' = 0.75$ .

Under conditions of natural convection:

$$Nu = 4(Pr \cdot Ar)^{0.108}, \text{ for } (Pr \cdot Ar) = 3 \cdot 10^6 - 2 \cdot 10^8,$$

$$Nu' = 4(Pr' \cdot Ar)^{0.248}, \text{ for } (Pr' \cdot Ar) = 1 \cdot 10^4 - 3 \cdot 10^8.$$

When calculating these criteria, the characteristic size is taken as the side of a square equivalent to the liquid surface area  $Ar = \frac{l^3 g \Delta \gamma}{\nu^2 \gamma_p}$ .

Here,  $l$  is the length of the surface in the direction of the flow,  $g$  is the acceleration due to gravity ( $m/s^2$ ), and  $\Delta \gamma = \gamma_p - \gamma_c$  is the difference in density between the moist gas at the liquid surface and the bulk gas flow. In heat transfer, this density difference is replaced by the temperature difference and is known as the Grashof number criterion.

In all these equations, the thermal conductivity of the humid gas is calculated using  $\lambda = \lambda_0 + 0.0041\phi$ , where  $\lambda_0$  is the thermal conductivity of the dry gas. The mass transfer coefficient (diffusion coefficient relative to partial pressure differences) is calculated as

$$\lambda' = a'_0 \frac{M_v T}{R T_0^2} \left( \frac{P_0}{p_b} \right), \text{ where } a'_0 \text{ is the diffusion coefficient under normal conditions. For water vapor,}$$

$a'_0 = 0.079 \text{ m}^2/\text{h}$ ,  $M_v = 0.018 \text{ kg/mol}$  is the molecular weight of vapor,  $P_0 = 760 \text{ mmHg}$  is the total barometric pressure, and  $T_0 = 273.2 \text{ K}$  is the absolute temperature under normal conditions. The universal gas constant is  $R = 0.06237 \text{ m}^3 \text{ mmHg/K mol}$ , and the average absolute boundary layer temperature is  $T = 273 + \frac{1}{2}(t_c + t_p)$ , where  $p_b$  is the partial pressure of dry vapor in mmHg.

### Wood drying process.

Initially, drying proceeds rapidly and slows down towards the end. The first stage involves heating the wood in the chamber. The moisture in the wood does not decrease; instead, it slightly increases due to condensation of atmospheric moisture on the cold wood surface.

The second stage involves drying from high initial moisture content  $w_0$  to the critical moisture content  $w_{cr}$ , which is slightly higher than the hygroscopic boundary (which is 30 %). During this stage, free moisture is removed from the wood, making this phase the most intense.

The third stage involves drying from critical moisture to the desired final moisture content. Here, bound moisture is removed, and the process is slower than in the second stage.

### Stresses developing in wood.

During drying, moisture is initially removed from the surface, leading to an uneven distribution of moisture throughout the volume. When the moisture content falls below the hygroscopic limit, shrinkage begins. (The property of wood to reduce its linear dimensions and volume when bound

water is removed (at a moisture content below 30 %) is called shrinkage.) This leads to the formation of tensile moisture stresses in the surface layers, which can result in external cracks. To prevent this, drying should be slowed down by creating a highly saturated steam environment in the chamber (this is known as moisture-heat treatment).

As the moisture gradient across the thickness decreases, the stresses also decrease. When the moisture content of the inner layers of the wood falls below the hygroscopic limit, the inner part begins to shrink, while the outer, being dry and in tension, resists the shrinkage of the inner layer. This leads to the development of tensile stresses in the inner layer. If these tensile stresses continue to develop, internal cracks will form. Internal stresses can be reduced through thermal-humidity treatment of the wood.

### **Low-temperature and high-temperature drying processes.**

Depending on the temperature level, the drying process can be classified as low-temperature or high-temperature.

Low-temperature drying occurs when the wood temperature remains below the boiling point of water at the given pressure ( $< 100\text{ }^{\circ}\text{C}$ ).

High-temperature drying occurs when the temperature in the central zones exceeds  $100\text{ }^{\circ}\text{C}$ . In this case, vaporization characteristics differ at different temperature levels.

For the high-temperature process, it is necessary not only for the surrounding medium to exceed  $100\text{ }^{\circ}\text{C}$  but also for the material itself to reach this temperature while still containing free water capable of boiling. An example of such a process is the drying of wood with an initial moisture content higher than the hygroscopic limit in a superheated steam environment under atmospheric pressure. A key feature of high-temperature drying is the intense transfer of moisture in the form of steam from the central zones to the peripheral ones. There is also an intermediate transition process between high- and low-temperature drying.

Drying chamber air circulation and types of chambers.

The circulation of the drying agent can be natural or forced, one-way or reversible. It is achieved using fans inside the chamber or through ejector nozzles, in which case the chambers are called ejection chambers.

Drying chambers are classified based on the drying agent:

- air chambers (where drying is done with heated air);
- superheated gas chambers;
- gas chambers, where the drying agents are combustion gases or natural gases mixed with humid air.

Based on operational principles, drying chambers can be:

- batch (periodic) operation: the material is loaded into the chamber in a full batch. If the chamber operates cyclically, the process consists of loading, drying, and unloading;
- continuous operation: the drying process does not stop for loading and unloading. The material moves continuously from the loading end to the unloading end of the chamber. With each unloading cycle, the stacks of material shift forward by the length of one stack [3].

## CONCLUSIONS

To calculate the optimal drying regime, which is determined by technological changes during the drying process, it is crucial to study the laws of moisture transfer to effectively control it. One possible way to manage the moisture transfer mechanism is by influencing the processes of diffusion and thermodiffusion.

When drying with heated air, the total moisture flux equals the difference in moisture gradients, which are determined by the gradients of moisture content and temperature  $q_m =$

$$= a_m \left| \frac{\Delta u}{\Delta x} \right| - a_m \delta \left| \frac{\Delta t}{\Delta x} \right|.$$

Under the influence of a temperature gradient, moisture moves inside the

material. The moisture flux directed toward the material surface decreases due to the thermodiffusion-induced moisture flux. The temperature gradient acts as a barrier to the movement of liquid from the central layers to the surface. At a constant drying intensity, conditions are created that facilitate the evaporation of liquid within the material. Thermodiffusion reduces the moisture gradient, slows down the movement of liquid moisture, and decreases the amount of water-soluble substances on the material surface. Changes in the magnitude and direction of the temperature gradient alter the conditions for moisture movement and the transfer of dissolved substances, leading to changes in the physicochemical properties of the material.

In the case of drying with heated air, the temperature gradient in the material leads to a significant moisture content gradient, generating high stresses that can cause cracking. By accelerating heating and cooling from the surface, it is possible to achieve values of the Postnov criterion

$$Pn = \frac{\delta \Delta t}{\Delta u},$$

where  $\delta$  is the thermogradient coefficient,  $\Delta t$  is the temperature difference, and

$\Delta u$  is the moisture content difference, at which the moisture content distribution will be close to uniform.

Under these conditions, moisture and temperature stresses in the material do not develop, allowing for fast drying without cracks.

The method of heat transfer to the material affects the substance and heat transfer mechanisms during thermal processing. In the steam-thermal method, saturated steam is used as the heat carrier. Heat is transferred to the material via convection from the steam-air environment. This creates a significant temperature gradient in the material, resulting in internal stresses. Since the material temperature is lower than that of the steam-air environment, a condensate film forms on the surface. According to the law of moisture-thermal conductivity, moisture migrates from the surface layers to the central ones, leading to moisture absorption by the material. Over time, developed reaction hydration contributes to the material's temperature exceeding that of the surrounding medium. Consequently, intense moisture evaporation occurs with a significant moisture content gradient, forming directed porosity within the material.

An important heat transfer method involves the interaction of an alternating magnetic field with ferromagnetic elements. The wet material, along with ferromagnetic heat-generating elements, is placed in an electromagnetic coil field powered by industrial-frequency current. The ferromagnetic materials heat up and transfer heat to the wet material. Depending on the material properties, the heat transfer method is selected, and it can be adjusted based on the technological scheme for placing ferromagnetic elements (in volume, in a layer, stack, or mass). This method prevents high stresses and deformations in the material, ensuring drying without warping or internal cracks.

During thermal treatment in an electromagnetic field, heat is conducted to the material from the formwork and reinforcement. This creates a minimal temperature gradient in the material. In this case, the surface temperature is higher than that of the environment, and evaporation occurs with a slight moisture content gradient. Such a thermal treatment method increases the number of closed pores compared to steaming, improving material quality. Using the principles of diffusion and thermodiffusion, the substance transfer mechanism can be controlled. Since diffusion is determined by the diffusion coefficient and thermodiffusion by the thermodiffusion coefficient, establishing the dependence of these coefficients on moisture content and temperature is crucial for regulating the transfer coefficient.

## REFERENCES

1. Nigmatulin, R. I. (1978). *Osnovy mekhaniki geterogennykh sred*. Moscow: Nauka, 336.
2. Gamaiunov, S. N., Misnikov, O. S. (1988). Usadochnye iavleniia pri sushke prirodnkh organomineralnykh dispersii. *Inzhenerno-fizicheskii zhurnal*, 71 (2), 233–236.
3. Mushtaev, V. I.; Planovskii, A. N. (Ed.) (1971). *Osnovnye teoreticheskie polozheniia konvektivnoi sushki i utochnennyi metod rascheta sushilnykh apparatov*. Moscow: MIKhM, 81.
4. Mushtaev, V. I., Ulianov, V. M. (1988). *Sushka dispersnykh materialov*. Moscow: Khimiia, 352.
5. Likov, A. V. (1968). *Teoriia sushki*. Moscow: Energiia, 472.
6. Sazhin, B. S. (1984). *Osnovy tekhniki sushki*. Moscow: Khimiia, 320.
7. Laitfud, U. (1977). *Iavleniia perenosa v zhivykh sistemakh*. Moscow: Mir, 210.
8. Tutova, E. G., Grinchik, N. N. (1984). Mekhanizm massoperenosa pri obezvozhivanii slozhnykh biologicheskikh sistem. *Teplomassoobmen* – 6. Vol. 7. Minsk: ITMO AN BSSR, 25–28.
9. Grinchik, N. N. (1991). Protsessy perenosa v poristyykh sredakh, elektrolitakh i membranakh. Minsk: ITMO im. A. V. Likova AN BSSR, 251.
10. Lutcik, L. P., Litevchuk, D. P. (1984). Vliianie porovoi struktury na pronitcaemost kapillarno-poristyykh tel. *Teplomassoobmen* – 6. Vol. 7. Minsk: ITMO AN BSSR, 74–77.
11. Likov, A. V. (1970). Metody resheniia nelineinykh uravnenii nestatsionarnoi teploprovodnosti. *Izv. AN SSSR, Energetika i transport*, 25, 109.
12. Zhuravleva, V. P. (1972). Masso-teploperenos pri termoobrabotke i sushke kapillarno-poristyykh stroitelnykh materialov. Minsk, 189.

13. Zhuravleva, V. P. (1971). Issledovanie protcessa obrazovaniia dispersnykh struktur. Minsk, 5, 35–40.
14. Kutc, P. S., Grinchik, N. N. (1984). Teplo- i massoperenos v kapilliarno-poristyykh telakh pri intensivnom paroobrazovanii s uchedom dvizheniia fronta ispareniiia. Teplomassoobmen – 6. Vol. 7. Minsk: ITMO AN BSSR, 93–96.
15. Lutcik, P. P. (1985). Uravneniia teorii sushki deformiruemykh tverdykh tel. Promyshlennaia teplotekhnika, 7 (6), 20.
16. Lutcik, P. P. (1984). Massotermicheskoe deformirovanie kapilliarno-poristyykh kolloidnykh tel v protsessakh sushki. Teplomassoobmen – VII. Vol. 6. Minsk: ITMO AN BSSR, 90.
17. Haivas, B. I. (2010). Pro opys lokalnogo stanu kapiliarno-poristyykh ta shchilno upakovanykh zernistyykh materialiv v protsesi sushinnia. Chastyna I. Modeliuvannia ta informatsiini tekhnologii. Kyiv: Instytut problem modeliuvannia v enerhetytsi im. H.Ie. Pukhova NAN Ukrainy, 57, 95–104.
18. Haivas, B. I. (2010). Kliuchova systema rivnian dla doslidzhennia protsesu sushinnia poristyykh til. Chastyna 2. Modeliuvannia ta informatsiini tekhnologii. Kyiv: Instytut problem modeliuvannia v enerhetytsi im. H. Ye. Pukhova NAN Ukrainy, 58, 116–125.
19. Haivas, B. (2010). Matematychnie modeliuvannia konvektyvnoho sushinnia materialiv z urakhuvanniam mekhanotermodyfuziinykh protsesiv. Fyzyko-matematychnie modeliuvannia ta informatsiini tekhnologii. Lviv: TsMM IPPMM im. Ya.S. Pidstryhacha NAN Ukrainy, 12, 9–37.
20. Hayvas, B., Torsky, A., Chapla, Y. (2012). On an approach to solution of problems of porous bodies drying. Fyzyko-matematychnie modeliuvannia ta informatsiini tekhnologii. Lviv: TsMM IPPMM im. Ya.S. Pidstryhacha NAN Ukrainy, 16, 42–51.
21. Haivas, B., Boretska, I. (2011). Vplyv rezhymu sushylnoho ahenta na osushennia poristyykh til. Kompiuterni tekhnologii drukarstva, 26, 231–240.
22. Romankov, P. G., Rashkovskaia, N. B. (1968). Sushka vo vzveshenom sostoianii. Lviv: Khimiiia, 360.
23. Teplitckii, Iu. S. (2002). Diagramma fazovogo sostoianiiia dispersnoi sistemy s voskhodiashchim potokom gaza. Inzhenerno-fizicheskii zhurnal, 75 (1), 117–121.
24. Kalenderian, V. A., Karnaraki, V. V. (1982). Teploobmen i sushka v dvizhushchemsia plotnom sloe. Kyiv: Vishcha shkola, 160.
25. Buevich, Iu. A., Bugkov, V. V. (1978). O sluchainykh pulsatsciakh v grubodispersnom psevdoozhizhenom sloe. Inzhenerno-fizicheskii zhurnal, 35 (6), 1089–1097.
26. Buevich, Iu. A., Korolev, V. N. (1991). Obtekanie tel i vneshnii teploobmen v psevdoozhizhenom sloe. Sverdlovsk: Izd. Uralskogo universiteta, 188.
27. Nagornov, S. A. (2002). Upravlenie protcessami perenosu teploty v neodnorodnykh psevdoozhizhenykh i vibrotcirkuliatcionnykh sredakh. Tambov: GNU VIITKN, 101.
28. Razumov, I. M. (1972). Psevdoozhizhenie i pnevmotransport sypuchikh materialov. Moscow: Khimiiia, 240.

29. Antonishin, N. V., Geller, L. A., Ivaniutenko, I. I. (1982). Teploperedacha v psevdoturulentnom sloe dispersnogo materiala. *Inzhenerno-fizicheskii zhurnal*, 43 (3), 360–364.
30. Kheifets, L. I., Neimark, F. M. (1982). *Mnogofaznye protsessy v poristyykh sredakh*. Moscow: Khimiia, 320.
31. Akulich, P. V., Milittcer, K. U. (1998). Modelirovanie neizotermicheskogo vlagoperenosa i napriazhenii v drevesine pri sushke. *Inzhenerno-fizicheskii zhurnal*, 71 (3), 404–411.
32. Shubin, G.S. (1985). *Sushka i teplovaia obrabotka drevesiny*. [Extended abstract of Doctoral thesis].
33. Shimanskii, V. M. (2015). *Matematichne modeliuвання neizotermichnogo vologoperenesenia ta v'iazkopruzhnogo deformuvannya u seredovishchakh z fraktalnoiui strukturoiu*. [Extended abstract of PhD thesis].
34. Sokolovskii, Ia. I., Shimanskii, V. M. (2011). Dvovimirna matematichna model vologoperenosu kapilarno-poristikh materialakh z fraktalnoiui strukturoiu. *Naukovii visnik NLTU Ukraini*, 21 (2), 341–348.
35. Voronov, V. G., Mikhailetskii, Z. N. (1982). *Avtomaticheskoe upravlenie protsessami sushki*. Kyiv: Tekhnika, 109.
36. Gayvas, B., Markovych, B., Dmytruk, A., Havran, M., Dmytruk, V. (2024). The methods of optimization and regulation of the convective drying process of materials in drying installations. *Mathematical Modeling and Computing*, 11 (2), 546–554. <https://doi.org/10.23939/mmc2024.02.546>
37. Dmytruk, A. (2024). Modeling mass transfer processes in multicomponent capillary-porous bodies under mixed boundary conditions. *Mathematical Modeling and Computing*, 11 (4), 978–986. <https://doi.org/10.23939/mmc2024.04.978>
38. Sokolovskyy, Y., Drozd, K., Samotii, T., Boretska, I. (2024). Fractional-Order Modeling of Heat and Moisture Transfer in Anisotropic Materials Using a Physics-Informed Neural Network. *Materials*, 17 (19), 4753. <https://doi.org/10.3390/ma17194753>
39. Decker, Ž., Tretjakovas, J., Drozd, K., Rudzinskas, V., Walczak, M., Kilikevicius, A. et al. (2023). Material's Strength Analysis of the Coupling Node of Axle of the Truck Trailer. *Materials*, 16(9), 3399. <https://doi.org/10.3390/ma16093399>
40. Gayvas, B. I., Markovych, B. M., Dmytruk, A. A., Havran, M. V., Dmytruk, V. A. (2023). Numerical modeling of heat and mass transfer processes in a capillary-porous body during contact drying. *Mathematical Modeling and Computing*, 10 (2), 387–399. <https://doi.org/10.23939/mmc2023.02.387>

Edited by  
Bogdana Gayvas, Veronika Dmytruk

DRYING PROCESSES: APPROACHES TO IMPROVE EFFICIENCY

Bogdana Gayvas, Bogdan Markovych, Anatolii Dmytruk, Veronika Dmytruk, Yevhen Chaplya

Collective monograph

Technical editor I. Prudius  
Desktop publishing T. Serhiienko  
Cover photo Copyright © 2025 Canva

---

TECHNOLOGY CENTER PC®

Published in March 2025

Enlisting the subject of publishing No. 4452 – 10.12.2012

Address: Shatylova dacha str., 4, Kharkiv, Ukraine, 61165

---